UC Berkeley
UC Berkeley Electronic Theses and Dissertations

Title

Characterization of microRNA oncogenes and tumor suppressors in a mouse B-lymphoma model.

Permalink

https://escholarship.org/uc/item/54v2057p

Author

Bennett, Margaux Joy

Publication Date

2014

Peer reviewed|Thesis/dissertation

eScholarship.org Powered by the California Digital Library
University of California

Characterization of microRNA oncogenes and tumor suppressors in a mouse B-lymphoma model.

By
Margaux Joy Bennett

A dissertation submitted in partial satisfaction of the

requirements for the degree of

Doctor of Philosophy

in

Molecular and Cell Biology

in the

Graduate Division

of the

University of California, Berkeley

Committee in charge:

Professor Lin He, Chair
Professor Danica Chen
Professor Richard Harland
Professor Astar Winoto

Spring 2014

© by Margaux Joy Bennett
May 2014
All Rights Reserved

Abstract

Characterization of microRNA oncogenes and tumor suppressors in a mouse B-lymphoma model.

By
Margaux Joy Bennett

Doctor of Philosophy Molecular and Cell Biology
University of California, Berkeley

Professor Lin He, Chair

Cancer of any cell type, including B-cell lymphoma, arises from a series of genetic lesions that ultimately transforms normal cells into tumor cells. These genetic lesions allow the cells to accumulate traits such as uncontrolled proliferation, resistance to cell death, and invasive growth. Functional characterization of these genetic lesions will help us to understand the molecular alterations required for lymphomagenesis, and to provide better therapeutic strategies. Several major lesions that drive oncogenesis have been well-characterized, but the complex signaling network that cooperates with and regulates these oncogenic drivers has yet to be understood. In the last decade, it has become clear that non-coding RNAs, particularly microRNAs, both as oncogenes and tumor suppressors, play a large role in cancer initiation, progression, and maintenance.

In this dissertation, I discuss the roles that the oncogenic miRNA cluster *mir-17-92*, and the tumor suppressive *mir-34* miRNA family play in B-cell lymphomagenesis, using the *Eμ-myc* mouse model that mimics human Burkitt's lymphoma. First, I present our work dissecting the *mir-17-92* cluster. In mammals, the *mir-17-92* cluster of miRNAs has an unconventional gene structure compared to protein-coding genes in that one *mir-17-92* primary transcript yields six individual miRNAs. The *mir-17-92* cluster is found to be amplified in several human B-cell malignancies, and overexpression of *mir-17-92* is known to accelerate *Eμ-myc* lymphomagenesis. To determine the mechanism behind *mir-17-92's* acceleration of lymphomagenesis, we dissected the components of the cluster and found that *mir-19* is both necessary and sufficient to accelerate *Eμ-myc* B-cell lymphomagenesis. While miRNAs regulate many pathways and targets, the oncogenic ability of *mir-19* is due at least in part to its capacity to downregulate the tumor suppressor phosphatase and tensin homolog (Pten). *mir-19* thus promotes cell survival over c-Myc induced apoptosis. We next show a new paradigm illustrating the internal oncogenic and tumor suppressive crosstalk that occurs within the unique polycistronic cluster of *mir-17-92*. We show that, fascinatingly, *mir-92* antagonizes *mir-19*'s oncogenic ability in this B-cell lymphoma model by downregulating Fbw7, a negative regulator of c-Myc. Consequently, *mir-92* increases the levels of c-Myc imposing a strong coupling between excessive proliferation and apoptosis. Therefore, during lymphomagenesis there is a selection to disrupt this internal antagonism of *mir-17-92* to favor the development of lymphoma cells that express less *mir-92* relative to that of *mir-19*.

In the final chapter of this dissertation I switch gears from analyzing oncogenic effects to investigating the tumor suppressive roles the *mir-34* miRNA family members have in *Eμ-myc*

lymphomagenesis. The *mir-34* miRNA family consists of six miRNAs that have identical seed sequences, which are located in three genomic loci with different cistronic arrangements; in humans *mir-34a* is transcribed from chromosome 1*, mir-34b/mir-34c* is transcribed as a single transcript from chromosome 11*,* and the *mir-449* family is transcribed as a single transcript containing *mir-449a/mir-449b/mir-449c* from chromosome 5. p53 transcriptionally induces the expression of *mir-34a,* and *mir-34b/mir-34c*, while the *mir-449* cluster is induced by E2f1. We found that the deletion of each of these three miRNA loci exhibit an acceleration of *Eμ-myc* lymphomagenesis. Surprisingly, however, the complete deletion of *mir-34a* and *mir-34b/mir-34c* loci abolishes the acceleration that is seen upon the deletion of the individual miRNAs. In the B-cells of the complete *mir-34* knockout, we found that the homologous *mir-449* family is upregulated. We demonstrate that the *mir-34* knockout mice also upregulate E2f1, which is likely driving the compensatory upregulation of *mir-449.* The compensatory responses of these homologous *mir-34* miRNAs further the crosstalk between the E2f1 and p53 pathways. These studies provide two clear examples of how miRNAs play a major role in cancer progression. The discovery of this interesting internal antagonism within the *mir-17-92* cluster, and the fine-tuned compensatory responses between the *mir-34* and *mir-449* miRNAs helps illuminate how miRNAs have evolved to maintain their unique polycistronic structures, and seemingly redundant families, in order to cross-activate regulatory pathways and rein in potentially oncogenic cell signals.

"What I love most about science is that it is such a deeply, intensely human enterprise. The success of the enterprise of science, and of the individual scientist, is derived precisely from the fact that we do it together. Science is among the best things we do as a species."
- Victor Ambros, 2010

Table of Contents

Table of Figures and Tables ..... **iii**

Acknowledgments ..... **v**

Introduction ..... **vii**
An introduction of microRNAs vii
microRNA Biogenesis and Function vii
microRNAs in Cancer ix
Oncogenic miRNAs: a focus on *mir-17-92* xiii
microRNAs as Tumor Suppressors xv
microRNAs and p53 xvii
P53 induced tumor suppressive miRNAS: A focus on *mir-34* xx
The *E*μ-*myc* mouse model xxii
Directions of Study xxiv

Chapter 1: *miR-19* is a key oncogenic component of *mir-17-92* **1**
Summary 2
Introduction 2
Results 3
Discussion 8
Methods 9

Chapter 2: A component of the *mir-17-92* polycistronic oncomir promotes oncogene-dependent apoptosis **28**
Summary 29
Introduction 29
Results 30
Discussion 37
Methods 38

Chapter 3: *mir-34* and *mir-449* microRNA families act as tumor suppressors in a B-lymphoma mouse model **68**
Summary 69
Introduction 69
Results 71
Discussion 76
Materials and Methods: 77

Conclusions **93**

References **94**

Appendix A: *Eμ-myc*$^{+}$*;p53*+/- tumors have increased numbers of T regulatory cells **116**

Appendix B: *Eμ-myc*$^{+}$*;mir-34b/c*+/- mice exhibit increased lymphoma dissemination to the meningeal space **119**

Table of Figures and Tables

Table of Figures and Tables ..... **iii**

Acknowledgments ..... **v**

Introduction ..... **vii**

Figure 1. microRNA Biogenesis and Post-transcriptional mechanisms of Regulation. viii

Table 1. Oncogenic microRNAs xii

Table 2. Tumor Suppressive microRNAs xvii

Chapter 1 ..... **1**

Figure 1. *miR-19b* phenocopies the oncogenic effects of *mir-17-92* in the *Eμ-myc* model. 13

Figure 2. *Eμ-myc/17-19* and *Eμ-myc/19b* lymphomas have similar pathological and immunological features. 15

Figure 3. *miR-19* miRNAs are essential for the oncogenic activity of *mir-17-19b*. 17

Figure 4. *Pten* is a *mir-17-19b* target specifically regulated by *miR-19*. 19

Figure 5. *miR-19b* functionally antagonizes *pten*-induced apoptosis in *Xenopus* embryos. 20

Figure 6. *miR-19* and *mir-17-19b* activates the Akt–mTOR pathway. 21

Supplementary Figure S1. Oncogenic potential of *mir-17-92* components in the *Eμ-myc* lymphoma model. 22

Supplementary Figure S2. Representative data from flow cytometric immunophenotyping of *Eμ-myc* lymphomas with different *mir-17-92* sub-clusters. 23

Supplementary Figure S3. *Eμ-myc/19* and *Eμ-myc/17-19b-Mut19* tumors are highly proliferative. 24

Supplementary Table S1. Flow cytometric immunophenotyping of *Eμ-myc* lymphomas with enforced expression of different *mir-17-92* sub-clusters. 27

Chapter 2 ..... **28**

Figure 1. *miR-92* negatively regulates the *mir-17-92* oncogenic activity in the *Eμ-myc B-lymphoma* model. 46

Figure 1 – supplement 1. Functional antagonism between *miR-19:miR-92* regulates the balance between proliferation and apoptosis. 48

Figure 2. The *miR-92* deficient *mir-17-92* cooperates with c-Myc to promote highly aggressive B-lymphomas. 50

Figure 3. *miR-92* enhances both c-Myc-induced apoptosis and c-Myc-induced proliferation. 52

Figure 3 - supplement 1. *miR-92* enhances c-Myc-induced apoptosis both in vitro and in vivo. 54

Figure 4. *miR-92* induces apoptosis through the activation of the p53 pathway. 56

Figure 4 - supplement 1. *miR-92* overexpression triggers the activation of the p53 pathway. 57

Figure 5. *miR-92* promotes the accumulation of c-Myc protein through repressing Fbw7. 59

Figure 5 - supplement 1. *miR-92* overexpression enhances c-Myc protein level by repressing Fbw7. 61

Figure 6. The antagonistic interaction between *miR-19* and *miR-92* regulates the balance between proliferation and apoptosis. 63

Figure 6 - supplement 1. Functional antagonism between *miR-19:miR-92* regulates the balance between proliferation and apoptosis. 64
Figure 7. The *miR-19*:*miR-92* antagonism is disrupted during malignant transformation. .. 66
Table 1. Flow cytometric immunophenotyping of *Eμ-myc* lymphomas with enforced expression of different *mir-17-92* derivatives..... 67

Chapter 3..... 68
Figure 1. Deletion of *mir-34a* or *mir-34b/c* accelerates lymphomagenesis..... 80
Supplemental Figure 1. 81
Figure 2. Deletion of *mir-34a* or *mir-34b/c* increases proliferation, while deletion of *mir-34b/c* inhibits apoptosis..... 82
Figure 3. *mir-34* miRNAs inhibit proliferation and induce apoptosis by targeting cell cycle and anti-apoptotic genes..... 83
Supplemental Figure 3. 84
Figure 4. Complete deletion of the *mir-34* miRNA family abolishes the acceleration of lymphoma seen in the both single knockout mice. 86
Supplemental Figure 4. 88
Figure 5. Deletion of *mir-449* accelerates *Eμ-myc*$^+$ lymphomagenesis. 89
Supplemental Figure 5 90
Figure 6. The complete deletion of *mir-34*/*mir-449* miRNAs seems to inhibit E2f1 induced apoptosis seen in the *mir-34a-/-;mir-34b/c-/-* mice. 91
Supplemental Figure 6. 92

Conclusions 93

References 94

Appendix A: 116
Figure 1. *Eμ-myc*$^+$*;p53*+/- tumors have increased numbers of T regulatory cells 118

Appendix B: 119
Figure 1: *Eμ-myc*$^+$*;p53*+/- mice exhibit increased lymphoma dissemination to the meningeal space..... 121
Figure 2: *Eμ-myc*$^+$*;mir-34b/c*+/- mice exhibit increased lymphoma dissemination to the meninges. 123

Acknowledgments

I came to the MCB Department here at Berkeley because of the people, and there are many to thank. First and foremost, I thank my advisor Lin He for taking me on as her first graduate student. Lin helped me cultivate confidence in myself in many ways, teaching me to independently navigate scientific experiments, conferences, and presentations. While the pressure she placed on me to become a better scientist could at times be a struggle, I would not change a thing about my graduate school experience as I have have grown both as a scientist and a person, and I thank her for that.

I thank my dissertation committee Danica Chen, Richard Harland, and Astar Winoto for their guidance. With regard to this thesis, I thank Richard for his humorous critiques and for helping me rework my sentence structure. I would like to thank the rest of the MCB professors who have both taught me and given me advice through the years. In particular, I thank Mark Schlissel for reminding me that I am in control of my own life. I also thank Iswar Hariharan for his comment on how I must be able to survive anything since I swim in the Pacific Ocean, thereby reminding me of my own strength.

I thank Virginie Olive for being there for me through every step of the way. I have never had so much fun doing science with someone. From my first day of lab trying to shave mice, to sleeping in lab between expedited cloning, to running to Jupiter before 11pm for pizza and beer – these experiences I will never forget. As a mentor, she encouraged me to try new experiements, she helped me edit my talks (as well as this thesis), and taught me more about how to handle life's hiccups than I can say. I thank her whole family for their support, particularly Lea for helping me keep my chin up.

A great amount of thanks is owed to Nico Sponer for helping me with life and experiments when I was overwhelmed and tired, and also for making sure I was properly caffeinated. I thank Iris Jiang for pipet help and qual party planning, Marcelo Ribeiro for laughter and 1pm mandatory lunches, and YeeAnn Chen for being the most positive and professional undergrad. I must thank all the other "He lab-ites" for making lab what it is, in particular: Yong Jin for being best and funniest bay mate; Paul, Jenn, and Mona for encouragement and amazing dance moves; Erich for keeping the lab clean, and the internet functioning; Em for teaching me the ways of Sandwhich Zone; Pengcheng for making the best enzymes; as well as everyone else along the way.

As a new student, I sought help from many people outside of my lab. Without these people, my science would not be what it is. I thank James Walker for being the senior graduate student I looked up to, and for being willing to collaborate with us on our papers. I thank Jennifer Young, Ivan Dzhagalov, and Hector Nolla for teaching me FACS. I thank Kathleen Pestal for teaching me how to perform tail vein injections, and Heather Melichar for teaching me how to do bone marrow chimeras. I thank Greg Timblin for always being available to give me vials of cells. I thank Andrea Wills for for teaching me frog injections, and that sometimes you should just buy all new reagents.

I am so blessed to have so many friends who have supported me through graduate school. I thank Megan Burger for accepting to be my " real friend." I am so glad that our love of the same scientific fields and wine could bring us together. She has taught me both how to work and play hard, and that running is more fun if you frolick. I thank Nikki Kong for being the best "co-ton," and for instilling in me a sense of spontaneity – like Hawaii after qualifying exams. I thank Ruchi Schock for being there since to the first day of graduate school to discuss the future of our

lives whenever needed. I thank Jess Lyons for her pragmatism, big smile, and cheerful outfis. I thank Tera Levin for the four leaf clovers, Nate Krefman for the science raps, and Nicole Fay and Robin Beckwith for teaching me biochemistry and commiserating.

While I have many friends outside of MCB, each who have supported me in their own way, no one has been as supportive as Julia Hellman. When I was too busy to be a proper friend, she stepped up and was enough "friend" for the both of us, bringing me tea at the microscope. I thank Alvin Lo for being the best running buddy, and always waiting for me to finish in lab. I thank Kendall Olsen for getting me through late labs nights both at Stanford, and Berkeley.

Before coming to MCB, I developed a love for science, first and foremost, from Rog McGeHee in Adv. Bio class at the Branson School. At Stanford, Tim Stearns and Martha Cyert set me on the path to research by accepting me in their Bio54/55 Adv. Lab Research class. In particular, I thank Tim for encouraging me to go to graduate school, and for getting me into both the Hartzog and Talbot labs. I thank Will Talbot for taking me on Tim's recommendation, giving me the chance to have my own project, and creating the environment in which I could fall in love with science. I thank Nitzan Sternheim for teaching me that everybody does the same experiments differently, and that family is the most important thing. I thank Kelly Monk for her rescue when I was lost in the zebrafish genome - without her I would not have mapped the *st64* zebrafish mutation. I thank Julie Perlin for welcoming "undergrad me" as if I were a grad student.

I thank my soon to be husband, Matt, for more than I can say. Growing up together has been so much fun, I know it will only get better. I thank my parents and my brother and new sister Caroline for their love and support, free home cooked meals and margaritas, for picking me up at lab, loaning me cars, and for finally understanding that I do not always want to talk about research. I am so lucky to have the most supportive and fun-loving family.

Lastly, hats off to MCB entering class of 2008. I wish you all luck in the future. I will not forget our times together.

Introduction

An introduction of microRNAs

microRNAs (miRNAs) were first identified in 1993 by the Ambros and Ruvkun labs in an effort to understand the function of *lin-4*, a gene involved in larval developmental timing (Lee et al, 1993; Wightman et al., 1993). *lin-4* was found to code for a small regulatory RNA which initially seemed unique to worms, until 2000, where the discovery of *let-7* in worms, and its subsequent homologs in flies, mice, and humans suggested that these small regulatory miRNAs are an evolutionarily conserved mechanism for gene regulation (Reinhart el al, 2000). Two decades after the original discovery of *lin-4,* more than 1,761 miRNAs have been confidently mapped across 38 species, with 278 of those being human miRNAs (Kozomara et al., 2014). Unlike coding genes, miRNAs are often organized in unique polycistronic clusters that allow for simultaneous or compounded regulation of signaling pathways. Additionally, the small size of miRNA (18-22 nucleotides) has allowed miRNAs to duplicate within genomes throughout evolution without disrupting other gene structures. These duplications have allowed several miRNA families to reinvent their role in cell fate decisions, populating various genomic loci that are differentially regulated according to signals for specific cell types and contexts.

microRNA Biogenesis and Function

The majority of nascent miRNA transcripts, known as primary miRNAs (pri-miRNAs), are first transcribed from the genome by polymerase II (Lee et al., 2002; Lee et al., 2004), with some being transcribed by polymerase III (Borchert et al., 2006). The pri-miRNAs transcripts are consequently 5'capped and polyadenylated, and may contain introns similar to coding genes (Lee et al., 2004). These pri-miRNA transcripts can be kilobases in length, contain multiple miRNA precursor hairpins, and undergo splicing similar to coding mRNA transcripts (Kim and Kim 2007). In fact, about 30 percent of miRNAs originate from the intronic region of a coding mRNA transcript (Kim and Kim 2007).

Most pri-miRNA transcripts contain 60-80 nucleotide hairpin structures created from semi-complementary base-pairing. These hairpins are processed by the microprocessor complex into individual stem loop, precursor miRNAs (pre-miRNAs) in the nucleus (Lee et al., 2003; Denli et al. 2004; Han et al., 2004; Fig. 1). In humans and mice, the microprocessor consists of the ribonuclease III enzyme Drosha, and it's cofactor DiGeorge syndrome critical region gene 8 (DGCR8). Drosha and Dgcr8 are the critical components for pri-miRNA processing, but more recently it has been found that differential cell signaling can affect the presence of additional cofactors in the microprocessor complex, such as p68/72, p53, and Smad (Fukuda et al., 2007; Davis et al., 2008; Suzuki, et al., 2009 – See the *microRNAs in Cancer* section for more detail). Intronic miRNAs, also known as mirtrons, skip this microprocessor cleavage step, and are instead spliced out from the coding transcript into pre-miRNA by the spicing machinery (Ruby et al., 2007).

These pre-miRNAs are then exported from the nucleus by Exportin-5 along with RanGTP and are processed by a second RNAse III enzyme, Dicer, into a mature miRNA duplex ranging from 18-24nt in length (Yi et al., 2003; Lund et al., 2004; Hutvágner et al., 2001; Grishok et al., 2001). One strand of the miRNA duplex, presumably the strand with the least stability at the 5'end, is selected by the Argonaute family proteins, and loaded into the RNA-induced silencing complex (RISC) (Martinez et al., 2002; Khvorova et al., 2003; Seitz et al., 2008). In the RISC complex, a miRNA can target specific mRNAs through imperfect base-pairing to downregulate their expression by post-transcriptional gene silencing mechanisms. The specificity of a miRNA for its target genes is generally

thought to depend on the seed sequence – positions 2 through 8 of the mature miRNAs – and how well this seed sequence base-pairs to its target sequence (Bartel 2009). Additionally, the mature miRNA can exhibit target cleavage using "centered sites" consisting of 11-12 contiguous Watson-Crick paired nucleotides in the center of the mature miRNA (Shin et al., 2010). Other sequences in the pri-miRNA and pre-miRNA may also have the ability to inhibit gene expression. One such controversial example comes from the Chen group, who shows that the hairpin loop of *mir-181a* and *mir-181c* affects the function of these miRNAs in T-cell development (Liu et al., 2008).

miRNA mediated post-transcriptional gene silencing mechanisms have been long debated, but there are several possibilities that may or may not be mutually exclusive under different contexts: inhibition of translation initiation, deadenylation of mRNA, inhibition of translation elongation, and sequestration of mRNA in cytoplasmic processing bodies (P-bodies) (Filipowicz et al., 2008; Fig. 1). It is thought miRNAs maneuver the RISC complex to associate with their target mRNAs. Though most agree that functional miRNA target sites reside in the 3'UTRs of their target transcripts, others have found target sites that reside in the coding sequence or the 5'UTRs of the mRNA (Tay et al., 2008; Lytle et al., 2007; Gu et al., 2009). Once bound to the target mRNAs, the RISC complex is thought to block translation initiation by interfering with cap-recognition of the mRNA, and thereby preventing ribosomal assembly (Pillai et al., 2005; Kiriakidou et al., 2007; Eulalio et al., 2010). After inhibition of translation initiation, the RISC complex deadenylates the target transcript and induces its subsequent degradation (Lim et al., 2005; Wu et al., 2006). In some cases, this deadenylation is thought to occur before translation inhibition can even happen (Giraldez et al., 2006). More controversially, the RISC complex is thought to inhibit translation elongation potentially by inducing the ribosomes to drop off prematurely (Maroney et al., 2006; Petersen et al., 2006). Lastly, the RISC is thought to mediate post-transcriptional gene silencing by forming transcript degrading P-bodies, complexing with decapping and deadenylating proteins. These P-bodies either degrade the transcript or transiently sequestering target mRNAs from translation machinery (Liu et al., 2005; Schratt et al., 2006). Though the exact mechanisms and protein components of these four post-transcriptional gene silencing pathways are not fully understood, most agree that the endpoint of these mechanisms most often involves deadenylation and destabilization of target mRNAs, allowing for screening of most miRNA targets by mRNA transcript level analyses.

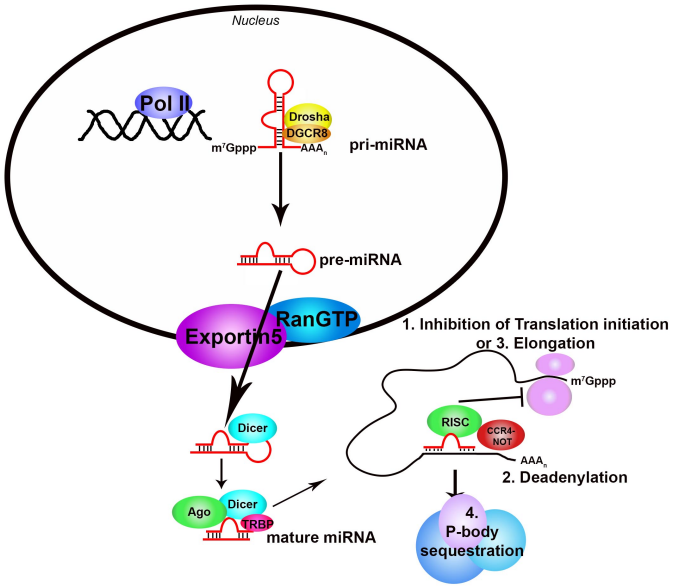

Figure 1. microRNA Biogenesis and Post-transcriptional mechanisms of Regulation.

microRNAs in Cancer

With their ability to repress many target genes and temper gene expression, it is only fitting that miRNAs have been found to play a large role in cancer biology. Before technology allowed for profiling of such small RNAs, there was already evidence pointing towards a role for miRNAs in cancer progression. The first two miRNAs discovered, *lin-4* and *let-7*, when deleted in *C. elegans* prevented larval differentiation, with the cells instead undergoing extra divisions creating more undifferentiated cells of their same larval stage (Lee et al., 1993, Wightman et al., 1993, Reinhart et al., 2000, and Slack et al., 2000). The loss of function of *lin-4* and *let-7* therefore somewhat resembled the phenotypes seen upon the loss of tumor suppressor protein coding genes. Soon after, forward genetic screens in *Drosophila* uncovered two miRNAs, *bantam* and *mir-14*, that were oncogenic in nature as *bantam* promoted proliferation and both *bantam* and *mir-14* inhibited apoptosis (Brennecke et al., 2003; Xu et al., 2003). Simultaneously, Carlo Croce's group discovered that *mir-15* and *mir-16* are deleted or downregulated in ~70% of all chronic lymphocytic leukemia (CLL), a discovery that was the start of intensive research on miRNAs and cancers (Calin et al., 2002).

miRNAs were subsequently identified to be frequently located at fragile sites in the genome, and found to display frequent genomic alteration and dysregulated expression in various human tumors (Calin et al., 2004; Lu et al., 2005; Sonoki et al., 2005; Ota et al., 2004). To determine if global downregulation of miRNAs aided tumorigenesis, the Jacks group knocked down the processing components, Drosha, DiGeorge syndrome critical region gene 8 (DGCR8), and Dicer, and saw that their partial knockdown enhanced cellular transformation, presumably by decreasing miRNA maturation (Kumar et al., 2007). Subsequently, several groups found Dicer to be a haploinsufficient tumor suppressor in solid cancers such as lung cancer and retinoblastoma (Kumar et al., 2007; Kumar et al., 2009; Nittner et al., 2012). However, interestingly, in the *Eμ-myc* B-lymphoma mouse model, heterozygosity for Dicer did not accelerate tumorigenesis, suggesting that certain miRNAs may be required for B-cell development, for transformation in a hematological setting or for Myc-driven tumorigenesis (Arrate et al., 2010). In fact, the *mir-17-92* cluster of miRNAs has been shown to be required for B-cell development (Ventura et al., 2008).

While it is clear that miRNA suppression enhances tumorigenesis, the mechanisms by which miRNAs are globally repressed only recently have come to light. Though Myc has been seen to globally repress transcription of pri-miRNAs (Chang et al., 2008), most tumors exhibit a downregulation of mature miRNAs without a change in the pri-miRNA levels suggesting global repression through alteration of miRNA processing (Lee et al., 2008; Thomson et al., 2006). Some studies have reported rare mutations in Dicer (Hill et al., 2009), TRBP2 (Melo et al., 2009) and XPO5 (Melo et al., 2010), but the surprising paucity of such mutations has stimulated work on how other signaling pathways might regulate miRNA biogenesis.

The Hammond group showed some of the first evidence that the miRNA biogenesis is likely regulated in most tumors at the Drosha/Microprocessor step (Thomson et al., 2006). Subsequent studies identified numerous cofactors that can associate with the Microprocessor and affect biogenesis of numerous miRNAs. These cofactors include p68 and p72 (Fukuda et al., 2007), transforming growth factor beta (TGFβ) and bone morphogenic proteins 2/4/7 (BMP2/4/7) (Davis et al., 2008), and FUS/TLS (Morlando et al., 2012). The KH-type splicing regulatory protein (KHSRP) was found to assist the biogenesis of 34 miRNA at both the pri- to pre-miRNA cleavage, and the pre- to mature Dicer regulated cleavage step (Trabucchi et al.,

2009). Recently, an elegant study showed that constitutively activated Yes-associated protein 1 (YAP), a transcription factor, can sequester p72 in the nucleus away from the microprocessor, thereby causing downregulation of a large percentage of miRNAs (Mori et al, 2014). Constitutively activated, nuclear YAP is seen in a great number of cancers including hepatocellular carcinoma, and lung cancer (Harvey et al., 2013), and therefore this study may explain why some cancers show a global downregulation of miRNAs. While constitutively activated YAP represses miRNA production, activated epidermal growth factor receptor (EGFR) can directly phosphorylate Ago2, which inhibits Ago2 from binding Dicer and assisting in the processing of tumor suppressive miRNAs (Shen et al., 2013). Increased processing of oncogenic miRNAs happens when TAR RNA-binding protein (TRBP) is phosphorylated by the mitogen-activated protein kinase (MAPK) downstream of Erk signaling. Phospho-TRBP then enhances the processing of growth promoting miRNAs such as *miR-17,* and *mir-20*, while inhibiting processing of growth inhibitory miRNA *let-7* (Paroo et al., 2009).

There are a few examples of other proteins that interact with the biogenesis of specific miRNAs. The heterogenous nuclear ribonucleoprotein A1 (hnRNP A1) assists in the processing of *pri-mir-18* by recognizing *mir-18's* stem loop (Guil and Caceres, 2007). Something similar may be occurring when p53 and breast cancer 1, early onset (BRCA1) assist in the processing of a subset of tumor suppressive miRNAs such as *mir-16*, *mir-34a*, and *mir-145* (Suzuki, et al, 2009; Kawai and Amano, 2012). In the case of *let*-7 processing, Lin-28 recruits a terminal uridylyl transferase or TUTase, Zcchc11, that causes poly-uridilaytion of pre-*let-7,* preventing it from being cleaved by Dicer into mature miRNA (Heo et al., 2008; Hagan et al., 2009). Fascinatingly, in somatic cells, the absence of Lin-28 allows the terminal uridylyl transferases TUT7/4/2 to mono-uridylate *let-7;* this mono-uridylation enhances the processing of *let-7,* while poly-uridylation inhibits its processing (Heo et al., 2012). The interactions of cofactors with specific primary miRNA transcripts may provide an alternative mechanism to amplification, methylation, and deletion for the dysregulation of different subsets of oncogenic or tumor suppressive miRNAs in cancer.

Alterations that occur in miRNA biogenesis in the context of cancer are continually being uncovered, as regulation of processing is likely to be cell-type and oncogenic-driver specific. While this section provides an overview of many of the aspects of miRNA biogenesis, it by no means comprehensive.

microRNAs as oncogenes

While cancer cells tend to exhibit global downregulation of miRNAs, there are a number of miRNAs that are upregulated and have been shown to promote oncogenesis in subsets of cancers. This section will provide an overview of a few of the most well characterized oncogenic miRNAs and the studies of their effects in specific types of cancer (see Table 1. Oncogenic miRNAs). This overview should be considered with the knowledge that many miRNAs may have alternative oncogenic or tumor suppressive properties depending on the cell type.

mir-21

mir-21 was one of the first miRNAs found to be upregulated in many different types of cancers, including glioblastoma (Chan et al., 2005), colon, prostate, breast, pancreas, lung, and stomach (Volinia et al., 2006). In various cancer cell types, *mir-21* was found to target a number of tumor suppressive genes including PTEN (Meng et al., 2007), tropomyosin 1 (TPM1) (Zhu et al., 2007), and programmed cell death 4 (Pdcd4) (Asangani et al., 2008). To determine the true

oncogenic potential of *mir-21,* the Slack lab generated transgenic mice that overexpressed *mir-21* throughout mice and observed development of pre-B cell malignant-like lymphoma (Medina et al., 2010). They further illustrated the dependence of these lymphomas on *mir-21* using their controllable Tet-off system. They showed that upon addition of the Tet agonist. doxycycline, the tumors regressed, thereby identifying the first example of oncogene addiction for a microRNA. At the same time, the Olson group showed that in a model where constitutively active Kras, $Kras^{G12D}$, drives lung cancer that overexpression of *mir-21* increases tumor burden, while deletion of *mir-21* lessens tumor burden (Hatley et al., 2010). These oncogenic effects were likely due to *mir-21* targeting negative regulators of the Ras/MEK/ERK pathway such as sprout homologs 1/2 (Spry1/2), B-cell translocation gene 1 (Btg1), and Pdcd4 (Hatley et al., 2010). Lastly, mice constitutively lacking *mir-21* appeared phenotypically normal but displayed a decrease in papillomas induced by 7,12-dimethylbenz[*a*]anthracene (DMBA) or 12-*O*-tetradecanoylphorbol-13-acetate (Ma et al., 2011).

mir-22

Recently*,* Song *et al* thoroughly illustrated the oncogenic effects of *mir-22* in two different cancer cell types (Song et al., 2013*).* First, they demonstrated that overexpression of *mir-22* in human breast cancer induced EMT, invasion, and metastasis in a xenograft model. They further showed MMTV-*miR-22* mice exhibit increased mammary gland side-branching, stemness, and tumor development; they also showed that overexpression of *mir-22* in the hematopoetic compartment triggers myelodysplastic syndrome (Song et al., 2013). These tumorigenic effects are ascribed to downregulation of the TET2/3 family by *mir-22*, thus preventing TET2/3 from demethylating and activating the promoters of the tumor suppressive *mir-200* family. Furthermore, the increase in expression of *mir-22* along with the decrease in TET expression correlates with poor prognosis for both breast and myelodysplastic patients.

mir-125b

mir-125b is the ortholog of the first identified *C. elegans* miRNA, *lin-4* (Bousquet et al., 2010). *mir-125b* is dysregulated in human megakaryoblastic leukemia (Klusmann et al., 2010). Additional clinical examples indicate that *mir-125b's* translocation into the immunoglobulin heavy chain locus can give rise to lymphoblastic lymphoma (Sonoki et al., 2005). Subsequently, overexpression of *mir-125b* was shown to accelerate BCR-ABL induced lymphomagenesis (Bousquet et al., 2010). Mimicking the clinically found translocation, the *E*μ-*mir-125b* transgenic mice develop lethal B-cell malignancies (Gefen et al., 2010). *mir-125b* at least partially furthers oncogenesis in B-cells by targeting tumor necrosis factor, alpha-induced protein 3 (TNFAIP3), a negative regulator of nuclear factor kappa-light-chain-enhancer of activated B cells (NF-KB). Thus, *mir-125b* upregulates NF-KB and activates its signaling. Consequently, *mir-125b* can further transcription of its own locus, and generate a feed forward loop (Kim et al., 2012). Many oncogenic effects of *mir-125b* are likely also due to *mir-125b* repressing p53 both directly, and indirectly (See section on "*Negative Regulation of p53 by microRNAs*").

mir-155

Before the identification of *mir-155,* the gene containing *pri-mir-155, BIC,* was found to induce leukemia when expression was stimulated by a proviral insertional of avian leukemia virus (Tam et al., 1996). More recently, the *E*μ-*mir-155* expressing B-cells have been found to recapitulate this phenotype, transforming into pre-B cell lymphoma (Sandhu et al., 2012). This

transformation is at least in thought in part be due to the repression of histone deacetylase 4 (Hdac4), which negatively regulates oncogenes such as *Id2*, *c-Myc*, *Il-6*, and *Cyclin D1*.

In spite of its clear role in leukemogenesis, *mir-155* has actually been most extensively studied in breast cancer. *mir-155* has been found to be regulated by the TGFBeta/Smad pathway and to contribute to epithelial cell plasticity by inhibiting *RhoA* expression (Kong et al., 2008). Downregulation of RhoA, as well as Foxo3a likely contributes to *mir-155's* promotion of breast cancer (Kong et al., 2008). Most recently, *mir-155* has been shown to increase glycolysis in breast cancer cells (Jiang et al., 2012). By inhbiting C/EBPβ, *mir-155* downregulates C/EBPβ's transcriptional target, the bicistron *mir-143/mir-145* (Jiang et al., 2012). The repression of *mir-143* allows for the upregulation of its target hexokinase 2, which enhances the ability of breast cancer cells to undergo glycolysis (Jiang et al., 2012). *mir-155* ultimately increases glycolysis by indirectly repressing *mir-143*.

Interestingly, amongst all its oncogenic effects, *mir-155* also exhibits anti-cancer effects in a non-cell autonomous manner as *mir-155* expression is required for CD8 T cells to effectively clear cancer cells (Dudda et al., 2013). *mir-155* is thought to increase both the survival and anti-cancer activity of the CD8 T cells in the tumor microenvironment.

Oncogenic microRNA	Cancer Association	Gene Target	Reference
mir-17-92	B-cell lymphoma; Lung, breast, stomach, prostate, colon, and pancreatic tumors	Pten (*miR-19*); E2F1 (*miR-17/20*);Rbl2/p130 (*miR-17*);	Ota et al, 2004; He et al, 2005; O'Donnell et al, 2005; Volinia et al, 2006; Sylvestre et al, 2007; Xiao et al 2008; Olive et al, 2009;Lu et al, 2007; Ma et al, 2012
mir-21	Lung, colorectal, breast, prostate, pancreas stomach cancer; Hepatocellular carcinoma; Glioblastoma; pre-B lymphoma	Apaf1; Spry1; Spry2; Btg2; Pdcd4; Faslg; RhoB; Pten; Tmp1	Hatley et al, 2010; Asangani et al, 2008; Meng et al, 2007; Zhu et al, 2007; Chan et al, 2005; Volina et al, 2006; Medina et al, 2010
mir-22	Breast cancer; Myelodysplastic syndrome	Tet2/3	Song et al, 2013
mir-25/mir-30d	Multiple myeloma	p53	Li et al, 2010; Kumar et al 2011
mir-125b	B-cell malignancies	TNFAIP3; p53; Puma; Bak1; p14/arf	Gefen et al, 2010; Kim et al, 2012; Le et al, 2009; Shi et al, 2011; Sumaira et al, 2013; Klusmann et al, 2010; Sonoki et al, 2005
mir-155	B-cell leukemia Breast cancer	Hdac4 RhoA; Foxo3a; C/EBPBeta	Sandhu et al, 2012 Kong et al, 2008; Jiang et al, 2012
mir-380-5p	N-Myc amplified neuroblastoma	p53	Swarbrick et al, 2009
mir-504	Colon cancer; oral squamous cell carcinoma	p53	Hu et al, 2010; Yang et al, 2012

Table 1. Oncogenic microRNAs

This table provides an overview of microRNAs and their targets with references supporting their oncogenic function.

Oncogenic miRNAs: a focus on *mir-17-92*

The *mir-17-92* cluster, also known as *oncomir-1,* was originally identified due to its amplification in B-cell lymphoma as part of the *C13orf25* locus (Ota et al., 2004). The *mir-17-92* primary transcript has a polyscistronic structure that contains six hairpin loops which generate six miRNAs. These six miRNAs fall into three separate miRNA families: *miR-17, miR-20, miR-*18 as one family, *miR-19a* and *miR-19b* as the second family, and *miR-92* as its own family. While mature *miR-18* exhibits sequence identity with *miR-17* and *miR-20,* one should note that *miR-18* differs by one nucleotide in the "seed" sequence. Duplications of the *mir-17-92* cluster in evolution generated two *mir-17-92* paralogs in mammals: *mir-106b-25* on chromosome 7 and *mir-106a-363* on chromosome X. Both the sequence and placement of each miRNA in the cluster is highly conserved across species (Olive et al., 2009; Chapter 2 of this thesis). There is some evidence that the organization of the *mir-17-92* polycistron is conserved for effective processing by the microprocessor (Chakraborty et al., 2012).

After initially finding the *mir-17-92* locus amplified in B-cell lymphoma, many groups set out to determine whether *mir-17-92* could, in fact, drive tumorigenesis. To do so, He et al., overexpressed *mir-17-92* in the *Eμ-myc* mouse model of B-lymphoma and found that *mir-17-92* overexpression accelerated lymphomagenesis (He et al., 2005). Subsequently, it was found that the *mir-106a-363* and *mir-17-92* are often dysregulated in hematopoietic and solid tumor malignancies (Petrocca et al., 2008;Volinia et al., 2006) and are commonly found as insertion sites in retrovirus-induced leukemias (Wang et al., 2006; Cui et al., 2007; Landais et al., 2007).

While the whole cluster can aid in tumorigenesis, we noted that overexpression of *mir-17-19b,* a variant lacking *mir-92,* could induce lymphoma more rapidly than the full cluster (Olive et al., 2009 and 2013). Therefore, in order to determine the extent to which each of the *mir-17-92* miRNAs contribute to oncogenesis, we and others have dissected the activity of the *mir-17-92* locus in different cancer types. Collectively we found that in the context of B-cell lymphoma, *mir-19* acts as a major driver of oncogenesis by targeting *Pten* and inhibiting Myc-induced apoptosis (Takakura et al., 2008; Xiao et al., 2008; Mu et al., 2009; Chapter 1 of this thesis). In contrast, the *mir-17/mir-20* family drives tumor development in prostate and colorectal cancer by directly repressing TIMP metallopeptidase inhibitor 3 (Timp3) and p130 and thereby increasing cell survival (Yang et al., 2013; Ma et al., 2012).

Most of the effects of each of the miRNAs in the *mir-17-92* cluster have been shown to be oncogenic, however, there are a few instances where individual miRNAs within the cluster may actually antagonize tumorigenesis. For example, *mir-17-5p* inhibits anchorage-independent growth of breast cancer cells by targeting amplified in breast cancer 1 protein (AIB1), a transcriptional coactivator with histone acetyltransferase activities (Hossain et al., 2006); *mir-17-5p* also inhibits proliferation and cell migration by targeting fibronectin type-III domain containing 3A (FNDC3A) in prostate cancer cells (Shan et al., 2009). In addition to the antagonistic effects of *mir-17* in these cell types, *mir-92* antagonizes *Eμ-myc* lymphomagenesis by repressing Fbw7 and increasing the amount of Myc-induced apoptosis (Olive et al., 2013 - Chapter 2 of this thesis). Therefore, it is likely that these miRNAs may be poised to balance each other's activity, but when their ratio becomes dysregulated they may promote tumorigenesis.

More and more evidence suggests that the expression of the *mir-17-92* cluster is highly regulated both transcriptionally and post-transcriptionally, thereby allowing it to exert both pleiotropic and specific functions across cell types. O'Donnell *et al* found that the *mir-17-92* cluster contains an E-box promoter element (O'Donnell et al., 2005), making it a downstream

target of the proto-oncogene c-Myc, and not surprisingly, N-myc also (Schulte et al., 2008). E2f1 and E2f3 also drive *mir-17-92* transcription, explaining why *mir-17-92* is upregulated in proliferating cells (Sylvestre et al., 2007; Woods et al., 2007). Fascinatingly, *mir-17-92* miRNAs exert negative feedback on their own transcription factors. Specifically, *mir-17* and *mir-20*, with their identical seed sequences, have been shown to inhibit translation of E2f1, E2f2, and E2f3 (Sylvestre et al., 2007; Woods et al., 2007). Additionally, *mir-92* indirectly induces the upregulation of c-Myc by targeting its negative regulator, Fbw7 (Olive et al., 2013 - Chapter 2 of this thesis). These observations suggest that under certain contexts *mir-17-92* can limit cellular proliferation by targeting E2fs and in other contexts promote cellular proliferation by upregulating c-Myc. Additionally, as both E2F and c-Myc have been shown to induce apoptosis, *mir-17-92* can also regulate cell survival signaling, as well as proliferation, through these same targets (Hershko et al., 2005; Meyer et al., 2008).

The mature *mir-17-92* miRNAs, while being derived from the same transcript, have been found to be each expressed at different levels depending on the cell type. For the cell specific expression changes, each miRNA must either experience differential processing or stability in each cell type (Chapter 2). Analysis of the tertiary structure of the *mir-17-92* primary transcript has suggested that *mir-19b* and *mir-92*a form the core of the *mir-17-92* molecule and are encapsulated by *mir-17, mir-18a,* and *mir-20*a (Chaulk et al., 2011). This tertiary form suggests that the outer *mir-17, mir-18a,* and *mir-20* miRNAs might be more efficiently processed than the inner, relatively inaccessible ones. Yet, *in vivo* studies have claimed that *mir-19b* and *mir-92a* are often the most efficiently processed miRNAs in the cluster (Manni et al., 2009). This group, however, used Northern blot analyses to compare relative levels of miRNA species within the cluster, which can be inaccurate as radio-labeled detection probes bind miRNA sequences with different efficiencies. The same technical problem occurs in their quantitative PCR analyses as each miRNA sequence is bound by primer sets and amplified at different rates. While technical difficulties may diminish the significance of their results, such studies suggest that *mir-19b* and *mir-92* may not be expressed a significantly decreased level compared to the other *mir-17-92* miRNAs. If this is true, there are likely other mechanisms that either promote the stability or the processing of *mir-19b* and *mir-92a in vivo*. For example, hnRNP A1 facilitates the processing of *mir-18* by Drosha, and it is likely that there are other cofactors that promote the processing of *mir-17-92* under different contexts (Guil and Caceres, 2007).

Many potentially oncogenic genes are required for proper development of the organism, and *mir-17-92* is a prime example. Unlike most single locus miRNA knockout mice, which lack a strong phenotype, *mir-17-92-/-* mice exhibit completely penetrant perinatal lethality, dying by day 1 after birth likely due to severe lung hypoplasia and cardiac defects (Ventura et al., 2008). It is likely that many of these *mir-17-92-/-* defects are due to hypoplasia of tissues from decreased cellular proliferation. Transgenic mice overexpressing *mir-17-92* in the lung exhibit lung hyperplasia, further supporting the role of *mir-17-92* in lung development and proliferation (Lu et al., 2007). It is also thought that *mir-17* aids development by regulating lung branching through signal transducer and activator of transcription 3 (Stat3) and Mapk14 (Carraro et al., 2009). The *mir-17-92-/-* mice also exhibit a block at the pro-B to pre-B transitional stage of B-cell development though this defect in B-cell differentiation seems to be due to an increase in apoptosis instead of a decrease in proliferation (Ventura et al., 2008). This developmental block is mirrored by the lymphoproliferative disease and autoimmunity that develops from mice overexpressing *mir-17-92* (Xiao et al., 2008). While this lymphoproliferative disease likely arises from both an inhibition of apoptosis and an increase in proliferation, the expansion of the B and

T cell compartments in the lympho-specific *mir-17-92* overexpressing mice does not transition into full-blown neoplasia (Xiao et al., 2008). Thus, under these circumstances, other lesions are required for complete cellular transformation, such as amplified Myc expression.

While much has been revealed about the regulation of *mir-17-92* in both oncogenesis and development, there is still much to learn about this important miRNA cluster. The degree to which, and under what contexts the two paralogs functionally overlap is not yet known. Additionally, each of the miRNAs within the cluster likely plays overlapping and distinct roles in between cell types. By further dissecting the individual effects of the *mir-17-92* miRNAs in different cell types we will better understand the importance of this cluster in both development and disease, and potentially be able to use our knowledge for improved therapeutic measures.

microRNAs as Tumor Suppressors

As miRNAs are globally repressed in tumors compared to normal cells (Kumar et al., 2007), it is natural to suspect that many miRNAs may have tumor suppressive potential. In this section, I will briefly highlight some of the most well characterized tumor suppressive miRNAs. However, I will discuss the numerous p53 regulated tumor suppressive miRNAs - *mir-34, mir-107, mir-192,* and *mir-200* - in the next section on *p53 transcriptionally regulated miRNAs*.

The *let-7* family

let-7 is frequently lost in cancer, which is not surprising considering that loss of *let-7* in *C. elegans* gives rise to extra cell divisions in the vulva (Reinhart et al., 2000). First, it was found that *let-7* exhibits reduced expression in lung cancer cells (Takamizawa et al., 2004) and that *let-7* targets and represses oncogenic RAS and High-mobility group AT-hook 2 (HMGA2), which both have the potential to aid in the transformation of lung and breast tissue (Johnson et al., 2005; Yu et al., 2007). The overexpression of HMGA2 coding sequence without *let-7* target sites was found to be sufficient to promote tumorigenesis, however, cancers overexpressing an HMGA2 without *let-7* sites are rarely observed (Lee and Dutta, 2007; Zaidi et al., 2006). Recently, the Pandolfi group has illustrated how *Hmga2* can act as a sponge for *let-7* in lung cancer, preventing *let-7* from targeting its other targets such as transforming growth factor beta receptor 3 (Tgfbr3) (Kumar et al., 2014). This mechanism of a target mRNA acting as a sponge, or competing endogenous (ceRNA), for its miRNAs may yet be one of the major ways to suppress miRNA function.

The *mir-15/mir-16* cluster

mir-15 and *mir-16* were among the first miRNAs found to be involved in human tumorigenesis. The 13q14.3 locus containing the bicistronic *mir-15* and *mir-16* often undergoes hemizygous or homozygous deletion in chronic lymphocytic leukemia (CLL) (Calin et al., 2002). This fragile locus was the first of many found to contain miRNAs and to be dysregulated in cancer (Calin et al., 2004). *mir-15* and *mir-16* are downregulated in many other types of cancer including prostate cancer (Bonci et al., 2008), and adenomas (Bottoni et al., 2005). Loss of *mir-15* and *mir-16* likely enhances tumorigenesis partially through the upregulation of their targets: anti-apoptotic B-cell lymphoma 2 (BCL-2) (Cimmino et al., 2005), pro-proliferative cyclin D1 (CCND1), and wingless-type MMTV integration site family, member 3A (WNT3A) (Bonci et al., 2008 (Bonci et al., 2008). The clearest analysis of *mir-15* and *mir-16* function in tumorigenesis comes from the deletion of *mir*-15/*mir-16* alone or *mir*-15/*mir-16* and their parent *DLEU2* gene that is also lost by translocation in CLL. This analysis showed that loss of *mir-15/mir-16* can give rise to

monoclonal B-cell lymphocytosis, but that malignant CLL only arises in the mice that lack *DLEU2/mir-15/mir-16* altogether (Klein et al., 2010). This study suggests that *mir-15* and *mir-16* are greatly involved in regulating B-cell proliferation, but that additional mutations are required for transformation.

mir-29 family

mir-29 has been postulated to have a potential tumor suprressor role however, the recent generation of the *mir-29a/b-1* knockout mice should further the analysis of its tumor suppressive capabilities (Smith et al., 2012). The *mir*-29 miRNA family consists of four miRNAs encoded in two bicistronic clusters: *mir-29a* and *mir-29b-1* on human chromosome 7, and *mir-29b-2* and *mir-29c* encoded on human chromosome 1. Overexpression of *mir-29b* has been found to target T-cell leukemia 1 (Tcl-1) in leukemogenesis (Pekarsky et al., 2006), myeloid leukemia cell 1 (MCL-1) in cholangiocarcinoma cell lines (Mott et al., 2007) and vascular endothelial growth factor A (VEGF-A) in breast cancer inhibiting metastasis (Chou et al., 2013). *mir-29a* was found to target v-myb avian myeloblastosis viral oncogene homolog-like 2 (B-myb) inducing senescence in breast cancer cells (Martinez et al., 2011), and enforced expression of *mir-29a* induced differentiation of acute myeloid leukemia blasts (Wang et al., 2012). Collectively, the *mir-29* family was shown to revert aberrant methylation in lung cancer by targeting DNA methyltransferases DMNT3a and DMNT3b (Fabbri et al., 2007). While its role as a classic tumor suppressor has yet to be determined using the knockout mice, overexpression of *mir-29* clearly exhibits tumor suppressive capabilities.

mir-146 family

mir-146a and *mir-146b* are two highly conserved miRNAs located on human chromosomes 5 and 10 respectively. This miRNA family was first identified in a screen for miRNAs upregulated by NF-κB innate immune signaling in response to lipopolysaccharides (LPS) (Taganov et al., 2006**).** Analysis of the *mir-146*a and *mir-146b* knockout mice led to the convincing theory that *mir-146* is upregulated by NF-κB in order to dampen NF-κB signaling by targeting downstream signal transducers: TNF Receptor-Associated Factor 6 (Traf6) and Interleukin-1 receptor-associated kinase 1 (Irak1) (Boldin et al., 2011). This inhibition of Traf6 in mice overexpressing *mir-146a* and *mir-146b* has been recently shown to block transformation of Pten deficient T-cells (Burger et al., 2014). As increased NF-κB signaling is a driver of myeloproliferative disorders it is not surprising that *mir-146*a expression is found to be disrupted in myeloproliferative disease patients, such as the 5q- syndrome subset of patients (Starczynowski et al., 2010). The *mir-146a* knockout mice frequently exhibit splenomegaly, mostly from myeloid proliferation, with 20% of the mice developing neoplastic lesions by 12 months (Boldin et al., 2011). *mir-146a* has been more recently found to be dysregulated in other cancer types, including NK/T lymphoma that exhibit *mir-146a* promoter methylation (Paik et al., 2011), as well as thyroid carcinoma, breast, and ovarian cancers where single nucleotide polymorphisms in *mir-146* have been identified (Jazdzewski et al., 2008; Shen et al., 2008).

More and more studies have identified miRNAs to be implicated in complex signaling loops involving other miRNAs. For example, *mir-146* has been shown to be linked in the regulation of *mir-155* through NF-κB signaling. Interestingly, many of the same inflammatory signals upregulate *mir-155* and *mir-146,* but while *mir-146* acts to negatively regulate NF-κB, *mir-155* positively regulates NF-κB suggesting that these two miRNAs may counterbalance each other (Wang et al., 2010). The balancing effects of *mir-146a* and *mir-155* are supported by the

fact that *mir-146a* knockout mice exhibit myeloproliferative disorders and B-cell lymphoma (O'Connell et al., 2008) that resemble the disorders seen in transgenic mice overexpressing *mir-155* (Sandhu et al., 2012; So et al., 2013).

Tumor Suppressive microRNA	Cancer/Disease Association	Gene Target	Reference
let-7	Lung cancer	RAS; HMGA2; Tgfbr3	Takamizawa et al, 2004; Johnson et al 2005; Yu et al, 2007; Kumar et al, 2014
mir-15/mir-16	Chronic lymphocytic leukemia	BCL-2; CCND1; WNT3A	Calin et al, 2004; Cimmino et al, 2005; Bonci et al, 2008
*mir-17**	Breast cancer	AIB1	Hossain et al, 2006
mir-29a/b	Leukemogenesis; cholangiocarcinoma; lung and breast cancer; Hutchinson-Gilford progeria syndrome	Tcl-1; MCL-1; VEGF-A; B-myb; DMNT3a/b; Cdc42; p85alpha; Ppm1d	Pekarsky et al, 2006; Mott et al, 2007; Fabbri et al, 2007; Park et al, 2009; Ugalde et al, 2011; Martinez et al, 2011; Chou et al, 2013
mir-34/449 family	Colon, prostate, lung, non-small lung, pancreatic cancer; neuroblastoma; cardiovascular disease; oxidative liver	SIRT1; HMDX ; HDAC1; CD44; c-MET; SNAIL; CD44; CD133; BMI; C-MYC; ZEB1; Wnt1/3; Lef1; Notch1; c-Kit; Axl; HK1/2; LDHa; E2F3; N-MYC; PNUTS; Sp1; Nrf2; Sirt1; and Mgst1; CDK4; CDK6; c-MET; Cyclin E; BCL-2	Welch et al, 2007; Wei et al, 2008; Yamakuchi et al, 2008; Fujita et al, 2008; Nalls et al, 2011; Mandke et al, 2012; Okada et al, 2014; Noonan et al, 2009; Zhao et al, 2013; Liu et al, 2011; Mudduluru et al, 2011; Li et al 2011; Cheng et al, 2014; Siemens et al, 2011; Kim et al, 2011; Bu et al, 2013; Siemens et al, 2013; Boon et al 2013; Chang et al, 2007; He et al, 2007; Raver-Shapira et al, 2007; Tarasov et al, 2007
*mir-92**	B-cell lymphoma	Fbw7	Olive et al, 2013
mir-107	Glioma, colon cancer, chronic lymphocytic leukemia, and bladder urothelial carcinoma	HIF-1; CDK6, Rbl2/p130	Yamakuchi 2010; Bohlig et al, 2011; Chen et al, 2013; Pallasch et al 2009; de la Pena et al, 2011).
mir-146a/b	T-cell lymphoma; 5q- myeloproliferative syndrome; NK/T lymphoma; thyroid carcinoma, breast, and ovarian cancers	Traf6; Irak1	Paik et al, 201; Jazdzewski et al 2008; Shen et al, 2008; Starczynowski et al, 2010; Boldin et al, 2011; Burger et al, 2014
mir-192/mir-215	Multiple myeloma; Colon cancer; hepatocellular carcinoma	ZEB1/2; MDM2; Bcl-2; Vegf-a	Pichiorri et al, 2010; Geng et al, 2013; Kim et al, 2011
mir-200	Breast cancer	BMI-1; ZEB1/2	Shimono et al, 2009; Gibbons et al, 2009; Kim et al 2011; Chang et al, 2011

* These miRNAs are not classically thought of as tumor suppressive miRNAs but in these contexts they repress tumorigenesis

Table 2. Tumor Suppressive microRNAs
This table provides an overview of microRNAs and their targets with references that support their tumor suppressive function.

microRNAs and p53
Oftentimes called the "guardian of the genome," p53 is a transcription factor that drives transcription of anti-proliferative and pro-apoptotic proteins, and thereby has tumor suppressive

capabilities (Levine and Oren, 2009). In the past several years, p53 has been found to positively and negatively regulate a number of miRNAs that could be involved in many of p53's tumor suppressive functions. As the p53 pathway is disabled in 30% of all cancers, and as more and more miRNAs are found to be positively upregulated in response to p53 activation, the global downregulation of miRNAs in cancer could be at least partially attributed to the deletion of p53 in tumorigenesis. This section will cover several ways in which crosstalk between p53 pathways and miRNAs occur.

p53 transcriptionally regulated miRNAs

An increasing number of miRNAs have been found to be expressed upon p53 activation, with p53 directly inducing their transcription. As far as we know, the miRNA downstream targets of p53 exert tumor suppressive properties similar to the p53-regulated protein coding genes. Below is a summary of the miRNAs that are transcriptionally regulated by p53.

mir-107

mir-107 is a mirtron that resides in the p53-inducible gene *PANK1,* which encodes for pantothenate kinase 1 (Yamakuchi et al., 2010; Bohlig et al., 2011). Upon p53 activation, *mir-107* targets hypoxia inducible factor 1 (HIF-1) to prevent angiogenesis, and targets cyclin-dependent kinase 6 (CDK6) to repress cell cycle progression (Yamakuchi 2010; Bohlig et al., 2011). *mir-107* has been found to be in a number of cancer cell types that lack p53, including glioma, chronic lymphocytic leukemia, and bladder urothelial carcinoma (Chen et al., 2013; Pallasch et al., 2009; de la Pena et al., 2011). Upon reexpresion of *mir-107,* the cells undergo proliferative arrest, which further supports in how miRNAs contribute to p53's tumor suppressive abilities (Yamakuchi 2010; Chen et al., 2013)

mir-192 family

mir-192 and *mir-215* are homologous miRNAs located at human chromosome 11 and 1, respectively. They were originally found to be upregulated in two different cancer cell lines upon doxorubicin-induced p53 activation (Braun et al., 2008; Georges et al., 2008). The *mir-192* family was subsequently found to be silenced in multiple myeloma (Pichiorri et al., 2010), as well as in breast cancer stem cells (Kim et al., 2011). Similar to *mir-200,* reexpression of *mir-192* represses zinc finger E-box-binding homeobox 1 and 2 (ZEB1/2), and inhibits the epithelial-mesenchymal transition (EMT) (Kim et al., 2011). *mir-192* inhibits metastasis by additionally targeting Bcl-2, and Vegf-a (Geng et al., 2013). *mir*-192 has also been shown to form a positive feedback loop with p53 by targeting and downregulating mouse double minute 2 (MDM2), the E3 ubiquitin-protein ligase responsible for tagging p53 for degradation by the proteasome (Pichiorri et al., 2010).

mir-200 family

The *mir-200* miRNA family was first found downregulated in cancer in a screen for differential miRNA expression in breast cancer stem cells (Shimono et al., 2009). The *mir-200* miRNA family consists of five family members, *miR-200a*, *miR-200b*, *miR-200c*, *miR-429*, and *miR-141*, all five of which were identified by Shimono *et al* to be downregulated in breast cancer stem cells. The *mir-200* family was found to downregulate the polycomb complex protein BMI-1, thereby repressing proliferation, breast cancer stem cell clonogenicity, and mammary epithelial branching (Shimono et al., 2009). Soon there after, the *mir-200* family was found to be regulated

transcriptionally by p53 (Chang et al., 2011). p53-induced upregulation of *mir-200* targets BMI-1 and ZEB1 to suppress EMT (Gibbons et al., 2009; Kim et al., 2011; Chang et al., 2011). The regulation of ZEB1 by *mir-200* has also been identified to form a double-negative feedback loop as ZEB1 represses *mir-200* transcription (Bracken et al., 2008).

In addition to those mentioned above, there are even more p53 transcriptionally regulated miRNAs. *mir-15* and *mir-16* and their mother gene DLEU2 are transcriptionally regulated by p53 target (Shi et al., 2014). Another putative tumor suppressive miRNA, *mir-29*, has been shown by a few groups to be transcriptionally regulated by p53 as well, and to form yet another positive feedback loop with p53 by targeting p53's negative regulators: cell division control protein 42 (Cdc42), p85alpha, and protein phosphatase 1 D (Ppm1d) (Park et al., 2009; Ugalde et al., 2011).

P53's direct regulation of microRNA processing

The link between p53 (as well as p14/ARF, alternative reading frame) and miRNA processing was first observed when p53 was activated upon the deletion of Dicer (Mudhasani et al., 2008). Deletion of ARF or p53 was also found to rescue senescence induced upon the deletion of Dicer (Mudhasani et al., 2008). Subsequently, it was found that p53 can directly interact with Drosha in the microprocessor complex to enhance processing of the two tumor-suppressive, bicistronic clusters *mir-16/mir-15* and *mir-143/mir-145* to precursor miRNAs (Suzuki, et al., 2009; Kawai and Amano, 2012).

Positive Regulation of p53 by microRNAs

There are many miRNAs that have been found to target negative regulators of p53, thereby upregulating p53 activity. Many of these miRNAs form a positive feedback loop on p53 as they themselves are regulated by p53. The *mir-34/449* miRNA family is the most characterized example of these positive feedback loops, and upregulates p53 by targeting sirtuin 1 (SIRT1) (Yamakuchi et al., 2008), and Mdm4 (Okada et al., 2014). This family will be discussed in the next section, *P53 induced tumor suppressive miRNAS: A focus on mir-34*.

Another positive feedback loop is formed by the p53-inducible *mir-192* and *mir-215* family that upregulates p53 via the downregulation of Mdm2 (Georges et al., 2008; Pichiorri et al., 2010). This is a similar feedback loop to the one created by *mir-605* also targeting Mdm2 (Xiao et al., 2011).

mir-122 has also been found to upregulate p53 via a more indirect mechanism. *mir-122* directly downregulates cyclin G1, and thereby inhibits the recruitment of PP2A phosphatase to Mdm2. Increased phosphorylation of Mdm2 prevents ubiquitination of p53 and increases p53 activity. In this way, ectopically expressed *mir-122* increases sensitivity hepatocellular carcinoma cell to doxorubicin (Fornari et al., 2009), and induces apoptosis in cutaneous T-cell lymphoma (Manfe et al., 2012). *mir-122* was also found to increase the stabilization and increase the translation of *p53* transcripts by downregulating the cytoplasmic polyadenylation element binding protein (CPEB) (Burns et al., 2011).

Negative Regulation of p53 by microRNAs

Several miRNAs act in an oncogenic manner by negatively regulating the p53 pathway; they either directly repress p53 transcripts, downregulate p53's transcriptional targets, or indirectly activate negative regulators of p53. *mir-25* and *mir-30d* are upregulated in multiple myeloma,

and repress p53 in these cells by binding to sites in p53's 3'UTR (Li et al., 2010; Kumar et al., 2011). *mir-380-5p* downregulates p53 by targeting the p53 3'UTR directly, and this downregulation is associated with poor prognosis for N-Myc amplified neuroblastoma patients (Swarbrick et al., 2009).

mir-504 is another miRNA that downregulates p53 expression through two binding sites in the p53 3'UTR therefore enhancing tumorigenesis of HCT116 cells in xenografts (Hu et al., 2010). Enhanced expression of *mir-504* by repression of connective tissue growth factor (CTGF) signaling also increases invasion and metastasis of oral squamous cell carcinoma (Yang et al., 2012). The authors ascribe the increase in metastasis to the downregulation of Forkhead box protein P1 (FOXP1), but *mir-504's* downregulation of p53 could also increase metastasis (Yang et al., 2012).

mir-125b was one of the first miRNAs found to directly target the p53 3'UTR and downregulate its expression (Le et al., 2009). Le *et al* found that overexpression of *mir-125b* could repress apoptosis in neuroblastoma cells and lung cancer cells, but most interestingly, they found that gamma-irradiation actually repressed *mir-125b* expression and upregulated p53. Unlike the previously listed miRNAs that so far have been found to only repress p53 by directly downregulating its transcripts, *mir-125b* has also been found to inhibit downstream components of the p53 pathway such as p53 upregulated modulator of apoptosis (Puma) (Shi et al., 2011) and p14/Arf (Sumaira et al., 2013) as well as p53. *mir-125b*'s multi-faceted effects in repressing p53 signaling likely contribute to its highly oncogenic nature.

P53 induced tumor suppressive miRNAS: A focus on *mir-34*

In 2007, several groups simultaneously found that activation of the tumor suppressor p53 drives transcription of the *mir-34* miRNA family (Chang et al., 2007; He et al., 2007; Raver-Shapira et al., 2007; Tarasov et al., 2007). The *mir-34* miRNA family consists of three miRNAs that reside at two loci in the genome: *mir-34a* is on human chromosome 1 and *mir-34b/mir-34c* are transcribed as a bicistron from human chromosome 11 (He et al., 2007; Chapter 3, Fig1). p53 activates transcription of both *mir-34* primary transcripts through direct p53 binding elements in their promoters (He et al., 2007).

While *mir-34* is transcriptionally regulated by p53, it should be noted that there is another cluster, the *mir-449* cluster, which is a part of this miRNA family. The *mir-449* polycistronic cluster is transcribed from chromosome 13 and consists of *mir-449a, mir-449b,* and *mir-449c,* all three of which have identical seed sequences to the *mir-34* miRNA family (Yang et al., 2009). Interestingly, the *mir-449* miRNA family is not transcriptionally regulated by p53, but instead is driven by E2F (Yang et al., 2009). Therefore, depending on the cellular circumstances, the *mir-449* family may repress the same targets as *mir-34*.

Overexpression of the *mir-34* family *in vitro* has profound tumor suppressive properties akin to those of p53 – the ability to induce apoptosis (Raver-Shapira et al., 2007), cell cycle arrest and senescence (He et al., 2007), and to inhibit metastasis (Mudduluru et al., 2011). A number of *mir-34* targets have been identified to explain each of its different tumor suppressive capabilities, but a unifying explanation is that enforced expression of *mir-34* itself increases the activity of p53 (Yamakuchi et al., 2008; Okada et al., 2014). The primary mechanism underlying *mir-34's* ability to activate p53 appears to be through *mir-34's* downregulation of SIRT1 (Yamakuchi et al., 2008; Fujita et al., 2008; Nalls et al., 2011). Additionally, *mir-34* has been shown to activate p53 through the downregulation of HMDX (Mandke et al., 2012; Okada et al.,

2014) and HDAC1 (Noonan et al., 2009; Zhao et al., 2013), suggesting that regulation of p53 could play a major role in *mir-34's* tumor suppressive functions.

However, *mir-34* can exert tumor suppressive functions in the absence of p53 since deletion of *mir-34* accelerates tumorigenesis of p53 null prostate cells (Cheng et al., 2014). In the absence of p53, *mir-34* could exert tumor suppressive properties via its direct downregulation of targets such as CDK4, CDK6, c-MET proto-oncogene, Cyclin E, and BCL-2, as well as many more (Chang et al., 2007; He et al., 2007; Raver-Shapira et al., 2007; Tarasov et al., 2007). Many of these targets are responsible for inducing apoptosis upon the enforced expression of *mir-34* (BCL-2) and cell cycle arrest (ex: CDK6) even in the absence of p53 (Hermeking, 2010; Ji et al., 2012). Additionally, *mir-34* has been found to inhibit tumorigenesis by suppressing invasion and migration (targeting SNAIL, C-MET, ZEB1/2 and Axl - Siemens et al., 2011; Mudduluru et al., 2011), metabolism (HK1/2, LDHa -Kim et al., 2013), and differentiation (CD44, CD133, BMI, Sox2, N-Myc, and Nanog, Wnt1, and Lef1) (Wei et al., 2008; Choi et al., 2010; Liu et al., 2011; Kim et al., 2011; Siemens et al., 2011).

With all its tumor suppressive capabilities, it is not surprising that the entire *mir-34*/*mir-449* miRNA family has been found to be dysregulated in many human cancers. The *mir-34a* locus 1p36 is deleted in neuroblastomas (Welch et al., 2007). The *mir-34b/c* locus is methylated in colorectal, pancreatic, and breast cancers (Lodygin et al., 2008; Vogt et al., 2011), and this methylation of *mir-34b/c* is also correlated with increased metastasis (Lujambio et al., 2008).

In addition to cancer, the *mir-34* family has been shown to play an important role in the process of aging. *mir-34a* is upregulated in aged cardiomyocytes, inducing DNA damage and telomere attrition by targeting protein phosphatase 1, regulatory subunit 10 (PPP1R10/PNUTS) (Boon et al., 2013). Consequently, the upregulation of *mir-34a* leads to physiological changes in the aged heart, such as increased fibrosis and hypertrophy, and inhibition of *mir-34a* reduced age-induced and infarction-induced cardiomyocyte cell death (Boon et al., 2013). In contrast to this study, Drosophila *mir-34* was shown to aid in prolonging life by downregulating the neurodegenerative inducing *Ecdysone-induced protein 74EF* (*Eip74EF*) in the brain (Liu et al., 2012). These two studies imply that *mir-34* can accelerate or inhibit the aging process depending on the tissue type. Lastly, *mir-34* has been found to increase oxidative stress in the liver of aged mice by targeting specificity protein 1 (Sp1), nuclear factor-like 2 (Nrf2), Sirt1, and microsomal glutathione S-transferase 1 (Mgst1) (Li et al., 2011), though no consequences of this oxidative stress were described.

Finally, *mir-34* has been shown to play a role in the development of specific tissues. In bone development for example, *mir-34b/c,* though not *mir-34a,* is required to repress proliferation and osteoblast differentiation (Wei et al., 2012). Mice conditionally deleted for *mir-34b/c* exhibit an increase in osteoblast numbers (Wei et al., 2012). More relevantly, *mir-34/449* deficient mice have most recently been shown to exhibit defects in ciliation, causing the mice to be infertile and exhibit phenotypes similar to primary cilia dyskinesia (Song et al., 2014). The role of *mir-34* in ciliogenesis is also conserved in *Xenopus laevis* (Marcet et al., 2011; Song et al., 2014).

Great progress has been made in determining how the *mir-34/449* miRNA family affects the process of cancer and development. However, future studies are needed to tease out the extent to which these miRNAs exhibit intrafamilial redundancy and in what cell types. The mechanisms regulating expression, interaction, and function of these miRNAs will help us to better understand how the precise balance of the *mir-34/449* miRNAs contribute to disease.

The *Eμ-myc* mouse model

In 1981, the *Eμ-myc* mice were the first, deliberately generated so-called "oncomice;" mice expressing an oncogenic transgene (Hanahan et al., 2007). The *Eμ-myc* mice carry a transgene, cloned from a plasmocytoma ABPC17, where the immunoglobulin heavy chain enhancer lies upstream from the first exon of *c-Myc* (Adams et al., 1985). These mice display hyperproliferation and an expansion of B-cells in the hematopoietic compartment, which eventually develops into pre-B and immature B-cell lymphomas with a latency of about 6 months and with 50% penetrance (Adams et al., 1985; Harris et al., 1988; Langdon et al., 1986). Both the translocation of *c-Myc* under the IgH enhancer, and the lymphoma phenotype mimic the pathology of human Burkitt's lympohoma patients. Therefore, the *Eμ-myc* mice have since been extensively used to tease out both tumorigenic and oncogenic lesions that affect human cancer development.

The *Eμ-myc* mouse model of B-lymphoma has been used to extensively characterize the tumor suppressive functions of the most commonly mutated tumor suppressor, p53. p53 provides a major check on Myc-induced proliferation as increased activation of c-myc induces an apoptotic response that is largely p53-dependent (Zindy et al., 1998). Myc activates p53 signalling by indirectly inducing the expression of p19/ARF, which stabilizes p53 through its binding and sequestering of Mdm2 (Levine and Oren, 2009). For milder stresses, it is thought that p53 tends to inhibit the cell cycle by binding to high affinity sites in the promoter of genes that regulate the cell cycle, such as *p21* (Vousden and Lu, 2002). In the case of Myc-induced p53 stabilization, p53 also binds to lower affinity sites in apoptosis-inducing downstream targets such as Noxa, a pro-apoptotic Bcl-2 homology 3 (BH3)-only member of the Bcl-2 family (Chen et al., 1996; Weber and Zambetti, 2003). Therefore the *Eμ-myc* cells have a strong selective pressure to block this apoptotic response in order to give rise to tumors. In fact it has been shown that the majority of mutations inhibiting apoptosis in *Eμ-myc* tumors occur in the p53 pathway (Eischen et al., 1999). Additionally, 75% of *Eμ-myc* tumors lose the functionality of the p53 pathway by loss of function mutations in p53, Arf or by overexpression of Mdm2 (Eischen et al., 1999). Not surprisingly, deletion of p53 or Arf (Eischen et al., 1999; Schmitt et al., 1999/2002), or overexpression of Mdm2 (Wang et al., 2008) markedly accelerates *Eμ-myc* lymphomagenesis. *Eμ-myc*$^{+}$;p53+/- animals exhibit greatly accelerated *Eμ-myc* lymphomagenesis, and 100% of the tumor cells arising in these mice lose the second copy of p53 by loss of heterozygosity (Schmitt et al., 1999; Eischen et al., 1999).

The pressure that *Eμ-myc* transgene places on the cells to lose the p53 pathway has been immensely helpful in determining in how the downstream targets of the p53 pathway provide a barrier to *Eμ-myc* transformation. There are four major ways to accelerate *Eμ-myc* lymphomagenesis: mutations in genes that induce apoptosis, induce senescence, inhibit proliferation, or inhibit dissemination. Below I will briefly discuss the genes that have been found to affect these pathways in the *Eμ-myc* mice.

Apoptosis is the predominant barrier to tumorigenesis in the *Eμ-myc* mouse model. The importance of blocking apoptosis for *Eμ-myc* transformation was first seen by crossing *Eμ-myc* mice to *Eμ-Bcl-2* mice to overexpress Bcl-2, the anti-apoptotic BH3-only protein that blocks mitochondria permeabilization (Strasser et al., 1990). This cross gave rise to tumors so quickly that they were thought to be early lymphoid progenitors. Bcl-2 is further entwined in Myc-induced apoptosis as Myc transcriptionally represses and downregulates Bcl-2 (Eischen et al., 2001; Patel and McMahon, 2007). Deletion of a pro-apoptotic BH3-only protein, Bim, also greatly accelerates *Eμ-myc* lymphomagenesis (average survival *Eμ-myc*$^{+}$*;Bim-/-* 8wks, vs. *Eμ-*

myc^{+}*;Bim*+/+ 15wks). Similar to overexpression of Bcl-2, deletion of Bim removes the selective pressure for the *Eμ-myc* cells to disable p53 (Egle et al., 2004). Also, similar to its p53 independent repression of Bcl-2, Myc can directly upregulate the pro-apoptotic Bim thereby inhibiting Bcl-2's anti-apoptotic activity (Hemann et al., 2005). These mutations in Myc that inhibit its interaction with the transcription of Bim are found clinically and accelerate *Eμ-myc* lymphomagenesis (Hemann et al., 2005).

By deleting individual p53 downstream BH3-only apoptotic target genes we can see their individual contributions to blocking *Eμ-myc* tumorigenesis. Deletion of the BH3-only pro-apoptotic Puma aceelerates lymphomagenesis (*Eμ-myc*$^{+}$*;Puma-/-* 66 days vs *Eμ-myc*$^{+}$*;Puma*+/+ 100 days), but does not remove the pressure to lose p53 (Garrison et al., 2008; Michalak et al., 2009). Fascinatingly, deleting Noxa, another p53 induced, BH3-only pro-apoptotic protein, does not even accelerate *Eμ-myc* lymphomagenesis, but increases malignancy upon simultaneous deletion of Puma (Michalak et al., 2009). Deletion of Bcl-2 associated X protein (Bax), yet another member of the BH3-only family of proteins, accelerates *Eμ-myc* lymphomagenesis, and removes the pressure to lose p53 as all *Eμ-myc*$^{+}$*;Bax-/-* tumors retain wild-type p53 (Eischen et al., 2001). The increased importance of Bax in preventing Myc driven tumorigenesis is made clear by the fact that Bax is directly induced by Myc/Max binding to the canonical E-box elements in its promoter, in addition to p53-inducing the expression of Bax (Mitchell et al., 2000). Moreover, Myc helps Bax oligomerize in the mitochondria and induce apoptosis (Cao et al., 2008). From these studies, the importance of apoptotic pathways to suppress Myc-driven tumorigenesis is clear; there is not one, but two separate pathways - p53-dependent and p53-independent - poised to terminate the cell upon overactivation of Myc.

While apoptosis has been identified as a main mechanism for preventing *Eμ-myc* driven transformation, the Lozano lab investigated the contributions of p53-induced cell cycle arrest and senescence on *Eμ-myc* lymphomagenesis. Using mice genetically engineered to express the *p53515C* allele of p53 that can activate cell cycle arrest targets such as p21, but cannot activate apoptotic p53 downstream target genes, Post *et al* observed a delay of lymphomagenesis as compared to the *Eμ-myc*$^{+}$*;p53*+/- mice (Post et al., 2010). While previously it was seen that the deletion of Rb in the *Eμ-myc* model had little effect on tumorigenesis (Schmitt et al., 1999), *Post et al,* showed that indeed other tumor suppressive signals, such as cell cycle arrest, could significantly inhibit *Eμ-myc* tumorigenesis (Post et al., 2010). The Greider lab showed that p53-induced senescence signaling activated by the presence of short telomeres could delay *Eμ-myc* lymphomagenesis even when apoptosis was blocked by overexpression of Bcl-2 (Feldser and Grieder, 2007). Fascinatingly, the strong delay in tumorigenesis caused by short telomeres was completely abolished upon deletion of p53.

While Feldser and Grieder analyzed senescence induced from an intrinsic cellular signal of short telemores, the Schmitt lab demonstrated that senescence induced from extrinsic macrophage production of TGFβ suppresses tumorigenesis (Reimann et al., 2010). They showed that *Eμ-myc*$^{+}$*;Suv39h1-/-,* lacking an H3K9 methyltranserfase responsible for inducing heterochromatization in S-phase promoting genes, could not undergo senescence and greatly accelerated *Eμ-myc* lymphomagenesis in a p53-dependent manner. They further discovered that macrophages were responsible for secreting TGFβ upon phagocytosing apoptotic lymphoma cells, and inducing senescence in the nearby lymphoma cells. Consequently, apoptosis inhibits *Eμ-myc* lymphomagenesis directly, by terminating the tumor cells, and indirectly, by enabling macrophages to secrete TGFβ and induce tumor cell senescence.

Lastly, the ability for lymphoma cells to disseminate and colonize specific organs can greatly contribute to the malignancy of *Eμ-myc* lymphoma. Rehm *et al*, showed that *Eμ-myc*$^{+}$*;CCR7-/-* exhibit a great delay *Eμ-myc* lymphomagenesis. Deletion of chemokine receptor 7 (CCR7) prevents B-lymphoma cell migration in response to chemokines such as CCL21 and CXCL12 (Rehm et al., 2011). As the *Eμ-myc*$^{+}$*;CCR7-/-* B-cells exhibited the same amount of apoptosis and proliferation as the controls, the delay in malignancy was due purely to an inability of the cell to migrate and colonize the secondary lymphoid organs.

Directions of Study

In this thesis, the work presented focuses on the oncogenic *mir-17-92* cluster, and the tumor suppressive, p53-regulated *mir-34* family and their effect on *Eμ-myc* lymphomagenesis. In Chapter 1, our work on *mir-17-92* focused on dissecting the cluster to determine which specific miRNA was responsible for the oncogenic effects of *mir-17*-92 in the *Eμ-myc* model. We found that *mir-19* is the miRNA that is mostly responsible for repressing apoptosis and accelerating lymphomagenesis in the *Eμ-myc*$^{+}$;*mir-17*-92 mice. In Chapter 2, inspired by previous observations that the *mir-17-92* cluster is more oncogenic upon the deletion of *mir-92,* we tease out how *mir-92* antagonizes the effects of *mir-19* by increasing the levels of Myc to induce apoptosis. Finally, in chapter 3, we switch focus to investigate the effects of the p53-regulated, tumor suppressive *mir-34* miRNA family. We comprehensively study the effects of the deletion of the *mir-34/449* family of miRNAs both individually and collectively on *Eμ-myc* lymphomagenesis, and illustrate the *mir-34/449* tumor suppressive capabilities.

Chapter 1

miR-19 is a key oncogenic component of *mir-17-92*

Virginie Olive*, Margaux J. Bennett*, James C. Walker, Cong Ma, Iris Jiang, Carlos Cordon-Cardo, Qi-Jing Li, Scott W. Lowe, Gregory J. Hannon and Lin He

Genes Dev. 2009 Dec 15;23(24):2839-49

This chapter is a reproduction of the paper by the same name published in Genes and Development December 2009. My contributions are as follows: I performed the histochemical staining and analyses in Figure 3D, 3E and 6D. I assisted in the generation Figure 4C. I conceived and initiated the collaboration shown in Figure 5, as well as minimally assisted in the execution. I assisted in designing the figures and editing the manuscript.

Summary
Recent studies have revealed the importance of multiple microRNAs (miRNAs) in promoting tumorigenesis, among which *mir-17-92* /*Oncomir-1* exhibits potent oncogenic activity. Genomic amplification and elevated expression of *mir-17-92* occur in several human B-cell lymphomas, and enforced *mir-17-92* expression in mice cooperates with c-myc to promote the formation of B-cell lymphomas. Unlike classic protein-coding oncogenes, *mir-17-92* has an unconventional gene structure, where one primary transcript yields six individual miRNAs. Here, we functionally dissected the individual components of *mir-17-92* by assaying their tumorigenic potential in vivo. Using the *Eμ-myc* model of mouse B-cell lymphoma, we identified *miR-19* as the key oncogenic component of *mir-17-92,* both necessary and sufficient for promoting c-myc-induced lymphomagenesis by repressing apoptosis. The oncogenic activity of *miR-19* is at least in part due to its repression of the tumor suppressor *Pten*. Consistently, *miR-19* activates the Akt–mTOR (mammalian target of rapamycin) pathway, thereby functionally antagonizing *Pten* to promote cell survival. Our findings reveal the essential role of *miR-19* in mediating the oncogenic activity of *mir-17-92*, and implicate the functional diversity of *mir-17-92* components as the molecular basis for its pleiotropic effects during tumorigenesis.

Introduction
MicroRNAs (miRNAs) encode small, regulatory RNAs that control gene expression predominantly through post-transcriptional repression (Ambros 2004; Zamore and Haley 2005; Bartel 2009). Nascent transcripts from miRNA genes (pri-miRNAs) contain one or multiple unique stem–loop structures. Mature miRNAs, ranging from 18 to 24 nucleotides (nt) in length, are initially embedded within one arm of the hairpin stems. These pri-miRNAs are processed sequentially by the ribonuclease III enzymes Drosha and Dicer to yield the mature miRNA duplexes (Kim et al., 2009). As the mature duplex is formed, the miRNA strand is then incorporated into the RNA-induced silencing complex (RISC) to mediate post-transcriptional regulation of specific mRNAs, primarily through mRNA degradation and/or translational repression (Filipowicz et al., 2008). The target recognition by miRNAs is achieved through imperfect complementarity. The seed region of the mature miRNA (nucleotides 2–8) is often complementary to sites within the target mRNAs, forming a "seed match" in an otherwise imperfect base-pairing (Bartel 2009). The small size of miRNAs, combined with imperfect target recognition, provide miRNAs with the enormous capacity and versatility to act as global gene regulators in diverse developmental and physiological processes. Recent bioinformatic predictions and several experimental validations also suggest that each miRNA is likely to regulate hundreds of mRNA targets and fine-tune their expression in a cell type-dependent and context-dependent manner (Baek et al., 2008; Selbach et al., 2008; Chi et al., 2009).

The connection between miRNAs and cancer was first implicated by their frequent genomic alteration and dysregulated ex *mir-17-92* pression in various human tumors (Calin et al., 2004; Lu et al., 2005; He et al., 2007b). Multiple miRNAs were subsequently identified to promote or

suppress oncogenesis, presumably by modulating gene expression in the oncogenic and tumor suppressor networks (He et al., 2005, 2007a; Johnson et al., 2005; Kumar et al., 2008; Kota et al., 2009). One of the first oncogenic miRNAs identified was *mir-17-92* (also known as oncomir-1), a miRNA polycistron with pleiotropic functions in cell survival, proliferation, differentiation, and angiogenesis (Hayashita et al., 2005; He et al., 2005; Lu et al., 2005; O'Donnell et al., 2005; Dews et al., 2006; Ventura et al., 2008). *mir-17-92* is the primary target of the genomic amplification 13q31 that occurs in Burkitt's lymphoma, diffuse large B-cell lymphoma (DLBCL), mantle cell lymphoma, follicular lymphoma, and several other solid tumor types (Ota et al., 2004; He et al., 2005; Tagawa and Seto 2005; Tagawa et al., 2007; Inomata et al., 2009; Navarro et al., 2009). Additionally, *mir-17-92* is highly expressed in a range of hematopoietic malignancies, particularly in B-cell lymphomas (Lu et al., 2005; Tagawa and Seto 2005; Navarro et al., 2009). Although transgenic mice with moderate *mir-17-92* overexpression only develop lymphoproliferative phenotypes (Xiao et al., 2008), enforced high-level expression of *mir-17-92* , in conjunction with c-myc, has potent transformation potential in mouse B-cells in vivo, largely due to its ability to repress apoptosis (He et al., 2005) This observation is consistent with the recurring *mir-17-92* amplifications in MYC-rearranged Burkitt's lymphomas and DLBCLs in humans (Tagawa et al., 2007). The survival effect of *mir-17-92* is also evident in the normal development of the B-cell compartment, as *mir-17-92* deficiency leads to premature cell death during pro-B-to-pre-B transition (Ventura et al., 2008).

Unlike classic protein-coding oncogenes, where one transcript generally gives rise to one protein product, the *mir-17-92* miRNA cluster produces a single polycistronic primary transcript that yields six individual mature miRNAs. The distinct mature miRNA sequence of these *mir-17-92* components dictates the specificity of their target regulation, and ultimately can determine the functional specificity. Here we report the functional dissection of *mir-17-92* in the context of B-cell transformation in vivo, and reveal the essential role of *miR-19* in mediating the oncogenic activity of *mir-17-92* . In the *Eμ-myc* model of Burkitt's lymphoma, *miR-19* is both necessary and sufficient for *mir-17-92* to promote c-myc-induced B lymphomagenesis. The oncogenic activity of *miR-19* is at least in part mediated by the PI3K (phosphatidylinositol 3-kinase)–Akt–mTOR (mammalian target of rapamycin) pathway, as enforced *miR-19* expression dampens the expression of the tumor suppressor *Pten*, thus activating the Akt–mTOR signaling to promote cell survival. Our findings demonstrate the functional diversity of *mir-17-92* components, and characterize the key molecular mechanism through which the *mir-17-92* polycistron promotes malignant transformation in the B-cell compartment.

Results

mir-17-92 encodes a miRNA polycistron that yields six individual components

The *mir-17-92* miRNA cluster produces a single polycistronic primary transcript that yields six mature miRNAs: *miR-17, miR-18a, miR-19a, miR-20a, mir-19b*, and miR-92a (Fig. 1A). This unique structural feature of *mir-17-92* , shared by a large number of miRNA genes in mammalian genomes, may constitute the molecular basis for its pleiotropic functions in a cell type-dependent and context-dependent manner. Based on sequence homology, the six *mir-17-92* components can be categorized into three miRNA families: *miR-17/20a/18a, miR-19a/19b*, and *miR-92a* (Fig. 1B). *miR-17* and *miR-20a* miRNAs are closely related homologs, differing by 2 nt outside the seed sequence (Fig. 1B). A related miRNA *miR-18a* has a similar yet not identical seed region, but shares significant sequence identity with *mir-17/20a* overall (Fig. 1B). The

second miRNA family contains *miR-19a* and *mir-19b*, which differ only by a single nucleotide at position 11, a region minimally important for target recognition (Fig. 1B; Lewis et al., 2003, 2005; Farh et al., 2005; Grimson et al., 2007). Finally, the unique seed region of *miR-92a* distinguishes it from all of the other *mir-17-92* components (Fig. 1B). All six *mir-17-92* miRNAs can repress many target mRNAs either cooperatively or individually; both mechanisms could lead to cell type-dependent and context-dependent functional readout.

***miR-19* exhibits potent oncogenic activity in the *Eμ-myc* model**

Previously, we chose the *Eμ-myc* model of Burkitt's lymphoma to evaluate the oncogenic activity of *mir-17-92* in vivo because genomic amplification and up-regulated expression of *mir-17-92* were both observed in human Burkitt's lymphomas (Tagawa et al., 2007). Recent studies also indicated the association between recurring *mir-17-92* genomic amplification and MYC rearrangement in Burkitt's lymphomas and DLBCLs, further implicating a functional cooperation between these two lesions (Tagawa et al., 2007). The *Eμ-myc* transgenic mice carry a c-myc oncogene driven by the immunoglobulin heavy-chain enhancer (Eμ), which is a powerful system in Burkitt's lymphoma. These mice exhibit c-myc overexpression specifically in the B-cell lineage, and ultimately acquire late-onset B-cell lymphomas with a latency of ~6 mo (Adams et al. 1985). To examine the oncogenic potentials of any candidate miRNA, the *Eμ-myc*/+ hematopoietic stem and progenitor cells (HSPCs) can be infected with murine stem cell viruses (MSCVs) overexpressing the miRNA, and then transplanted into lethally irradiated recipient animals (Supplemental Fig. S1B; Schmitt et al., 2000). The oncogenic potential can be evaluated by the acceleration of c-myc-induced lymphomagenesis in this adoptive transfer model (Supplemental Fig. S1B).

The first evidence that individual *mir-17-92* components may contribute differently to its oncogenic potential comes from our previous observation, in which *mir-17-19b*, a truncated *mir-17-92* cluster lacking miR-92a (Supplemental Fig. S1A), can greatly accelerate c-myc-induced tumorigenesis in the *Eμ-myc* model (He et al., 2005). The fact that miR-92a is dispensable for the oncogenic activity prompted us to further divide the *mir-17-19b* cluster to functionally dissect the oncogenic potentials of each individual miRNA component (Supplemental Fig. S1A). We initially divided the oncogenic *mir-17-19b* miRNA polycistron into three subclusters: *mir-17*, *miR-18a,* and *mir-19a/20a/19b* (Supplemental Fig. S1A). Overexpression of the control vector (MSCV) or *mir-17* in this adoptive transfer model had minimal oncogenic effects, causing late-onset B lymphomas with incomplete penetrance (Fig. 1C). In contrast, animals coexpressing *mir-19a/20a/19b* and c-myc developed highly malignant, early-onset B lymphomas, with a median survival at 84 d post-transplantation ($P < 0.0001$, log rank test) (Fig. 1C). Interestingly, miR-18a overexpression caused a moderate acceleration of lymphomagenesis in the *Eμ-myc* model (Fig. 1C). Although it is unlikely that miR-18a is the major oncogenic component of *mir-17-19b*, it may play accessory roles to facilitate *miR-19a/20a/19b* to promote malignant transformation in the *Eμ-myc* model. Retroviruses driving *mir-17-19b* and each of the subclusters had similar levels of overexpression, indicating that the observed difference in oncogenic effects reflected true functional differences among *mir-17-92* components, rather than differences in expression level (data not shown).

The three miRNAs encoded by *mir-19a/20a/19b* belong to two distinct families: *miR-19* (including *miR-19a* and *mir-19b*) and miR-20a. While *miR-20a* exhibited minimal oncogenic

collaboration with c-myc, *mir-19b* and c-myc resulted in highly malignant B lymphomas with nearly complete penetrance (median survival 87 d; $P < 0.0001$, log rank test) (Fig. 1D). Given the sequence homology between *miR-19a* and *mir-19b* and their 1-nt divergence at a region nonessential for miRNA target recognition, it is possible that *miR-19a* can also accelerate c-myc-induced lymphomagenesis. Similar to *mir-19a/20a/19b*, *mir-19b* phenocopied the oncogenic effects of *mir-17-19b*. Interestingly, mice overexpressing *mir-19b* exhibited a slightly longer life span after reconstitution (Fig. 3C, below) when compared with those overexpressing *mir-17-19b*, a difference likely due to functional cooperation among *mir-19b*, *miR-19a*, and possibly *miR-18a*.

Histopathological and immunophenotyping analyses confirmed the phenotypic similarities among the *Eμ-myc*/*mir-19b* (*Eμ-myc*/19b), *Eμ-myc*/*mir-19a/20a/19b* (*Eμ-myc*/*19a/20a/19b*), and *Eμ-myc*/*mir-17-19b* (*Eμ-myc*/*17-19b*) lymphomas. These mice developed advanced lymphomas, with massive enlargement of lymph nodes, splenic hyperplasia, and leukemia. In all cases, lymphoma cells invaded the thymus and bone marrow, as well as visceral organs outside the lymphoid compartment, including the liver, lung, and, occasionally, kidney (Fig. 2A; He et al., 2005). While control *Eμ-myc* lymphomas exhibited a high mitotic index accompanied by extensive cell death as shown by TUNEL staining (Fig. 2B; Supplemental Fig. S3), the *Eμ-myc*/*19a/20a/19b* and *Eμ-myc*/*19b* lymphomas, similar to *Eμ-myc*/*17-19b* lymphomas, had greatly reduced apoptosis without affecting cell proliferation (Fig. 2B; Supplemental Fig. S3). Although *mir-17-92* has been implicated to promote cell proliferation in other cellular contexts (Ventura et al., 2008), *mir-17-19b*, *mir-19a/20a/19b*, and *mir-19b* overexpression did not enhance cell proliferation in the *Eμ-myc* model. The lack of proliferative effects in the B-lymphoma cells is likely due to the high level of basal proliferation resulting from c-myc overexpression. Additionally, control *Eμ-myc* mice frequently develop more mature B-cell lymphomas, but the *Eμ-myc*/19b, *Eμ-myc*/*19a/20a/19b*, and *Eμ-myc*/*17-19b* tumors were derived primarily from progenitor B-cells (Fig. 2C; Supplemental Table S1; Supplemental Fig. S2), suggesting a functional preference for these miRNAs to transform B-cell progenitors under our experimental conditions. These observations were consistent with the B-cell phenotypes in the *mir-17-92* knockout mice, in which the pro-B-to-pre-B transition was marked by extensive apoptosis (Ventura et al., 2008).

miR-19 components are required for the oncogenic activity of _mir-17-92_

Among all of the *mir-17-92* components, *mir-19* is sufficient for accelerating c-myc-induced lymphomagenesis. To determine whether *miR-19* miRNAs are also necessary for the oncogenic effects of *mir-17-19b*, we introduced mutations into *miR-19a* and *miR-19b* within the *mir-17-19b* construct (designated as *mir-17-19b-Mut19*). In so doing, we disrupted the hairpin stem of both *miR-19a* and *miR-19b* to abolish the biogenesis of *miR-19* miRNAs while preventing generation of cryptic miRNAs. These mutations specifically disabled *miR-19* biogenesis, without affecting that of *miR-17, miR-18a*, and *miR-20a* within the same construct (Fig. 3A,B). Consistent with *miR-19* being the key oncogenic component, the *miR-19* mutations greatly compromised the oncogenic capacity of *mir-17-19b*, causing delayed tumor onset, incomplete penetrance, and extended life span (median survival 141 d; $P < 0.001$, log rank test) (Fig. 3C). In *Eμ-myc*/*mir-17-19b-Mut19* (*Eμ-myc*/*17-19b-Mut19*) animals that ultimately developed late-onset lymphomas, the *miR-19* mutations significantly compromised cell survival without affecting cell proliferation (Fig. 3D,E; Supplemental Fig. S3). In comparison, tumors derived from oncogenic collaboration

between c-myc and *mir-17-19b* or *miR-19b* alone exhibited greatly reduced apoptosis (Figs. 2B, 3D,E). The *miR-19* mutations not only disrupted cell survival, but also compromised the ability of *mir-17-19b* to preferentially transform progenitor B-cells. This was suggested by the immunophenotyping analyses on *Eμ-myc*/*17-19b-Mut19* B-cell tumors, which exhibited more cell type heterogeneity compared with *Eμ-myc*/*17-19b* tumors (Supplemental Table S1). Taken together, these findings establish *miR-19* miRNAs as the key oncogenic component within *mir-17-92*, promoting tumorigenesis seemingly through the repression of c-myc-induced apoptosis.

miR-19* specifically dampens the expression level of the tumor suppressor *Pten

miR-19 is the key oncogenic component of *mir-17-92* , and therefore *miR-19*-specific targets are likely to mediate the oncogenic effects of *mir-17-92* . Among hundreds of *miR-19* targets predicted by TargetScan and RNA22 (Lewis et al., 2005; Miranda et al., 2006; Grimson et al., 2007), the tumor suppressor *Pten* is a prominent candidate, due to its important functions in promoting apoptosis and tumor suppression. *Pten* is a negative regulator of the PI3K signaling. In response to a variety of extracellular signals, the PI3K pathway elicits diverse cellular responses to promote cell survival, rapid proliferation, and cell growth. *Pten* has been implicated as a target of *mir-17-92* by luciferase reporter assays and Western analyses in cell culture-based experiments (Takakura et al., 2008; Xiao et al., 2008). However, it is not clear how individual *mir-17-92* components contribute to the repression of *Pten* and, more importantly, whether the down-regulation of *Pten* by *mir-17-92* leads to any functional impact on cell survival. Overexpression of *miR-19b* and *mir-17-19b*—but not *miR-17*, *miR-18a*, *miR-20a*, or MSCV control—significantly down-regulated the endogenous level of *Pten* mRNA and protein in NIH-3T3 cells (Fig. 4C,D). Similarly, *Pten* down-regulation by *mir-19b* and *mir-17-19b* was observed in mouse primary B-cell culture (Supplemental Fig. S4B). The ability of *mir-17-19b* to down-regulate *Pten* in both cell types depended on the intact *miR-19* components within this cluster, since *mir-17-19b*/*Mut19* failed to dampen *Pten* expression in either 3T3 cells or primary B-cell culture (Fig. 4E,F; Supplemental Fig. S4A,B). These findings suggest that *miR-19* is the *mir-17-92* component that is both necessary and sufficient to mediate *Pten* repression. Interestingly, the level of *Pten* repression by *miR-19* was also dependent on cell types and physiological contexts, possibly due to differences in basal levels of *miR-19* and *Pten* expression (Hwang et al., 2009; data not shown).

The human *PTEN* 3′ untranslated region (UTR) contains two *miR-19*-binding sites (Fig. 4A; Miranda et al., 2006). A luciferase reporter, when fused with the wild-type human *PTEN* 3′UTR, was significantly repressed by overexpression of *miR-19b*, but not by *miR-17, miR-18a, miR-20a,* or *miR-1* control (Fig. 4B). Mutations of one or both *miR-19*-binding sites in the luc-*PTEN* 3′UTR construct either partially or completely derepressed the luciferase reporter when coexpressed with *miR-19b* (Fig. 4A,B). These findings suggest that direct binding between *miR-19* and *PTEN* 3′UTR is required for *PTEN* repression by *miR-19*.

***miR-19* functionally antagonizes *Pten* to promote cell survival**

miR-19 is evolutionarily conserved across many vertebrate species (Griffiths-Jones 2006). Between *Xenopus* and mammals, the sequences of *miR-19a* and *miR-19b* are identical, and two putative *miR-19*-binding sites are also present in the *Xenopus pten* mRNA. These observations implicate a selective pressure to preserve the *pten* regulation by *miR-19* during ~350 million years of evolution. To determine whether *Pten* down-regulation by *miR-19* had any functional

impact, we examined their functional interaction using an in vivo apoptosis assay in *Xenopus* embryos.

Not only is *miR-19* conserved at the sequence level in *Xenopus*, its anti-apoptotic function is also preserved, evident by its ability to repress hydroxyurea-induced cell death. When subjected to hydroxyurea treatment, *Xenopus* embryos undergo apoptosis, often characterized by a whitish color, cell blebbing, and disruption of cell adhesion after the mid-blastula transition (Walker and Harland 2009). Injection of *miR-19b* considerably rescued hydroxyurea-induced apoptosis (Fig. 5A,B). Consistent with *Pten* being a key target of *miR-19*, injection of *miR-19* and *Pten* individually gave rise to opposite phenotypes, with *miR-19* promoting cell survival (Fig. 5A,B) and *pten* inducing apoptosis (Fig. 5C,D). Coinjection of *miR-19b* and *pten*, however, significantly rescued *pten*-induced apoptosis, but a mutated *miR-19b* (*mut-19b*) with an altered seed sequence failed to impact the *Pten* function (Fig. 5C,D). When we introduced mutations in the two *miR-19*-binding sites in the *Pten* cDNA without affecting *Pten* protein coding, the mutated *Pten* mRNA (*Pten*-mut) retained the ability to potently induce cell death. In this case, *miR-19* injection failed to rescue the apoptotic effects of *pten-Mut* (Fig. 5E,F). Altogether, our findings indicate that the repression of *Pten* by *miR-19* occurs not only at the expression level, but also at the functional level, both of which are dependent on the intact *miR-19*-binding sites within the *Pten* mRNA.

miR-19 activates the Akt–mTOR pathway both in vitro and in vivo

PTEN is a tumor suppressor that is mutated or deleted in multiple tumor types with high frequency (Di Cristofano and Pandolfi 2000; Knobbe et al., 2008). It acts to repress the intracellular level of phosphatidylinositol-3,4,5-trisphosphate in cells, thus negatively regulating the PI3K pathway and its downstream effectors, Akt and mTOR (Comer and Parent 2002; Rossi and Weissman 2006). Consistent with the ability of *miR-19* to repress *Pten* expression and function, *miR-19b* overexpression in NIH-3T3 cells specifically activated the PI3K pathway, leading to increased phosphorylation of Akt without affecting the overall level of Akt (Fig. 6A). *miR-19b* or *mir-17-19b* overexpression also caused a significant increase in phosphorylation of S6 ribosomal protein due to the activated mTOR pathway (Supplemental Fig. S4D). Surprisingly, *miR-17* and *miR-20a* overexpression slightly increased the phospho-S6 level compared with the vector control, but this increase might be achieved through a mechanism independent of *Pten* or Akt (Fig. 6A,B). Using Western analyses and immunohistochemistry assays, a high level of phospho-S6 protein was observed in a cohort of *Eμ-myc*/*19b* and *Eμ-myc*/*17-19b* tumors, suggesting that *miR-19* and *mir-17-19b* were able to activate the mTOR pathway in vivo (Fig. 6C,D), at least in part through the repression on *Pten*. In comparison, the control *Eμ-myc* tumors generally exhibited a low level of phospho-S6 protein, although a certain degree of heterogeneity existed among different tumors. Although *mir-17-19b* and *miR-19b* were equally potent in inducing phospho-S6 in vitro (Supplemental Fig. S4D), the effect of *mir-17-19b* in vivo was more potent (Fig. 6C,D), possibly due to a degree of cooperative effects from the other miRNA components. The late-onset *Eμ-myc*/*17-19b-Mut19* lymphomas had varying levels of phospho-S6, yet this cohort of lymphomas as a whole exhibited a decrease in the phospho-S6 level compared with *Eμ-myc*/*17-19b* tumors (Supplemental Fig. S4E).

Although *Pten* deficiency in mice frequently gives rise to T-cell malignancy, *Pten* heterozygosity appears to partially phenocopy *mir-17-19b* overexpression, and cooperates with c-myc in the *Eμ-*

myc model to moderately accelerate B lymphomagenesis (Wendel et al., 2006). However, the oncogenic effect of *miR-19b* or *mir-17-19b* is more potent than *Pten* heterozygosity in the *Eμ-myc* lymphoma model. *Pten* is a haploinsufficient tumor suppressor whose dosage proportionally impacts its tumor suppressor activity and inversely correlates with tumor progression in a cell type-dependent manner (Trotman et al., 2003). It is likely that *miR-19b* or *mir-17-19b* overexpression, when compared with *Pten* heterozygosity, causes greater *Pten* repression (Supplemental Fig. S4C), and thus a stronger B-cell transformation in the *Eμ-myc* model. Interestingly, in non-Hodgkin's B-cell lymphomas (NHLs) including Burkitt's lymphoma and DLBCL, recurring deletions and rearrangements of 10q23, which harbors *PTEN*, are observed in 5%–10% of patients (Butler et al., 1999). In addition, the reduction or loss of *PTEN* expression is often associated with inferior survival (Abubaker et al., 2007; Robledo et al., 2009). These findings implicate the importance of the *PTEN* pathway in the progression and prognosis of specific human B-cell malignancies. Besides *PTEN* deletion and mutations, *mir-17-92* -mediated *PTEN* repression may be an additional mechanism to disrupt the *PTEN* function and to promote malignant transformation in human B-cells. In line with this hypothesis, a recent study described a subset of DLBCLs in which the amplification of *mir-17-92* and the deletion of *PTEN* are mutually exclusive (Lenz et al., 2008).

Discussion

The small size of miRNAs, combined with their imperfect base-pairing for target recognition, allows miRNAs to regulate many mRNA targets. The strong cooperation between *miR-19* and c-myc can result from the collective impacts on many *miR-19* targets, of which *Pten* is a key target, but it may not be the only one. Given the robust induction of phospho-S6 by *miR-19*, it is possible that other negative regulators of the PI3K–AKT–mTOR pathway, in addition to *Pten*, are coordinately regulated. It is also conceivable that additional pathways regulated by *miR-19* could synergize with down-regulated *Pten* to promote cell survival and malignant transformation. Increasing evidence suggests that the dosage of tumor suppressor genes has a significant impact on their functional readout. A number of tumor suppressors are haploinsufficient, and hypomorphic mutations in tumor suppressors are frequent in cancer (Payne and Kemp 2005). Given the importance of miRNAs in human cancer and their unique mechanism of action, partial repression of tumor suppressors is likely a novel mechanism through which miRNA oncogenes promote malignant transformation.

Polycistronic gene structure is frequently observed in miRNA loci (Ambros 2004; He and Hannon 2004; Zamore and Haley 2005). Since each miRNA has the potential to regulate hundreds of target mRNAs, a miRNA polycistron containing multiple components may possess a greater capacity for gene regulation, thus yielding pleiotropic biological effects through complex mechanisms of coordination. In the context of B-cell transformation in the *Eμ-myc* model, *miR-19* miRNAs are identified as the key oncogenic components of *mir-17-92* to cooperate with c-myc. The other *mir-17-92* components either are dispensable for oncogenesis, or, as in the case of *miR-18a*, may play an accessory role to enhance oncogenic potential. As a strong oncogene, *mir-17-92* can regulate multiple cellular processes to favor malignant transformation, causing decreased cell death, rapid cell proliferation, and increased angiogenesis (He et al., 2005; O'Donnell et al., 2005; Dews et al., 2006; Ventura et al., 2008). However, it remains unclear how this polycistronic miRNA regulates coordinated biological processes to achieve malignant transformation. It is conceivable that individual *mir-17-92* components function cooperatively to

impact multiple cellular processes, although more complex mechanisms of coordination may also exist. A recent study indicates that *miR-17* overexpression in mice decreases cell proliferation, adhesion, and migration, raising a possibility that components of *mir-17-92* can both positively and negatively regulate the same cellular process to achieve homeostasis (Shan et al., 2009). It is possible that cell types and biological contexts may also determine the exact mechanisms of coordination among polycistronic miRNA components. We are just beginning to understand the functional complexity of polycistronic miRNAs, which have an enormous capacity for gene regulation and complex coordination among different components. The unique gene structure of these miRNA polycistrons can ultimately underlie the molecular basis for their pleiotropic functions in the oncogenic and tumor suppressor network.

Methods

Molecular construction of *mir-17-92* subclusters

The subclusters of *mir-17-92* were amplified by PCR and subsequently cloned into the XhoI and EcoRI sites of the MSCV retrovirus vectors. In these vectors, miRNAs were placed downstream from the LTR promoter, which is followed by either a SV40-GFP cassette (for all in vivo experiments) or a PGK-Puro-Ires-GFP cassette (for all in vitro experiments) (Hemann et al., 2005). To construct the MSCV-*17-19b*/*Mut19* vector, a 12-nt mutation was introduced into the hairpin stem of *pre-mir-19a* and *pre-mir-19b* using the QuickChangeXL mutagenesis kit (Strategene). For the MSCV-*17-19b/Mut19* vector, the loss of *miR-19* expression and the normal expression of the other *mir-17-19b* components were validated using the TaqMan miRNA assays (Applied Biosystems).

Adoptive transfer of *Eμ-myc* HSPCs for lymphomagenesis

Fetal liver-derived HSPCs were isolated from embryonic day 13.5–15.5 (E13.5–E15.5) *Eμ-myc*/+ embryos, and were transduced with MSCV alone or MSCV expressing various *mir-17-92* subclusters. The MSCV retroviral vector used in our studies contains a SV40-GFP cassette that allows us to monitor transduced HSPCs both in vitro and in vivo. Infected HSPCs were subsequently transplanted into 8- to 9-wk-old, lethally irradiated C57BL/6 recipient mice. Tumor onset was subsequently monitored by weekly palpation, and tumor samples were either collected into formalin for histopathological studies, or prepared as single-cell suspension for FACS analysis.

Luciferase assays

Human *PTEN* 3′UTR were amplified from the genomic DNA (forward primer, 5′-CACCAAGATGGCACTTTCCCGTTT-3′; reverse primer, 5′-TGGCAAACATGTTCAAGAGGAGCT-3′), which contains two *miR-19*-binding sites that are also conserved in mice. Mutagenesis of these two *miR-19*-binding sites was carried out using the QuickChangeXL mutagenesis kit (Strategene). The wild-type *PTEN* 3′UTR, as well as the mutated *PTEN* 3′UTR fragments, were each cloned downstream from a firefly luciferase reporter. These firefly luciferase constructs that contain either the wild-type or the mutated *PTEN* 3′UTR were each transfected into the Dicer-deficient Hct116 cells (Cummins et al., 2006), together with a Renilla luciferase construct for normalization control, and 50 nM miRNA mimics for *mir-17*, *mir-18*, *miR-19b*, *miR-20a*, and *mir-1*, respectively. These miRNA mimics were generated by annealing two complementary RNA oligos (IDT). Luciferase activity of each construct was determined by dual luciferase assay (Promega) 48 h post-transfection.

Cell culture
NIH-3T3 cells were cultured in DMEM with 10% bovine serum, and were kept 30%–40% confluent throughout the entire cell culture experiment. Primary B-cells were prepared from mouse bone marrows, and were cultured in RPMI medium with 10% fetal bovine serum (FBS), 50 μM β-mercaptoethanol, and 2 ng/mL Il-7. NIH-3T3 cells and mouse primary B-cell cultures were infected by MSCV retroviruses expressing *mir-17-92* subclusters, and were selected by puromycin for 2 d. Serum-starved NIH-3T3 cells were prepared by incubating the cells with DMEM without serum for 12 h before harvesting the cell lysate. MSCV-infected primary B-cells were sorted based on GFP, and were then subjected to Western analyses or real-time PCR analyses as described below.

Real-time PCR analysis and Western analysis
TaqMan miRNA assays (Applied Biosystems) were used to measure the level of mature miRNAs. The mRNA level for *Pten* (forward primer, 5′-CACAATTCCCAGTCAGAGGCGC-3′; reverse primer, 5′-GCTGGCAGACCACAAACTGAGGA-3′) was determined using real-time PCR analysis with SYBR (Applied Biosystems). *Actin* was used as a normalization control in all our RT-QPCR experiments (forward primer, 5′-GATCTGGCACCACACCTTCT-3′; reverse primer, 5′-GGGGTGTTGAAGGTCTCAAA-3′). For Western analyses, *Pten* (Cell Signaling), Akt (Cell Signaling), phospho-Akt (Ser473; Cell Signaling), and phospho-S6 (Cell Signaling) antibodies were used at 1:1000, and tubulin antibody (Sigma) was used at 1:4000.

Histopathology
Tissue samples were fixed in formalin, embedded in paraffin, sectioned into 5-μm sections, and stained with haematoxylin and eosin (H&E). For Ki-67 (rabbit anti-Ki67; NovoCastra), caspase-3 (AF835; R&D Systems), and PCNA (MS-106P; Lab Vision Corp.) detection, representative sections were deparaffinized and rehydrated in graded alcohols before being subjected to antigen retrieval treatment in a vegetable steamer. Detection of antibody staining was carried out following standard procedures from the avidin-biotin immunoperoxidase methods. Diaminobenzidine (Invitrogen) was used as the chromogen and haematoxylin was used as the nuclear counterstain. Analysis of the apoptotic rate by TUNEL assay was performed according to a published protocol (Di Cristofano et al., 1998).

Flow cytometry
Lymphoma cells harvested from the animals were resuspended in 10% FBS/phosphate-buffered saline (PBS) to reach a concentration of 10^7 cells per milliliter. Twenty microliters of the cell suspension were stained with various antibodies diluted in 10% FBS/PBS for 1 h. Subsequently, cells were washed with 2% FBS/PBS and resuspended in 10% FBS/PBS for flow cytometry analysis. Antibodies used for our FACS analyses include PE anti-mouse IgM (eBioscience, 12-5790), APC-Cy7 B220 (BD Pharmingen, 552094), CD4 APC-Cy7 (BD Pharmingen, 552051), PE-CD8 (BD Pharmingen, 553032), PE-CD25 (BD Pharmingen, 553866), and APC-CD19 (Biolegend, 115511).

Apoptotic assays
Xenopus laevis eggs were collected and fertilized, and embryos were cultured by standard procedures. The *miR-19b* mimics were produced from the annealing products of 5′-

UGUGCAAAUCCAUGCAAAACUGA-3′ and 5′-AGUUUUGCAGGUUUGCAUCCAUU-3′ (IDT). Two complimentary RNA oligos were combined and diluted to a stock concentration of 1 μg/μL, heated for 1 min to 80°C, and then allowed to cool to room temperature to form duplexes. The same was done to generate the mutated *miR-19* mimics, *mut-19b*, using 5′-UCAGGUAAUCCAUGCAAAACUGA-3′ and 5′-AGUUUUGCAGGUUACCUUCGAUU-3′. The *Pten*-mut construct was made by two consecutive QuickChange reactions of accession plasmid BC161129 with primers 5′-ACAAATTTAGCTGCAGAGTAG-3′ and 5′-GGTCTTCAAACGGATACTGAG-3′, and 5′-GCAGAGTGAGGGGAGCGGGT-3′ and 5′-CGGGGAAAGGTTGGCACCCG-3′. *Xenopus tropicalis pten* and *pten-mut* RNAs were made using the mMessage SP6 kit (Ambion) on Not1-cut plasmid. Embryos were injected into both cells at the two-cell stage with 2 ng of each RNA. Hydroxyurea (Sigma) was diluted to a final concentration of 15 mM and embryos were treated from 2 h post-fertilization until stage 10.5. All embryos undergoing apoptosis of any cells were scored as positive.

Acknowledgements
We thank B. Zude, A. Basila, Y. Choi, and K. Lehet for technical assistance, and A. Winoto, D. Raulet, G. Barton, L. Coscoy, J. Liu, and R. Vance for stimulating discussions and helpful input. We also thank M. Schlissel and G.S. Martin for careful reading of our manuscript, and J.M. Silva, A. Economides, M. Schlissel, C. Miething, A. Thomas-Tikhonenko, D. Schulz, P. Garcia, M. Sohaskey, D. Stafford, M. Tokuyama, K. Chow, E. Cadera, W. Cousin, L.C. Trotman, and E. Hernando for sharing reagents and helpful discussions. We are particularly grateful to M. Schriock and B. Colpo for unconditional support. L.H. is a Searle Scholar, and is supported by the pathway to independence grant, an RO1 grant from the NCI, and the new faculty award from CIRM. S.W.L. and G.J.H. are both HHMI investigators, and are supported by a program project grant from the NCI.

Figure 1

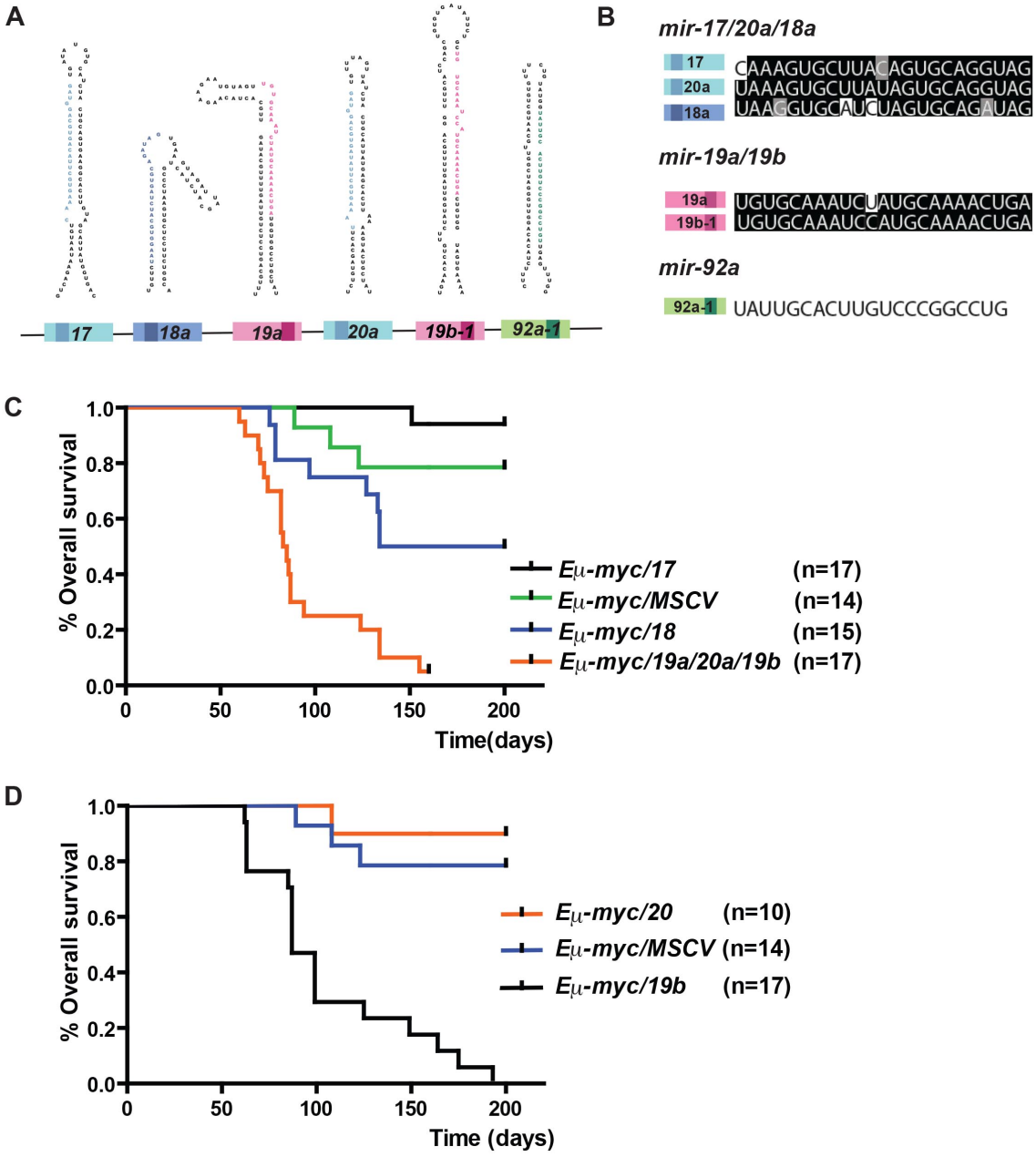
A
17
18a
19a
20a
19b-1
92a-1
B
mir-17/20a/18a
17 CAAAGUGCUUACAGUGCAGGUAG
20a UAAAGUGCUUAUAGUGCAGGUAG
18a UAAGGUGCAUCUAGUGCAGAUAG
mir-19a/19b
19a UGUGCAAAUCUAUGCAAAACUGA
19b-1 UGUGCAAAUCCAUGCAAAACUGA
mir-92a
92a-1 UAUUGCACUUGUCCCGGCCUG
C
% Overall survival
Time(days)
Eμ-myc/17 (n=17)
Eμ-myc/MSCV (n=14)
Eμ-myc/18 (n=15)
Eμ-myc/19a/20a/19b (n=17)
D
% Overall survival
Time (days)
Eμ-myc/20 (n=10)
Eμ-myc/MSCV (n=14)
Eμ-myc/19b (n=17)

Figure 1. *miR-19b* phenocopies the oncogenic effects of *mir-17-92* in the *Eμ-myc* model. **(A)** Gene structure of the *mir-17-92* polycistronic cluster. (Light-colored boxes) Pre-miRNAs; (dark-colored boxes) mature miRNAs. Homologous miRNA components are indicated by the same or similar colors. **(B)** *mir-17-92* components belong to three miRNA families: *miR-17/20a/18* (blue), *miR-19* (red), and *miR-92a* (green). Mature miRNA sequence alignments are shown for each family. Based on sequence identity, *miR-17* and *miR-20a* are closely related homologs, sharing significant sequence identity with miR-18a, but containing a slightly different seed (74% identity among all three). *mir-19a* and *mir-19b* differ by a single nucleotide at position 11, and are likely to regulate the same mRNA targets (96% identity). *miR-92a* has a unique seed sequence that distinguishes it from other components. **(C)** The *mir-19a/20/19b* subcluster accelerates c-myc-induced lymphomagenesis. Irradiated mice reconstituted with the Eμ-myc/+ HSPCs overexpressing *miR-17*, *miR-18a*, *mir-19a/20a/19b*, or a MSCV control vector were monitored weekly beginning 4 wk post-transplantation. The Kaplan-Meier curves represent percentage of overall survival. **(D)** *mir-19b* accelerates c-myc-induced lymphomagenesis. The *mir-19a/20/19b* subcluster was further divided into *mir-19b* and *miR-20a*, each overexpressed in the Eμ-myc/+ HSPCs before transplantation into lethally irradiated recipient animals. Reconstituted mice were monitored weekly starting 4 wk post-transplantation. The Kaplan-Meier curve indicates *mir-19b* has a strong oncogenic effect.

Figure 2

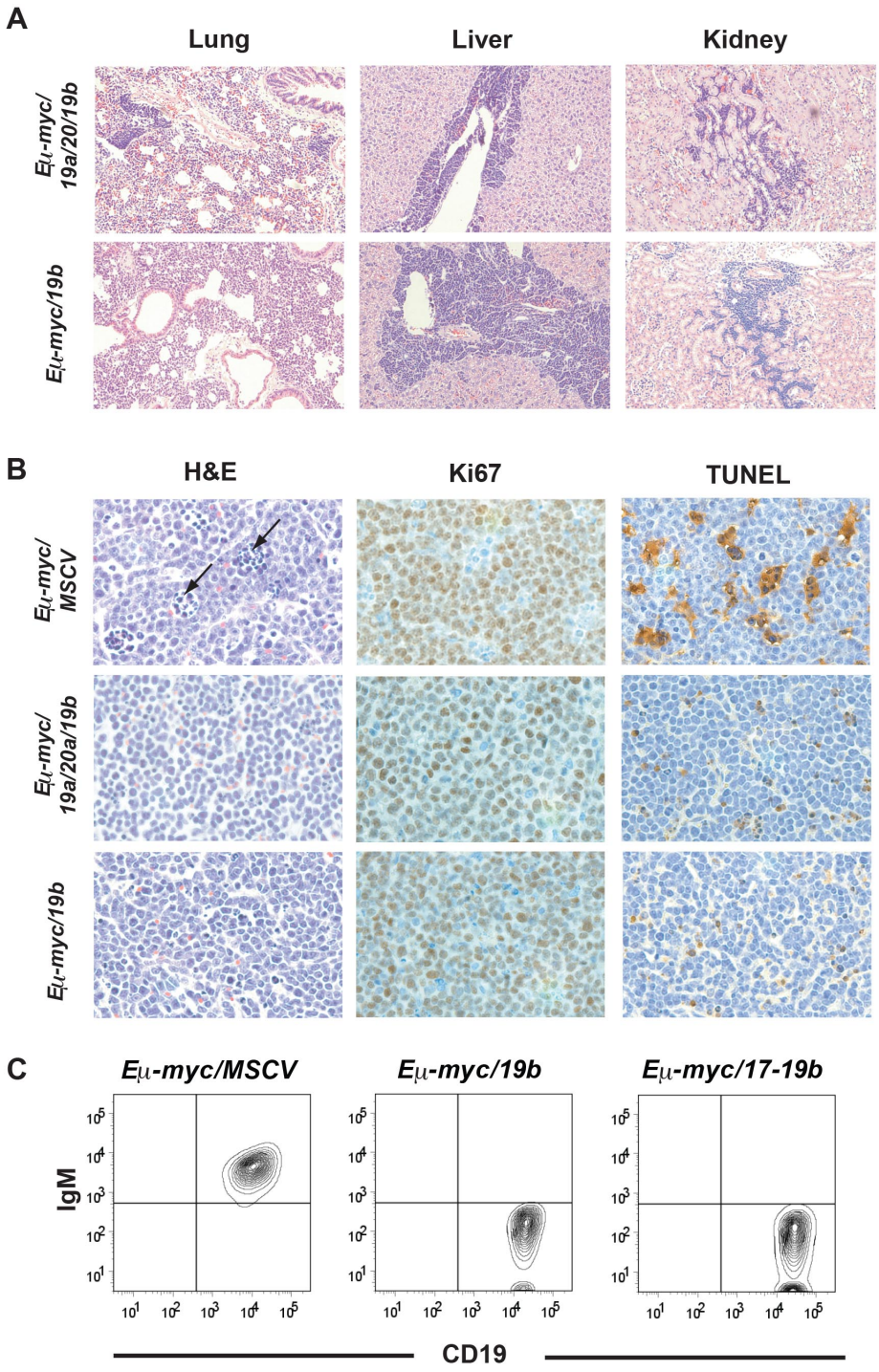
A
Lung
Liver
Kidney
Eμ-myc/ 19a/20/19b
Eμ-myc/19b
B
H&E
Ki67
TUNEL
Eμ-myc/ MSCV
Eμ-myc/ 19a/20a/19b
Eμ-myc/19b
C
Eμ-myc/MSCV
Eμ-myc/19b
Eμ-myc/17-19b
IgM
CD19

Figure 2. *Eμ-myc/17-19* and *Eμ-myc/19b* lymphomas have similar pathological and immunological features.

(A) *Eμ-myc/19b* lymphomas are highly invasive. H&E staining of the liver, lung, and kidney showed aggressive invasion by *Eμ-myc/19b* tumor cells, which was highly analogous to that of the *Eμ-myc/19a/20a/19b* lymphomas. In particular, both perivascular and parenchymal invasion of the liver were observed. **(B)** Overexpression of *mir-19b* represses c-myc-induced apoptosis. The *Eμ-myc/19b* and *Eμ-myc/19a/20a/19b* lymphomas had similar proliferation rates to those of Eμ-myc/MSCV controls, demonstrated by Ki67 staining. However, exogenous expression of *mir-19b* or *mir-19a/20/19b* greatly decreased apoptosis in the *Eμ-myc* tumors, confirmed by TUNEL and H&E staining of *Eμ-myc/17-19* lymph node tumors. The "starry sky" morphology of cell clusters undergoing apoptosis (black arrows), a hallmark of Eμ-myc/MSCV lymphomas, was absent in *Eμ-myc/19b* and *Eμ-myc/19a/20a/19b* tumors. **(C)** *mir-19b* and *mir-17-19b* preferably transform progenitor B-cells. Flow cytometric immunophenotyping of representative *Eμ-myc*, *Eμ-myc/17-19*, and *Eμ-myc/19* lymphomas. While the majority of *Eμ-myc* tumors consisted of CD19-positive and IgM-positive B-cells, the *Eμ-myc/19b* and *Eμ-myc/17-19* tumor cells bore cellular characteristics of progenitor B-cells, positive for CD19 but not for surface IgM.

Figure 3

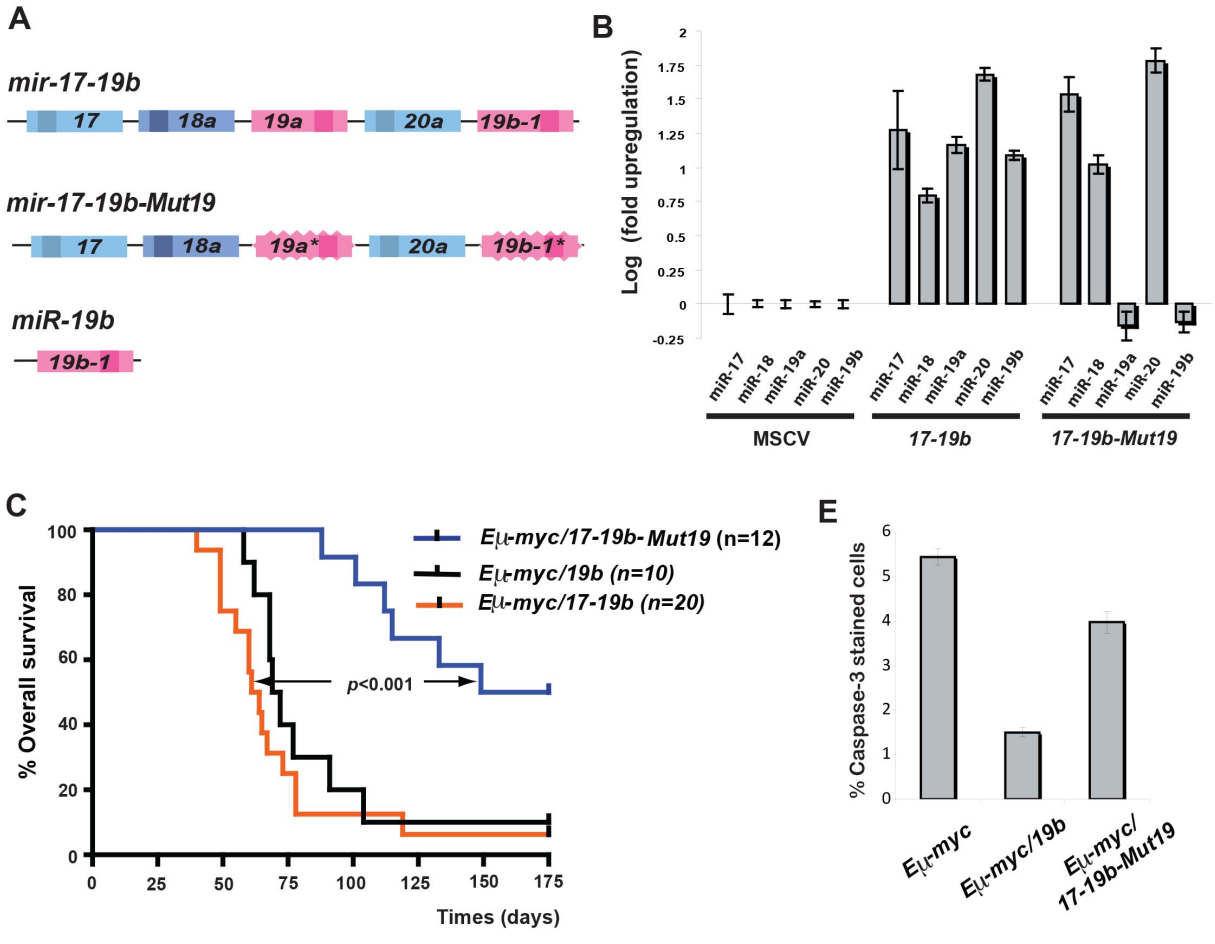
A
mir-17-19b
17
18a
19a
20a
19b-1
mir-17-19b-Mut19
17
18a
19a*
20a
19b-1*
miR-19b
19b-1
B
Log (fold upregulation)
2
1.75
1.5
1.25
1
0.75
0.5
0.25
0
-0.25
miR-17
miR-18
miR-19a
miR-20
miR-19b
MSCV
17-19b
17-19b-Mut19
C
% Overall survival
100
80
60
40
20
0
0
25
50
75
100
125
150
175
Times (days)
Eμ-myc/17-19b-Mut19 (n=12)
Eμ-myc/19b (n=10)
Eμ-myc/17-19b (n=20)
p<0.001
E
% Caspase-3 stained cells
6
5
4
3
2
1
0
Eμ-myc
Eμ-myc/19b
Eμ-myc/
17-19b-Mut19
D
Eμ-myc
Eμ-myc/19b
Eμ-myc/
17-19b-Mut19

Figure 3. *miR-19* miRNAs are essential for the oncogenic activity of *mir-17-19b*.
(A) A schematic representation of the gene structural organization of *mir-17-19b*, *mir-17-19b*-Mut19, and *mir-19b*. *19a** and *19b** indicate *miR-19* mutations. **(B)** *miR-19* mutations specifically affected *miR-19* expression in *mir-17-19b*. 3T3 cells were infected with MSCV-*mir-17-19b*, MSCV-*mir-17-19b*-Mut19, or control MSCV vectors. Expression levels of *miR-17*, *miR-18a*, *miR-19a*, *miR-20a*, and *mir-19b* were determined using TaqMan miRNA assays. *miR-19* mutations specifically affected the expression of *miR-19a* and *mir-19b*, but not that of the adjacent *mir-17-19b* components. Error bars indicate SD (n = 3). **(C)** *miR-19* is both necessary and sufficient for the oncogenic effect of *mir-17-19b*. Overexpression of *mir-19b* and *mir-17-19b* accelerated c-myc-induced lymphomagenesis to a similar degree, shown in Kaplan-Meier curves as the percentage of overall survival. Mutations in *miR-19* greatly decreased the oncogenic activity of *mir-17-19b* in the Eμ-myc model. We compared the oncogenic effects of *mir-17-19b*, *mir-19b*, and *mir-17-19b-Mut19* in the same adoptive transfer experiment. **(D)** *miR-19* is both necessary and sufficient for the cell survival effect of *mir-17-19b* in vivo. Representative lymphomas from *Eμ-myc*, *Eμ-myc/19b*, and *Eμ-myc/17-19b-Mut19* were stained for H&E and caspase-3, which indicated that the *miR-19* mutations significantly compromised cell survival effects of *mir-17-19b*, while *mir-19b* overexrepssion suppresses apoptosis. The Eμ-myc/19b and *Eμ-myc/17-19b-Mut19* tumors shown here were both IgM-negative B lymphomas. (Arrow) "Starry sky" feature of apoptotic tumor cells; (arrowhead) apoptotic cells with positive caspase-3 staining. Bar, 50 μm. **(E)** Quantification of caspase-3 staining of representative tumors from D as percentage of positive cells. For *Eμ-myc/19b* and *Eμ-myc/17-19b-Mut19* tumors, only IgM-negative tumors were selected for this comparison (n = 3; error bars represent SEM).

Figure 4

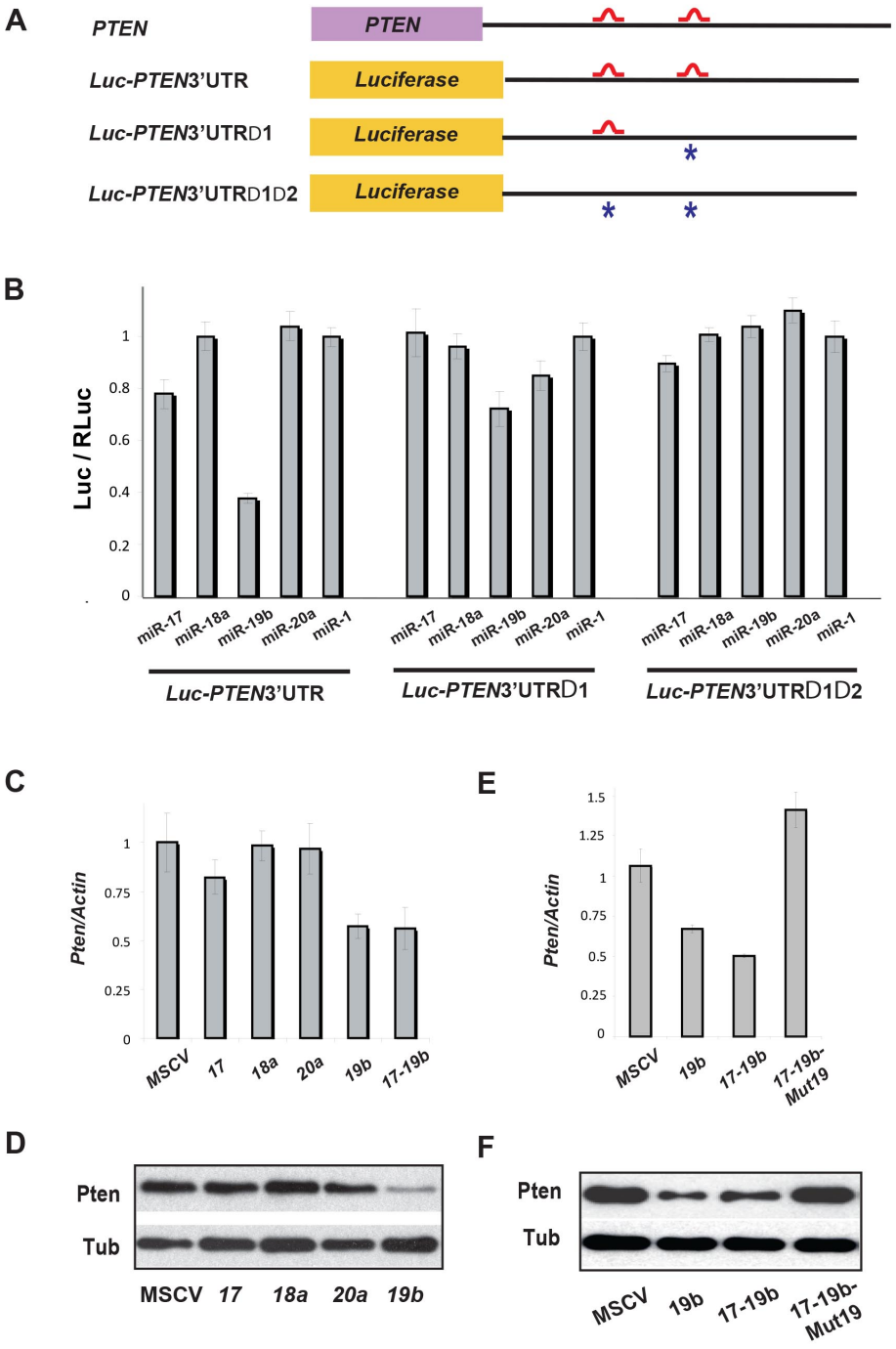
A
PTEN
PTEN
Luc-PTEN3'UTR
Luciferase
Luc-PTEN3'UTRD1
Luciferase
Luc-PTEN3'UTRD1D2
Luciferase
B
Luc / RLuc
0
0.2
0.4
0.6
0.8
1
miR-17
miR-18a
miR-19b
miR-20a
miR-1
Luc-PTEN3'UTR
Luc-PTEN3'UTRD1
Luc-PTEN3'UTRD1D2
C
Pten/Actin
0
0.25
0.5
0.75
1
MSCV
17
18a
20a
19b
17-19b
D
Pten
Tub
MSCV
17
18a
20a
19b
E
Pten/Actin
0
0.25
0.5
0.75
1
1.25
1.5
MSCV
19b
17-19b
17-19b-Mut19
F
Pten
Tub
MSCV
19b
17-19b
17-19b-Mut19

Figure 4. *Pten* is a *mir-17-19b* target specifically regulated by *miR-19*.
(A) Schematic representation of the *PTEN* 3′UTR and its *miR-19*-binding sites. Two *miR-19*-binding sites (shown in red) can be found in the human *PTEN* 3′UTR. The *PTEN* 3′UTR with mutations (designated with asterisks) at one (*PTEN3′UTRΔ1*) or both (*PTEN3′UTRΔ1Δ2*) *miR-19* sites, as well as the wild-type counterpart (*PTEN3′UTR*), were each cloned downstream from a luciferase reporter (Luc). **(B)** Specific repression of *Luc-PTEN3′UTR* reporter by *miR-19*. *Luc-PTEN3′UTR* was cotransfected with mimics of miR-17, miR-18a, *mir-19b*, miR-20a, and control miR-1. Only *mir-19b* significantly repressed the reporter expression. Cotransfection with a luciferase construct carrying one mutated *mir-19b* site in the *PTEN* 3′UTR (*Luc-PTEN3′UTRΔ1*) partially derepressed the Luc reporter, and cotransfection of a construct with mutations in both *miR-19* sites (*Luc-PTEN3′UTRΔ1Δ2*) completely derepressed the Luc reporter. **(C,D)** *mir-19b* specifically represses endogenous *Pten* expression level. Using real-time PCR analysis **(C)** and Western analysis **(D)**, down-regulation of endogenous *Pten* mRNA and protein can be detected in serum-starved NIH-3T3 cells infected with *mir-19b* and *mir-17-19b*. In comparison, overexpression of *miR-17*, *miR-18a*, *miR-20a*, and control vector (MSCV) in these cells has minimal effects on the endogenous *Pten* level. **(E,F)** *miR-19* is both necessary and sufficient to mediate the *Pten* repression by *mir-17-19b*. Repression of endogenous *Pten* mRNA **(E)** and protein **(F)** can be detected in serum-starved NIH-3T3 cells infected with *mir-19b* and *mir-17-19b*. In comparison, *mir-17-19b-Mut19* failed to repress the endogenous *Pten* level.

Figure 5

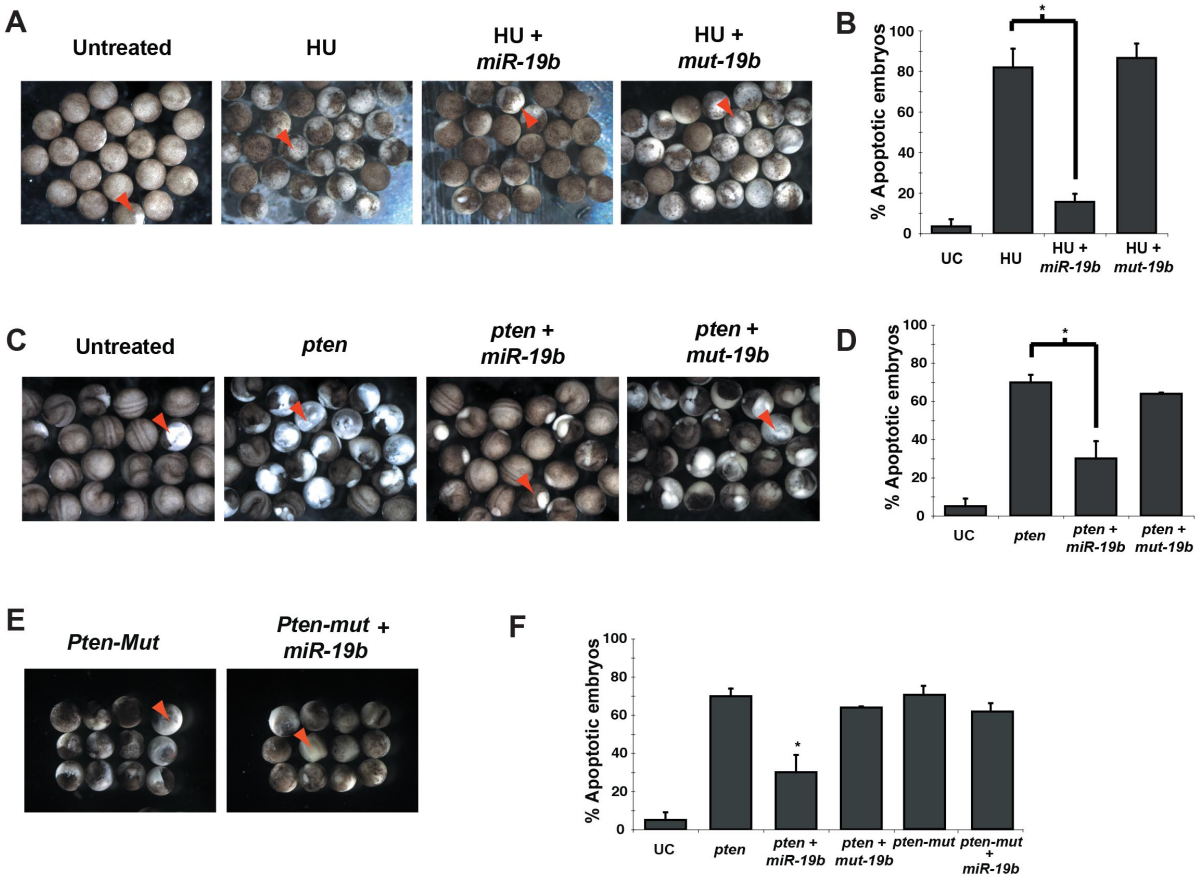

Figure 5. *miR-19b* functionally antagonizes *pten*-induced apoptosis in *Xenopus* embryos. **(A,B)** *mir-19b* rescues hydroxyurea (HU)-induced apoptosis in *X. laevis* embryos. Injection of *mir-19b* mimics into *X. laevis* embryos rescued apoptosis caused by hydroxyurea treatment. The mutated *mir-19b* with an altered seed region (*mut-19b*) failed to rescue hydroxyurea-induced apoptosis. Embryos undergoing apoptosis were marked by cell blebbing, disruption of cell adhesion, and a characteristic white color (red arrowhead). Hydroxyurea-treated embryos appeared more pigmented than control embryos, largely due to developmental arrest. **(B)** Apoptosis was quantified for untreated and hydroxyurea-treated embryos, as well as the hydroxyurea-treated embryos coinjected with either *mir-19b* mimics or mut-19b mimics (n = 3 experiments with >25 embryos in each group; [*] $P < 0.05$). **(C,D)** Injection of *mir-19b* rescued *Pten*-induced apoptosis in *Xenopus* embryos. Injection of full-length *Pten* mRNA into *Xenopus* embryos led to widespread apoptosis. Injection of *mir-19b*, but not *mut-19b*, significantly rescued the proapoptotic effect of *Pten*. **(E,F)** Disruption of base-pairing between *miR-19* and *pten* mRNA abolished their functional antagonism. Mutations in the *miR-19*-binding sites within the *pten* mRNA (*pten-mut*) did not abrogate the proapoptotic effects of *Pten*, but did eliminate the ability of *mir-19b* to repress the apoptosis (n = 3 experiments with >25 embryos in each group; [*] $P < 0.05$). All error bars represent SEM.

Figure 6

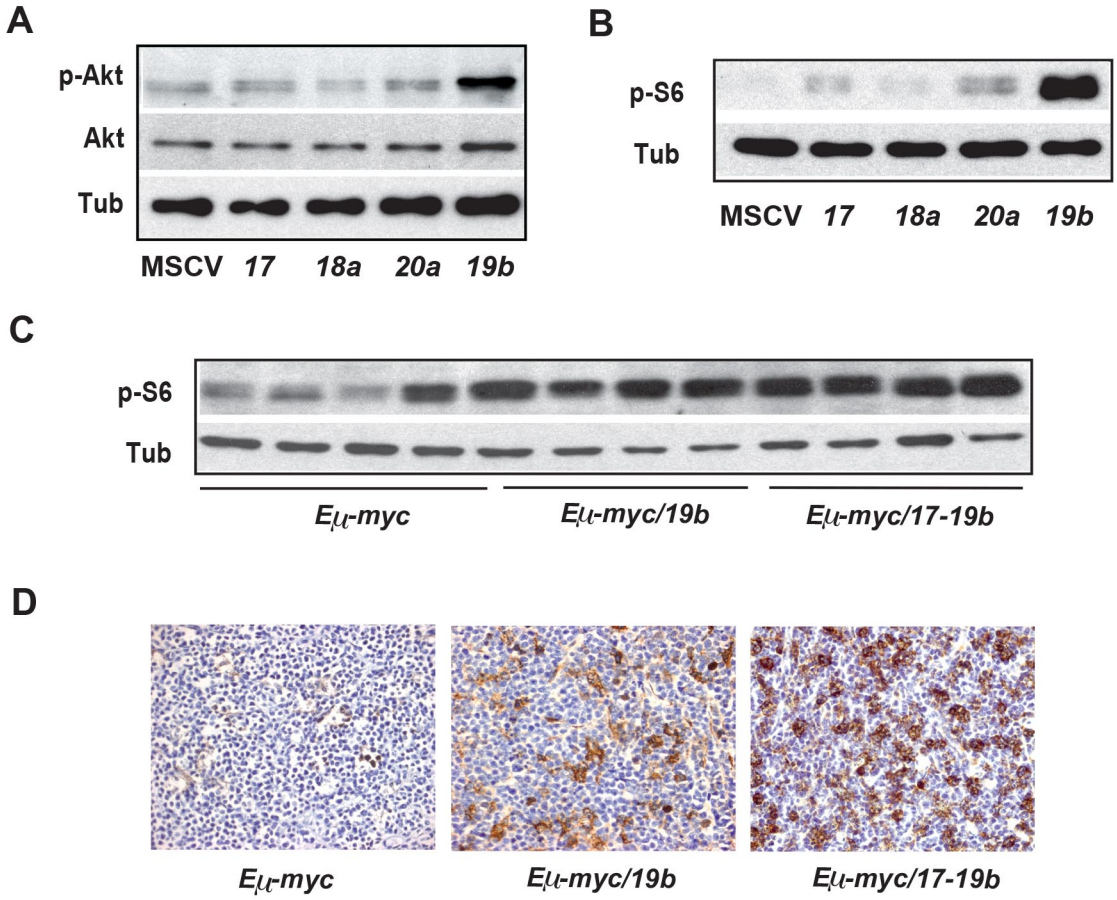

Figure 6. *miR-19* and *mir-17-19b* activates the Akt–mTOR pathway.
(A) *miR-19* is a key *mir-17-19b* component to activate the Akt–mTOR pathway. Using Western analysis, increased phospho-Akt level was detected in serum-starved 3T3 cells infected with *mir-19b*, but not *miR-17, miR-18a, miR-20a,* and the control vector (MSCV). In comparison, the overall Akt level was not affected by *mir-19b*. **(B)** *miR-19* induces an increase in phosphorylation of S6 ribosomal protein. Enforced expression of *mir-19b* strongly promoted the S6 phosphorylation as compared with the rest of *mir-17-19b* components. **(C,D)** Enforced *mir-19b* or *mir-17-19b* expression in the Eμ-myc model led to an increased level of phospho-S6 in lymphomas. Cells derived from the Eμ-myc, Eμ-myc/19b, and Eμ-myc/17-19b lymphomas were analyzed by Western **(C)** and immunohistochemistry **(D).** Both *Eμ-myc/19b* and *Eμ-myc/17-19b* lymphomas exhibited a high level of phospho-S6, although *mir-17-19b* seemed to have a stronger effect. In comparison, *Eμ-myc* tumors exhibited a low level of phospho-S6 and more variation among different samples, possibly reflecting the differences in the secondary oncogenic lesions. In all Western analyses, tubulin (Tub) was used as a normalization control.

Supplementary Figure S1

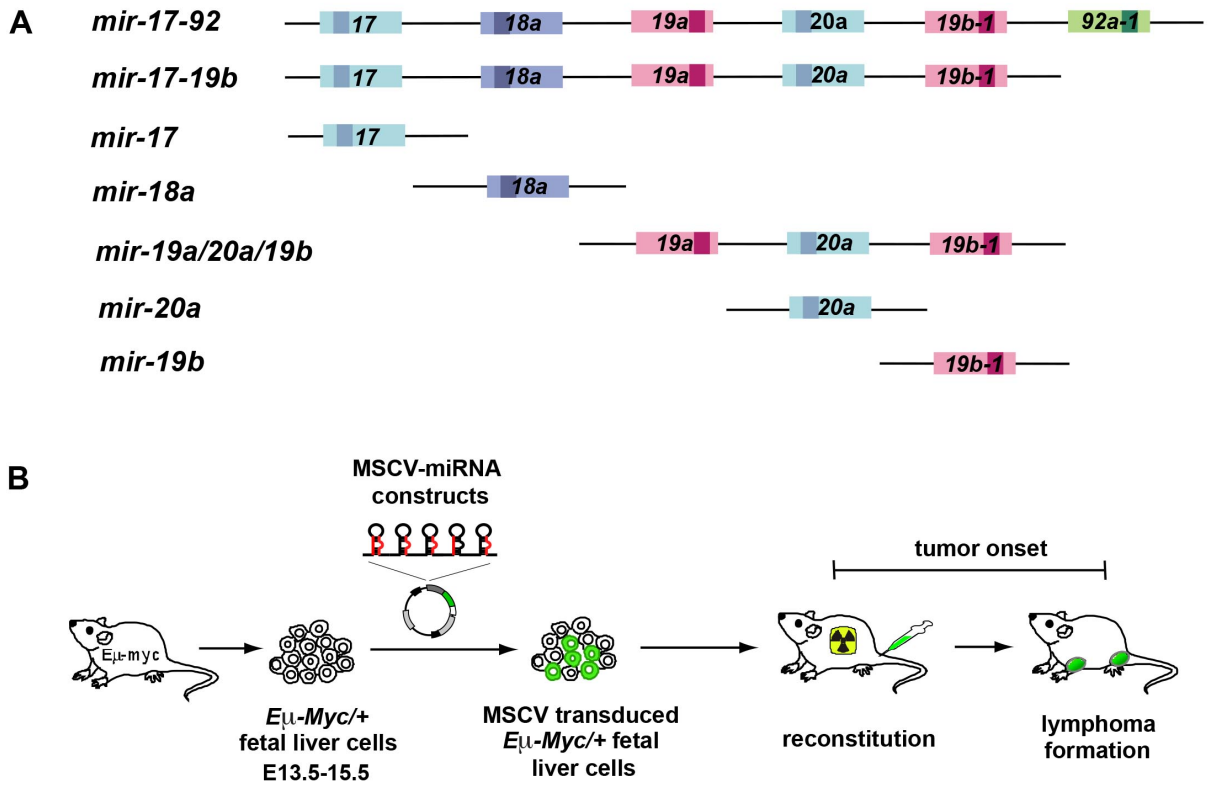

Supplementary Figure S1. Oncogenic potential of *mir-17-92* components in the *Eμ-myc* lymphoma model.
(A) Schematic representation of the gene structure of *mir-17-92* and its sub-clusters used in our studies. **(B)** Schematic representation of the adoptive transfer protocol using *Eμ-myc* HSPCs. *Eμ-myc*/+ fetal livers were extracted from E13.5-E15.5 embryos, then infected with MSCV retroviral vectors overexpressing specific miRNAs, and finally injected into lethally irradiated recipient mice. Lymphoma onset of the adoptive transferred mice was monitored to determine the oncogenic collaboration between *c-myc* and the miRNAs.

Supplementary Figure S2

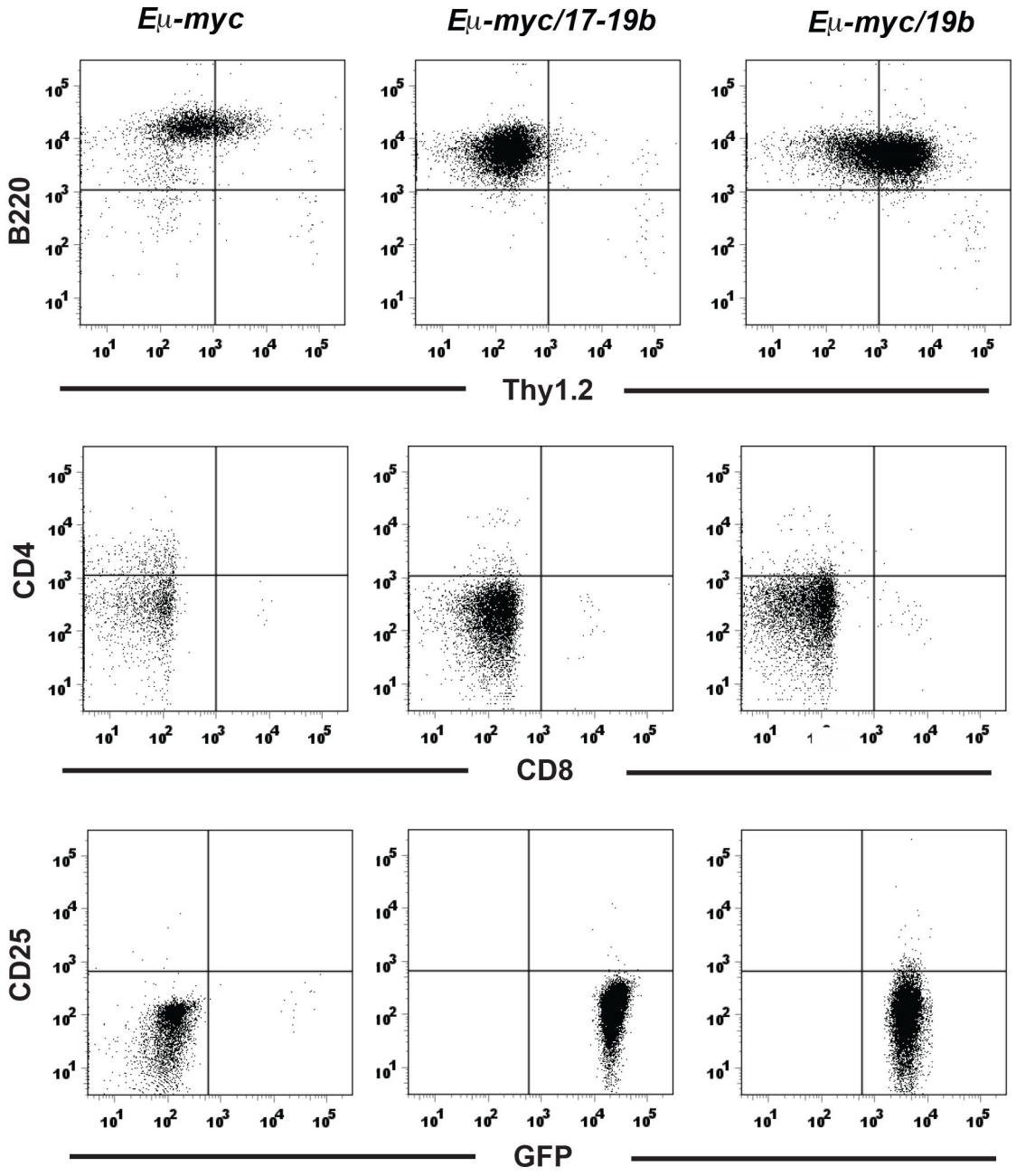

Supplementary Figure S2. Representative data from flow cytometric immunophenotyping of *Eμ-myc* lymphomas with different *mir-17-92* sub-clusters.
Representative lymphomas from *Eμ-myc, Eμ-myc/19,* and *Eμ-myc/17-19b* animals were stained with cell surface antibody B220, Thy1.2, CD4, CD8, CD25, respectively, and gated on the basis of forward scatter, side scatter, and GFP. The immunophenotypes of these tumors indicated that they were of a B-cell origin.

Supplementary Figure S3

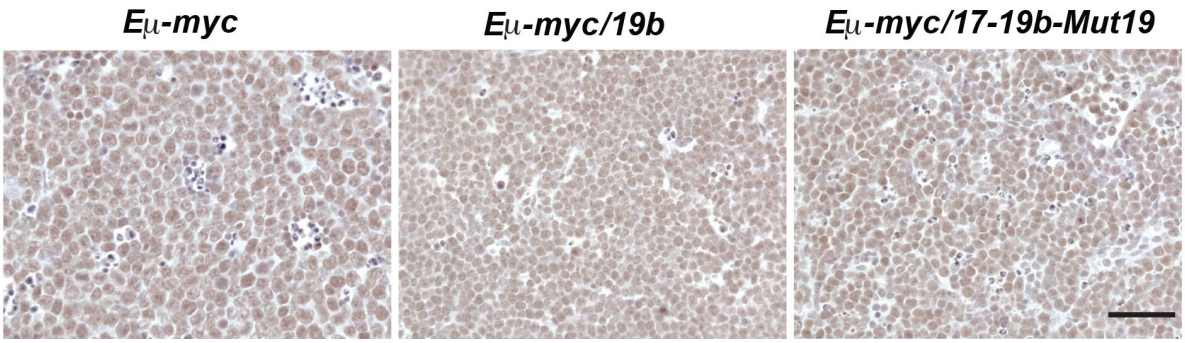

Supplementary Figure S3. *Eμ-myc/19* and *Eμ-myc/17-19b-Mut19* tumors are highly proliferative.

Representative lymphomas from *Eμ-myc, Eμ-myc/19* and *Eμ-myc/17-19b-Mut19* animals were stained with PCNA, a marker for cell proliferation. For all three types of lymphomas, ~80-90% of lymphoma cells were positive for PCNA, indicating the highly proliferative nature of these tumor cells. Scale bar, 50um.

Supplementary Figure S4

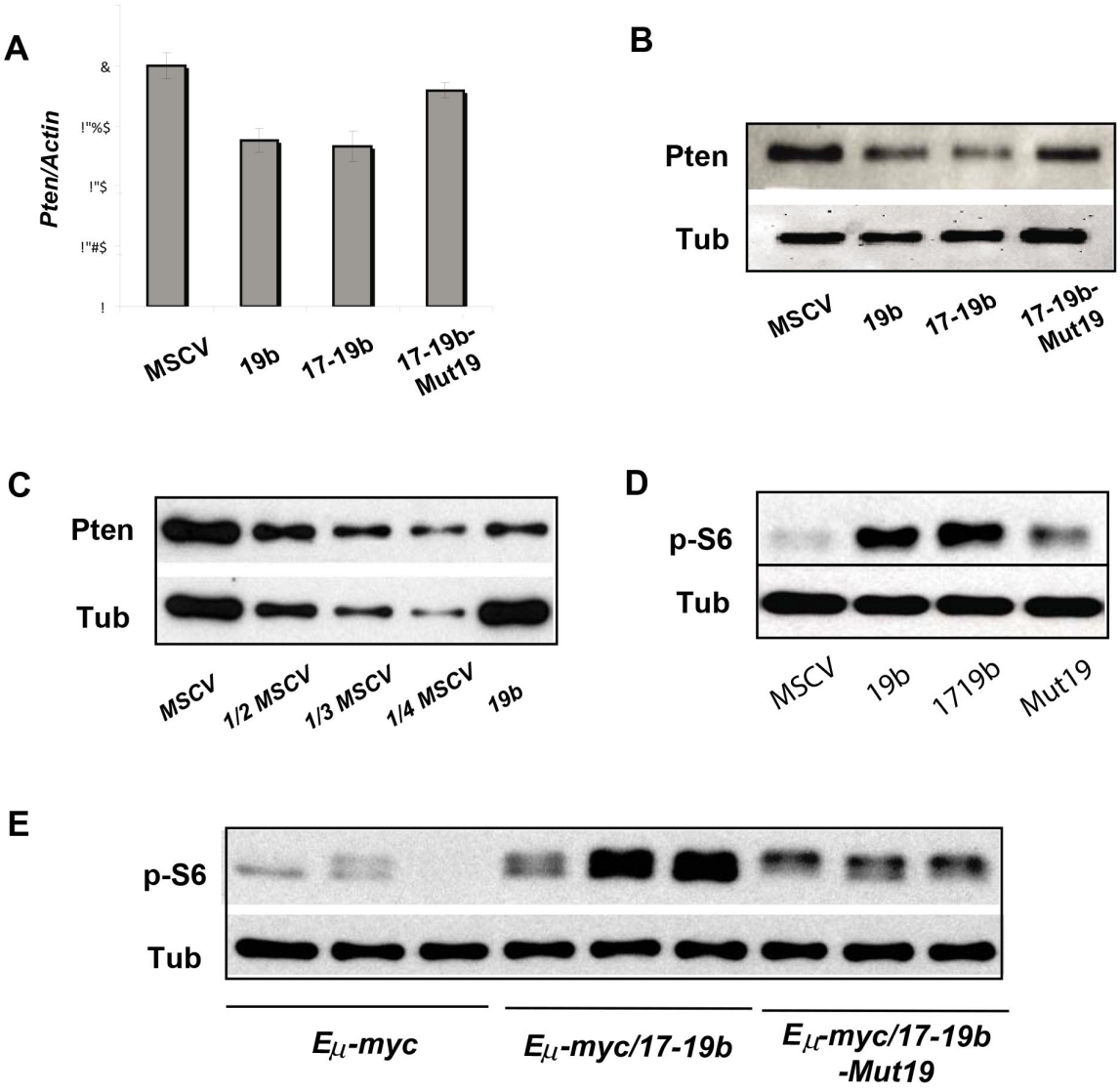

Supplementary Figure S4. *miR-19* is the key component of *mir-17-19b* to downregulate Pten.

(A, B) *miR-19* is necessary and sufficient for *mir-17-19b* to repress endogenous *Pten* in primary B-cells. Using real time PCR analysis (**A**) and western analysis (**B**), downregulation of endogenous *Pten* mRNA and protein were detected in primary B-cells infected with *miR-19b* and *mir-17-19b*, but not *mir-17-19b-Mut19*. Error bars indicate s.d. (n = 3). **C**. Semi-quantitative measurement of *Pten* repression achieved by *miR-19*. NIH 3T3 cells infected with control vector (MSCV), *miR-19b* and *mir-17-19b*, were compared side by side for the level of *Pten* protein. The control lysate (MSCV) were serially diluted by two fold (1/2 MSCV), three fold (1/3 MSCV) and four fold (1/4 MSCV), respectively, for a more quantitative comparison. **D, E.** *miR-19* mutations compromise the ability of *mir-17-19b* to induce S6 phosphorylation. Using western analysis, NIH 3T3 cells (**D**) and *Em-myc* tumors (**E**) with overepxression of control vector (MSCV), *miR-19b*, and *mir-17-19b* and *mir-17-19b-Mut19* were compared for the level of for phospho-S6. In both cases, *mir-17-19b-Mut19* reduced the phospho-S6 level compared to cells overexpressing *mir-17-19b*, although sample to sample variation was found for different tumor samples. Interestingly, *Em-myc/17-19b-Mut19* lymphomas exhibited stronger phospho-S6 compared to *Em-myc* lymphomas.

Supplementary Table 1 Flow cytometric immunophenotyping of *Eμ-myc* lymphomas with enforced expression of different *mir-17-92* subclusters.

Genotype	n	Percentage	Immunotype
Eμ-myc (n=7)	5	71.0%	$B220^+$, IgM^+,$CD19^+$, $CD4^-$, $CD8^-$, $CD25^-$ [a]
	2	29.0%	$B220^+$, IgM^-,$CD19^+$, $CD4^-$, $CD8^-$, $CD25^-$
Eμ-myc/17-19b (n=22)	17	77.3%	$B220^+$, IgM^+,$CD19^+$, $CD4^-$, $CD8^-$, $CD25^-$
	4	9.1%	predominantly $B220^+$, IgM^+,$CD19^+$, $CD4^-$, $CD8^-$, $CD25^-$, and a small percentrage of $CD4^+$ and/or $CD8^+$
	1	4.5%	$B220^+$, IgM&IgM^+, $CD19^+$, $CD4^-$, $CD8^-$ [b]
Eμ-myc/19b (n=16)	11	68.8%	$B220^+$, IgM^-,$CD19^+$, $CD4^-$, $CD8^-$, $CD25^-$
	5	31.3%	$B220^+$, IgM^+,$CD19^+$, $CD4^-$, $CD8^-$, $CD25^-$
Eμ-myc/17-19b-mut19 (n=8)	4	50.0%	$B220^+$, IgM^-,$CD19^+$, $CD4^-$, $CD8^-$, $CD25^-$
	2	25.0%	$B220^+$, IgM^+,$CD19^+$, $CD4^-$, $CD8^-$, $CD25^-$
	1	12.5%	$B220^-$, IgM^-,$CD19^+$, $CD4^+$, $CD8^+$, $CD25^-$, $Thy1^+$
	1	12.5%	Predominantly $B220^-$, IgM^-,$CD19^+$, $CD4^+$, $CD8^-$, $CD25^-$, and a small percentage of $B220^+$, IgM^-,$CD19^+$, $CD4^-$, $CD8^-$, $CD25^-$
Eμ-myc/19a-19b (n=6)	5	83.3%	$B220^+$, IgM^-, $CD19^+$, $CD4^-$, $CD8^-$
	1	16.7%	$B220^+$, IgM^+, $CD19^+$, $CD4^-$, $CD8^-$

[a] The IgM staining is surface IgM staining.

[b] These tumors consist of a mixture of IgM positive and IgM negative B-cells.

Supplementary Table S1. Flow cytometric immunophenotyping of *Eμ-myc* lymphomas with enforced expression of different *mir-17-92* sub-clusters.

Chapter 2

A component of the *mir-17-92* polycistronic oncomir promotes oncogene-dependent apoptosis

Virginie Olive*, Erich Sabio*, Margaux J Bennett, Caitlin S De Jong, Anne Biton, James C McGann, Samantha K Greaney, Nicole M Sodir, Alicia Y Zhou, Asha Balakrishnan, Mona Foth, Micah A Luftig, Andrei Goga, Terence P Speed, Zhenyu Xuan, Gerard I Evan, Ying Wan, Alex C Minella, Lin He

Elife. 2013 Oct 15;2:e00822.

This chapter is a reproduction of the paper by the same name published in eLife October 2013. My contributions to this paper are as follows. I assisted in generating Figure 1C. I performed the immunohistochemical staining for figure 2B and 2C. I instigated the experiment generating the mice, and performing the experiment with V. Olive for figure 3A and 3B, which later led to follow-up experiments in Figure 5G, and Figure 6A and 6B where I generated the mice and executed the analysis with V. Olive. I also assisted in editing the manuscript.

Summary
mir-17-92, a potent polycistronic oncomir, encodes six mature miRNAs with complex modes of interactions. In the *Eμ-myc* Burkitt's lymphoma model, *mir-17-92* exhibits potent oncogenic activity by repressing c-Myc-induced apoptosis, primarily through its *miR-19* components. Surprisingly, *mir-17-92* also encodes the *miR-92* component that negatively regulates its oncogenic cooperation with c-Myc. This *miR-92* effect is, at least in part, mediated by its direct repression of Fbw7, which promotes the proteosomal degradation of c-Myc. Thus, overexpressing *miR-92* leads to aberrant c-Myc increase, imposing a strong coupling between excessive proliferation and p53-dependent apoptosis. Interestingly, *miR-92* antagonizes the oncogenic *miR-19* miRNAs; and such functional interaction coordinates proliferation and apoptosis during c-Myc-induced oncogenesis. This *miR-19:miR-92* antagonism is disrupted in B-lymphoma cells that favor a greater increase of *miR-19* over *miR-92*. Altogether, we suggest a new paradigm whereby the unique gene structure of a polycistronic oncomir confers an intricate balance between oncogene and tumor suppressor crosstalk.

Introduction
MicroRNAs (miRNAs) are a class of small, non-coding RNAs that regulate post-transcriptional gene repression in a variety of developmental and pathological processes (Ambros, 2004; Zamore and Haley, 2005; Bartel, 2009; Kim et al., 2009). Due to their small size and the imperfect nature of target recognition, miRNAs have the capacity to regulate many target mRNAs through translational repression and mRNA degradation, thereby acting as global regulators of gene expression (Lewis et al., 2005; Filipowicz et al., 2008). Unlike mammalian protein-coding genes that follow the one-transcript, one-protein paradigm, many miRNA genes are expressed as polycistronic primary transcripts, generating multiple mature miRNAs under the same transcriptional regulation (Megraw et al., 2007). miRNA polycistrons further expand the gene regulatory capacity, since different miRNA components can confer specific yet overlapping biological effects, and their functional interactions can yield unusual complexity.

Polycistronic miRNAs often exhibit pleiotropic biological functions with unique gene regulatory mechanisms (Megraw et al., 2007). One of the best example is *mir-17-92*, a potent oncomir (i.e., miRNA oncogene), whose genomic amplification and aberrant overexpression have been observed in many human tumors including Burkitt's lymphoma, diffuse large B-cell lymphoma (DLBCL), and lung cancer (Lu et al., 2005; Mendell, 2008). *mir-17-92* regulates multiple cellular processes during tumor development, including proliferation, survival, angiogenesis, differentiation, and metastasis (He et al., 2007; Uziel et al., 2009; Conkrite et al., 2011; Nittner et al., 2012).

As a polycistronic oncomir, *mir-17-92* produces a single precursor that yields six individual mature miRNAs (Figure 1A, Figure1—figure supplement 1A) (Tanzer and Stadler, 2004). Based on the seed sequence homology, the six *mir-17-92* components are categorized into four miRNA families (Figure 1A, Figure 1—figure supplement 1A): *miR-17 (miR-17* and *20*)*, miR-18, miR-19 (miR-19a* and *19b*)*,* and *miR-92a* (we will designate *miR-92a* as *miR-92* in the remainder of our paper). Interestingly, *miR-92* has a more ancient evolutionary history compared to the other *mir-17-92* components (Tanzer and Stadler, 2004). *miR-92* is evolutionarily conserved in vertebrates, chordates, and invertebrates, while the remaining *mir-17-92* components are only found in vertebrates (Figure 1—figure supplement 1B,C). Conceivably, the distinct mature miRNA sequence of each *mir-17-92* component determines the specificity of the target regulation. However, the functional significance of the *mir-17-92* polycistronic gene structure remains largely unknown.

The structural analogy to prokaryotic operons has led to the speculation that the co-transcribed *mir-17-92* components can collectively contribute to oncogenesis. However, our studies reveal an unexpected functional interaction among *mir-17-92* components. In the *Eμ-myc* mouse B-cell lymphoma model, while the intact *mir-17-92* acts as an oncogene, its *miR-92* component negatively regulates the oncogenic cooperation with c-Myc. This effect, at least in part, results from the ability of *miR-92* to yield aberrant c-Myc dosage, which promotes a strong coupling between oncogene stress and p53-dependent apoptosis. Surprisingly, *miR-92* functionally antagonizes *miR-19*, a key oncogenic *mir-17-92* component, in the context of c-Myc-induced oncogenesis. During B-cell transformation, this *miR-19:miR-92* antagonism is disrupted to favor a greater increase of *miR-19* than *miR-92*. Thus, the polycistronic *mir-17-92* employs an antagonistic interaction among its encoded miRNA components to confer an intricate crosstalk between the oncogene and tumor suppressor networks.

Results

Since *mir-17-92* is overexpressed in human Burkitt's lymphomas (Tagawa et al., 2007), we set out to functionally dissect *mir-17-92* components in the *Eμ-myc* model of Burkitt's lymphoma (Figure 1B). The *Eμ-myc* mice carry a *c-myc* transgene downstream of the immunoglobulin (*Ig*) heavy chain enhancer *Eμ* (Langdon, 1986; Adams et al., 1985)*,* which functionally resembles the *Ig-MYC* translocations that occur frequently in Burkitt's lymphomas (Tagawa et al., 2007). The resulting B-cell specific, aberrant c-Myc activation promotes excessive proliferation, yet also evokes potent, p53-dependent apoptosis (Schmitt et al., 2002; Hemann et al., 2003). Thus, c-Myc-induced apoptosis enables a self-defense mechanism against malignant transformation, producing B-lymphomas with a late onset (Lowe et al., 2004). In our adoptive transfer model (Olive et al., 2009), *Eμ-myc/+* hematopoietic stem and progenitor cells (HSPCs) were transplanted into lethally irradiated recipient mice, generating chimeric mice that faithfully recapitulated the late tumor onset of the *Eμ-myc* transgenic mice (Figure 1B).

When *Eμ-myc/+* HSPCs were infected with MSCV (murine stem cell virus) retrovirus to overexpress the intact *mir-17-92* oncomir, we observed a considerable acceleration in tumor onset compared to the *Eμ-myc*/MSCV control mice ($p<0.01$, Figure 1C).

Unexpectedly, the oncogenic cooperation between c-Myc and *mir-17-92* was significantly stronger when *miR-92* was deleted within this oncomir (Figure 1C). The average survival of *Eμ-myc*/*17-92Δ92* mice was 66 days, significantly shorter than that of *Eμ-myc*/*17-92* mice (112 days, $p<0.0001$). *mir-17-92Δ*92 carried a deletion of *miR-92* pre-miRNA and its flanking sequences, which might alter the expression of the remaining *mir-17-92* components (Figure 1D, Figure 1—figure supplement 1D). We then engineered a 12-nucleotide *miR-92* seed mutation within *mir-17-92* to abolish the functional *miR-92* with minimal disruption to the overall gene structure. The resulting *mir-17-92Mut92* phenocopied *mir-17-92Δ*92 in vivo (Figure 1C), significantly enhancing the oncogenic cooperation with c-Myc without altering the level of any remaining *mir-17-92* components (Figure 1D, Figure 1—figure supplement 1D). This unexpected effect was specifically attributable to *miR-92*. Mutations of *miR-20* or *miR-17* failed to affect oncogenesis in the *Eμ-myc* model (Figure 1C, Figure 1—figure supplement 1D and data not shown), and mutations of both *miR-19* miRNAs nearly abolished this oncogenic cooperation (Olive et al., 2009). This finding suggests that, although *mir-17-92* acted as a potent oncogene as a whole, its *miR-92* component confers an internal negative regulation on its oncogenic cooperation with c-Myc. This effect of *miR-92* clearly contrasts with that of *miR-19*, a key oncogenic *mir-17-92* component that promotes c-Myc-induced lymphomagenesis by repressing apoptosis (Mu et al., 2009; Olive et al., 2009; Mavrakis et al., 2010).

In the *Eμ-myc* model, a strong oncogenic lesion often leads to the B-cell transformation at an earlier developmental stage (Hemann et al., 2003). The greater oncogenic activity of *mir-17-92Mut92* in comparison with *mir-17-92* was consistent with *mir-17-92Mut92* preferentially transforming IgM negative progenitor B-cells, and *mir-17-92* frequently transforming IgM positive B-cells (Figure 2A; Table 1). In comparison to *Eμ-myc*/*17-92* mice, both *Eμ-myc*/*17-92Δ92* and *Eμ-myc*/*17-92Mut92* mice developed more aggressive B-lymphomas, characterized by massive lymph node enlargement, splenic hyperplasia, leukemia, and widespread dissemination into visceral organs outside of the lymphoid compartment (Figure 2B, data not shown).

During Myc-induced tumorigenesis, aberrant c-Myc dosage yields simultaneous induction of proliferation and apoptosis, imposing a unique selective pressure for pro-survival lesions (Evan and Vousden, 2001). Thus, we compared the extent of Myc-induced apoptosis in the *Eμ-myc*/*17-92, Eμ-myc*/*17-92Δ92, Eμ-myc*/*17-92Mut92*, and control *Eμ-myc*/*MSCV* lymphomas. The control *Eμ-myc/MSCV* lymphomas invariably exhibited a high proliferation index accompanied by extensive cell death, as evidenced by the widespread 'starry sky' pathology (Figure 2C,D) and cleaved caspase 3 staining (Figure 2C,E). The potent oncogenic activity of *mir-17-92Δ*92 and *mir-17-92Mut92* was consistent with the strong reduction of apoptosis in the lymph node tumors. In comparison, the intact *miR-92* significantly attenuated the repression of c-Myc-induced apoptosis by *mir-17-92* in vivo (Figure 2C–E).

We next investigated the effect of *miR-92* alone in regulating c-Myc-induced apoptosis. In the *Eμ-myc* model, *miR-92* overexpression significantly enhanced c-Myc-induced apoptosis in vivo (Figure 3A,B, Figure 3—figure supplement 1A), consistent with a rapid

depletion of *miR-92*-infected cells in premalignant *Eμ-myc* B-cells (Figure 3—figure supplement 1B). Similar *miR-92* effects on c-Myc-induced apoptosis were observed in vitro. The *R26MER/MER* mouse embryonic fibroblasts (MEFs) carry a switchable variant of Myc, MycERT2, downstream of the constitutive *Rosa26* promoter, which allows acute activation of the *MycER* transgene by 4-OHT (4-Hydroxytamoxifen) induced nuclear translocation (Murphy et al., 2008). The *R26MER/MER* MEFs recapitulate c-Myc-induced apoptosis in vitro, as activated MycERT2 induces p53-dependent apoptosis in response to serum starvation (Murphy et al., 2008). Enforced *miR-92* expression in *R26MER/MER* MEFs invariably enhanced Myc-induced apoptosis (Figure 3C, Figure 3—figure supplement 1C).

In addition to promoting c-Myc-induced apoptosis, *miR-92* unexpectedly enhanced c-Myc-induced cell proliferation. A significant increase of BrdU incorporation was observed in *R26MER/MER* MEFs overexpressing *miR-92*, both under normal culture conditions and, more evidently, under serum starvation (Figure 3D). The same proliferative effect of *miR-92* was also observed in primary B-cells. Comparison of the proliferative effect of each *mir-17-92* component in bone marrow derived primary B-cells revealed that the *miR-92* component yielded one of the strongest effects (Figure 3E,F). In addition, *miR-92* deficiency significantly compromised the ability of *mir-17-92* to promote cell cycle progression in B-cells (Figure 3—figure supplement 1D). Interestingly, strong proliferative effects have been reported for nearly all *mir-17-92* components, yet the exact cell type and biological context can select specific components as the predominant drivers for cell proliferation. Taken together, our data suggest that *miR-92* is a unique *mir-17-92* component that functionally couples c-Myc-induced cell proliferation and c-Myc-induced apoptosis in the B-cell compartment.

To investigate the molecular mechanism underlying *miR-92* functions, we performed microarray analyses comparing gene expression profiles of *R26MER/MER* MEFs overexpressing *miR-92* or the control MSCV vector. These MEFs were serum starved and 4-OHT treated to trigger strong Myc-induced apoptosis. *miR-92*-upregulated genes were significantly enriched for the cell cycle pathway, including *ccnd1*, *ccnb1*, *ccnb2*, *cdc25b, cdc25c,* and *cdk4* (Figure 4A,B), consistent with the ability of *miR-92* to promote Myc-induced cell proliferation. Genes upregulated by *miR-92* were also enriched for the *p53* pathway, including the classic *p53* target *mdm2*, as well as the pro-apoptotic p53 targets—*noxa*, *bax*, *puma*, *perp*, and *bid* (Figure 4A,B, Figure 4—figure supplement 1A). Since aberrant c-Myc activation triggered a p53-dependent apoptotic response (Lowe et al., 2004), our observation is consistent with *miR-92* further enhancing p53 activation downstream of c-Myc. Interestingly, *p21*, a canonical p53 target, was not induced by *miR-92* in the MycERT2 activated *R26MER/MER* MEFs (Figure 4—figure supplement 1A). It is likely that the transcriptional repression of *p21* by c-Myc renders *p21* irresponsive to p53 activation under this biological context (Heasley et al., 2002). Using real-time PCR, we validated the ability of *miR-92* to induce cell cycle genes and activate p53 targets in both *R26MER/MER* MEFs, as well as primary B-cells (Figure 4C, Figure 4—figure supplement 1A,B). Hence, the molecular signature imposed by *miR-92* overexpression is consistent with its functional readout.

The activation of the p53 pathway by c-Myc is essential for the induction of the apoptotic response in the *Eμ-myc* model (Schmitt et al., 2002). A major mechanism that governs Myc-induced p53 activation is the transcriptional induction of the gene encoding *Arf*, which inhibits Mdm2-mediated p53 ubiquitination and degradation (Lowe et al., 2004; Campaner and Amati, 2012). The ability of *miR-92* to enhance c-Myc-induced apoptosis and to increase the expression of p53 targets raised the possibility that *miR-92* overexpression activates p53 possibly through elevated Arf. In both *R26MER/MER* MEFs and wild-type primary B-cells, *miR-92* overexpression alone caused significant accumulation of Arf mRNA and protein (Figure 4C,D, Figure 4—figure supplement 1C), consistent with the rapid stabilization of the p53 protein (Figure 4D, Figure 4—figure supplement 1C) without alteration of *p53* mRNA (Figure 4—figure supplement 1D). Notably, the ability of *miR-92* to induce p53 activation occurred not only in 4-OHT treated *R26MER/MER* MEFs with MycERT2 activation, but also in untreated *R26MER/MER* MEFs with normal c-Myc level. This was clearly demonstrated by the elevation of p53 protein level, as well as the increased p53 target expression (Figure 4—figure supplement 1B,C).

The induction of p53 by *miR-92* prompted us to investigate the functional importance of p53 in *miR-92*-induced apoptotic response. Knockdown of *p53* in *R26MER/MER* MEFs not only led to a suppression of c-Myc-induced apoptosis, but also completely abolished the effect of *miR-92* to enhance c-Myc-induced apoptosis (Figure 4E). These findings suggested that an intact p53 pathway is required for the apoptotic effect of *miR-92*. Consistently, the *miR-92* induction of the pro-apoptotic genes, including *noxa*, *perp,* and *mdm2*, also was mediated by the intact p53 (Figure 4F). Thus, aberrant c-Myc activation triggers an apoptotic response through p53 activation; and co-expression of *miR-92* with c-Myc leads to an even stronger p53 activation, and subsequently apoptotic response.

Our findings suggest parallels between *c-myc* and *miR-92*: both are potent oncogenes that promote excessive cell proliferation coupled with p53-dependent apoptosis, and both are capable to induce expression of cell cycle genes (*ccnb1, ccnd1, cdk4,* and *cdc25*) (Lowe et al., 2004; Campaner and Amati, 2012) and p53 pathway components (*Arf, puma, noxa, perp,* and *mdm2*) (Lowe et al., 2004; Campaner and Amati, 2012). The functional analogy between c-Myc and *miR-92*, as well as the molecular overlap between their downstream pathways, led us to investigate the effect of *miR-92* on c-Myc. Intriguingly, *miR-92* expression significantly enhanced c-Myc protein level both in MEFs and in primary B-cells (Figure 5A), without affecting the *c-myc* mRNA level (Figure 5—figure supplement 1A, data not shown). Consistent with the stabilization of endogenous c-Myc, *miR-92* overexpression in *R26MER/MER* MEFs stabilized the MycERT2 protein (Figure 5B). The dosage of c-Myc protein is crucial for its biological readout (Murphy et al., 2008). While c-Myc dosage determines the extent of cell cycle gene induction and cell proliferation, it also regulates the degree of p53 activation and subsequent apoptosis (Murphy et al., 2008) (Figure 5—figure supplement 1B). Thus, the ability of *miR-92* to induce aberrant c-Myc accumulation likely constitutes the molecular basis for its ability to promote both cell proliferation and p53-dependent apoptosis.

Based on our findings, we speculated that *miR-92* targets could include negative

regulators of c-Myc protein accumulation. Therefore, we searched genes known to negatively regulate *c-myc* for the presence of putative *miR-92* binding sites. Using the Targetscan and RNA22 algorithms (Lewis et al., 2005; Miranda et al., 2006; Bartel, 2009), we identified eight candidate *miR-92* targets, each of which contained one or more predicted *miR-92* binding sites in the 3′ untranslated region (3′UTR). Real-time PCR analysis of these candidate genes confirmed *fbw7* (F-box and WD repeat domain-containing 7) as a likely target of *miR-92* (Figure 5C, Figure 5—figure supplement 1C). *fbw7*, which contains two *miR-92* target sites within its 3′UTR (Figure 5C), is the substrate recognition component of an SCF-type E3 ubiquitin ligase that mediates the degradation of several proto-oncoproteins, including Myc, Cyclin E, c-Jun, and Notch (Welcker and Clurman, 2008; Crusio et al., 2010; Wang et al., 2012). A luciferase reporter or a FLAG-tagged *fbw7*-encoding ORF (open reading frame), when fused to the wild-type *fbw7* 3′ UTR, were both significantly repressed in a *miR-92* dependent manner (Figure 5D, Figure 5—figure supplement 1D). Yet enforced *miR-92* expression failed to repress the luciferase reporter that contained an *fbw7* 3′UTR with two mutated *miR-92* binding sites (Figure 5D), suggesting that *miR-92* binding to *fbw7* 3′UTR is required for this repression. Furthermore, *miR-92* effectively repressed endogenous Fbw7 protein level, as demonstrated by the decreased *fbw7* mRNA level and Fbw7 immunoprecipitation (Figure 5E). Consistent with *fbw7* as an important target for *miR-92*, enforced *miR-92* expression upregulated multiple *Fbw7* substrates at their protein levels, including c-Myc and cyclinE (Figure 5F). Observations from our in vivo experiments also supported this post-transcriptional regulation of Fbw7 by *miR-92*, as we observed an inverse correlation between the level of *miR-92* and *fbw7* when comparing *Eμ-myc/17-92Δ92 and Eμ-myc/17-92* lymphoma cells (Figure 5—figure supplement 1E).

fbw7 has previously been postulated as a potential *miR-92* target based on the presence of *miR-92* target sites (Mavrakis et al., 2011), yet it remains unclear how *fbw7* mediated the pro-apoptotic effects of *miR-92*, given its well-characterized functions as a tumor suppressor. Recent findings indicate that the acute inactivation of tumor suppressor Fbw7 imposes a strong oncogenic stress to induce p53-dependent apoptosis, conferring a selective advantage to cells with deficient p53 function (Minella et al., 2007; Onoyama et al., 2007; Matsuoka et al., 2008; Grim et al., 2012). This p53-dependent apoptosis is, at least in part, due to an aberrant increase of c-Myc dosage (Onoyama et al., 2007; Matsuoka et al., 2008). These findings suggested that a major mechanism through which *miR-92* enhanced the c-Myc protein level, and subsequently, c-Myc-induced apoptosis, could be through its direct repression of Fbw7. In support of this hypothesis, *miR-92* overexpression significantly increased the c-Myc protein level in wild-type Hct116 cells, but not in *FBW7*−/− Hct116 cells (Figure 5—figure supplement 1F), suggesting *FBW7* was essential for *miR-92* to induce c-MYC increase. Functionally, acute *fbw7* knockdown in *R26MER/MER* MEFs partially phenocopied the effect of *miR-92* to enhance c-Myc-induced apoptosis (Figure 5G, Figure 5—figure supplement 1G); while overexpression of an *fbw7α* open reading frame (ORF), albeit above its physiological level, completely abolished this apoptotic effect of *miR-92* (Figure 5H, Figure 5—figure supplement 1H). Nevertheless, it is still likely that additional mechanisms downstream of *miR-92* also promote its apoptotic effects, because *fbw7* knockdown largely recapitulated the extent of c-Myc upregulation by *miR-92* (Figure 5—figure supplement 1G), yet only partially

phenocopied its pro-apoptotic effects (Figure 5G). In addition, overexpression of *fbw7* above its physiological level might amplify the extent of functional interactions between *fbw7* and *miR-92* in regulating apoptosis. Despite these caveats, our results strongly argue that the *miR-92*-Fbw7 axis constitutes a major mechanism underlying the pro-apoptotic effects of *miR-92*.

Downregulation of Fbw7 by *miR-92* significantly enhanced the protein level of c-Myc in *R26MER/MER* MEFs and in primary B-cells (Figure 5A). It is conceivable that the ability of *miR-92* to repress Fbw7 in vivo could similarly enhance the c-Myc accumulation in the *Eμ-myc/92* premalignant B-cells, promoting rapid cell proliferation and a p53-dependent apoptotic response. Unfortunately, due to technical limitations, we were not able to demonstrate an increased c-Myc protein level as a result of *miR-92* overexpression in the *Eμ-myc* premalignant B-cells. There was a significant depletion of the *Eμ-myc/92* premalignant B-cells due to excessive apoptosis (Figure 3—figure supplement 1B), making it difficult to collect enough cells to analyze the c-Myc protein level by western analyses. Similarly, we could not obtain enough cells to compare the protein level of c-Myc in the premalignant B-cells from the *Eμ-myc/17-92*, *Eμ-myc/17-92Δ92,* and *Eμ-myc/MSCV* animals. Nevertheless, our functional studies in cell culture, combined with the inverse expression correlation between *fbw7* and *miR-92* in vivo, strongly argue the importance of the *miR-92*-Fbw7-Myc axis to promote the pro-apoptotic effects of *miR-92*.

In the context of the c-Myc cooperation, *mir-17-92* encodes miRNA components with opposing biological functions. While *miR-19* miRNAs repress c-Myc-induced apoptosis to promote *Eμ-myc* lymphomagenesis (Mu et al., 2009; Olive et al., 2009), *miR-92* enhances c-Myc-induced apoptosis to attenuate the tumorigenic effects. Consistent with the opposing effects of *miR-19* and *miR-92*, co-expression of these two miRNAs as a dicistron attenuated the apoptotic effect of *miR-92* in premalignant *Eμ-myc* B-*cells* in vivo (Figure 6A,B, Figure 6—figure supplement 1A). A similar antagonistic interaction was also observed in *R26MER/MER* MEFs; and introducing a *miR-19b* mutation within *mir-19b-92* dicistron abolished this interaction (Figure 6C). Since *miR-19* represses *pten* to promote the PI3K/AKT pathway, the activation of AKT signaling would lead to increased phosphorylation of Mdm2, thus destabilizing p53 to dampen the apoptotic response induced by *miR-92* (Gottlieb et al., 2002; Ogawara et al., 2002). Consistent with this hypothesis, we observed a decreased p53 induction and an unaltered c-Myc level when *miR-92* was co-expressed with *miR-19* (Figure 6D, Figure 6—figure supplement 1B).

This *miR-19:miR-92* antagonism appears to be conserved evolutionarily. In *Xenopus laevis, miR-19* and *miR-92* have identical sequence to their mammalian orthologs (Figure 1—figure supplement 1B). Based on Targetscan and RNA22 miRNA target prediction algorisms (Lewis et al., 2003, 2005; Miranda et al., 2006; Grimson et al., 2007), their target specificity is also conserved for key miRNA targets, although the exact binding sites may or may not be conserved (Olive et al., 2009) (Figure 6—figure supplement 1C). In addition, the biological functions of *miR-19* and *miR-92* exhibit evolutionary conservation between *Xenopus laevis* and mammals. Individual injection of *miR-19*

promoted cell survival of hydroxyurea-treated *Xenopus* embryos, while co-injection of *miR-19a* and *miR-92* significantly attenuated this pro-survival effect (Figure 6E). This functional antagonism was specific for *miR-92* and *miR-19*, since co-injection of other *mir-17-92* components or a mutated *miR-92* did not yield any functional interactions in combination with *miR-19* (Figure 6F).

Given the opposing biological effects of *miR-19* and *miR-92* during c-Myc-induced lymphoma development, differential regulation of these two miRNA families could determine the oncogenic activity of *mir-17-92*. Under normal physiological conditions, this *miR-19*:*miR-92* antagonism could attenuate the detrimental oncogenic signaling by inducing apoptosis in cells with inappropriate *mir-17-92* induction. During malignant transformation, and particularly during c-Myc-induced oncogenesis, this *miR-19*:*miR-92* antagonism could be disrupted to favor cell survival. Using real time PCR analyses, we compared the relative abundance of *miR-19*a, *miR-19*b, and *miR-92* in normal splenic B-cells, premalignant *Eμ-myc* B-cells, and *Eμ-myc* lymphomas (Figure 7A). Comparing to normal splenic B-cells, the levels of all three mature miRNA species were elevated in both premalignant and malignant *Eμ-myc* B-cells, possibly due to transcriptional activation of *mir-17-92* by c-Myc (Donnell et al., 2005). However, the *miR-19* to *miR-92* ratios significantly increased during c-Myc-induced lymphomagenesis (Figure 7B). In other words, when normalized to the respective miRNA levels in normal splenic B-cells, mature *miR-19* (including *miR-19a* and *miR-19b*) exhibited a greater increase in premalignant and malignant *Eμ-myc* B-cells than mature *miR-92* (Figure 7A–C). This differential increase was most evident in premalignant *Eμ-myc* B-cells; the fully transformed *Eμ-myc* B-lymphoma cells exhibited a lesser difference (Figure 7A,B). This observation is consistent with premalignant *Eμ-myc* B-cells having an intact p53-dependent apoptotic response, thus a stronger selective pressure for a greater *miR-19:miR-92* ratio. In comparison, most *Eμ-myc* B-lymphomas have a defective p53 response, hence a less strong selective pressure to maintain a high *miR-19:miR-92* ratio. We also validated this observation using northern analysis. Comparing normal splenic B-cells and multiple *Eμ-myc* lymphoma cells, the levels of the mature *miR-19a, miR-19b* and *miR-92* were all elevated in transformed B-cells; however, the degree of increase for *miR-19a* and *miR-19b* was significantly higher than that of *miR-92* (Figure 7C). This differential increase of *miR-19* and *miR-92* was also observed in human Burkitt's lymphoma cell lines when compared to normal B-cells isolated from the periphery blood (Figure 7D). More importantly, this phenomenon was not limited to *c-myc* driven B-lymphomas. In the LT2-MYC murine model of hepatocellular carcinoma (HCC), where tumor development was initiated by tetracycline-inducible c-Myc expression, *miR-19a* and *miR-19b* also exhibited a stronger increase than *miR-92* when comparing tumor cells and the normal counterpart (Figure 7E).

These observations were consistent with a previous finding, where the inducible *c-myc* activation in a human Burkitt's lymphoma cell line induced both *miR-19a* and *miR-19b* to a greater extent than *miR-92* (Donnell et al., 2005). Although *miR-19* and *miR-92* are co-transcribed from the *mir-17-92* precursor, the differential increase of *miR-19* vs *miR-92* occurs in multiple c-Myc-driven tumor types. Thus, the relative abundance of *miR-19* and *miR-92* could constitute an important molecular basis to regulate the initiation and

progression of c-Myc-induced tumor development.

Discussion

The unique polycistronic structure of *mir-17-92* constitutes the basis for its pleiotropic functions and the complex mode of interactions among its miRNA components. A high level of *mir-17-92* in normal or premalignant cells could lead to suboptimal consequences that are counter-balanced through an intrinsic negative regulation by *miR-92* (Figure 7F). As we demonstrated in vitro where *miR-92*, by directly downregulating Fbw7, enhances c-Myc protein level to promote apoptosis, the ability of *miR-92* to repress Fbw7 in vivo could similarly constitute a major mechanism to enhance c-Myc-induced apoptosis. This effect of *miR-92* is a double edged sword in c-Myc driven tumors, as its overexpression gives rise to a strong and obligated coupling between excessive proliferation and a potent, p53-dependent apoptosis (Figure 7F). This coupling is consistent with the previous observation that a lower level of constitutive c-Myc acts more effectively to promote tumor initiation, while a higher level of c-Myc is selected by the terminal tumors with defective apoptosis machinery (Murphy et al., 2008). Therefore, *mir-17-92* encodes an internal component to confer a negative regulatory feedback on its oncogenic activity, imposing a strong selection for anti-apoptotic lesions to shape the path of malignant transformation. More interestingly, c-Myc transcriptionally activates *mir-17-92* that encodes *miR-92* (Hemann et al., 2005), which in turn enhances c-Myc dosage, at least in part, by repression Fbw7. It is possible that aberrant c-Myc activation triggers a positive feedback loop to further increase c-Myc dosage to strengthen the apoptotic response and to eliminate cells with oncogenic potential. It is worth noting that the *miR-92* apoptotic effect described in this study depends on an intact p53 response. Consequently, in terminal *Eμ-myc* B-lymphoma cells that often carry a defective p53 response, *miR-92* failed to enhance c-Myc-induced apoptosis (Mu et al., 2009).

The functional readout of *miR-92* heavily depends on cell types and biological contexts. It is important to recognize that *miR-92* is not a tumor suppressor miRNA. Like c-Myc, *miR-92* elicits potent oncogene stress to engage tumor suppressor response, at least in part, by activating p53. In the premalignant *Eμ-myc/92* B-cells, the effect of *miR-92* to repress Fbw7 most likely results in an increase of c-Myc level, which coupled with the intact p53 response to strongly sensitize the cells to *miR-92*-induced apoptosis. Under other contexts when proliferation becomes a rate-limiting event for oncogenesis, or when p53-dependent apoptosis is compromised, *miR-92* could render a pro-proliferative effect that is strictly oncogenic (Tsuchida et al., 2011). Likewise, the functional readout of other *mir-17-92* components also heavily depends on cell types and biological contexts. *miR-19* promotes c-Myc-induced B-lymphomas by repressing apoptosis (Mu et al., 2009; Olive et al., 2009), yet has little effects in promoting *Rb*-deficient retinoblastomas (Conkrite et al., 2011); *miR-17* allows the bypass of Ras-induced senescence by promoting proliferation (Hong et al., 2010), yet fails to affect c-Myc-induced lymphomas, possibly due to its functional redundancy with c-Myc.

Both cooperative and antagonistic interactions operate among subsets of *mir-17-92* components. The *miR-19:miR-92* antagonism constitutes a novel mechanism to confer an intricate balance between oncogene signaling and innate tumor suppressor responses

(Figure 7F). This balance can be disrupted in premalignant and malignant cells that exhibit c-Myc overexpression, as an increase in the *miR-19*:*miR-92* ratio is likely to favor the suppression of c-Myc-induced apoptosis and to promote oncogenesis. Although all *mir-17-92* components are co-transcriptionally regulated, different changes of *miR-19* vs *miR-92* during oncogenesis could be a result of differential miRNA biogenesis and/or turn-over. It has been shown that specific RNA-binding proteins, such as hnRNP A1, promote the processing of a specific *mir-17-92* component, *miR-18* (Guil and Cáceres, 2007). Future studies are likely to reveal important mechanisms underlying cell type- and context-dependent differential regulation of *mir-17-92* components, which will generate important insights on the biology of polycistronic miRNAs.

Our current study mostly focuses on the antagonistic interaction between *miR-19* and *miR-92* in c-Myc driven oncogenesis, yet it reveals a more general mechanism underlying the structural function relationship of polycistronic miRNAs. It is likely that the complex interactions among polycistronic miRNA components can coordinate and balance a multitude of cellular and molecular processes during normal development and disease. Interestingly, in the case of *mir-17-92*, *miR-92* has a different evolutionary history compared to the other *mir-17-92* components. *miR-92* is evolutionary conserved in Deuterostome (including vertebrates and chordates), Ecdysozoa (including flies and worms), and Lophotrochozoa, yet the remaining *mir-17-92* components are only found in vertebrates (Figure 1—figure supplement 1C). The functional antagonism between the more ancient *miR-92* and the newly evolved *mir-19* might result from the convergence of these two separate evolutionary paths at the origin of vertebrates. This antagonism could evolve to regulate cell proliferation and cell death downstream or independent of c-Myc in both normal development and disease. Thus, our studies suggest a novel mechanism by which a crosstalk between oncogene and tumor suppressor pathways has been hardwired through evolution into the unique gene structure of a polycistronic oncomir.

Methods

Molecular cloning

mir-17-92 Δ92 and *mir-17-92* were amplified by PCR and subsequently cloned into the XhoI and EcoRI sites of the MSCV retrovirus vectors. In these vectors, miRNAs were placed downstream of the LTR promoter, which is followed either by a SV40-GFP cassette (for all in vivo experiments), a PGK-Puro-IRES-GFP cassette, or a SV40-CD4 cassette (for in vitro experiments) (Hemann et al., 2005). To construct MSCV-*17-92Mut92*, MSCV-*17-92Mut20*, and *MSCV-17-92Mut19b* vectors, a 12-nucleotide mutation was introduced into the seed region of the mature *miR-92*, *miR-20*, or *miR-19b* using the Quikchange XL mutagenesis kit (200521; Stratagene) and the following primers:

Mut20 primers:

GACAGCTTCTGTAGCACTAAtaaacaataatcGCAGGTAGTGTTTAGTTATC and

GATAACTAAACACTACCTGCGATTATTGTTTATTAGTGCTACAGAAGCTGTC.

Mut92 primers:

CAATGCTGTGTTTCTGTATGGTtaacattaacatCCGGCCTGTTGAGTTTG and

CAAACTCAACAGGCCGGATGTTAATGTTAACCATACAGAAACACAGCATTG.

Mut19b primers:

CTGTGTGATATTCTGCTGacatttaagtacCAAAACTGACTGTGGTAGTG and CACTACCACAGTCAGTTTTGGTACTTAAATGTCAGCAGAATATCACACAG. The loss of *miR-92, miR-20* or *miR-19b* expression and the intact expression level of the remaining *mir-17-92* components were validated using the TaqMan MicroRNA Assays (4427975; Applied Biosystems, Foster City, CA). *mir-19b-92*, *mir-19bMut92*, and *mir-19b-92Mut19b* were similarly amplified by PCR (ACTGCTCGAGAGCTTCGGCCTGTCGCCC and GTAGAATTCATGTATCTTGTAC) from the *mir-17-92*, *mir-17-92Mut92*, and *mir-17-92Mut19b* construct described above and subsequently cloned into the XhoI and EcoRI sites of the MSCV retrovirus vectors.

To construct the MSCV-Shp53 vector, shRNA against p53 was placed downstream of the LTR promoter of the MSCV-SV40-HuCD4 retroviral vector (Xue et al., 2007). MSCV-Shfbw7 construct was kindly provided by Dr Hans Guido Wendel (Mavrakis et al., 2011). To construct the pRetroX-fbw7-IRES-DsRedExpress (Xu et al., 2010), *fbw7α* ORF was placed downstream of the LTR promoter followed by an IRES-DsRed cassette.

Adoptive transfer of *Eμ-myc* HSPCs for lymphomagenesis

The hematopoietic stem and progenitor cells (HSPCs) were isolated from E13.5-E15.5 *Eμ-myc*/+ mouse embryos and were transduced with MSCV alone or MSCV vectors expressing various *mir-17-92* derivatives. The MSCV retroviral vector used in our adoptive transfer model contains a SV40-GFP cassette that allows us to monitor transduced HSPCs both in vitro and in vivo. Infected HSPCs were subsequently transplanted into an 8- to 10-week-old, lethally irradiated C57BL/6 recipient mice. Tumor onset was subsequently monitored by weekly palpation, and tumor samples were either collected into formalin for histopathological studies, or prepared as single cell suspension for FACS analysis and for cell culture studies. Both the *Eμ-myc*/+ mice and the recipient mice are on C57BL/6 background.

LT2-MYC mouse liver tumor model

The LT2-MYC mouse model for human hepatocellular carcinoma (HCC) is a double transgenic mouse model, in which the tetracycline transactivator protein (tTA) is driven by the hepatocyte-specific promoter, the liver activator protein (LAP) promoter, while the human c-MYC gene is driven by the tetracycline response element (TRE). The LT2-MYC model exhibits 'dox-off' regulation, where c-Myc expression is turned on in hepatocytes in the absence of doxycycline.
LT2-MYC mice taken off doxycycline-containing food, between 3–5 weeks of age, develop distinct tumor nodules around 8–12 weeks on an average (Kistner et al., 1996; Shachaf et al., 2004). Total RNA was extracted from liver tumor samples from three independent mice, as well as normal livers from the doxycycline treated LT2 mice. Total RNAs were prepared using Trizol (15596018; Invitrogen) and subjected to real time PCR analyses as described below.

Cell culture and retroviral infection

Primary murine B-cells were prepared from bone marrows of 4- to 6-week-old mice and were cultured in RPMI with 10% fetal bovine serum (FBS), 50 μM beta-mercaptoethanol

(M3148; Sigma) and 2 ng/ml Il-7 (407-ML-005; R&D). *R26MER/MER* and *R26MER/+* MEFs were kindly provided by Gerald Evan's laboratory. MEFs were cultured in DMEM with 10% fetal bovine serum. *Eμ-myc* tumor cells were derived from lymphomas from the terminal-stage *Eμ-myc* animals. *Eμ-myc* lymphoma cells overexpressing various *mir-17-92* derivatives were cultured in 45% DMEM, 45% IMDM with 10% fetal bovine serum, and 50 μM β-mercaptoethanol (M3148; Sigma) on irradiated NIH-3T3 feeder cells. Immortalized human B-cell lines were cultured in RPMI with 10% FBS and 90 μM beta-mercaptoethanol. *Dicer*-deficient Hct116 cells, kindly provided by Dr Bert Vogelstein (Cummins et al., 2006), and *Fbxw7*-deficient Hct116 cells (Grim et al., 2012) were cultured in McCoy's 5A media with 10% fetal bovine serum. Human Burkitt's lymphoma cell lines, including BL41, BL2, MutuI, Daudi, Raji (provided by Dr Terry Rabbitts), Manca, and Jiyoje were cultured in RPMI with 10% FBS.
Mouse primary B-cell cultures or MEFs were infected by MSCV retroviruses expressing various *mir-17-92* derived miRNA clusters, shRNA against p53 (Xue et al., 2007), shRNA against fbw7 (Mavrakis et al., 2011), or fbw7 cDNA (pRetroX-fbw7-IRES-DsRedExpress). In Figure 4E,F, double infection was performed to obtain *R26MER/MER* MEFs that co-expressed shRNA *p53* and *miR-92*. In this experiment, MEFs were initially infected with an ecotropic MSCV-*p53shRNA-SV40huCD4* retrovirus to a nearly 100% infection efficiency, as validated by FACS analysis using huCD4 antibody. The second infection was achieved using an amphotropic MSCV-*miR-92-PGK-Puro-IRES-GFP* retrovirus. Doubly infected cells were then selected using puromycin. In Figure 5H, double infection of *R26MER/MER* MEFs with pRetroX-*fbw7*-IRES-DsRedExpress and MSCV-*miR-92-PGK-Puro-IRES-GFP* were similarly performed. For all experiments with primary murine B-cells, bone marrow cells were cultured for 48 hr before retroviral infection and collected or analyzed 72 hr after infection. After 5 days in culture, the percentage of B220-positive cell is 100%. In Figure 3E, Figure 3—figure supplement 1, B-cells were infected with MSCV retrovirus containing a PGK-Puro-IRES-GFP cassette. FACS analysis was performed after gating on the GFP-positive population. In Figure 5A, the collected B-cells were infected with retrovirus containing SV40-CD4 cassette. Infected cells were purified with Human CD4 Micro-beads (130-045-101; Miltenyi Biotec) using MACS Purification Columns MS (130-042-201; Miltenyi Biotec).

The collection of normal and malignant B-cells in vivo
Normal mouse B-cells were isolated from the spleen or the bone marrow of 4- to 6-week-old C57B/6J mice, using CD19 Micro-Beads (Miltenyi Biotec) or by negative selection (Easysep 19754; STEMCELL). Similarly, premalignant *Eμ-myc* B-cells were extracted from the bone marrow of 5- to 6-week-old *Eμ-myc* transgenic mice. Malignant *Eμ-myc* B-cells were extracted from the lymph node tumors of terminal-stage *Eμ-myc* mice. In addition, the normal human B-cells from peripheral blood were FACS sorted from the peripheral blood of healthy donors.

Histopathology and immunotyping
Mouse tissue samples were fixed in formalin (SF100-4; Fisher), embedded in paraffin (AC41677-0020; Fisher), sectioned into 5 μm tissue samples, and stained with hematoxylin and eosin (7211 & 7111, Fisher). For caspase-3 (AF835, 1:200; R&D Systems), PCNA (MS-106P, 1:200; Lab Vision Corp.), and B220 (14-0452-85, 1:100;

eBioscience) detection, representative sections were deparaffinized and rehydrated in graded alcohols before subjected to antigen retrieval treatment with 10 mM sodium citrate buffer 10 min in a pressure cooker. Detection of antibody staining was carried out following standard procedures from the avidin-biotin immunoperoxidase methods. Diaminobenzidine (002014, Invitrogen) was used as the chromogen and hematoxylin as the nuclear counter stain. Quantitation of apoptosis was evaluated by counting the number of starry sky foci in three fields (40X) from seven representative animals of each genotype, as well as by counting the number of caspase-3 positive cells in three fields (40X) from five representative animals of each genotype.
To determine the cell surface markers of the lymphoma cells harvested from the animals, cells were resuspended in 10% FBS/PBS to reach a concentration of 107 cells/ml. 20 μl of this cell suspension was stained with antibodies diluted in 10% FBS/PBS for 1 hr. Subsequently, cells were washed with 2% FBS/PBS and resuspended in 10% FBS/PBS for flow cytometry analysis. Antibodies used for FACS analyses include PE anti-mouse IgM (12-5790, 1:200; eBioscience), APC-Cy7 anti-mouse B220 (552094, 1:200; BD Pharmingen), APC-Cy7 anti-mouse CD4 (552051, BD Pharmingen, 1:200), PE anti-mouse CD8 (553032, 1:200; BD Pharmingen), PE anti-mouse CD25 (553866, 1:200; BD Pharmingen), and APC anti-mouse CD19 (115511, 1:100; Biolegend).

Apoptosis assays and proliferation assays
Subconfluent MSCV- or *miR-92*-infected *R26MER/MER* MEFs were induced and serum starved by incubating the cells with 100 nM of 4-hydroxytamoxifen (H6278; Sigma) in DMEM with 0.2% fetal bovine serum for 12–24 hr before harvesting the cells for apoptosis analyses using APC-Annexin V antibody (550475, 1:50; BD Pharmingen) and 7AAD staining solution (559925; BD Pharmingen). To evaluate the apoptotic effects of *miR-92* in our adoptive transfer model in vivo, we collected premalignant *Eμ-myc* B-cells from spleen or bone marrow of well-controlled *Eμ-myc/92* and *Eμ-myc/MSCV* mice at 5 weeks after adoptive transfer and measured the extent of apoptosis by FACS. Apoptosis in GFP-positive B220-positive premalignant B-cells was measured using the Caspase Detection Kit (Calbiochem, Red-VAD-FMK) following the manufacturer's instructions. To quantitate cell proliferation, 10 μM of BrdU was used to label primary B-cells for 4 hr and MEFs for 30 min. The percentage of BrdU-positive cells was determined using the Flow BrdU kit (552598; BD Pharmingen).

Real time PCR and western analyses
TaqMan MicroRNA Assays (Applied Biosystems) were used to measure the level of mature miRNAs, including *miR-17, 18, 19a, 20, 19b*, and *92* (4427975; ABI). mRNA level for *perp* (GACCCCAGATGCTTGTTTTC, GGGTTATCGTGAAGCCTGAA), *noxa* (GGAGTGCACCGGACATAACT, TGAGCACACTCGTCCTTCAA), *puma* (GCGGCGGAGACAAGAAGA, AGTCCCATGAAGAGATTGTAC), p21 (ACGGTGGAACTTTGACTTCG, CAGGGCAGAGGAAGTACTGG), *bax* (GTTTCATCCAGGATCGAGCAG, CCCCAGTTGAAGTTGCCATC), *mdm2* (CTCTGGACTCGGAAGATTACAGCC, CCTGTCTGATAGACTGTCACCCG), *p53* (AACCGCCGACCTATCCTTAC, TCTTCTGTACGGCGGTCTCT), *ccnb1* (AAGGTGCCTGTGTGTGAACC, GTCAGCCCCATCATCTGCG), *ccnb2* (GCCAAGAGCCATGTGACTATC, CAGAGCTGGTACTTTGGTGTTC), *cdc20*

(AGACCACCCCTAGCAAACCT, GACCAGGCTTTCTGATGCTC), *cdc25b* (ATTCTCGTCTGAGCGTGGAC, GCTGTGGGAAGAACTCCTTG), *fbw7* (CGGCTCAGACTTGTCGATACT, CTTGATGTGCAACGGTTCAT), *gtse1* (GCTTTGCCTGTGAGAGGAAG, CACTCTGGGATCCCTTTTCA), *bid* (CTGCCTGTGCAAGCTTACTG, GTCTGGCAATGTTGTGGATG), *pten* (CACAATTCCCAGTCAGAGGCG, GCTGGCAGACCACAAACTGAG), *bim* (ACCACTATCTCAGTGCAATGGCTTCC, CGGTAATCATTTGCAAACACCCTCCTTG), *cdk4* (TGGTACCGAGCTCCTGAAGT, GTCGGCTTCAGAGTTTCCAC), *c-myc* (GTGCTGCATGAGGAGACACCGCC, GCCCGACTCCGACCTCTTGGC), *Pirh2* (TGCAGTGCATCAACTGTGAA, CAAACAGGTGGCAAATACTGC), *Ppp2r5d* (CCGTGATGTTGTCACTGAGG, ACTCTGCTCCTGTGGGATTC), *Dyrk2* (CCAGCAACGCTACCACTACA, AACAGCTGCTGAACCTGGAT), *Romo1* (ATTCGGAGTGAGACGTCGAG, TGACGAAGCCCATCTTCAC), *Pak2* (TTGGCTTTGATGCTGTTACG, CACTGCCTGAGGGTTCTTCT), *Trpc4ap* (CGCAAATGTCCTTCCTCTTC, GCCAGCATCAGGATTACCAG), and *Axin1* (AGGACGCTGAGAAGAACCAG, CTGCTTCCTCAACCCAGAAG) were determined using real time PCR analyses with SYBR (KK4605; Kapa Biosystems). *Actin* (GATCTGGCACCACACCTTCT, GGGGTGTTGAAGGTCTCAAA) was used as a normalization control in all our real time PCR analysis with SYBR. U6 snRNA assay (4427975; ABI) was used as a normalization control in all our TaqMan MicroRNA Assays (Applied Biosystems).
For western analyses, all samples were directly collected into Laemmli buffer. p53 (1C12; Cell Signaling), Arf (5-C3-1; Novus), and c-Myc (1472-1; Epitomics) antibodies were used at 1:1000 dilution. FLAG (M2; Sigma) and Tubulin (12G10) were used at 1:2500 dilution. HRP conjugated secondary antibodies (Santa Cruz Biotechnology, sc-2004 sc-2005 and sc-2006) were used at 1:5000.

Microarray analyses
Three independent *R26MER/MER* MEF lines were infected by MSCV vector alone or by MSCV vector encoding *miR-92*. These MEFs were induced and serum starved by incubating the cells with 100 nM of 4-hydroxytamoxifen (H6278; Sigma) in DMEM with 0.2% fetal bovine serum for 12 hr before harvesting the cells for RNA preparation. Total RNAs were prepared using Trizol (15596018; Invitrogen), and subjected to microarray analysis using Affymetrix chip Mouse 430_2. To identify differentially expressed genes that could be regulated by *miR-92*, we used gcRMA in the bioconductor package (Wu et al., 2004) and SAM (Significance Analysis of Microarrays) (Tusher et al., 2001) for statistical analysis of our microarray data. Gene expression signals were estimated from the probe signal values in the CEL files using statistical algorithm gcRMA. This data processing at the probe level includes background signal subtraction and quantile normalization to facilitate the comparison among microarrays. SAM was then used to identify the genes with significant expression level alterations between *miR-92* overexpressing MEFs and the control MEFs. The genes with at least 1.5-fold expression level change and FDR <1% were regarded as differentially expressed genes. Pathway analyses were performed on upregulated and downregulated genes using the KEGG database (Dennis et al., 2003).

Xenopus embryo apoptosis assays

Xenopus laevis eggs were collected, fertilized, and embryos cultured by standard procedures. The *miR-19b* mimics were produced from the annealing products of 5′UGUGCAAAUCCAUGCAAAACUGA3′ and 5′AGUUUUGCAGGUUUGCAUCCAUU3′ (IDT).
The *miR-17* mimics were produced from the annealing products of 5′CAAAGUGCUUACAGUGCAGGUAGU3′ and 5′UACUGCAGUGAAGGCACUUGUAG3′(IDT).
The *miR-18* mimics were produced from the annealing products of 5′UAAGGUGCAUCUAGUGCAGAUAG3′ and 5′ACUGCCCUAAGUGCUCCUUCUG3′(IDT).
The *miR-19a* mimics were produced from the annealing products of 5′AGUUUUGCAUAGUUGCACUA3′ and 5′UGUGCAAAUCUAUGCAAAACUGA3′(IDT).
The *miR-20* mimics were produced from the annealing products of 5′UAAAGUGCUUAUAGUGCAGGUAG3′ and 5′ACUGCAUAAUGAGCACUUAAAGU3′(IDT).
The *miR-92* mimics were produced from the annealing products of 5′UAUUGCACUUGUCCCGGCCUG3′ and 5′AGGUUGGGAUUUGUCGCAAUGCU3′(IDT).
The annealing of miRNA mimics were performed by combining two complimentary RNA oligos at a stock concentration of 1 μg/μl, heating the oligos to 80°C for 1 min, and then cooling down to room temperature to allow duplexes to form. The same was done for generating the mutated *miR-19* mimics (*Mut-miR-19*), by annealing 5′UCAGGUAAUCCAUGCAAAACUGA3′ and 5′AGUUUUGCAGGUUACCUUCGAUU3′, and mutated *miR-92* mimics (*Mut-miR-92*) by annealing 5′UUAUCGACUUGUCCCGG3′ and 5′GGUUGGGAUUGGUUCGA 3′.
Xenopus embryos were injected into both cells at the two-cell stage with 2 ng of each RNA (Walker and Harland, 2009). The pcDNA3-*myc-AGO2* vector, kindly provided by Dr Greg Hannon, was cut using ScaI; and the synthetic *hAGO2* mRNAs were transcribed using mMessage mMachine T7 kit (Ambion). When indicated, a total of 0.5 ng *hAGO2* mRNA (Liu et al., 2004) was injected into two-cell stage embryos either alone or with 2 ng of each miRNA (Lund et al., 2011). The embryos were then treated with hydroxyurea (H8627; Sigma) at a final concentration of 5 mM from stage 3 until stage 10. Apoptotic embryos were scored as those containing any apoptotic cells based on morphological changes.

Luciferase assays

A luciferase reporter fused with the *fbw7* 3′UTR was kindly provided by Dr Hans-Guido Wendel (Mavrakis et al., 2011). In this psiCHECK-2 based reporter, the *fbw7* 3′UTR was cloned downstream of the *Renilla* luciferase reporter, and a separate *firefly* luciferase cassette was used as a transfection control. Because the two predicted *miR-92* binding sites are close to each end of the 3′UTR, we mutated the *miR-92* binding sites by PCR using the following primers:
3′UTR-Fbw7-Mut-Xho1-F (GATCTCGAGCAAGACGACTCTCTAAATCCAACTATTCTTT) and 3′UTR-Fbw7-

mut-Not1-R (ATGCGGCCGCAACACATTTAGTTATAAGAAAATAAAATTT). The PCR fragment was subsequently cloned into the XhoI and Not1 sites of the psiCHECK-2 vector. The reporter construct, together with 50 nM *miR-92* mimics, was transfected into *Dicer*-deficient Hct116 cells (Cummins et al., 2006), with transfection of *miR-17* or *miR-18* as negative controls. Luciferase activity of each construct was determined by dual luciferase assay (E19100; Promega) 48 hr post-transfection following the manufacturer's instructions. The *miR-17* mimics were produced by annealing 5′CAAAGUGCUUACAGUGCAGGUAGU3′ and 5′UACUGCAGUGAAGGCACUUGUAG3′. The *miR-18* mimics were produced by annealing 5′UAAGGUGCAUCUAGUGCAGAUAG3′ and 5′ACUGCCCUAAGUGCUCCUUCUG3′.
The *miR-92* mimics were produced by annealing 5′UAUUGCACUUGUCCCGGCCUG3′ and 5′AGGUUGGGAUUUGUCGCAAUGCU3′.

Fbw7α immunoprecipitation and western analyses
Because Fbxw7-substrate degradation was regulated in a cell-cycle-dependent manner, we used serum starvation synchronized MEFs to study Fbw7 regulation by *miR-92* during cell cycle progression. MEFs were made quiescent by serum starvation; then Fbw7 expression was examined following release into serum. Cells were lysed in NP-40 buffer supplemented with protease inhibitors. Lysates were normalized and immunoprecipitated with polyclonal anti-Fbw7 antibody kindly provided by Dr Bruce Clurman (Grim et al., 2008), followed by immunoblotting with polyclonal anti-Fbw7 antibody (A301-720A; Bethyl Laboratories). Wild-type and *FBW7−/−* Hct116 cells were used, respectively, as positive and negative controls.
The construction of the pFLAG-Fbw7α-3′UTR plasmid was previously described (Xu et al., 2010). The construct was transfected into the *Dicer*-deficient Hct116 cells together with 50 nM of *miR-92* mimics or siRNA against GFP as indicated. Anti-FLAG (M2; Sigma) antibody was used to detect the FLAG-Fbw7α by western blot 48 hr after transfection.

Cyclin E-dependent kinase assays
Cyclin E-CDK complexes were immunoprecipitated from MSCV or *miR-92* infected *Rosa26MER/MER* MEFs extracts using affinity-purified polyclonal antibody, provided by Dr Bruce Clurman (Minella et al., 2008). Cyclin E immunoprecipitates were then incubated with purified histone subunit H1 (Sigma) and (gamma-32P)ATP to measure cyclin E-dependent kinase activity. The anti-Grb2 monoclonal (BD Biosciences) antibody was used a normalization control.

Figure 1

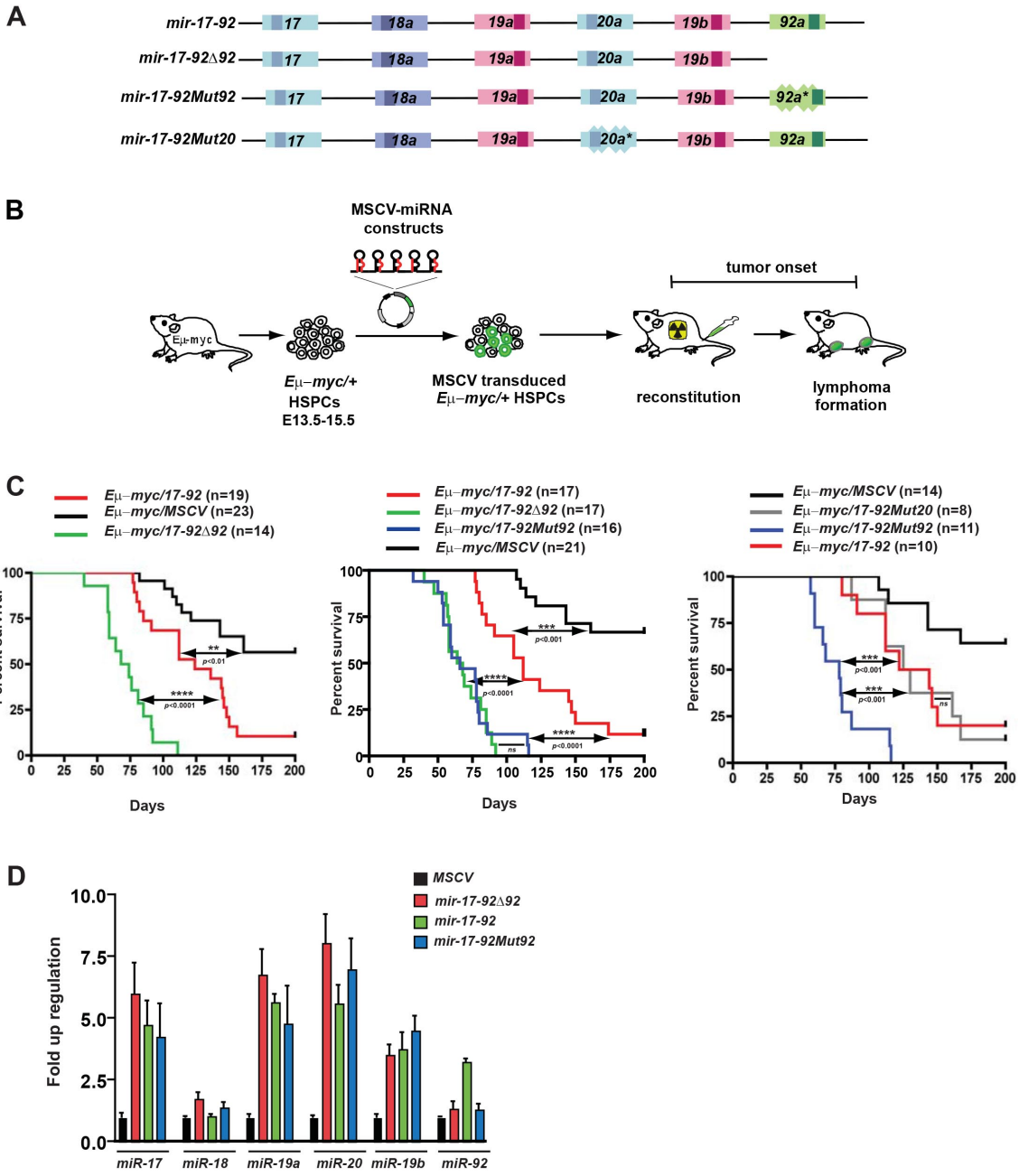
A
mir-17-92
17
18a
19a
20a
19b
92a
mir-17-92Δ92
mir-17-92Mut92
92a*
mir-17-92Mut20
20a*
B
MSCV-miRNA constructs
tumor onset
Eμ-myc
Eμ–myc/+ HSPCs E13.5-15.5
MSCV transduced Eμ–myc/+ HSPCs
reconstitution
lymphoma formation
C
Eμ–myc/17-92 (n=19)
Eμ–myc/MSCV (n=23)
Eμ–myc/17-92Δ92 (n=14)
Percent survival
Days
Eμ–myc/17-92 (n=17)
Eμ–myc/17-92Δ92 (n=17)
Eμ–myc/17-92Mut92 (n=16)
Eμ–myc/MSCV (n=21)
Eμ–myc/MSCV (n=14)
Eμ–myc/17-92Mut20 (n=8)
Eμ–myc/17-92Mut92 (n=11)
Eμ–myc/17-92 (n=10)
D
MSCV
mir-17-92Δ92
mir-17-92
mir-17-92Mut92
Fold up regulation
miR-17
miR-18
miR-19a
miR-20
miR-19b
miR-92

Figure 1. *miR-92* negatively regulates the *mir-17-92* oncogenic activity in the *Eμ-myc B-lymphoma* model.
(**A**) The gene structure of the *mir-17-92* polycistron and its mutated derivatives. Light colored boxes, pre-miRNAs; dark colored boxes, mature miRNAs. Homologous miRNA components are indicated by the same color. (**B**) Schematic representation of the adoptive transfer protocol using *Eμ-myc* hematopoietic stem and progenitor cells (HSPCs). *Eμ-myc/+* HSPCs were extracted from E13.5–E15.5 mouse embryos, infected with MSCV retroviral vectors overexpressing *mir-17-92* and its derivatives, and finally transplanted into lethally irradiated recipient mice. Lymphoma onset of the adoptive transferred mice was monitored to evaluate the oncogenic collaboration between c-Myc and a specific miRNA. (**C**) *miR-92* deficiency specifically accelerates the oncogenic activity of *mir-17-92* in the *Eμ-myc* model. Using the *Eμ-myc* adoptive transfer model, we compared the oncogenic effects between *mir-17-92* and *mir-17-92Δ92* and observed a significant acceleration of tumor onset in *Eμ-myc/mir-17-92Δ92* mice ($p<0.0001$, left). When the oncogenic effects of *mir-17-92, mir-17-92Δ92* and *mir-17-92Mut92* were compared in the same adoptive transfer model, *mir-17-92Δ92* and *mir-17-92Mut92* similarly accelerated *Eμ-myc*-induced lymphomagenesis compared to *mir-17-92* ($p<0.0001$ for both comparisons, middle). Deficiency of *miR-20* failed to affect the oncogenic cooperation between *mir-17-92* and *Eμ-myc*, having minimal effects on tumor onset (right). (**D**) The mutation of *miR-92* has minimal effects on the levels of the remaining *mir-17-92* components. *Eμ-myc* B-lymphoma cells were infected with MSCV retrovirus overexpressing *mir-17-92*, *mir-17-92*Δ92 and *mir-17-92Mut92* at an MOI (multiplicity of infection) of 1. Expression levels of *miR-17, 18a, 19a, 20a, 19b* and *92* were subsequently determined using Taqman miRNA assays. Error bars indicate standard deviation ($n = 3$). **p<0.01, ***p<0.001, ****p<0.0001.

Figure 1– figure supplement 1

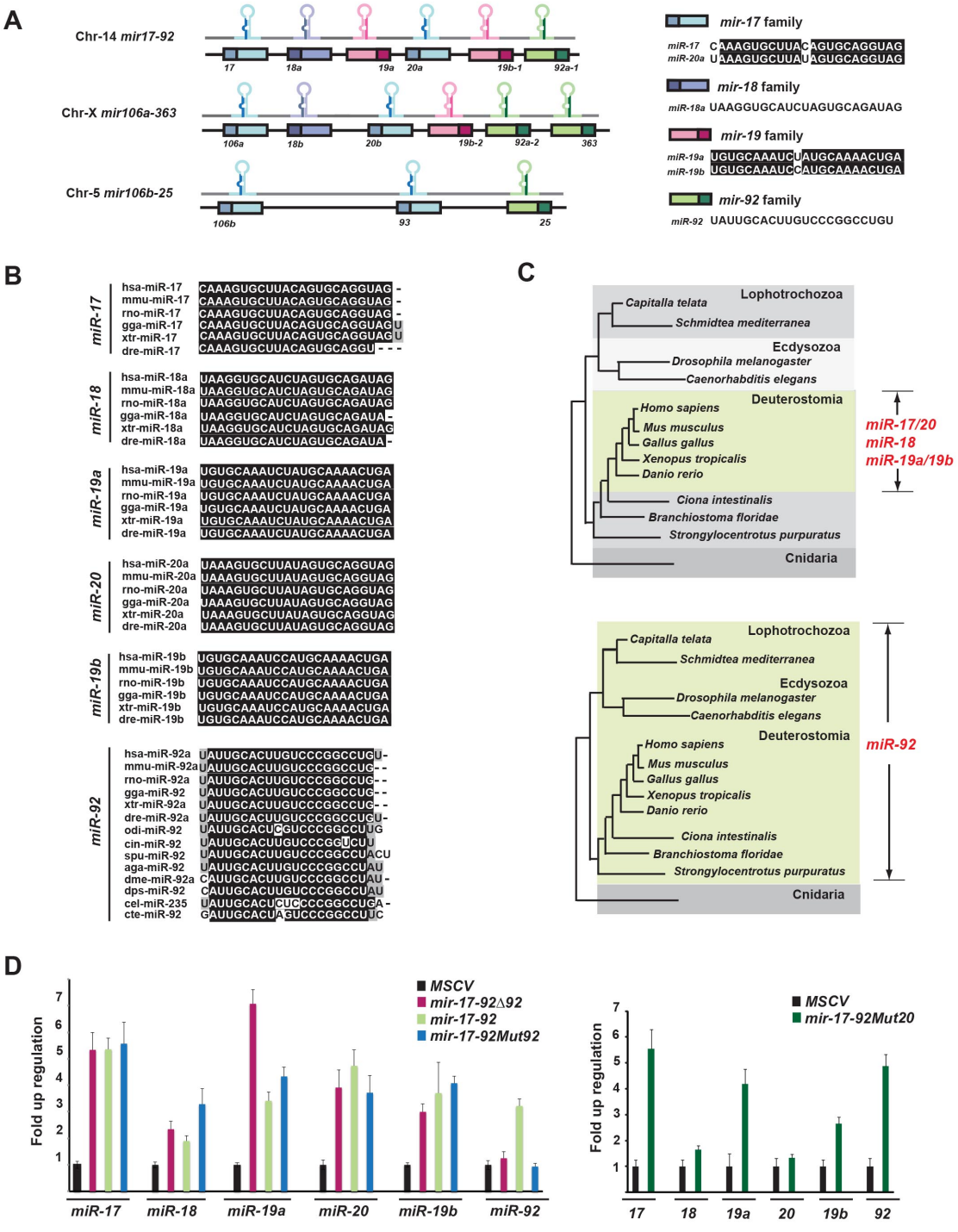

Figure 1 – supplement 1. Functional antagonism between *miR-19:miR-92* regulates the balance between proliferation and apoptosis.
(**A**) *miR-19* antagonizes the apoptotic effects of *miR-92* in vivo. *miR-92* overexpression enhanced apoptosis in premalignant *Eμ-myc* bone marrow B-cells in vivo, while co-expression of *miR-19* and *miR-92* as a dicistron (*mir-19b-92*) abolished this apoptotic effect (left three panels). A quantitative analysis of apoptosis by FACS was shown for three independent experiments (right). (**B**) *miR-19* has no effects on the level of c-Myc protein. While *miR-92* overexpression significantly enhanced the level of c-Myc in *R26MER/MER* MEFs, co-expression of *miR-19b* and *miR-92* did not reverse the increase in c-Myc expression. In addition, *miR-19b* expression alone did not impact the dosage of c-Myc protein. (**C**) *Xenopus fbw7* contains one predicted target site for *miR-92*. This predicted *miR-92* binding site is conserved between *Xenopus* and mouse.

Figure 2

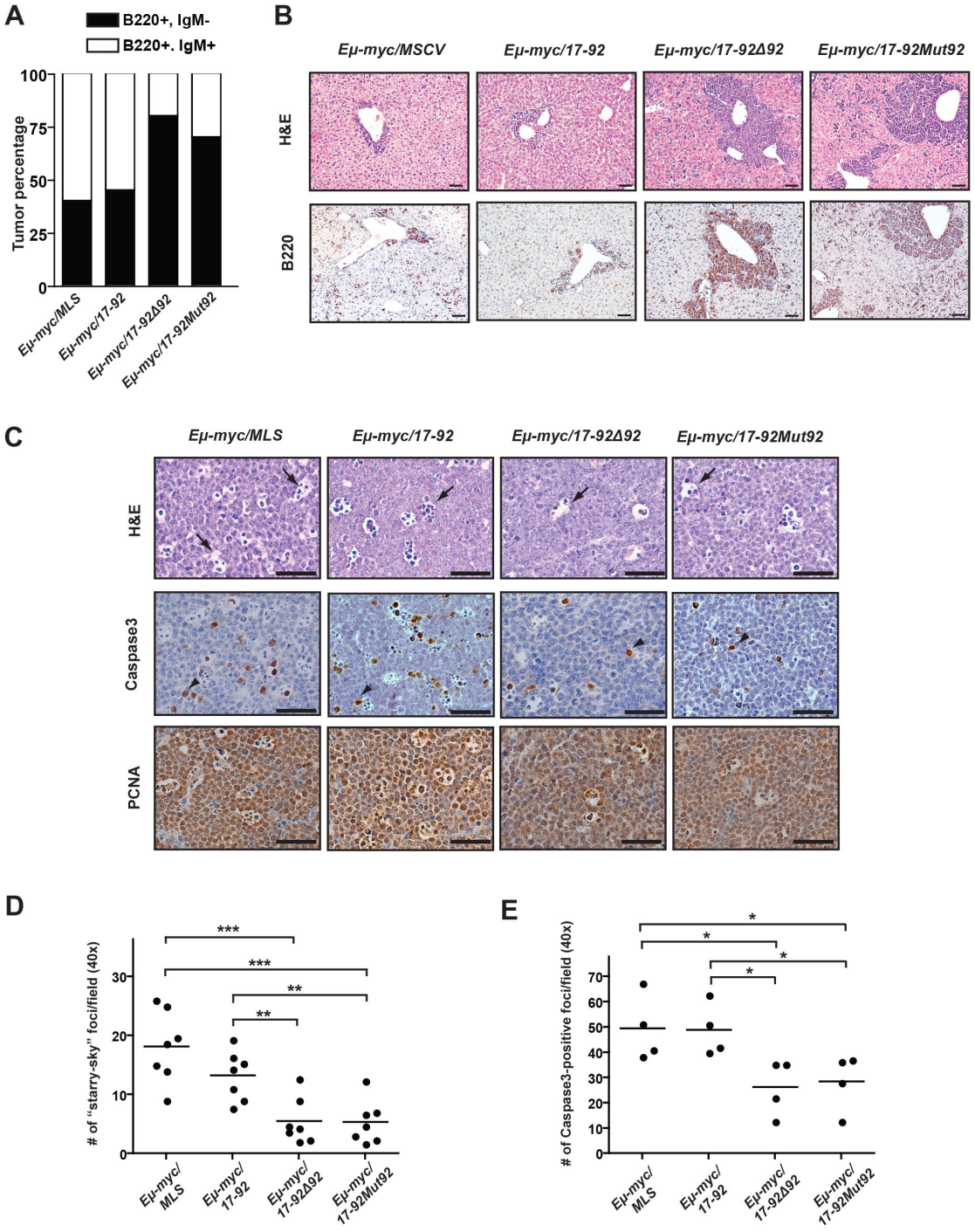
A
B220+, IgM-
B220+. IgM+
Tumor percentage
100
75
50
25
0
Eμ-myc/MLS
Eμ-myc/17-92
Eμ-myc/17-92Δ92
Eμ-myc/17-92Mut92
B
Eμ-myc/MSCV
Eμ-myc/17-92
Eμ-myc/17-92Δ92
Eμ-myc/17-92Mut92
H&E
B220
C
Eμ-myc/MLS
Eμ-myc/17-92
Eμ-myc/17-92Δ92
Eμ-myc/17-92Mut92
H&E
Caspase3
PCNA
D
of "starry-sky" foci/field (40x)
30
20
10
0
***
***
**
**
Eμ-myc/ MLS
Eμ-myc/ 17-92
Eμ-myc/ 17-92Δ92
Eμ-myc/ 17-92Mut92
E
# of Caspase3-positive foci/field (40x)
70
60
50
40
30
20
10
0
*
*
*
*
Eμ-myc/ MLS
Eμ-myc/ 17-92
Eμ-myc/ 17-92Δ92
Eμ-myc/ 17-92Mut92

Figure 2. The *miR-92* deficient *mir-17-92* cooperates with c-Myc to promote highly aggressive B-lymphomas.
(**A**) The percentage of IgM positive and IgM negative B-lymphomas was calculated for each genotype (*Eμ-myc/MSCV,* n = 10*; Eμ-myc/17-92,* n = 9; *Eμ-myc/17-92Δ92,* n = 10; *Eμ-myc/17-92Mut92,* n = 10). (**B**) The *Eμ-myc/17-92Mut92 and Eμ-myc/17-92Δ92* mice developed high grade B-lymphomas that were frequently disseminated into the liver. When compared to *Eμ-myc/MSCV* and *Eμ-myc/17-92* mice, *Eμ-myc/17-92Mut92 and Eμ-myc/17-92Δ92* lymphomas gave rise to more liver dissemination, as indicated by H&E and B220 staining. (**C**) *Eμ-myc/17-92Mut92* and *Eμ-myc/17-92Δ92* lymphomas exhibited a decreased apoptosis compared to *Eμ-myc/MSCV* or *Eμ-myc/17-92* lymphomas. Representative lymphomas were stained for H&E, cleaved caspase-3 and PCNA. Arrow, 'starry sky' feature of apoptotic lymphoma cells; arrowhead, apoptotic cells with positive staining for cleaved caspase-3; scale bar, 50 μm. (**D** and **E**) Apoptosis was quantitatively measured in representative lymphomas of each genotype using the 'starry sky' features (**D**) and cleaved caspase-3 staining (**E**). *$p<0.05$, **$p<0.01$, ***$p<0.001$.

Figure 3

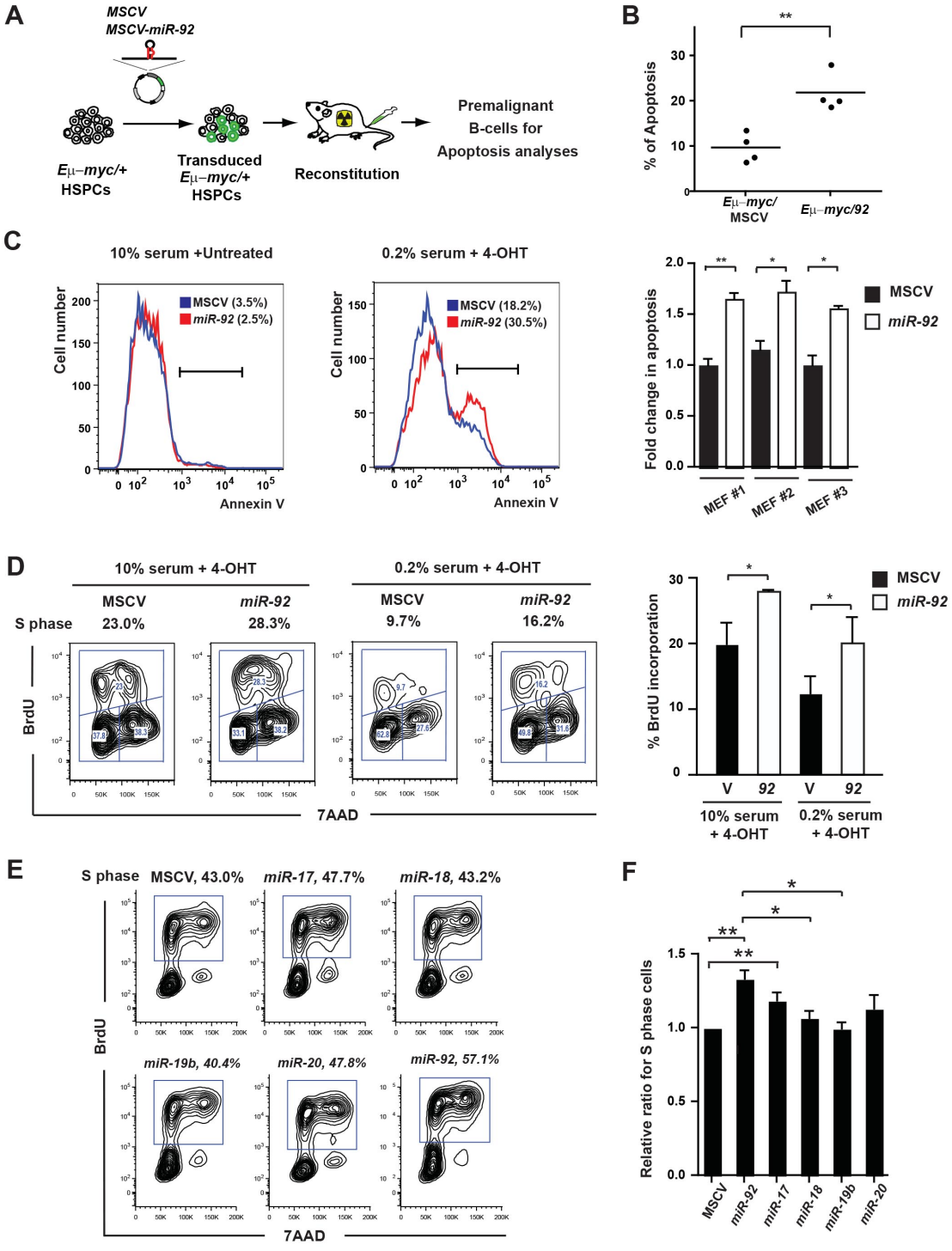
A
MSCV
MSCV-miR-92
Eμ–myc/+ HSPCs
Transduced Eμ–myc/+ HSPCs
Reconstitution
Premalignant B-cells for Apoptosis analyses
B
% of Apoptosis
Eμ–myc/ MSCV
Eμ–myc/92
C
10% serum +Untreated
0.2% serum + 4-OHT
Cell number
MSCV (3.5%)
miR-92 (2.5%)
MSCV (18.2%)
miR-92 (30.5%)
Annexin V
Fold change in apoptosis
MSCV
miR-92
MEF #1
MEF #2
MEF #3
D
10% serum + 4-OHT
0.2% serum + 4-OHT
MSCV
miR-92
S phase
23.0%
28.3%
9.7%
16.2%
BrdU
7AAD
% BrdU incorporation
V
92
10% serum + 4-OHT
0.2% serum + 4-OHT
E
S phase
MSCV, 43.0%
miR-17, 47.7%
miR-18, 43.2%
miR-19b, 40.4%
miR-20, 47.8%
miR-92, 57.1%
BrdU
7AAD
F
Relative ratio for S phase cells
MSCV
miR-92
miR-17
miR-18
miR-19b
miR-20

Figure 3. *miR-92* enhances both c-Myc-induced apoptosis and c-Myc-induced proliferation.
(**A**) The schematic representation of the adoptive transfer model to evaluate the *miR-92* effects on the *Eμ-myc* premalignant B-cells in vivo. (**B**) *miR-92* overexpression enhances the apoptotic response in the premalignant *Eμ-myc* B-cells in vivo. Using the *Eμ-myc* adoptive transfer model, we generated well-controlled *Eμ-myc/MSCV* and *Eμ-myc/92* mice reconstituted from donor matched *Eμ-myc* HSPCs. Premalignant *Eμ-myc* splenic B-cells were isolated from the *Eμ-myc/MSCV* and *Eμ-myc/92* mice 6 weeks after reconstitution. The in vivo apoptosis was measured by the level of caspase activation using Red-VAD-FMK, a fluorescently labeled caspase inhibitor that specifically bound to cleaved caspases. The percentage of *Eμ-myc* B-cells positive for cleaved caspases was shown for four independent experiments. (**C**) Enforced *miR-92* expression in *R26MER/MER* MEFs significantly enhanced c-Myc-induced apoptosis. *miR-92* overexpressing and the control *R26MER/MER* MEFs were serum starved, and the MycERT2 transgene was activated by 4-OHT treatment. The level of apoptosis of each MEF was measured using Annexin V staining before (left) and after (middle) 4-OHT treatment and serum starvation. Quantification of c-Myc-induced apoptosis was performed in three independent MEF lines that overexpressed MSCV or *miR-92* (right panel, error bars represent SEM). (**D**) Enforced *miR-92* expression in *R26MER/MER* MEFs significantly enhanced c-Myc-induced proliferation. Proliferative effects of *miR-92* was measured by BrdU incorporation in MycERT2 activated *R26MER/MER* MEFs. *miR-92* cooperated with c-Myc to promote BrdU incorporation in both 10% (left) and 0.2% (middle) serum culture conditions. Quantification of BrdU incorporation was performed in two independent experiments (right). (**E**) *miR-92* is a potent *mir-17-92* component to promote primary B-cell proliferation. The proliferative effects of all *mir-17-92* miRNAs were measured individually in primary B-cells using BrdU incorporation. (**F**) The quantification of BrdU incorporation in experiments described in (**E**) was performed in four independent experiments. Error bars represent standard deviation, *$p<0.05$, **$p<0.01$.

Figure 3–figure supplement 1

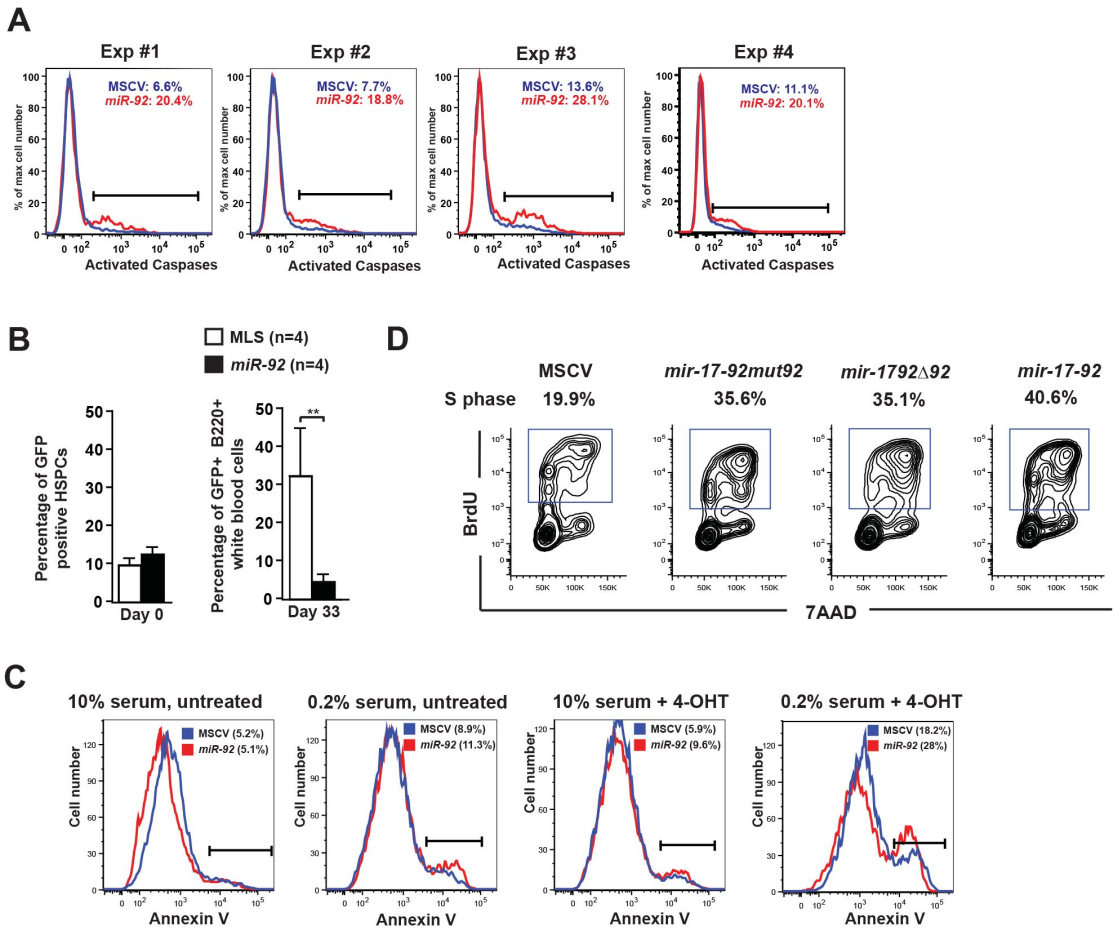

Figure 3 - supplement 1. *miR-92* enhances c-Myc-induced apoptosis both in vitro and in vivo.

(**A**) *miR-92* enhances the apoptotic response in the premalignant *Eμ-myc* B-cells in vivo. Using the *Eμ-myc* adoptive transfer model, we generated well-controlled *Eμ-myc/MSCV* and *Eμ-myc/92* mice that were reconstituted from the same *Eμ-myc* HSPCs. The in vivo apoptosis was measured by the level of caspase activation 6 weeks after the transplantation. The percentage of *Eμ-myc* B-cells positive for cleaved caspases was shown for four independent experiments. (**B**) *miR-92* infected, premalignant *Eμ-myc* B-cells is significantly depleted in the *Eμ-myc* adoptive transfer model. We generated well-controlled *Eμ-myc*/MSCV and *Eμ-myc*/92 mice reconstituted from the same *Eμ-myc* HSPCs. We measured the percentage of retrovirally infected cells (GFP+) before reconstitution (left), and demonstrated similar infection efficiency in *Eμ-myc*/MSCV and *Eμ-myc*/92 mice. At day 33 post adoptive transfer, we isolated white blood cells from the peripheral blood of these mice, and measured the percentage of retrovirally infected, *Eμ-myc* B-cells (B-220-positive; GFP-positive cells) using FACS. Error bars indicate standard deviation, n = 4, **p<0.01. (**C**) Enforced *miR-92* expression in *R26MER/MER* MEFs significantly enhanced c-Myc-induced apoptosis. The *miR-92* effect was most evident when the infected *R26MER/MER* MEFs were serum starved and treated with 4-OHT. (**D**) *miR-92* is required for the potent proliferative effect of *mir-17-92* in primary B-cells. *miR-92* deficient *mir-17-92* miRNA polycistrons exhibited a reduced BrdU incorporation in primary B-cell culture in vitro.

Figure 4

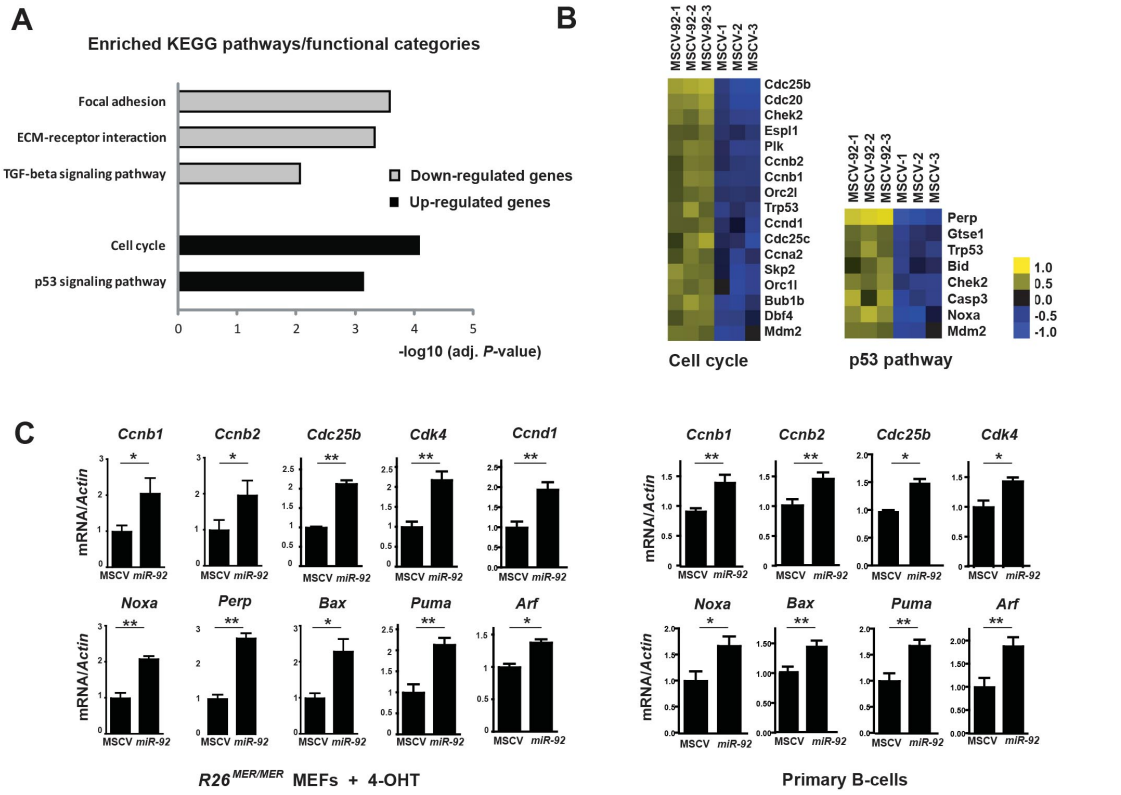
A
Enriched KEGG pathways/functional categories
Focal adhesion
ECM-receptor interaction
TGF-beta signaling pathway
Cell cycle
p53 signaling pathway
Down-regulated genes
Up-regulated genes
-log10 (adj. P-value)
B
MSCV-92-1
MSCV-92-2
MSCV-92-3
MSCV-1
MSCV-2
MSCV-3
Cdc25b
Cdc20
Chek2
Espl1
Plk
Ccnb2
Ccnb1
Orc2l
Trp53
Ccnd1
Cdc25c
Ccna2
Skp2
Orc1l
Bub1b
Dbf4
Mdm2
Cell cycle
Perp
Gtse1
Trp53
Bid
Chek2
Casp3
Noxa
Mdm2
p53 pathway
1.0
0.5
0.0
-0.5
-1.0
C
Ccnb1
Ccnb2
Cdc25b
Cdk4
Ccnd1
Noxa
Perp
Bax
Puma
Arf
mRNA/Actin
MSCV
miR-92
R26 MER/MER MEFs + 4-OHT
Primary B-cells
D
R26 MER/MER MEFs
#1
#2
MSCV
miR-92
Arf
p53
Tub
Primary B-cells
E
MSCV
MSCV-shp53
miR-92: 23.3%
MSCV: 14.4%
miR-92: 10.7%
MSCV: 8.7%
% of max cell number
AnnexinV
% Annexin V-positive cells
Shp53
4OHT
Serum (%)
F
noxa
perp
mdm2
noxa/Actin
perp/Actin
mdm2/Actin
ns

Figure 4. *miR-92* induces apoptosis through the activation of the p53 pathway. (**A**) The genes upregulated by *miR-92* were enriched for the cell cycle pathway and the *p53* pathway. Microarray analyses compared gene expression profiles of serum starved and 4-OHT treated *R26MER/MER* MEFs overexpressing either *miR-92* or a control MSCV vector (n = 3). The differentially expressed genes were defined as those with at least 1.5-fold expression level change using SAM (Significance analysis of microarrays, false discovery rate <1%). Pathway analyses were performed on upregulated and downregulated genes using the KEGG database. (**B**) The heatmaps of the *miR-92* upregulated genes enriched for the cell cycle and p53 pathways. (**C**) Components of the cell cycle and p53 pathways were upregulated upon *miR-92* overexpression in both MEFs (left) and primary B-cells (right). The quantitation of gene expression was performed using real time PCR. (**D**) *miR-92* overexpression induces the accumulation of Arf and p53 proteins in MEFs and primary B-cells from bone marrow. Western analyses were performed on the *R26MER/MER* MEFs (left) and primary B-cells (right) that overexpressed *miR-92* or a control MSCV vector in two independent experiments. The infected *R26MER/MER* MEFs were assayed at 6 hr after serum starvation and 4-OHT treatment; the infected primary B-cells were collected 72 hr post infection. (**E**) The apoptotic effect of *miR-92* requires an intact p53 pathway. We infected *R26MER/MER* MEFs with two MSCV retrovirus, MSCV-p53shRNA and MSCV-92, to obtain doubly infected cells. Knocking down *p53* in *R26MER/MER* MEFs abolished the ability of *miR-92* to enhance c-Myc-induced apoptosis, as measured by Annexin V staining (two left panels). The percentage of apoptotic MEFs of each experimental condition was quantitatively measured (right). (**F**) The induction of the p53 pathway components by *miR-92* is dependent on an intact p53. Knocking down *p53* in *R26MER/MER* MEFs abolished the ability of *miR-92* to induce pro-apoptotic p53 targets and other canonical p53 targets, including *noxa*, *perp* and *mdm2*. Error bars represent standard deviation, *p<0.05, **p<0.01, ***p<0.001.

Figure 4–figure supplement 1

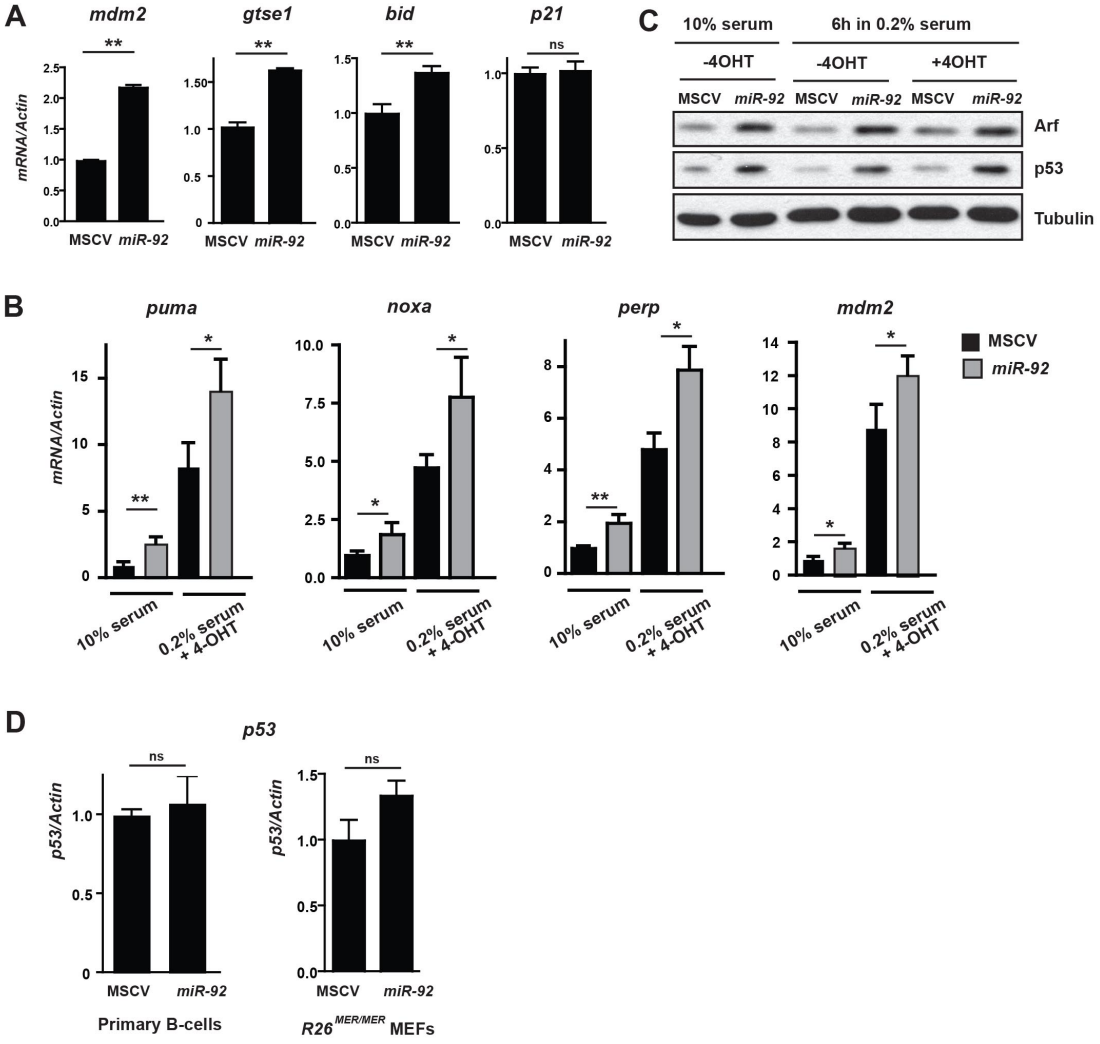

Figure 4 - supplement 1. *miR-92* overexpression triggers the activation of the p53 pathway.
(**A**) *miR-92* overexpression in *R26MER/MER* MEFs induced several p53 target genes in addition to those described in Figure 3C, including *mdm2*, *Gtse1* and *Bid,* but not *p21*. (**B**) Induction of p53 targets by *miR-92* in *R26MER/MER* MEFs with and without MycERT2 activation. (**C**) *miR-92* overexpression alone enhanced Arf and p53 protein level in *R26MER/MER* MEFs with and without 4-OHT treatment. (**D**) *miR-92* overexpression did not affect p53 mRNA levels in either primary B-cells or in *R26MER/MER* MEFs. Error bars indicate standard deviation, n = 3, *p<0.05; **p<0.01.

Figure 5

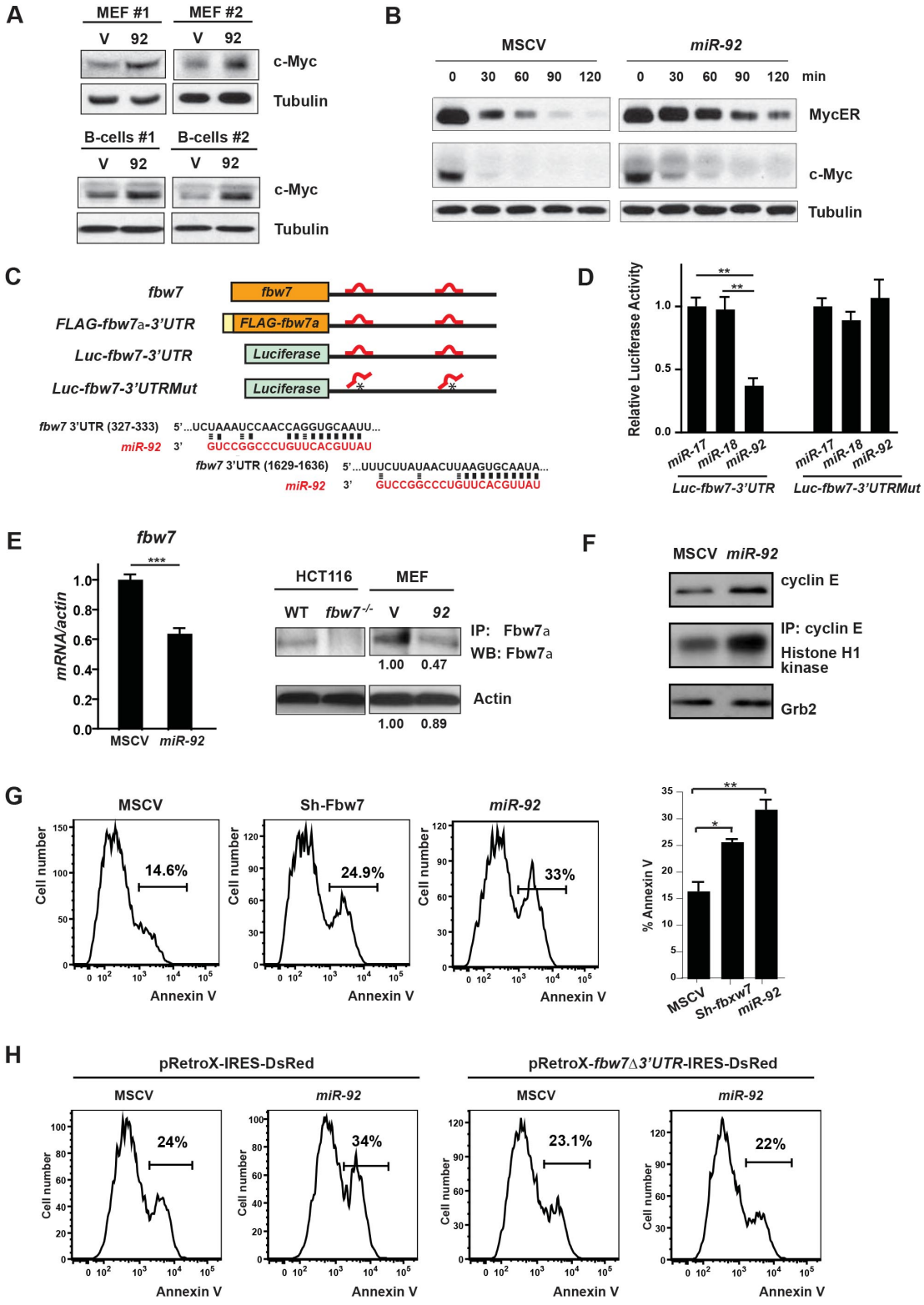
A
MEF #1
MEF #2
V 92
V 92
c-Myc
Tubulin
B-cells #1
B-cells #2
V 92
V 92
c-Myc
Tubulin
B
MSCV
miR-92
0 30 60 90 120
0 30 60 90 120 min
MycER
c-Myc
Tubulin
C
fbw7
FLAG-fbw7a-3'UTR
Luc-fbw7-3'UTR
Luc-fbw7-3'UTRMut
Luciferase
fbw7 3'UTR (327-333) 5'...UCUAAAUCCAACCAGGUGCAAUU...
miR-92 3' GUCCGGCCCUGUUCACGUUAU
fbw7 3'UTR (1629-1636) 5'...UUUCUUAUAACUUAAGUGCAAUA...
miR-92 3' GUCCGGCCCUGUUCACGUUAU
D
Relative Luciferase Activity
1.0
0.5
0.0
**
**
miR-17 miR-18 miR-92
miR-17 miR-18 miR-92
Luc-fbw7-3'UTR
Luc-fbw7-3'UTRMut
E
fbw7
***
mRNA/actin
1.0 0.8 0.6 0.4 0.2 0.0
MSCV miR-92
HCT116
MEF
WT fbw7-/-
V 92
IP: Fbw7a
WB: Fbw7a
1.00 0.47
Actin
1.00 0.89
F
MSCV miR-92
cyclin E
IP: cyclin E
Histone H1 kinase
Grb2
G
MSCV
Sh-Fbw7
miR-92
Cell number
14.6%
24.9%
33%
Annexin V
% Annexin V
**
*
MSCV
Sh-fbxw7
miR-92
H
pRetroX-IRES-DsRed
pRetroX-fbw7Δ3'UTR-IRES-DsRed
MSCV
miR-92
MSCV
miR-92
Cell number
24%
34%
23.1%
22%
Annexin V

Figure 5. *miR-92* promotes the accumulation of c-Myc protein through repressing Fbw7.

(**A**) *miR-92* enhances the accumulation of c-Myc protein in synchronized *R26MER/MER* MEFs (upper), as well as primary B-cells (lower). The *miR-92* overexpression and the control *R26MER/MER* MEFs were synchronized by serum starvation and were collected 12 hr after being released into serum culture conditions to determine the c-Myc protein level. This synchronization approach in *R26MER/MER* MEFs has provided us with the most consistent measurement for c-Myc protein level, because it is regulated in a cell-cycle-dependent manner. (**B**) *miR-92* overexpression decreases the turnover of c-Myc protein. Serum-synchronized *R26MER/MER* MEFs that overexpress either *miR-92* or the control MSCV vector were released into the serum for 6 hr, treated with cycloheximide, collected at the indicated time points, then analyzed by western blot to determine the levels of MycER and the endogenous c-Myc protein. (**C**) Schematic representation of the two *miR-92* binding sites in the murine *fbw7* 3′UTR. Additionally, a luciferase reporter and a *FLAG* tagged *fbw7* ORF were each placed upstream of a wild-type *fbw7* 3′UTR, or a mutated *fbw7* 3′UTR that abolished the predicted *miR-92* binding. (**D**) The expression of *Luc-fbw7-3′UTR* was specifically repressed by *miR-92* in *Dicer*−/− HCT116, while mutations of the two putative *miR-92* binding sites within the *fbw7-3′UTR (Luc-fbw7-*3′UTRMut) abolished this repression. (**E**) The endogenous *fbw7* gene was downregulated by *miR-92* post-transcriptionally. Both the endogenous *fbw7* mRNA (left) and the endogenous Fbw7 protein (right) were repressed upon *miR-92* overexpression in *R26MER/MER* MEFs. Due to the lack of a proper antibody to detect endogenous Fbw7 in regular western analysis, we demonstrated the downregulation of endogenous Fbw7 by *miR-92* using immunoprecipitation followed by immunoblotting with a polyclonal anti-Fbw7 antibody. (**F**) *miR-92* enhances the accumulation of Cyclin E protein. Overexpression of *miR-92* increased the accumulation of Cyclin E protein, which was further confirmed by the increased Cyclin E-dependent kinase activity. (**G**) The knockdown of *fbw7* resembles the effect of *miR-92* to enhance c-Myc-induced apoptosis. Knocking down *fbw7* in *R26MER/MER* MEFs enhanced c-Myc-induced apoptosis, partially recapitulating the phenotype caused by *miR-92* overexpression. Apoptosis was quantitatively measured by Annexin V staining in two independent lines of *R26MER/MER* MEFs upon serum starvation and 4-OHT treatment. (**H**) Overexpression of *fbw7* abolished the apoptotic effects of *miR-92* in *R26MER/MER* MEFs. *R26MER/MER* MEFs were doubly infected by pRetro-*fbw7αΔ3′UTR*-IRES-dsRed and MSCV-*miR-92*. The c-Myc-induced apoptosis was quantitatively measured by Annexin V staining in doubly infected *R26MER/MER* MEFs upon serum starvation and 4-OHT treatment. Error bars represent standard deviation). *$p<0.05$; **$p<0.01$.

Figure 5–figure supplement 1

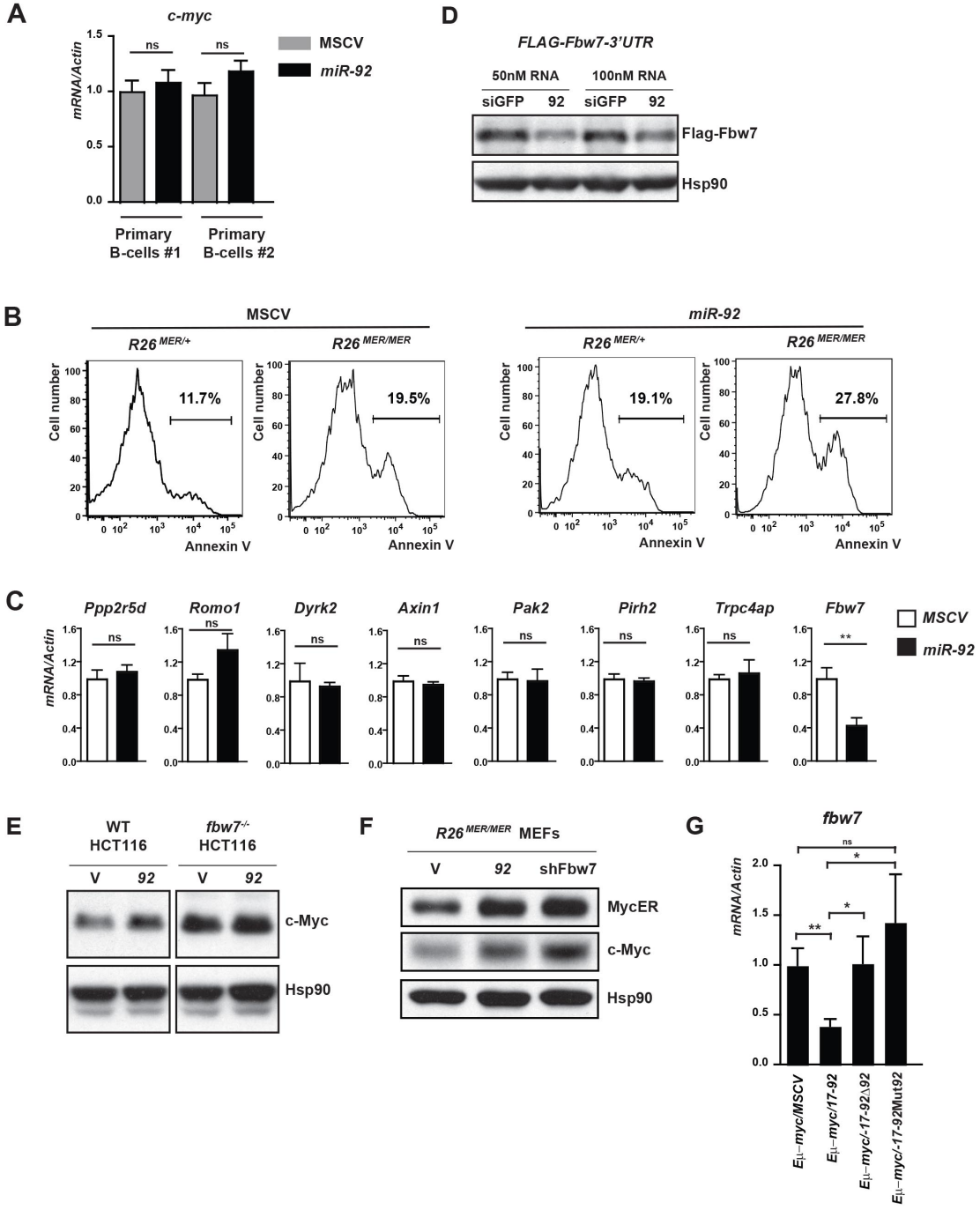

Figure 5 - supplement 1. *miR-92* overexpression enhances c-Myc protein level by repressing Fbw7.
(**A**) *miR-92* overexpression did not affect *c-myc* mRNA levels in two independent primary B-cells. (**B**) The c-Myc dosage determines the degree of c-Myc-induced apoptosis in *R26MER/MER* MEFs. When *R26MER/MER* MEFs were compared with *R26MER/+* MEFs, a twofold increase in the MycERT2 dosage significantly enhanced the c-Myc-induced apoptotic response upon serum starvation. This effect was observed in *R26MER/MER* MEFs either with or without *miR-92* overexpression. (**C**) Negative regulators of c-Myc that contain a putative *miR-92* binding site(s) were screened for *miR-92*-mediated repression in *R26MER/MER* MEFs that overexpress *miR-92* or a control MSCV vector. Only *fbw7* exhibited a *miR-92*–mediated repression. (Error bars indicate standard deviation, n = 3, **p<0.01). (**D**) The expression of *FLAG-fbw7*-3′UTR was significantly repressed by *miR-92* in *Dicer−/−* HCT116 cells. (**E**) *fbw7* is downregulated in *Eμ-myc* lymphomas that overexpress *miR-92*. A panel of *Eμ-myc/MSCV* (n = 9), *Eμ-myc/17-92* (n = 7), *Eμ-myc/17-92Δ92* (n = 6) and *Eμ-myc/17-92Mut92* (n = 5) lymphomas were compared for their expression level of endogenous *fbw7*. *Eμ-myc/17–92* lymphomas exhibited a specific decrease of *fbw7* compared to the other genotypes, possibly due to the *miR-92* overexpression. (**F**) The c-MYC upregulation by *miR-92* requires an intact *fbw7*. The effect of *miR-92* to upregulate c-MYC protein level was observed in wild-type Hct116 cells, but largely absent in *FBW7−/−* Hct116 cells. (**G**) *fbw7* knockdown by RNAi in *R26MER/MER* MEFs recapitulated the c-Myc upregulation by *miR-92*. (**H**) *fbw7* expression level in *R26MER/MER* MEFs infected with pRetroX-*fbw7*-IRES-DsRedExpress. Error bars indicate standard deviation, *p<0.05; **p<0.01.

Figure 6

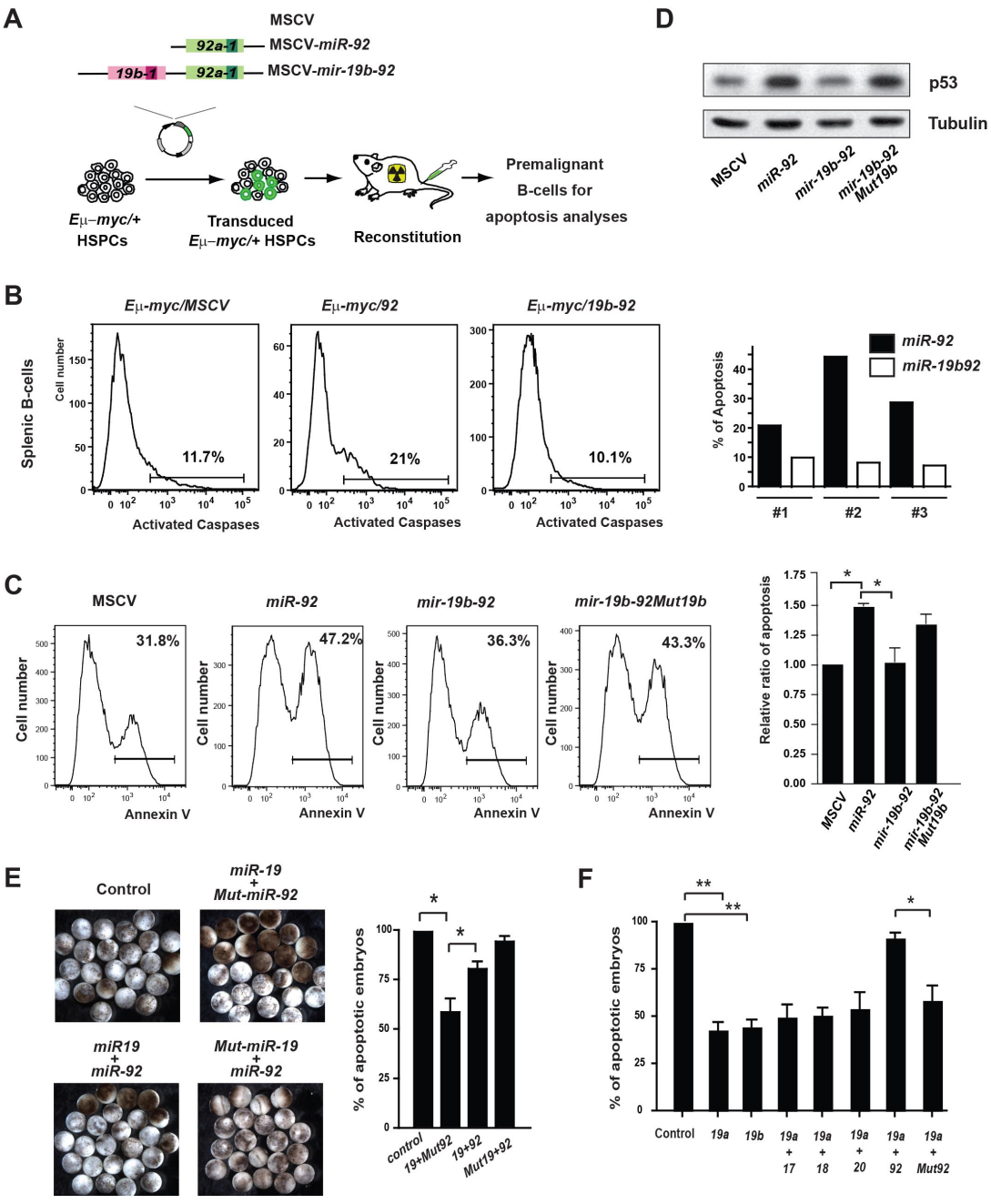
A
MSCV
92a-1
MSCV-miR-92
19b-1
92a-1
MSCV-mir-19b-92
Eμ–myc/+ HSPCs
Transduced Eμ–myc/+ HSPCs
Reconstitution
Premalignant B-cells for apoptosis analyses
D
p53
Tubulin
MSCV
miR-92
mir-19b-92
mir-19b-92 Mut19b
B
Eμ-myc/MSCV
Eμ-myc/92
Eμ-myc/19b-92
Splenic B-cells
Cell number
11.7%
21%
10.1%
Activated Caspases
% of Apoptosis
miR-92
miR-19b92
#1
#2
#3
C
MSCV
miR-92
mir-19b-92
mir-19b-92Mut19b
31.8%
47.2%
36.3%
43.3%
Cell number
Annexin V
Relative ratio of apoptosis
E
Control
miR-19 + Mut-miR-92
miR19 + miR-92
Mut-miR-19 + miR-92
% of apoptotic embryos
control
19+Mut92
19+92
Mut19+92
F
% of apoptotic embryos
Control
19a
19b
19a + 17
19a + 18
19a + 20
19a + 92
19a + Mut92

Figure 6. The antagonistic interaction between *miR-19* and *miR-92* regulates the balance between proliferation and apoptosis.
(**A**) The schematic representation of the *Eμ-myc* adoptive transfer model to evaluate the functional interaction between *miR-92* and *miR-19* in vivo. Light colored boxes, pre-miRNAs; dark colored boxes, mature miRNAs. (**B**) *miR-19* antagonizes the apoptotic effects of *miR-92* in vivo. *miR-92* overexpression in the *Eμ-myc* adoptive transfer model enhanced apoptosis in premalignant *Eμ-myc* splenic B-cells, while the *mir-19b-92* dicistron expression abolished this apoptotic effect (left three panels). A quantitative analysis of apoptosis by FACS was shown for three independent, well-controlled experiments (right). (**C**) *miR-19b* dampens the *miR-92*-induced apoptosis in MycERT2 activated *R26MER/MER* MEFs. *R26MER/MER* MEFs were infected by *miR-92*, *mir-19b-92*, *mir-19b-92Mut19b* and the MSCV control vector, and were subsequently serum starved and treated with 4-OHT to activate MycERT2. Apoptosis in these samples was measured quantitatively using Annexin V staining (left four panels). The extent of apoptosis induced by MSCV, *miR-92*, *mir-19b-92*, *mir-19b-92Mut19b* was normalized to that of MSCV infected *R26MER/MER* MEFs and then averaged from four independent experiments (right). (**D**) *miR-19b* dampens the *miR-92*-induced p53 activation. *R26MER/MER* MEFs that overexpress the indicated constructs (*miR-92*, *mir-19b-92Mut19b* and *mir-19b*-92) were collected 48 hr after infection and then analyzed by western blot to determine the level of p53 protein. (**E**) *miR-92* and *miR-19* exhibit antagonistic effects to regulate hydroxyurea (HU)-induced cell death in *Xenopus* embryos. Representative images of HU-treated *Xenopus* embryos that were co-injected with human Ago2 and the indicated miRNA mimics (left). Co-injection of *miR-92* dampened the cell survival effects of *miR-19* on HU-induced apoptosis (right, n = 3, with >20 embryos in each group). (**F**) *miR-92* exhibits a specific antagonistic interaction with *miR-19*. Injection of *miR-19a* or *miR-19b* rescued HU-induced apoptosis in *Xenopus* embryos. Co-injection of *miR-92*, but not a mutated *miR-92*, or other *mir-17-92* components, dampened the cell survival effect of *miR-19* (n = 3, with >20 embryos in each group). Error bars represent standard deviation, *$p<0.05$; **$p<0.01$.

Figure 6–figure supplement 1

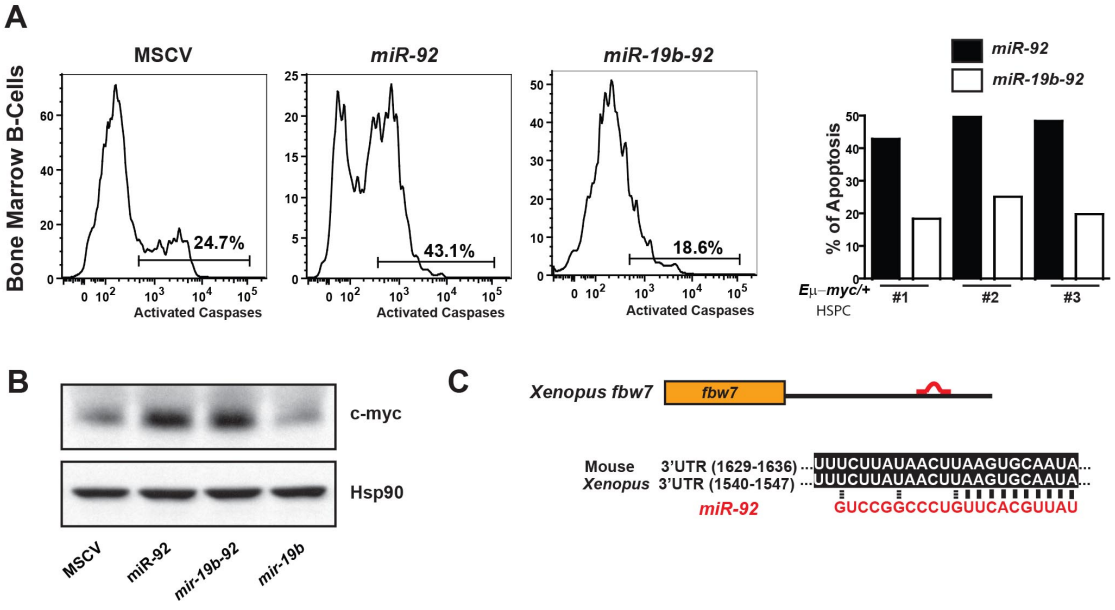

Figure 6 - supplement 1. Functional antagonism between *miR-19:miR-92* regulates the balance between proliferation and apoptosis.
(**A**) *miR-19* antagonizes the apoptotic effects of *miR-92* in vivo. *miR-92* overexpression enhanced apoptosis in premalignant *Eμ-myc* bone marrow B-cells in vivo, while co-expression of *miR-19* and *miR-92* as a dicistron (*mir-19b-92*) abolished this apoptotic effect (left three panels). A quantitative analysis of apoptosis by FACS was shown for three independent experiments (right). (**B**) *miR-19* has no effects on the level of c-Myc protein. While *miR-92* overexpression significantly enhanced the level of c-Myc in *R26MER/MER* MEFs, co-expression of *miR-19b* and *miR-92* did not reverse the increase in c-Myc expression. In addition, *miR-19b* expression alone did not impact the dosage of c-Myc protein. (**C**) *Xenopus fbw7* contains one predicted target site for *miR-92*. This predicted *miR-92* binding site is conserved between *Xenopus* and mouse.

Figure 7

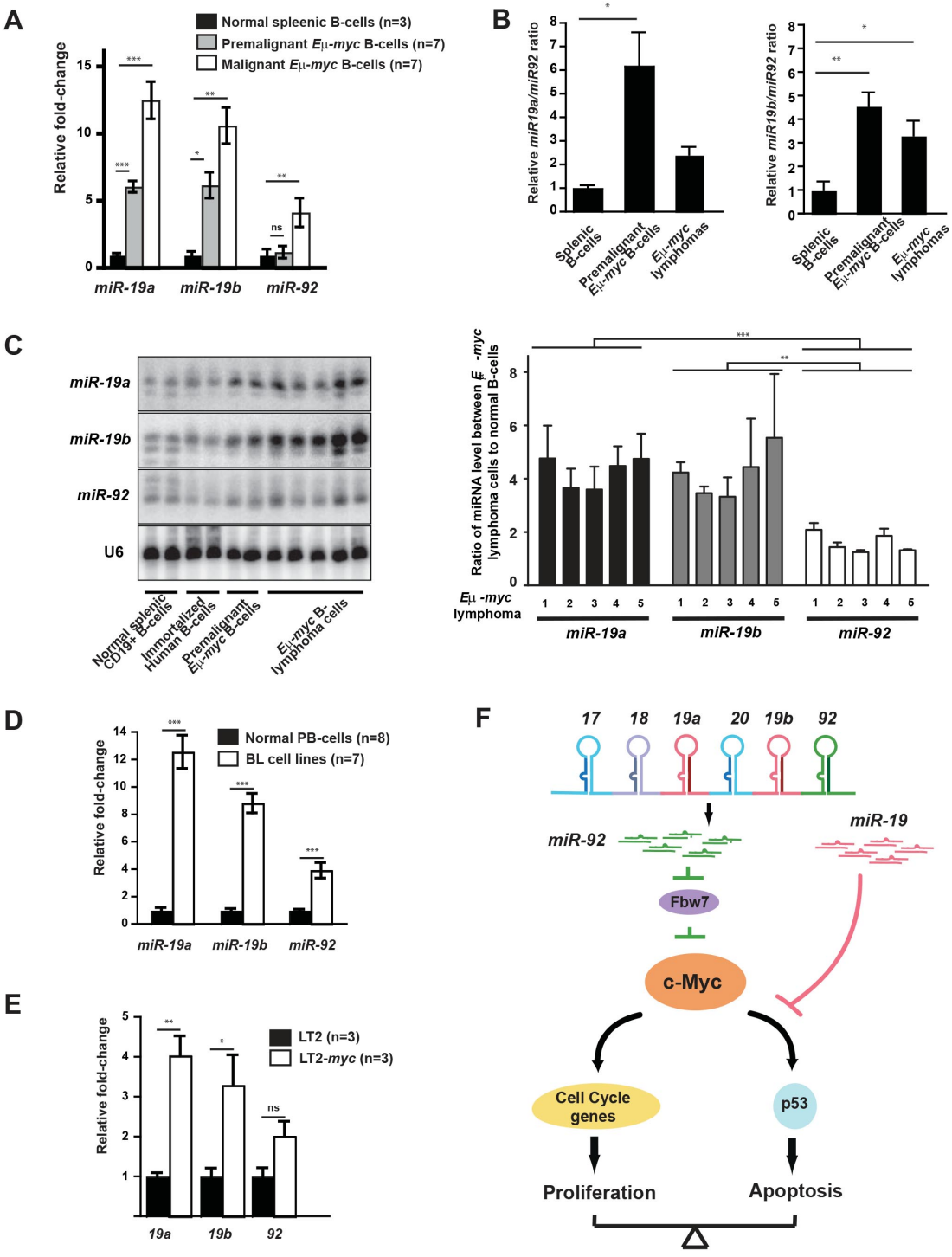
A
Normal spleenic B-cells (n=3)
Premalignant Eμ-myc B-cells (n=7)
Malignant Eμ-myc B-cells (n=7)
Relative fold-change
miR-19a
miR-19b
miR-92
ns
B
Relative miR19a/miR92 ratio
Relative miR19b/miR92 ratio
Splenic B-cells
Premalignant Eμ-myc B-cells
Eμ-myc lymphomas
C
miR-19a
miR-19b
miR-92
U6
Normal splenic CD19+ B-cells
Immortalized Human B-cells
Premalignant Eμ-myc B-cells
Eμ-myc B-lymphoma cells
Ratio of miRNA level between Eμ -myc lymphoma cells to normal B-cells
Eμ -myc lymphoma
D
Normal PB-cells (n=8)
BL cell lines (n=7)
Relative fold-change
E
LT2 (n=3)
LT2-myc (n=3)
19a
19b
92
F
17
18
19a
20
19b
92
miR-92
miR-19
Fbw7
c-Myc
Cell Cycle genes
p53
Proliferation
Apoptosis

Figure 7. The *miR-19*:*miR-92* antagonism is disrupted during malignant transformation.
(**A** and **B**) Compared to normal splenic B-cells, premalignant and malignant *Eμ-myc* B-cells favored a greater increase in mature *miR-19* (*miR-19a* and *miR-19b*) than *miR-92*. The purified normal splenic B-cells, premalignant *Eμ-myc* bone marrow B-cells and malignant *Eμ-myc* B-lymphoma cells were subjected to Taqman miRNA assays to determine the expression level of *miR-19a*, *miR-19b* and *miR-92*. Comparing premalignant/malignant *Eμ-myc* B-cells vs normal splenic B-cells, all three miRNAs exhibited an increased level, although the increase in *miR-19a* or *miR-19b* was significantly higher than that of *miR-92* (**A**). In the same experiment, the relative ratios for *miR-19a:miR-92* and *miR-19b:miR-92* were measured for all normal splenic B-cells and *Eμ-myc* B-cells (**B**). (**C**) Mature *miR-19* and *miR-92* are differentially expressed in normal splenic B-cells and *Eμ-myc* B-lymphoma cells. The normal splenic B-cells, immortalized human B-cells, premalignant *Eμ-myc/+* B-cells, and *Eμ-myc/+* B-lymphoma cells were subjected to Northern analysis. Compared to normal splenic B-cells, both malignant and premalignant *Eμ-myc/+* B-cells favored a greater increase of *miR-19* than *miR-92*. (**D**) Compared to normal B-cells isolated from peripheral blood, human Burkitt's lymphoma cell lines favor a greater increase in mature *miR-19* than *miR-92*. (**E**) Compared to normal livers (LT2), mouse hepatocellular carcinomas caused by the inducible c-Myc over-expression (LT2-*myc*) favor a greater increase in mature *miR-19* than *miR-92*. (**F**) A diagram describes our proposed model to explain the functional interactions between *miR-92* and *miR-19* in c-Myc-induced B-lymphomagenesis. Aberrant c-Myc expression couples rapid proliferation and p53-dependent apoptosis. *miR-92* overexpression further increases c-Myc dosage to strengthen this coupling, at least in part by repressing Fbw7. This *miR-92* effect ensures a potent mechanism to eliminate premalignant c-Myc overexpressing cells. Interestingly, *miR-92* and can be antagonized by the survival effects of the *miR-19* miRNAs encoded by the same *mir-17-92* miRNA polycistron. Taken together, while *miR-19* miRNAs repressed c-Myc-induced apoptosis to promote the oncogenic cooperation between *mir-17-92* and c-Myc, *miR-92* exhibits a negative regulation. Thus, the antagonistic interactions between *miR-92* and *miR-19* confer an intricate crosstalk between proliferation and apoptosis. Error bars represent standard deviation, *$p<0.05$; **$p<0.01$, ***$p<0.001$.

Figure2–table supplement 1

Flow cytometric immunophenotyping of Eμ-myc lymphomas with enforced expression of different mir-17-92 derivatives

Genotype	n	percentage	Immunotype
Eμ-myc/MSCV	4	40%	B220+, IgM-,CD19+, CD4-, CD8-
	6	60%	B220+, IgM+,CD19+, CD4-, CD8- [a]
Eμ-myc/17-92	4	40%	B220+, IgM-,CD19+, CD4-, CD8-
	5	50%	B220+, IgM+,CD19+, CD4-, CD8- [b]
	1	10%	B220-, IgM-,CD19-, CD4+, CD8+
Eμ-myc/17-92Mut92	7	70%	B220+, IgM-,CD19+, CD4-, CD8-
	3	30%	B220+, IgM+,CD19+, CD4-, CD8- [c]
Eμ-myc/17-92Δ92	8	80%	B220+, IgM-,CD19+, CD4-, CD8-
	2	20%	B220+, IgM+,CD19+, CD4-, CD8- [d]

[a] 1 out of 6 samples predominantly contains IgM+ cells, with a small percentage of IgM- cells

[b] 3 out of 5 samples predominantly contain IgM+ cells, with a small percentage of IgM- cells

[c] 1 out of 3 samples predominantly contains IgM+ cells, with a small percentage of IgM- cells

[d] 1 out of 2 samples predominantly contains IgM+ cells, with a small percentage of IgM- cells

Table 1. Flow cytometric immunophenotyping of *Eμ-myc* lymphomas with enforced expression of different *mir-17-92* derivatives

Chapter 3

mir-34 and *mir-449* microRNA families act as tumor suppressors in a B-lymphoma mouse model.

Margaux J. Bennett, YeeAnn Chen, Virginie Olive, Nicole Sponer, Lin He
Unpublished 2014

Summary
The *mir-34* miRNA family has long been thought to act as tumor suppressor microRNAs both independently and in response to p53 activation. However, previous studies of *mir-34* knockout mice have not revealed a significant role for this family in inhibiting tumorigenesis. In the *Eμ-myc* mouse model of B-lymphoma, we show that deletion of either the *mir-34a* locus or the *mir-34b/c* locus accelerates *Eμ-myc* lymphomagenesis. Surprisingly, however, we found that the complete deletion of *mir-34a* and *mir-34b/mir-34c* loci abolishes the acceleration that is seen upon the deletion of each individual locus. We propose that the lack of *Eμ-myc* lymphoma acceleration in the complete *mir-34* knockout mice is due in part to an upregulation of E2f1, which is driving the compensatory upregulation of the additional *mir-34* family members encoded in the *mir-449* miRNA cluster. The fine-tuned compensatory responses between the loci of *mir-34/mir-449* miRNAs further the crosstalk between the E2f1 and p53 pathways, and provide an explanation for the conservation of seemingly redundant miRNAs.

Introduction
p53 acts as a barrier to transformation and tumorigenesis by activating or repressing a large number of downstream targets, which trigger cell cycle arrest, apoptosis, or senescence depending on the type of cell and stimulus. Historically, p53 is known for transcriptionally regulating the expression of several protein coding genes, but increasing studies have characterized several microRNAs as part of p53's tumor suppressor networks (Hermeking et al., 2012).

The most extensively studied p53-regulated miRNAs are those in the *mir-34* miRNA family. The *mir-34* miRNA family consists of *mir-34a*, encoded at mouse chromosome 4, and *mir-34b/34c,* which is transcribed from chromosome 9 as a bicistronic miRNA (Figure 1A). Both *mir-34* loci are transcribed in response to p53 activation (Chang et al., 2007; He et al., 2007; Raver-Shapira et al., 2007; Tarasov et al., 2007). Enforced expression of these *mir-34* miRNAs *in vitro* recapitulate several biological effects of p53, including cell cycle arrest, senescence and apoptosis, all of which are likely due to *mir-34*'s post-transcriptional repression of such targets as Cyclin D1, Cyclin E2, Cdk4, c-Met, c-Myc, Bcl2, and Sirt1 (Hermeking, 2009). In addition to functionally mimicking p53 activation *in vitro*, the *mir-34* miRNA family is frequently inactivated through chromosomal deletion, promoter methylation, or dysregulated expression in hematopoietic malignancies and several solid tumors (Kaghad et al., 1997; Lodygin et al., 2008; Hermeking 2010; Wang et al., 2011; Tanaka et al., 2012). Additionally, overexpression of *mir-34* leads to tumor repression *in vivo* both in xenograft models, and a lung adenocarcinoma model **(**Wiggins et al., 2010; Kasinski and Slack 2012).

However, in spite of *mir-34*'s links to p53 and to tumor suppressive capabilities, analysis of the *mir-34* knockout mice did not lead to obvious defects in the p53 pathway (Choi et al., 2011; Concepcion et al., 2012). *In vitro* analysis of *mir-34* deficient embryonic fibroblasts exhibit no defects in p53-dependent cell cycle arrest, apoptosis or replicative senescence (Choi et al., 2011; Concepcion et al., 2012). In fact, most miRNA knockout mice have mild phenotypes, with very few exhibiting strong developmental defects (Mendell and Olson, 2012). Many have speculated that the redundancy within

miRNA families could cause single miRNA knockout mice to exhibit no phenotypic changes, while the complete loss of redundant miRNAs might exhibit a phenotype. There are a few examples of this redundancy: only *mir-133a-1* and *mir-133a-2* double knockouts exhibit lethal cardiac defects (Liu et al., 2008), and only the *mir-208b* and *mir-499* double knockouts exhibit a decrease in slow muscle fibers while single knockouts have no phenotype (van Rooij et al., 2009).

Alternatively, another source of redundancy among miRNAs could occur at the target level. Loss of one miRNA could induce a compensatory response of other miRNAs that share an overlapping set of targets genes, even for miRNAs that do not share sequence similarity. While specific examples of this hypothesis are not yet widely known, studies in *C. elegans* have shown that specific miRNAs deletions give rise to synthetic phenotypes in combination with loss of function of argonaute like 1 (*alg-1)* (Brenner et al., 2010). This global reduction of miRNAs upon *alg-1* deletion could possibly remove compensatory miRNAs, and elucidate a phenotype for the specific miRNA deletion. Moreover, extensive depletion of miRNAs, such as in the case of the *alg-1* deletion, could instead induce stress that exposes the phenotype. Due to the varied possibilities for redundancy and overlapping targets, miRNA knockout mice that do not exhibit a phenotype under normal conditions, exhibit phenotypes upon exposure to different physiological stresses (Mendell and Olson, 2012). For example, under normal conditions, deletion of the cardiomyocyte specific *mir-208* exhibits no phenotype, but under the stress of hypothyroidism, the *mir-208* knockout cells failed to remodel the heart (van Rooj et al., 2007). Consequently, we hypothesized that the *mir-34* miRNA knockout mice may reveal tumor suppressive functions *in vivo* if exposed to constitutive oncogenic stresses.

The *Eμ-myc* mouse model of B-cell lymphoma has been used to study the p53 tumor suppressor network in great detail. Loss of p53 in this model greatly accelerates *Eμ-myc* lymphomagenesis by inhibiting apoptosis and by promoting proliferation and dissemination (Eischen et al., 1999; Schmitt et al., 1999). The *miR-34* miRNAs are effectors of p53, and so we hypothesized that deletion of the *miR-34* miRNAs in the *Eμ-myc* mouse model would also accelerate lymphomagenesis. Fascinatingly, deletion of each individual locus containing the *mir-34* family members accelerated lymphomagenesis to different degrees. The *Eμ-myc*$^{+}$*;mir-34a-/-* mice had mildly accelerated lymphomagenesis, while the *Eμ-myc*$^{+}$*;mir-34b/c-/-* mice had more greatly accelerated lymphomagenesis, possibly due to a dosage effect of deleting two of the *mir-34* miRNAs (Fig 2). Surprisingly, however, in the complete *mir-34* miRNA knockout mouse (*Eμ-myc*$^{+}$*;mir-34a-/-;b/c-/-)* the acceleration seen in the individual knockout mice was abolished, which is consistent with Concepcion *et al's* observations. We found that upon deletion of the *mir-34* miRNAs, the *mir-449* locus is upregulated, which transcribes a tricistronic cluster of miRNAs that are homologous to *mir-34.* We demonstrate that the *mir-34a-/-;b/c-/-* mice also upregulate E2f1, which is likely driving the upregulation of *mir-449,* and preventing the acceleration of Myc driven tumorigenesis. These observations illustrate how the signaling pathways of the two transcription factors, E2f1 and p53, are further intertwined in cell fate decisions. In this study we will further discuss how *mir-34/mir-449* mediates crosstalk between the p53 and E2f1 pathways.

Results

Deletion of *mir-34a* or *mir-34b/c* accelerates lymphomagenesis.

The *mir-34* miRNAs share the exact same seed sequence, but are located in two places of the genome: *mir-34a* is located on chromosome 4; *mir-34b* and *mir-34c* are transcribed as a single transcript from chromosome 9 (Fig. 1A). We previously generated knockout mice for each *mir-34a* and *mir-34b/c* (Choi et al., 2011), and determined that deletion of either *mir-34a* or *mir-34b/c* did not affect the expression of the other locus in the B-cells of the mice (Fig. 1B.). As *mir-34a* and *mir-34b/c* are transcriptionally regulated by p53 and their expression is lost in many hematopoietic malignancies (Eischen et al., 1999; Schmitt et al., 1999; Schmitt et al., 2002), we chose to investigate the tumor suppressive capabilities of each of the *mir-34* miRNA family members in the *Eμ-myc* mouse model, in which the p53 pathways has been greatly characterized (Eischen et al., 1999; Schmitt et al., 1999; Schmitt et al., 2002). The *Eμ-myc* mice carry a *c-Myc* transgene downstream of the immunoglobulin heavy chain enhancer, *Eμ.* The resulting aberrant c-Myc activation in primarily the B-cell compartment promotes excessive proliferation, as well as potent, p53-dependent apoptosis to eliminate the expansion of premalignant cells (Langdon et al., 1986; Eischen et al., 1999; Schmitt et al., 1999; Schmitt et al., 2002**)**. Thus, lesions that further enhance proliferation, or inhibit c-Myc-induced apoptosis accelerate *Eμ-myc* lymphomagenesis. Interestingly, *Eμ-myc*$^{+}$ mice from *Eμ-myc*$^{+}$ mothers exhibit a maternal effect of accelerated lymphomagenesis, and therefore we generated our survival curve cohort from littermates of the illustrated crosses (Fig. 1C). Surprisingly, while Concepcion *et al* did not observe accelerated lymphomagenesis in their *Eμ-myc*$^{+}$*;mir-34a-/-;mir-34b/c-/-* mice, we see that deletion of each individual *mir-34* miRNA locus accelerates lymphomagenesis (Fig. 1D) (Concepcion et al., 2012). The *Eμ-myc*$^{+}$*;mir-34a-/-* mice succumb to lymphoma at an average of 109 days compared to an average of 134 days in the *Eμ-myc*$^{+}$ mice (Fig. 1D; Log rank Mantel: $p<0.0051$). The *Eμ-myc*$^{+}$*;mir- 34b/c-/-* mice succumb to lymphoma at an even greater accelerated rate compared to even the *Eμ-myc*$^{+}$*;mir-34a-/-* (Fig. 1E; 90 days, $p<0.0045$). The *Eμ-myc*$^{+}$*;mir-34b/c+ /-* mice exhibit the same acceleration of lymphomagenesis and phenotypes as their *Eμ-myc*$^{+}$*;mir- 34b/c-/-* littermates (Supplemental Fig. 1A). Additionally, the *Eμ-myc*$^{+}$*;mir-34b/c+/-* mice do not exhibit a loss of heterozygosity indicating that deletion of one allele is sufficient to accelerate lymphomagenesis (Supplemental Fig. 1B).

Both the *mir-34* miRNA family members are direct transcriptional targets of p53, but interestingly the loci are differentially regulated during *Eμ-myc* tumorigenesis and during normal B-cell development (Fig. 1E, Supplemental Fig. 1C). It is know that c-Myc represses *mir-34a* (Chang et al., 2008; Craig et al., 2011), and indeed *mir-34a* is repressed in the *E*μ-*myc* mouse model both in premalignant (4-6week) CD19+ bone marrow cells, and in the *E*μ-*myc* tumors, while *mir-34c* expression does not change (Fig. 1E). During normal B-cell development, *mir-34c* has greater expression in the pro-B-cell compartment, unlike *mir-34a* that is more greatly expressed in the pre-B cell compartment (Sup.Fig. 1C). The varied expression patterns of the *mir-34* miRNAs suggest that these loci experience distinct transcriptional control likely by other transcription factors in addition to p53. This differential regulation of the *mir-34a* and *mir-34b/c* loci is supported by the difference in their relative expression levels in osteoblasts, where *mir-34b/*c expression increases through osteoblast differentiation, but

mir-34a remains constant (Wei et al., 2012). Upon phosphorylation by mitogen-activated protein kinase-activated protein kinase 5 (MK5), forkhead box O3 (Foxo3a) induces *mir-34b/*c but not *mir-34a* expression (Kress et al., 2012). Foxo3a could therefore possibly be a mechanism of differential regulation in B-cells.

Deletion of *mir-34a* or *mir-34b/c* increase proliferation, while deletion of *mir-34b/c* inhibits apoptosis.

In the *Eμ-myc*$^+$ mouse model, it has been shown that loss of p53 accelerates lymphomagenesis through both an increase in proliferation and a decrease in apoptosis. Therefore, in order to understand the differential rates of lymphoma progression in the *mir-34a* and *mir-34b/34c* knockout mice, we analyzed the lymphomas of the mice for proliferative differences by performing immunohistochemistry of phospho-H3 as a marker of mitosis. We observed that tumors of *Eμ-myc*$^+$*;mir-34a-/- and Eμ-myc*$^+$*;mir-34b/c-/-* exhibit an increase in phospho-H3 compared to the *Eμ-myc*$^+$ mice (Fig. 2A). This level of phospho-H3 is comparable to that seen in *Eμ-myc*$^+$*;p53*+/- tumors (Fig. 2A). Additionally, total cell lysates from *Eμ-myc*$^+$*;mir-34a-/-* and *Eμ-myc*$^+$*;mir-34b/c-/-* terminal stage tumors showed a slight trend of a decrease in the number of p16 positive tumors, with *Eμ-myc*$^+$*;mir-34b/c-/-* exhibiting the least number of p16 positive tumors (Fig. 2B). p16 has been shown as a marker of delayed lymphomagenesis in the *Eμ-myc* mouse model (Moser et al., 2012). Therefore, deletion of either *mir-34a* or *mir-34b/c* accelerates lymphomagenesis in part by increasing the number of cells that are proliferating throughout tumorigenesis.

The *Eμ-myc*$^+$*;mir-34b/c-/-* tumors exhibit a decrease in apoptosis as seen by caspase-3 staining (Fig. 2C), which correlates with the *Eμ-myc*$^+$*;mir-34b/c-/-* mice exhibiting the fastest rate of lymphomagenesis. The decrease in apoptosis seen in *Eμ-myc*$^+$*;mir- 34b/c-/-* tumors is supported by the decrease in IgM+ tumors, suggesting that the *Eμ-myc*$^+$*;mir- 34b/c-/-* B-cells presumably undergo transformation earlier in B-cell development (Fig. 2D). Most anti-apoptotic lesions in the *Eμ-myc* mouse model transform early stage pre-B cells likely because reduced cell death allows more pre-B cells to survive and acquire transforming mutations. In summary, the *Eμ-myc*$^+$*;mir-34b/c-/-* mice develop tumors at the fastest rate likely due to an increase in both proliferation and apoptosis, while *Eμ-myc*$^+$*;mir-34a-/-* only exhibit an increase in proliferation, as compared to the *Eμ-myc* mice alone.

***mir-34* miRNAs inhibit proliferation and induce apoptosis by targeting cell cycle activating and anti-apoptotic genes.**

To explore whether *mir-34* miRNAs can inhibit cellular proliferation and induce apoptosis in B-cells, we investigated the effects of enforced expression of *mir-34*. Interestingly, while the *Eμ-myc*$^+$*;mir-34a-/-* mice only show an increase in proliferation, overexpression in an Abelson transformed B-cell line of both *mir-34a* and *mir-34b/c* inhibit proliferation, as seen by a decrease in BrdU incorporation in S-phase (Fig. 3A), and induce apoptosis, as seen by an increase in Annexin V positive cells (Fig. 3B). *mir-34b/c* has both a stronger effect on proliferation and apoptosis than *mir-34a* as seen by overexpressing each miRNA at comparable levels with an infection efficiency of MOI 1 (Fig 3A,B.). It is interesting to note, that overexpression of *mir-34b* alone did not induce apoptosis, but when expressed with *mir-34c*, the effects of *mir-34c* were compounded to

significantly induce more apoptosis compared to overexpression of *mir-34a* alone (Fig. 3B). *mir-34b*, however, did repress the cell cycle at the same level as *mir-34c,* but the combination of the two further repressed the cell cycle (Supplemental Fig. 3; Fig. 3A). This data suggests that an increase in copy number of the *mir-34* miRNAs has the ability to induce a stronger phenotype.

We immunoblotted for *mir-34* miRNA targets to identify mechanisms through which the *mir-34* miRNAs induce apoptosis and inhibit proliferation in B-cells. Both *mir-34a* and *mir- 34b/c* inhibit the cell cycle in part by targeting these cell cycle regulators: Cyclin E2, Cyclin D1, and CDK6 (Fig. 3C) (Hermeking et al., 2009; Zauli et al., 2011). We have seen *mir-34* miRNAs downregulate CDK4 at the transcript level, but not at the protein level in these Abelson transformed cells. *mir-34a* and *mir-34b/c* induce apoptosis in part by downregulating the expression of the anti-apoptotic protein Survivin and the p53 negative regulator, Sirt1 (Fig. 3C). *mir-34's* repression of Sirt1 activates p53 and drives the expression of p53 downstream targets (Supplemental Figure 3) (Yamakuchi et al., 2008; Audrito et al., 2011). These same *mir-34* targets are upregulated in bone marrow derived B-cell cultures of *mir-34a-/-* and *mir-34b/c-/-* mice (Fig. 3D), and therefore likely contribute to the acceleration of *Eμ-myc*$^+$*;mir- 34a-/-* and *Eμ-myc*$^+$*;mir-34b/c-/-* mice.

Complete deletion of the *mir-34* miRNA family abolishes the acceleration of lymphoma seen in the both single knockout mice.

We expected to see a stronger phenotype upon a collective loss of the *mir-34* miRNAs, but in fact we saw the opposite phenotype. While *Eμ-myc*$^+$*;mir-34a-/-* and *Eμ-myc*$^+$*;mir-34b/c-/-* mice exhibit accelerated *Eμ-myc* lymphomagenesis, when both *mir-34a* and *mir-34bc* are knocked out, the acceleration is abolished (Fig. 4A). This result is consistent with the results from Concepcion *et al* who also do not observe an acceleration of lymphomagenesis in the *Eμ-myc*$^+$*;mir-34a-/-;mir-34b/c-/-* mice. The lack of accelerated lymphomagenesis correlates with the lack of increase of phospho-H3 staining in the premalignant spleens of *Eμ-myc*$^+$*;mir-34a-/-;34b/c-/-* mice (Fig. 4B). Both the *Eμ-myc*$^+$*;mir-34a-/-* and *Eμ-myc*$^+$*;mir-34b/c-/-* premalignant spleens exhibit an increase in phospho-H3 staining, which correlates with their accelerated onset of tumorigenesis (Fig. 4B). Additionally, the terminal tumors of the *Eμ-myc*$^+$*;mir-34a-/-;mir-34b/c-/-* mice do not exhibit a decreased percentage of p16 positive samples unlike the *Eμ-myc*$^+$*;mir-34b/c-/-* tumors (Fig. 2B). In fact there may even be a slight increase in the percentage of p16 positive tumors in the *Eμ-myc*$^+$*;mir-34a-/-;mir-34b/c-/-* mice. The *Eμ-myc*$^+$*;mir-34a-/-;mir-34b/c-/-* tumors also do not exhibit a decrease in caspase-3 staining (Fig. 4D), and they seem to transform from the later stage B-cells like the *Eμ-myc*$^+$ tumors (Supplemental Fig. 4A).

Given that the *mir-34* miRNAs share the same "seed" sequence with the *mir-449* miRNAs (Fig. 4F), we hypothesized that *mir-449* might be potentially upregulated in the *Eμ-myc*$^+$*;mir-34a-/-;mir-34b/c-/-* B-cells to compensate for the loss of the *mir-34* miRNAs. The *mir-449* locus consists of three miRNAs (*a, b,* and c) that are transcribed on one pri-miRNA transcript (Fig. 4E). Therefore, upregulation of the *mir-449* locus actually upregulates three miRNAs. To investigate a compensatory response of *mir-449* in *mir-34a;34b/c* deficient mice, we compared *mir-34a-/-;b/c-/-* and wild-type bone marrow, culture-derived B-cells for expression of *mir-449*. We consistently see a 2-fold

upregulation of the primary *mir-449* transcript in the *mir-34a-/-;34b/c-/-* B-cells but not in the *mir-34a-/-* or *34b/c-/-* B-cells (Fig. 4F). We also do not see compensatory upregulation of *mir-34a* or *mir-34c* in their respective *mir-34* single knockouts (Fig. 1B).

mir-449 is regulated by the transcription factor E2F1 (Yang et al., 2009). E2F1 is repressed by both *mir-34a* and *mir-34b/c* (Supplemental Fig. 4B; Zauli et al., 2011). We hypothesized that deletion of *mir-34a* and *mir-34b/c* might cause a de-repression of E2f1, and thereby allow E2f1 to induce this compensatory expression of *mir-449* (Fig. 4F). In this way, *mir-34* and *mir-449* could complete a feedback loop that links their tumor suppressive capabilities together. Consequently, we analyzed the *mir-34a-/-;34b/c-/-* cultured B-cells for upregulation of E2f1 protein levels (Fig . 4G). We see that E2f1 is in fact upregulated and induces the upregulation of its target gene of p19/Arf (Fig. 4G). One function of p19/Arf is to inhibit Mdm2 from inducing degradation of p53 (Levine and Oren, 2009). In this context upregulation of p19 surprisingly does not seem to significantly affect the levels of p53 (Fig. 4G; Supplemental Fig. 4C). In spite, of not stabilizing p53 levels, known p53 downstream targets, such as Puma and Noxa, are upregulated (Supplemental Fig. 4C).

E2f1 is a known target of Myc (Meyer and Penn, 2008). Therefore, *the Eμ-myc+;mir-34a-/-;34b/c-/-* B-cells could actually be negatively affected by an even greater increase in E2f1 activity. E2f1 is indeed upregulated in premalignant *Eμ-myc*$^{+}$*;mir-34a-/-;34b/c-/-* B-cells, in both culture derived and uncultured, sorted premalignant B-cells (Fig. 4H; Supplemental Fig. 4E). Interestingly, in premalignant *Eμ-myc*$^{+}$*;mir-34a-/-;34b/c-/-* cultured derived B-cells, we see that *p21* is upregulated in addition to *p19* being upregulated (Fig. 4I). Similar to the culture derived B-cells from the animals lacking Myc, we did not see stabilization of p53 in the cultured *Eμ-myc*$^{+}$*;mir-34a-/-;34b/c-/-* B-cells, and thus *p21* is likely upregulated and *Cyclin D1* is likely repressed by E2f1 directly (Radhakrishnan et al., 2004; Watanabe et al., 1998). In fact, in the culture-derived B-cells without the *Eμ-myc* allele, *Puma* and *Noxa* might also be directly upregulated by E2f1 (Hershko et al., 2005).

E2f1's downregulation of *Cyclin D1* accounts for the decrease in proliferation seen in the *Eμ-myc*$^{+}$*;mir-34a-/-;34b/c-/-* premalignant spleens (Fig. 4B). However, we have yet to seen consistent upregulation of *mir-449* in the *Eμ-myc*$^{+}$*;mir-34a-/-;34b/c-/-* B-cells. We have analyzed both the premalignant B-cells and terminal tumors of the *Eμ-myc*$^{+}$*;mir-34a-/-;34b/c-/-* mice for *mir-449* compensation. While *mir-449* expression changes during normal B-cell development (Supplemental Fig. 4G), more importantly we see that *mir-449* is upregulated in response to Myc itself, and then subsequently lost later in tumor development (Supplemental Fig. 4G). Consequently, *Eμ-myc* tumorigenesis is dependent on a loss of *mir-449* expression, and thus we do not see compensatory expression of *mir-449* in the *Eμ-myc*$^{+}$*;mir-34a-/-;34b/c-/-* tumors (data not shown). However, in 3 out of 5 premalignant *Eμ-myc*$^{+}$*;mir-34a-/-;34b/c-/-* mice we see compensatory expression of *mir-449* in the primary CD19+ bone marrow cells that we do not see in *Eμ-myc*$^{+}$*;mir-34a-/-* (data not shown) or *Eμ-myc*$^{+}$*;mir-34b/c-/-* premalignant animals (Supplemental Fig. 4H). This compensatory expression of *mir-449* in the *Eμ-myc*$^{+}$*;mir-34a-/-;34b/c-/-* premalignant B-cells may be difficult to see due to the fact that Myc itself raises the basal level of *mir-449* in the *Eμ-myc*$^{+}$mice, and the variability of tumor onset makes staging premalignancy difficult.

Deletion of *mir-449* accelerates *E*μ-*myc*$^+$ lymphomagenesis.

While it is clear that the increase in E2f1 inhibits proliferation in the *Eμ-myc*$^+$*;mir-34a-/-;34b/c-/-* mice by repressing Cyclin D1, it seems likely that the possible compensation of *mir-449* in the *E*μ-*myc*$^+$*;mir-34a-/-;34b/c-/-* mice may also be playing a role in inhibiting tumorigenesis. Even the two-fold upregulation of *mir-449* occaisionally seen in the *E*μ-*myc*$^+$*;mir-34a-/-;bc-/-* mice could inhibit tumorigenesis as even deletion of a single copy of *mir-449* accelerates *E*μ-*myc*$^+$ lymphomagenesis (Fig. 5A). The *mir-449-/-* mice exhibit no overt phenotypes similar to the *mir-34a-/-;b/c-/-* (Bao et al., 2012). Interestingly, while the complete knockout of *mir-449* accelerates lymphomagenesis, there is, however, a compensatory upregulation of *mir-34a* and *mir-34c* in culture-derived *mir-449-/-* B-cells (Sup. Fig. 5B). While these observations do indeed close the feedback loop between the *mir-34* and *mir-449* loci, we speculate that the compensating *mir-34* expression in the *mir-449-/-* B-cells is not present in the *Eμ-myc*$^+$*;mir-449-/-* for two reasons: 1. Myc represses *mir-34a* (O'Donnell et al., 2005; Craig et al., 2011), and 2.) we see that complete deletion of *mir-449* accelerates of *E*μ-*myc* lymphomagenesis (Fig. 1E). Therefore, the *mir-34* likely do not compensate in the *Eμ-myc*$^+$*;mir-449-/-* mice. We have preliminary data suggesting that in the presence of Myc, *mir-34a* and *mir-34c* do not compensate the deletion of *mir-449,* but more numbers are required to be conclusive (Supplemental Fig. 5C).

The *Eμ-myc*$^+$*;mir-449+/-* and *Eμ-myc*$^+$*;mir-449-/-* mice both exhibit an increase in proliferation in the premalignant spleens as seen by phospho-H3 staining (Fig. 5B; $p<0.0021$), and a decrease in caspase-3 positive cells in the terminal tumors (Fig. 5C; $p<0.0048$). Again, in accordance with decreased apoptosis, the *E*μ-*myc*$^+$*;mir-449+/-* and *E*μ-*myc*$^+$*;mir-449-/-* animals exhibit predominantly IgM- tumors, suggesting an earlier stage of transformation (Sup. Fig 5A). Similar to the *mir-34a-/-* and *mir-34bc-/-* B-cells, the *mir-449-/-* B-cells exhibit an increase in cell cycle and anti-apoptotic targets Cyclin A, Survivin, and Sirt1 (Fig. 5D). While *mir-449* miRNAs are known to target E2f1, it seems as though the *mir-449-/-* B-cells do not upregulate E2f1 to the level seen in the *mir-34a-/-;mir-34b/c-/-* B-cells (Supplemental Fig. 5D). In summary, a complex feedback loop interconnects *mir-34* and *mir-449* seemingly redundant tumor suppressive functions through E2f1 and p53 signaling (Fig. 5E).

The complete deletion of *mir-34*/*mir-449* miRNAs seems to inhibit E2f1 induced apoptosis seen in the *mir-34a-/-;mir-34bc-/-* mice.

In order to investigate the effects of the complete loss of the *mir-34* and *mir-449* miRNAs, we crossed the *mir-449-/-* mice to the *mir-34a-/-;mir-34b/c-/-* mice. Generation of mice from the *mir-34a-/-;mir-34b/c-/-;mir-449+/-* intercrosses yielded *mir-34a-/-;mir-34b/c-/-;mir-449-/-* mice that were smaller physically in size, due to an inability to thrive, and were infertile because of defects in multiciliated cells (Song et al., 2014). Additionally, about 60% of these animals died before adulthood (Song et al. 2014). The visible phenotypes of the *mir-34a-/-;mir-34b/c-/-;mir-449-/-* mice further support the idea that the *mir-34* and *mir-449* miRNAs are redundant, at least in certain tissues

While the inability of the *mir-34a-/-;mir-34b/c-/-;mir-449-/-* animals to thrive and mate makes it difficult to study the B-cells of *mir-34a-/-;mir-34b/c-/-;mir-449-/-* mice, let alone *E*μ-*myc*$^+$*;mir-34a-/-;mir-34b/c-/-;mir-449-/-* mice, we have observed decreased

basal apoptosis in the *mir-34a-/-;mir-34b/c-/-;mir-449-/-* B-cells (Fig. 6A). This decrease in apoptosis could be due to an even greater upregulation of anti-apoptotic *mir-34* targets in the *mir-34a-/-;mir-34b/c-/-;mir-449-/-* culture derived B-cells, but more investigation is required. Interestingly, we see a return to wild-type levels of p19 in the *mir-34a-/-;mir-34b/c-/-;mir-449-/-* culture derived B-cells (Fig. 6B). This wild-type level of p19 may be due to a concordant decrease in E2f1 (Fig. 6C.) While, E2f1 seems to be still upregulated in the *mir-34a-/-;mir-34b/c-/-;mir-449-/-* culture derived B-cells, it looks to be less upregulated compared to its littermate controlled *mir-34a-/-;mir-34b/c-/-;mir-449+/+*(Fig. 6C). Additionally, the more wild-type levels of p19 in the *mir-34a-/-;mir-34b/c-/-;mir-449-/-* B cells could be due to an even greater upregulation of Sirt1 upon deletion of the entire *mir-34/mir-449* miRNA family. It has been shown that Sirt1 can directly bind E2f1 and inhibit its transcription and ability to induce apoptosis (Wang et al., 2006).

We do not yet know whether *mir-34a-/-;mir-34b/c-/-;mir-449-/-* cells have an increased ability to undergo transformation. However, the decrease in apoptosis seen the *mir-34a-/-;mir-34b/c-/-;mir-449-/-* B-cells suggests that they might be more prone to tumorigenesis. However, as the *mir-34* and *mir-449* feedback loop is so complex, additional molecular changes may be occurring to prevent transformation. For example, the *mir-34* and *mir-449* miRNAs may regulate different targets through minimal differences in their mature or even pre-miRNA sequence. This differential target regulation could allow constitutively activated Myc to upregulate *mir-34* targets that may even inhibit tumorigenesis.

Discussion

The *mir-34/mir-449* miRNA family contains seemingly redundant family members under distinct regulation in order to generate feedback loops that keep cell signaling in check; the *mir-34/mir-449* family structure likely represents a common theme amongst miRNA families. In this study, we have shown that the deletion of the *mir-34* miRNA family induces a compensatory upregulation of *mir-449*, through an increase of E2f1(Fig. 4F). The reverse also occurs, whereupon the deletion of *mir-449* induces a compensatory upregulation of *mir-34* miRNAs (Sup. 5B). This balance seems to be disrupted under the context of *E*μ-*myc* as data suggests that deletion of the *mir-34* miRNAs induces the upregulation of *mir-449,* but not the reverse. This presumably occurs in part through Myc's ability to suppress *mir-34a* expression (O'Donnell et al., 2005; Craig et al., 2011). However, more work is needed to carefully determine the mechanism for the altered regulation of the *mir-34/449* family under the context of *E*μ-*myc.* Perhaps, the ability of Myc to repress the *mir-34a* locus underlies the evolutionary logic for why the *mir-34a* and *mir-34b/*c loci are separate, while the *mir-449* locus contains all three miRNAs. Still, the repression of *mir-34a* by Myc implies that seemingly highly regulated feedback loops have an Achilles heal where certain signals can inhibit molecular checks to tip the cell to favor oncogenic growth. It is possible that under less vigorous Myc expression or in cell types expressing different Myc binding partners, the repression of *mir-34a* does not occur, and a feedback loop remains intact. For example, under Braf induced senescence, *mir-34a* is upregulated by Elk1 and targets Myc itself (Chrisofferson et al., 2010). Consequently, in Braf-induced oncogenesis, upregulation of *mir-34* could potentially repress *mir-449* by downregulating c-Myc. Additionally, there may be contexts where the

repression of *mir-34a* by c-Myc may be required for normal cell function, even upon the loss of *mir-449*.

The complex signaling pathway formed by the *mir-34/mir-449* family suggests that under different contexts the loss of either *mir-34* or *mir-449* could be more or less oncogenic. We show above that in the context of Myc, it is more advantageous to lose the expression of *mir-449* than to lose all *mir-34* miRNAs, as Myc itself represses *mir-34a* but activates *mir-449*. Intriguingly, Concepcion *et al* show that in the absence of Rb it may be at least equally advantageous to lose the expression of *mir-34*. When they inhibit Rb by expressing E1A, there is an increase in colony formation upon the expression of constitutively active Kras in the *mir-34a-/-;mir-34b/c-/-* mouse embryonic fibroblasts (Concepcion et al., 2012). Future studies using different oncogenic signals to activate the *mir-34/449/p53/E2f1* feedback loop will help us to better understand the tumor suppressive properties of the these miRNAs.

While more work is needed to analyze how the complete deletion of *mir-34* and *mir-449* miRNAs affects tumorigenesis, we have data suggesting that completely abolishing the *mir-34/mir-449* miRNAs may at least allow B-cells to better resist apoptotic signaling (Fig 6A). Other groups previously saw that *mir-34* antagonists impair p53-induced apoptosis (Yamakuchi et al., 2008; Boon et al., 2013). p53 is not altered in the *mir-34a-/-;mir-34b/c-/-* animals, but may impaired by *mir-34* antagonists because the antagonists may indiscriminately inhibit both the *mir-34* and *mir-449* mature miRNAs due to identical seed sequences. Consequently, *mir*-34 antagonists may inhibit apoptosis by significantly impairing the function of the entire *mir-34/mir-449* family.

In conclusion, we have shown that the duplication of *mir-34* and *mir-449* miRNAs within the genome allows these miRNAs to better inhibit tumorigenesis. However, the cell context and the type of oncogenic signaling can severely inhibit the ability of the endogenous *mir-34/mir-449* loci to prevent cellular transformation. The conservation of the *mir-34/mir-449* miRNAs throughout evolution (Supplemental Fig. 6), and the manner in which they further the crosstalk between p53 and E2f1 highlights their functional importance in suppressing tumorigenesis in response to oncogenic signals.

Materials and Methods:

Cell culture

Primary murine B-cells were prepared from bone marrows of 4-6 week old mice, and were cultured in RPMI with 10% FBS, 50 uM Beta-mercaptoethanol (Sigma, M3148) and 2 ng/ml Il-7 (R&D, 407-ML-005) for 5-6days. Primary Eμ-myc^{+} bone marrow was cultured under the same conditions, however, Eμ-myc^{+} bone marrow cells could not be expanded off the original plate as they are dependent on their adherent endogenous stromal cells. The Abelson immortalized pro-B cell line (7GS) were kindly provided by Greg Timblin in the Schlissel lab, and were cultured in RPMI with 10% FBS, and 50 uM Beta-mercaptoethanol. The pro-B cell Abelson lines were infected by MSCV retroviruses expressing the *mir-34* derived miRNA clusters. Mouse embryonic fibroblasts were collected from E13 – 14, and cultured in DMEM with 10% FBS and 50/ml of Penicillin and streptomycin (Gibco, Life Tech 15070-063).

Histopathology

Mouse tissue samples were fixed in formalin (Fisher, SF100-4), embedded in paraffin

(Fisher, AC41677-0020), sectioned in 5 μm, and stained with haematoxylin and eosin (Fisher, 7211 & 7111). For caspase-3 (R&D Systems, AF835, 1:200), and phospho-H3 (ab5176) detection, representative sections were deparaffinized and rehydrated in graded alcohols before subjected to antigen retrieval treatment with 10mM sodium citrate buffer or DAKO Target Retrieval Solution for 10 minutes in a pressure cooker steamer at low pressure. Detection of antibody staining was carried out following standard procedures from the avidin-biotin immunoperoxidase methods. Diaminobenzidine (Invitrogen, 002014) was used as the chromogen and haematoxylin as the nuclear counter stain. Quantitation of apoptosis was evaluated by counting the number of caspase-3 positive cells in 5 fields (40X).

Immunnotyping and Flow Cytometry

To determine the cell surface markers of the lymphoma cells harvested from the animals, cells were stained for various markers in 3-5% FBS/PBS for flow cytometry analysis. Antibodies used for FACS analyses include:
eBioscience:
PE-IgD (Clone 11-26c) 1:200, PE-/APC-/PE-Cy7-B220 (Clone RA3-6B2) 1:200, FITC-CD25 (Clone PC61.5) 1:100, FITC -/PerCPCy5.5-CD19 (eBio1D3) 1:100, PE-huCD2 (RPA-2.10) 1:200, PE-Cy7-huCD4 (RPA-T4) 1:200, FITC-IgM (Clone 11/41) 1:100, PacBlue-CD8a (Clone 53-6.7) 1:600; PerCPCy5.5-CD4 (RM4-5) 1:100.
BD Pharmigen:
APC-Annexin V (Cat3#: 550475) 1:50, PE-CD43 (Cat#: 553271) 1:350

Bone marrow derived Pro-B (IgM-, B220+, CD43+) and Pre-B cells (IgM-, B220+, CD43-) were sorted on the Beckman Coulter MoFlo legacy.

Apoptosis assays and proliferation assays

To evaluate the apoptotic response to retrovirally expressed miRNAs, cells positive for the huCD2 vectors stained we PE anti-huCD2 (1:200) and were sorted with help from Hector Nolla and Alma Valeros on the MoFlo Cell Sorter 24 hours post single infection to equal concentrations in 96 well plates. 24 hours later cells were analyzed for apoptosis by Annexin V and 7AAD staining and analyzed by flow cytometry. For this we stained the cells with APC-Annexin V antibody (BD Pharmingen, 550475, 1:50) in Annexin buffer (10mM HEPES, 140mM NaCl, 5mM CaCl2, – pH to 7.4 with NaOH) for 15min, washed with 1ml Annexin buffer, resuspended in 10ul 7AAD staining solution (BD Pharmingen, 559925), and added 400ul of Annexin buffer.

To quantitate cell proliferation, BrdU was incubated at a concentration of 10 μM for 30min for experiments with the pro-Abelson cell line. The percentage of BrdU positive cells was determined using the Flow BrdU kit (BD Pharmingen, 552598).

Western Antibodies

Cdk6 (ab3126, 1:1000), E2F1 (sc-193x; 1:1000; sc-193, 1:1000), Sirt1 (Cell Signaling, #2028, 1:1000), Cyclin E2 (sc-22777), Cyclin D1 (sc-753), Survivin (Cell Signaling, # 2808, 1:1000).

Real time PCR and western analyses
TaqMan® MicroRNA Assays (Applied Biosystems) were used to measure the level of the pri- and mature miRNAs, including *miR-34a, 34c,* and *449a, 449b, 449c*. The *miR-34b* assay is not specific so we did not use it. For these assays, samples were normalized to TaqMan® MicroRNA Assays (Applied Biosystems) *U6*.

mRNA levels were measure for the following targets using primer sequences listed and SYBR (Kapa Biosystems, KK4605).
Actin (GATCTGGCACCACACCTTCT, GGGGTGTTGAAGGTCTCAAA) was used as a normalization control in all our real time PCR experiments.
Cdk4 (TGGTACCGAGCTCCTGAAGT, GTCGGCTTCAGAGTTTCCAC),
*Cdk6 (*AGAAGTCCTGCTCCAGTCCA, CACGTCTGAACTTCCACGAA)
Cyclin E2 (ATGTCAAGACGCAGCCGTTTA, GCTGATTCCTCCAGACAGTACA)
E2f1 (AGGCTGGATCTGGAGACTGA, GAAGCGTTTGGTGGTCAGAT)
Mdm2 (CTCTGGACTCGGAAGATTACAGCC,
CCTGTCTGATAGACTGTCACCCG),
Noxa (GGAGTGCACCGGACATAACT, TGAGCACACTCGTCCTTCAA),
p21 (ACGGTGGAACTTTGACTTCG, CAGGGCAGAGGAAGTACTGG,
Puma (GCGGCGGAGACAAGAAGA, AGTCCCATGAAGAGATTGTAC,)
*Sirt1 (*TCACACGCCAGCTCTAGTGA, GGTGGAGGAATTGTTTCTGG)
*Survivin (*CATCGCCACCTTCAAGAACT, AAAACACTGGGCCAAATCAG)

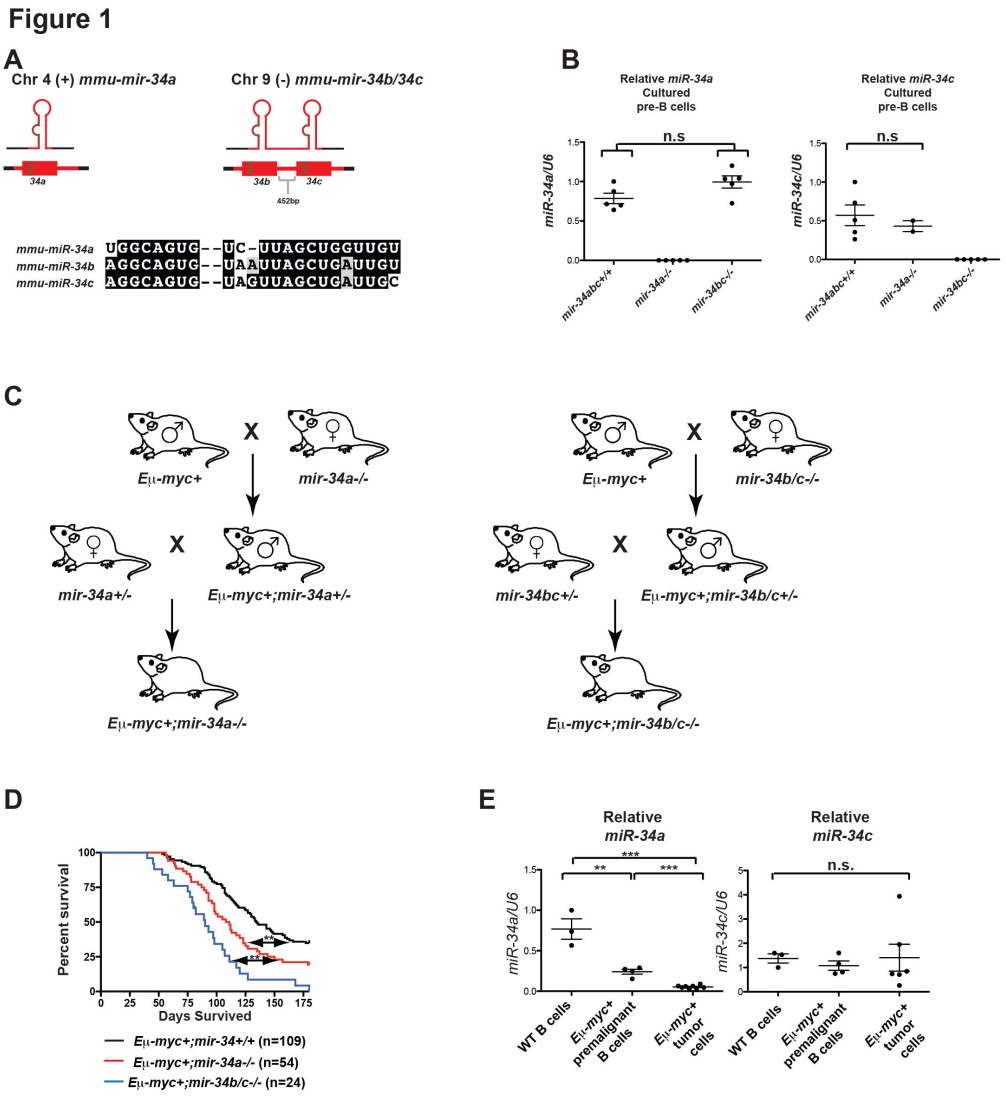

Figure 1. Deletion of *mir-34a* or *mir-34b/c* accelerates lymphomagenesis.
A. Gene structure of *mir-34a* and *mir-34bc,* and homology of the *mir-34* miRNA family. **B.** Deletion of each single *mir-34* locus does not induce compensatory expression from the other locus. **C.** Mating scheme for generating *Eμ-myc* $^{+}$*;mir-34a-/-* and *Eμ-myc* $^{+}$*;mir-34bc-/-* mice. Of note, there is a strong maternal effect in pups born of *Eμ-myc* $^{+}$. **D.** Deletion of *mir-34a* and *mir-34bc* accelerates *Eμ-myc* $^{+}$ lymphomagenesis (Em-*myc*$^{+}$ compared to *Eμ-myc* $^{+}$*;mir-34a-/-*, $p<0.0051$; *Eμ-myc* $^{+}$*;mir-34a-/-* compared to *Eμ-myc* $^{+}$*;mir-34b/c-/-* $p<0.0035$). **E.** *mir-34a* and *mir-34b/34c* are differentially regulated throughout B-lymphoma onset. The expression of *mir-34a* significantly decreases upon exposure to *Eμ-myc* $^{+}$ ($p<0.0026$), and further decreases as tumors progress ($p<0.0001$).

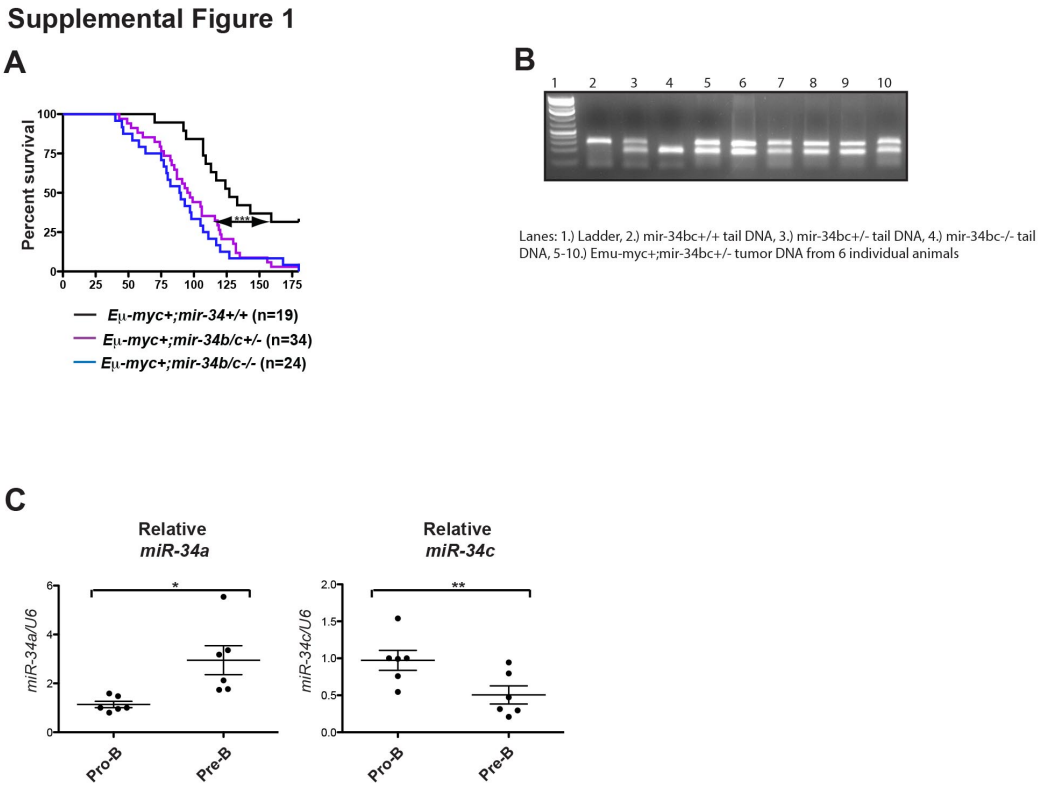

Supplemental Figure 1.

A. *Eμ-myc* $^{+}$*;mir-34bc+/-* mice accelerate lymphomagenesis at the same rate as *Eμ-myc;mir-34bc-/-* littermates. **B.** *Eμ-myc* $^{+}$*;mir-34bc+/-* tumors do not exhibit loss of heterozygosity of the second allele. **C.** *mir-34a* and *mir-34c* are preferentially expressed at different stages of B-cell development, with *mir-34a* being expressed relatively more highly in pre-B cells ($p<0.023$ paired *t* test), and *mir-34c* being expressed relatively more highly in pro-B cells ($p<0.0072$ paired *t* test).

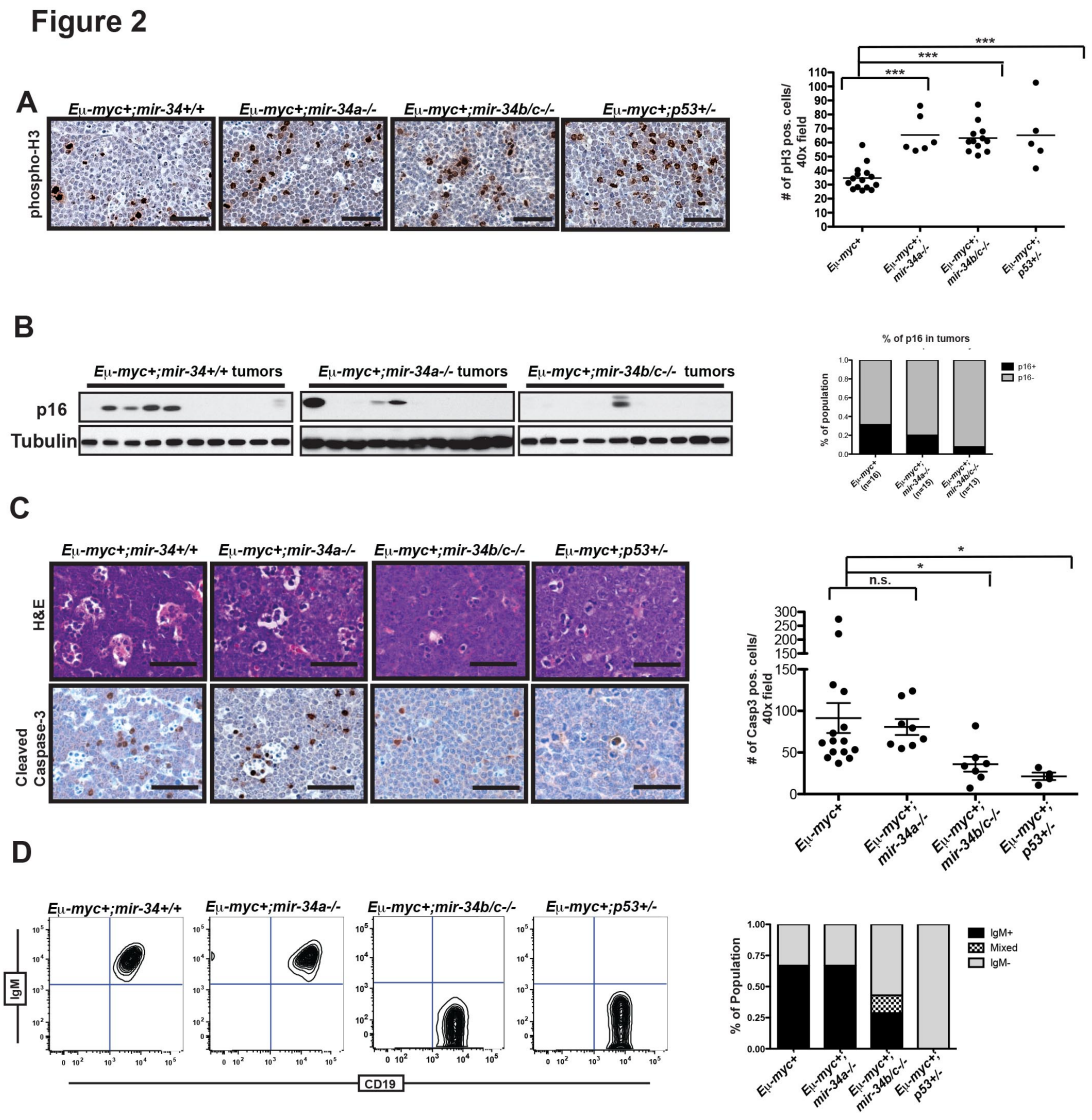

Figure 2. Deletion of *mir-34a* or *mir-34b/c* increases proliferation, while deletion of *mir-34b/c* inhibits apoptosis.

A. Lymph node tumors derived from *Eμ-myc* $^{+}$*;mir-34a-/-* and *Eμ-myc* $^{+}$*;mir-34b/c-/-* mice exhibit an increased rate of proliferation that is similar to *Eμ-myc* $^{+}$*;p53+/-* tumors as seen by phospho-H3 immunohistochemical staining. **B.** Additionally, protein lysate from these lymph node tumors exhibit a trending decrease in p16 expression, with a stronger phenotype seen in the *Eμ-myc* $^{+}$*;mir-34bc-/-* tumors. **C.** *Eμ-myc* $^{+}$*;mir-34b/c-/-* lymph node tumors, but not *Eμ-myc* $^{+}$*;mir-34a-/-* tumors exhibit less caspase-3 staining (*Eμ-myc* $^{+}$ compared to *Eμ-myc* $^{+}$*;mir-34b/c-/-, p*<0.0279; *Eμ-myc*$^{+}$ compared to *Eμ-myc* $^{+}$*;p53+/-, p*<0.0330). **D.** Immunophenotyping of tumors shows that *Eμ-myc* $^{+}$*;mir-34b/c-/-* tumors arise from progenitor IgM^{-} B-cells, similar to *Eμ-myc* $^{+}$*;p53+/-* while *Eμ-myc* $^{+}$*;mir-34a-/-* and *Eμ-myc* $^{+}$ develop tumors from later stages of B-cell development.

Figure 3

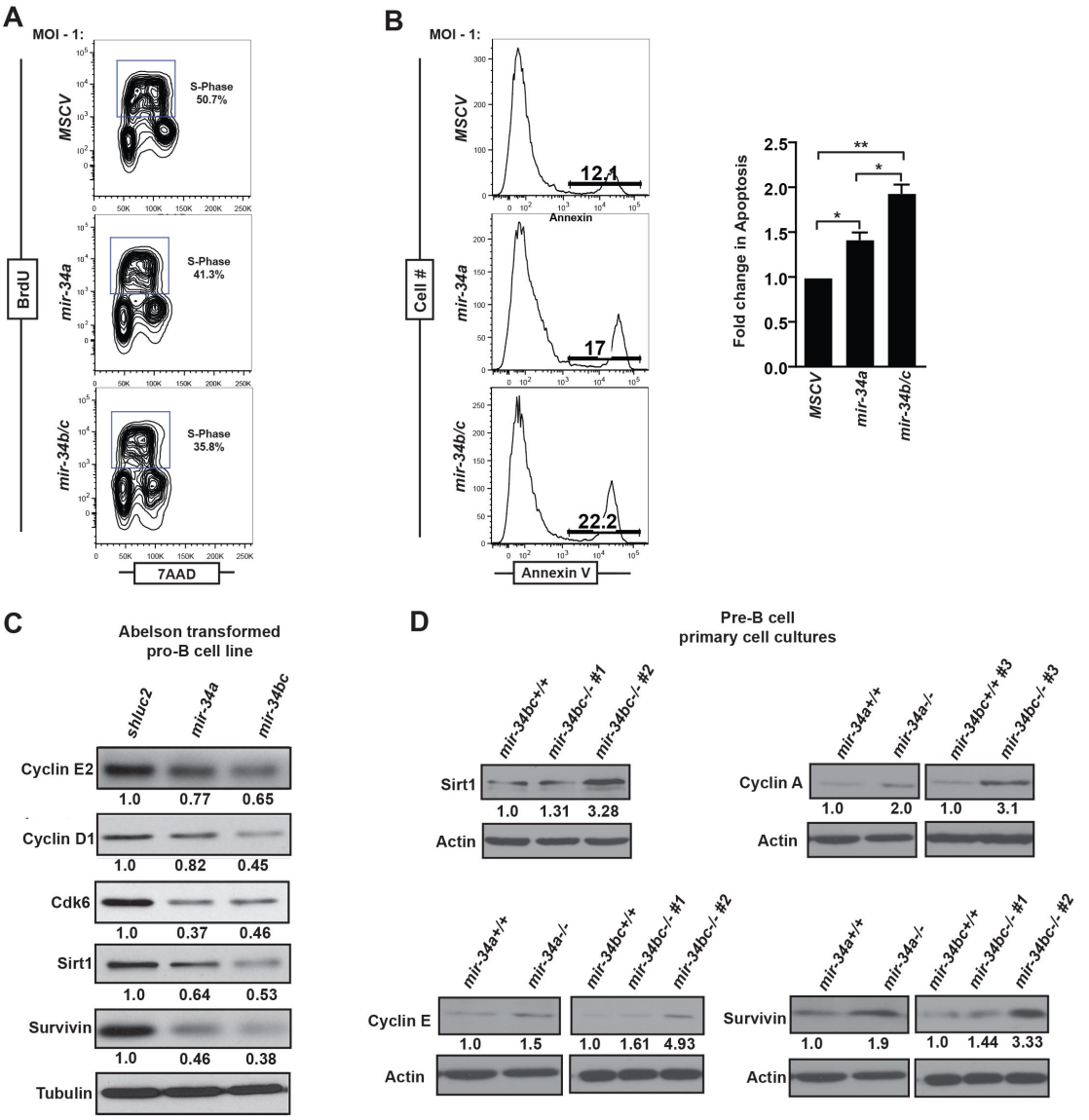

Figure 3. *mir-34* miRNAs inhibit proliferation and induce apoptosis by targeting cell cycle and anti-apoptotic genes.

A. Retroviral infection of MOI 1 shows *mir-34a* and, to a greater extent, *mir-34b/c* inhibiting cell cycle progression as seen by BrdU staining. **B.** Retroviral infection of MOI 1 shows that *mir-34a* and *mir-34b/c* to a greater extent induce apoptosis as seen by Annexin V staining. Graph displays quantification across three experiments. Paired *t* tests: MSCV vs. *mir-34a*, $p<0.0143$; MSCV vs. *mir-34b/c,* $p<0.0047$; *mir-34a* vs. *mir-34b/c,* $p<0.0395$ **C.** Overexpression of *mir-34a* and *mir-34b/c* downregulate cell cycle activators and anti-apoptotic targets. All of the above experiments were performed in an Abelson transformed pro-B cell line. **D.** Cultured primary B-cells from both *mir-34a-/-* and *mir-34b/c-/-* 4-6 week old mice exhibit an increase in protein levels of both cell cycle and anti-apoptotic target genes shown.

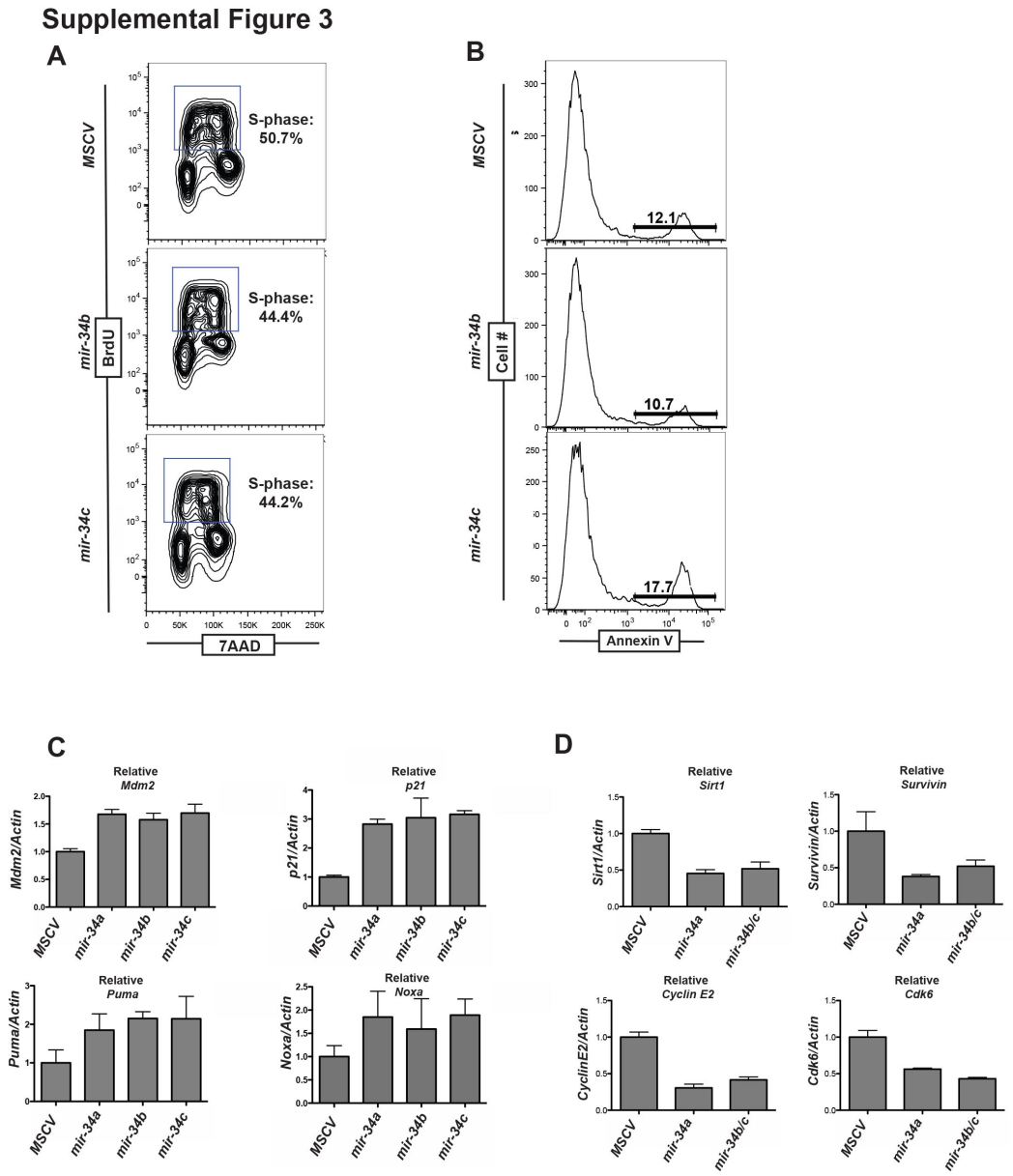

Supplemental Figure 3.

A. Overexpression of *mir-34b* and *mir-34c* at MOI of 1 exhibit a similar induction of cell cycle delay as seen by BrdU. The effects of *mir-34b* and *mir-34c* are compounded when expressed together (Fig. 3A). **B.** Overexpression of *mir-34b* at MOI 1 has less of an effect on apoptosis compared to *mir-34c,* however, more apoptosis is induced when *mir-34b/c* are overexpressed together (Fig. 3B). **C.** Overexpression of each *mir-34* miRNA induces the expression of p53 downstream targets *Mdm2, p12, Puma,* and *Noxa* in Abelson transformed pro-B cells. **D.** Overexpression of *mir-34a* or *mir-34b/c* downregulates target mRNA as well as protein levels (Fig. 3C).

Figure 4

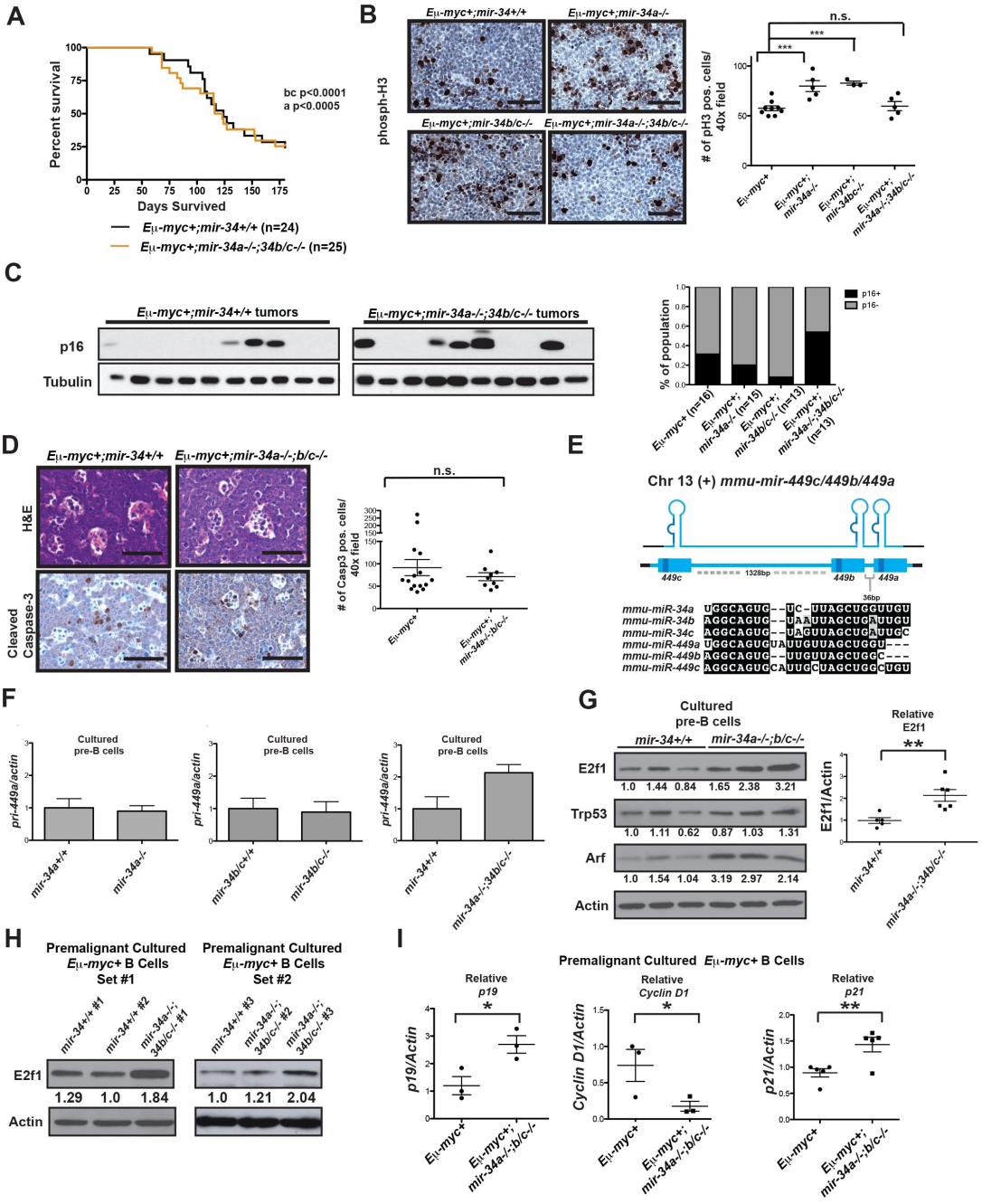
A
Percent survival
Days Survived
bc p<0.0001
a p<0.0005
Eμ-myc+;mir-34+/+ (n=24)
Eμ-myc+;mir-34a-/-;34b/c-/- (n=25)
B
Eμ-myc+;mir-34+/+
Eμ-myc+;mir-34a-/-
Eμ-myc+;mir-34b/c-/-
Eμ-myc+;mir-34a-/-;34b/c-/-
phosph-H3
# of pH3 pos. cells/ 40x field
n.s.
C
Eμ-myc+;mir-34+/+ tumors
Eμ-myc+;mir-34a-/-;34b/c-/- tumors
p16
Tubulin
% of population
p16+
p16-
D
H&E
Cleaved Caspase-3
# of Casp3 pos. cells/ 40x field
E
Chr 13 (+) mmu-mir-449c/449b/449a
449c
1328bp
449b
449a
36bp
mmu-miR-34a
mmu-miR-34b
mmu-miR-34c
mmu-miR-449a
mmu-miR-449b
mmu-miR-449c
F
Cultured pre-B cells
pri-449a/actin
mir-34a+/+
mir-34a-/-
mir-34b/c+/+
mir-34b/c-/-
mir-34+/+
mir-34a-/-;34b/c-/-
G
Cultured pre-B cells
mir-34+/+
mir-34a-/-;b/c-/-
E2f1
Trp53
Arf
Actin
Relative E2f1
E2f1/Actin
H
Premalignant Cultured Eμ-myc+ B Cells Set #1
Premalignant Cultured Eμ-myc+ B Cells Set #2
mir-34+/+ #1
mir-34+/+ #2
mir-34a-/-;34b/c-/- #1
mir-34+/+ #3
mir-34a-/-;34b/c-/- #2
mir-34a-/-;34b/c-/- #3
E2f1
1.29 1.0 1.84
1.0 1.21 2.04
Actin
I
Premalignant Cultured Eμ-myc+ B Cells
Relative p19
p19/Actin
Relative Cyclin D1
Cyclin D1/Actin
Relative p21
p21/Actin
Eμ-myc+
Eμ-myc+;mir-34a-/-;b/c-/-

Figure 4. Complete deletion of the *mir-34* miRNA family abolishes the acceleration of lymphoma seen in the both single knockout mice.
A. *Eμ-myc* $^{+}$*;mir-34a-/-;34b/c-/-* mice exhibit the same rate of lymphoma onset as *Eμ-myc* $^{+}$ control mice. **B.** Phospho-H3 immunohistochemistry of 4-6wk premalignant spleens show that *Eμ-myc* $^{+}$*;mir-34a-/-* ($p<0.0001$) and *Eμ-myc* $^{+}$*;mir-34b/c-/-* ($p<0.0005$) exhibit an increase in proliferation while *Eμ-myc* $^{+}$*;mir-34a-/-;34b/c-/-* do not. **C.** An immunoblot shows that there is no difference in the number of *Eμ-myc* $^{+}$*;mir-34a-/-;34b/c-/-* animals with tumors positive for p16 when compared to *Eμ-myc* $^{+}$ alone, and an increase when compared to *Eμ-myc*$^{+}$*;mir-34a-/-* and *Eμ-myc* $^{+}$*;mir-34b/c-/-*. **D.** *Eμ-myc* $^{+}$*;mir-34a-/-;34b/c-/-* lymph node tumors do not exhibit less caspase-3 staining. **E.** Gene structure of *mir-449* miRNA family, homologue to the *mir-34* miRNA family. **F.** Culture derived pre-B cells from *mir-34a-/-;34bc-/-* mice compensatorily upregulate *mir-449*, while *mir-34a-/-* and *mir-34b/c-/-* B-cells do not. **G.** Culture derived *mir-34a-/-;34b/c-/-* pre-B cells exhibit increased E2F1 and p19/Arf protein levels as compared to WT pre-B cells; p53 however seems unchanged. Quantification of two experiments shows E2f1 upregulation is significant $p<0.0029$. **H.** In the presence of *Eμ-myc*$^{+}$, cultured premalignant *Eμ-myc* $^{+}$*;mir-34a-/-;34b/c-/-* B-cells upregulate E2F1 compared to *Eμ-myc* $^{+}$ controls. **I.** *p19* and *p21* are upregulated ($p<0.0153$, and $p<0.005$) in premalignant cultured *Eμ-myc* $^{+}$*;mir-34a-/-;34b/c-/-* B-cells, while *Cylcin D1* is repressed ($p<0.035$).

Supplemental Figure 4

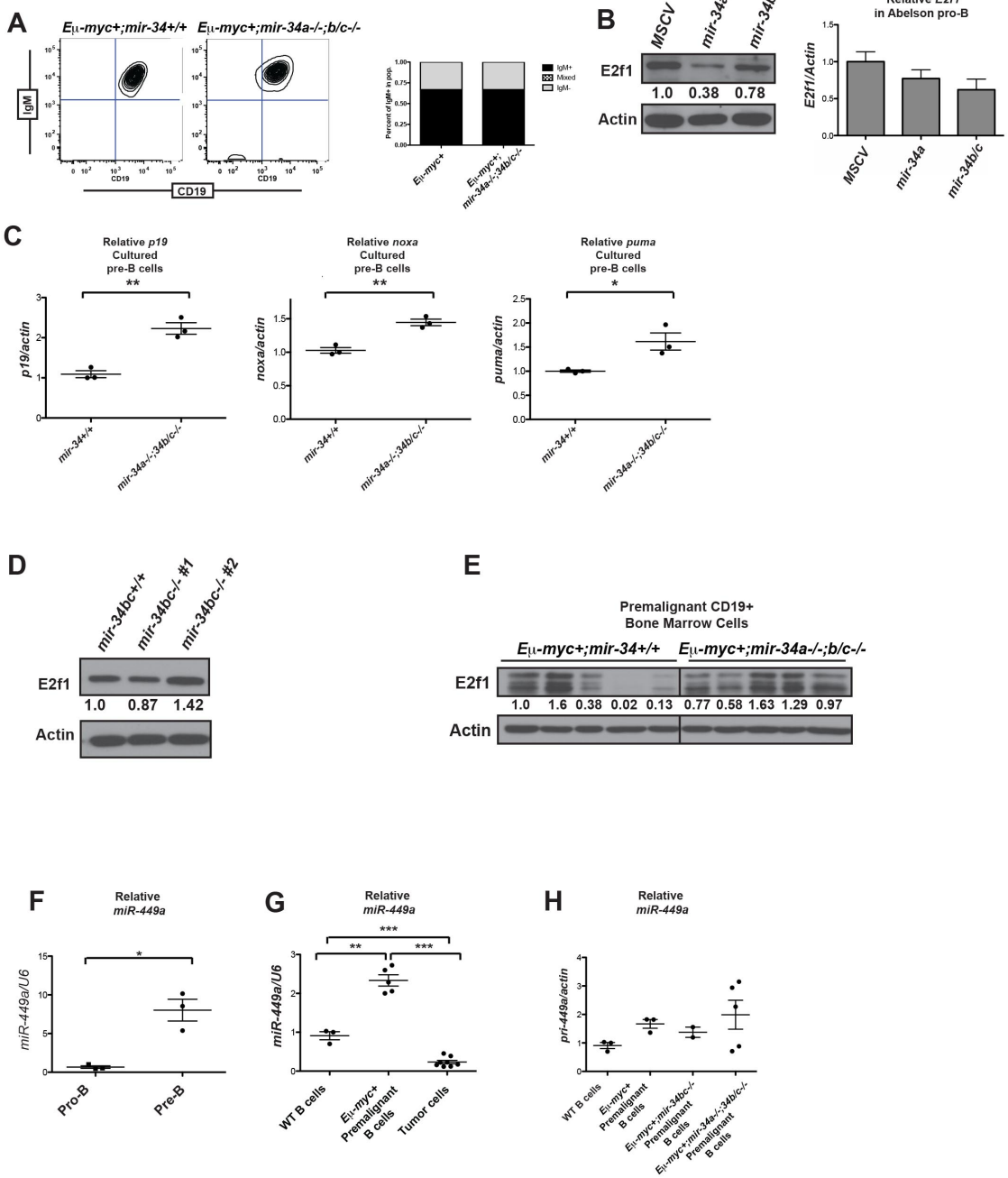

Supplemental Figure 4.
A. Immunophenotyping shows that *Eμ-myc* $^{+}$*;mir-34a-/-;34b/c-/-* tumors arise from immature B-cells like controls. **B.** E2f1 is a target of *mir-34* as overexpression of *mir-34a* or *mir-34b/c* downregulate E2f1 at the protein and RNA level. **C.** Bone marrow, culture-derived *mir-34a-/-;mir-34b/c-/-* B-cells exhibit an increase in E2F downstream targets *p19, puma*, and *noxa.* **D.** Single knockout *mir-34b/c-/-* culture derived B-cells do not seem to upregulate E2f1 to the same degree as *mir-34a-/-;mir-34b/c-/-* B-cells. **E.** Premalignant *Eμ-myc* $^{+}$*;mir-34a-/-;34b/c-/-* CD19+ B-cells upregulate E2F1 compared to *Eμ-myc* $^{+}$ controls. **F.** *miR-449a* is differentially regulated during B-cell development, with pre-B cells expressing about 8 fold higher levels than pro-B cells ($p<0.163$ paired *t* test). **G.** Expression of *mir-449* during tumor progression shows that *Eμ-myc* $^{+}$ induces *mir-449* expression that is eventually lost during tumor development. **H.** *mir-449* is sometimes upregulated in CD19+ premalignant B-cells from 4-6week old *Eμ-myc* $^{+}$*;mir-34a-/-b/c-/-* mice, but not in other single knockout genotypes.

Figure 5

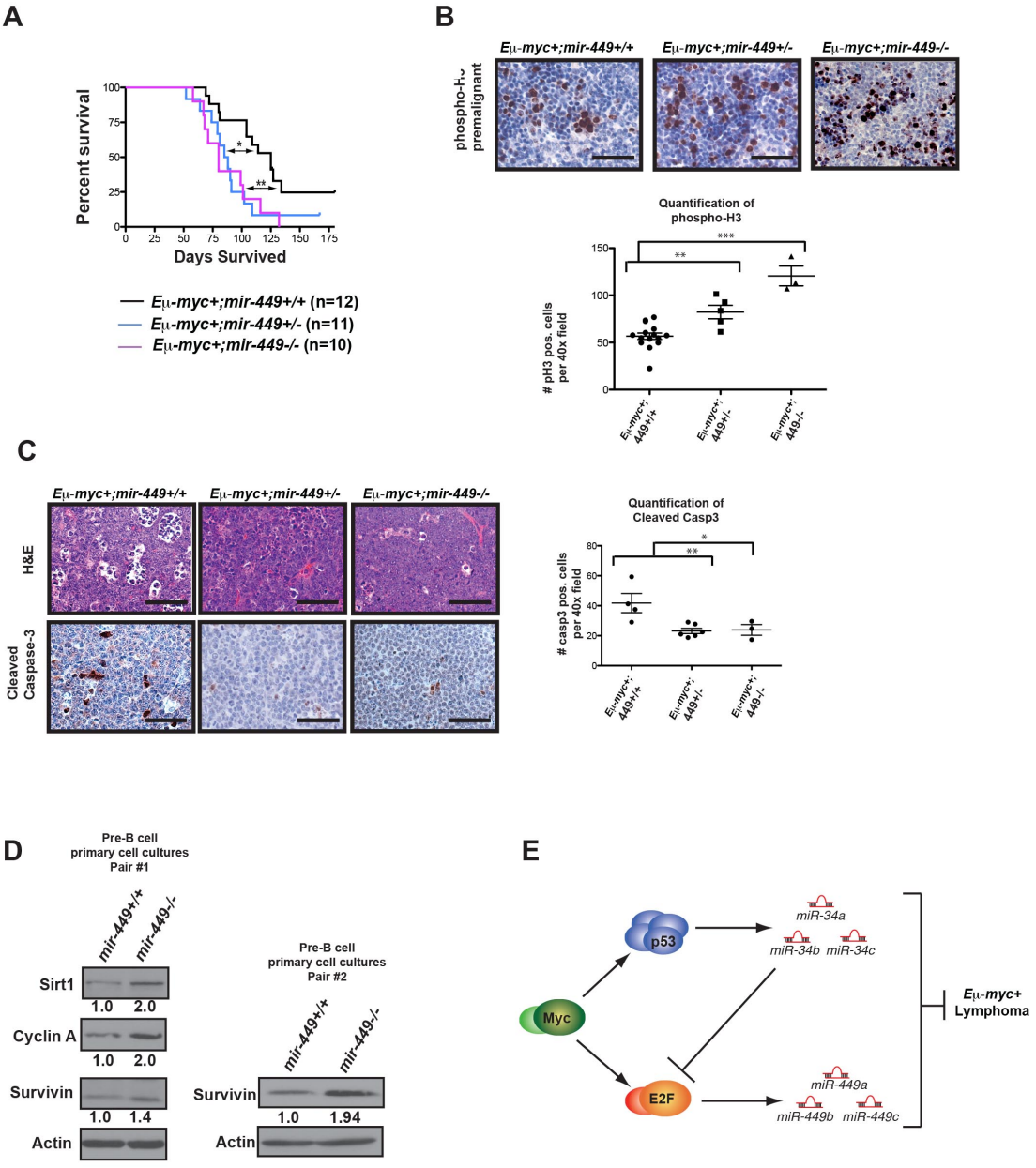

Figure 5. Deletion of *mir-449* accelerates *Eμ-myc* lymphomagenesis.
A. *Eμ-myc*$^{+}$*;mir-449+/-* and *Eμ-myc*$^{+}$*;mir-449-/-* mice have an increased rate of lymphomagenesis ($p<0.0133$ and $p<0.0046$ respectively). **B.** Phospho-H3 staining of premalignant spleens of 4-6week mice show that *Eμ-myc*$^{+}$*;mir-449+/-* and *Eμ-myc*$^{+}$*;mir-449-/-* mice exhibit an increase in proliferation($p<0.0011$ and $p<0.0001$). **C.** *Eμ-myc*$^{+}$*;mir-449+/-* and *Eμ-myc*$^{+}$*;mir-449-/-* lymph node tumors exhibit a decrease in caspase-3 staining and starry-skied morphology ($p<0.0048$ and $p<0.0394$). **D.** Culture pre-B *mir-449-/-* upregulate both cell cycle and anti-apoptotic target genes at the protein level. **E.** Diagram of the p53/*mir-34*/*E2f1*/*mir-449* feedback loop.

Supplemental Figure 5

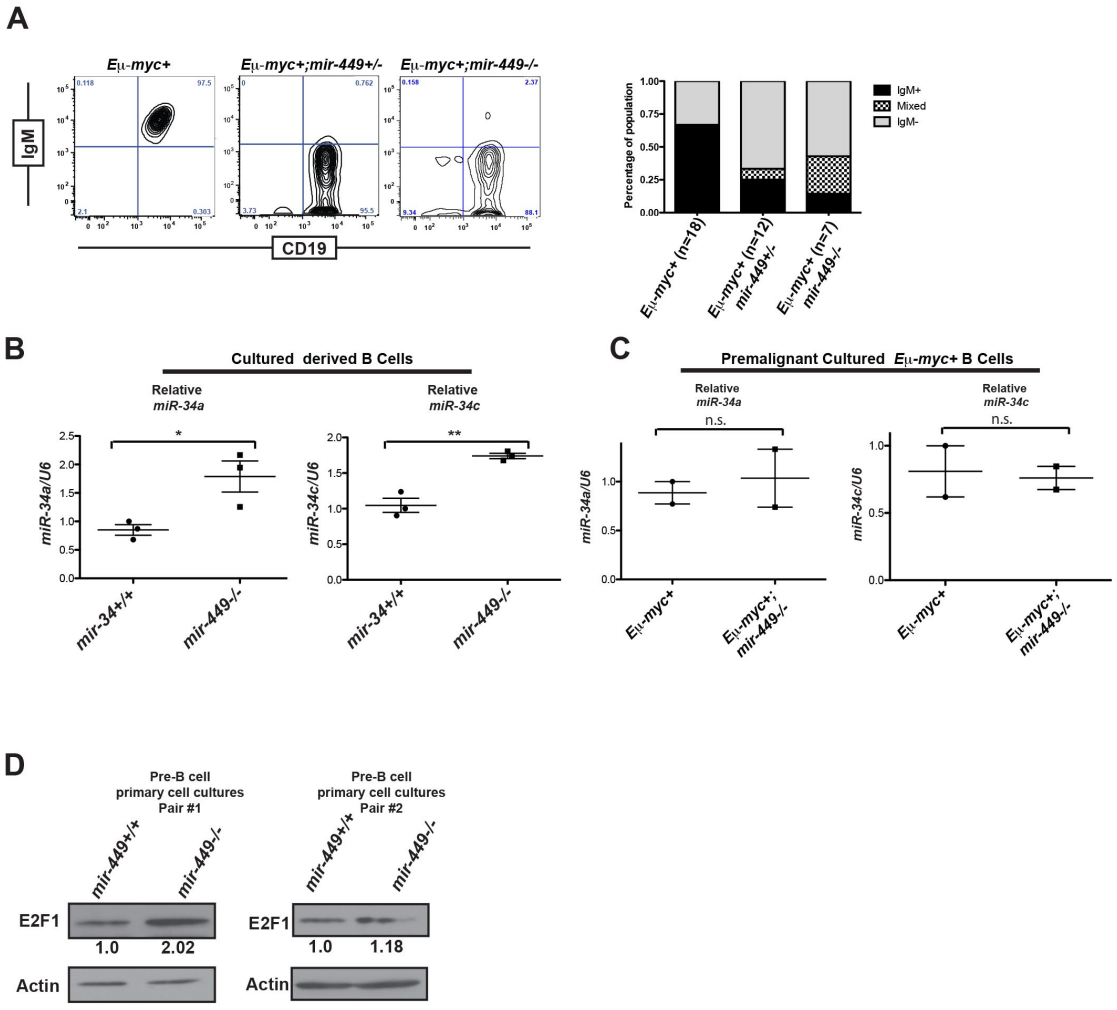

Supplemental Figure 5

A. Immunophenotyping indicates that *Eμ-myc* $^{+}$*;mir-449+/-* and *Eμ-myc* $^{+}$*;mir-449-/-* tumors arise from progenitor B-cells. **B.** *miR-34a* and *miR-34c* are upregulated in culture derived *mir-449-/-* B-cells. **C.** In the presence of *Eμ-myc*$^{+}$, it appears that *miR-34a* and *miR-34c* are not upregulated in premalignant cultured *Eμ-myc*$^{+}$*;mir-449-/-* B-cells. **D.** Single knockout *mir-449-/-* culture derived B-cells do not seem to upregulate E2f1 to the same degree as *mir-34a-/-;mir-34b/c-/-* B-cells.

Figure 6

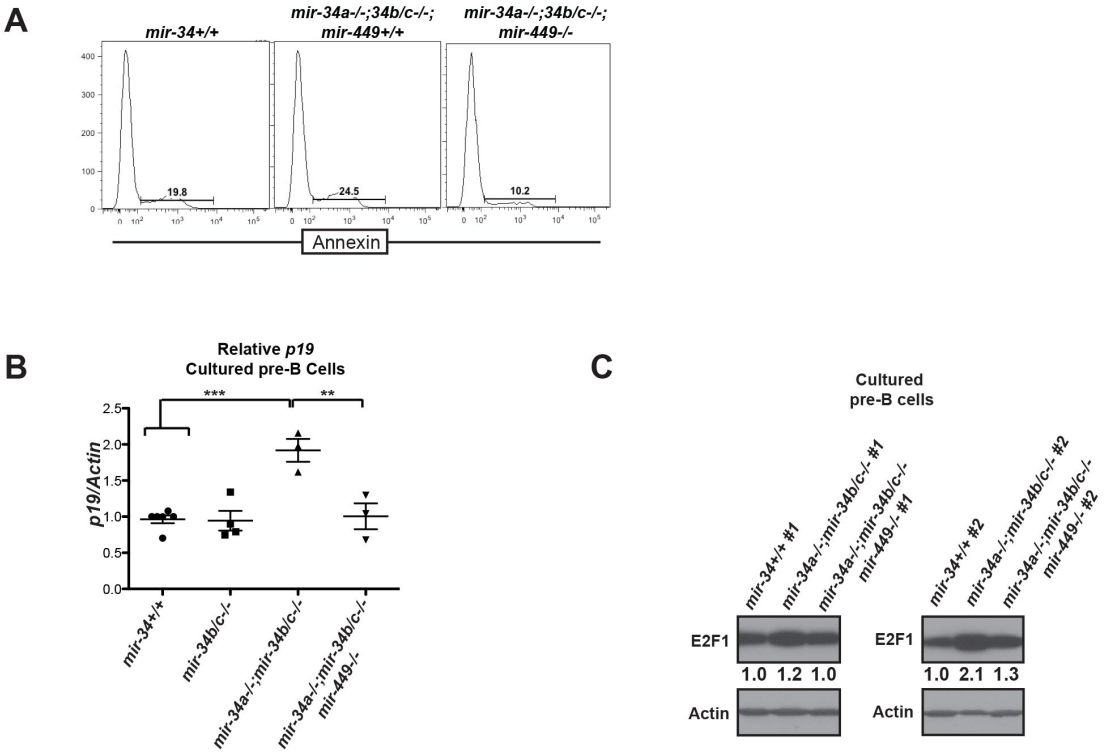

Figure 6. The complete deletion of *mir-34*/*mir-449* miRNAs seems to inhibit E2f1 induced apoptosis seen in the *mir-34a-/-;mir-34b/c-/-* mice.
A. *mir-34a-/-;mir-34b/c-/-;mir-449-/-* B-cells exhibit a decrease in basal cell-culture induced apoptosis compared to littermate *mir-34a-/-;mir-34b/c-/-;mir-449+/+* and age-matched wild-type controls. **B.** *p19* upregulation is rescued by deletion of *mir-449*, as seen in the *mir-34a-/-;mir-34b/c-/-;mir-449-/-* culture derived B-cells. **C.** There seems to be decrease in E2f1 levels in the *mir-34a-/-;mir-34b/c-/-;mir-449-/-* mice compared to their littermate controlled *mir-34a-/-;mir-34b/c-/-;mir-449+/+* mice, though there is likely a slight increase in E2f1 over wild-type B-cells.

Supplemental Figure 6

A

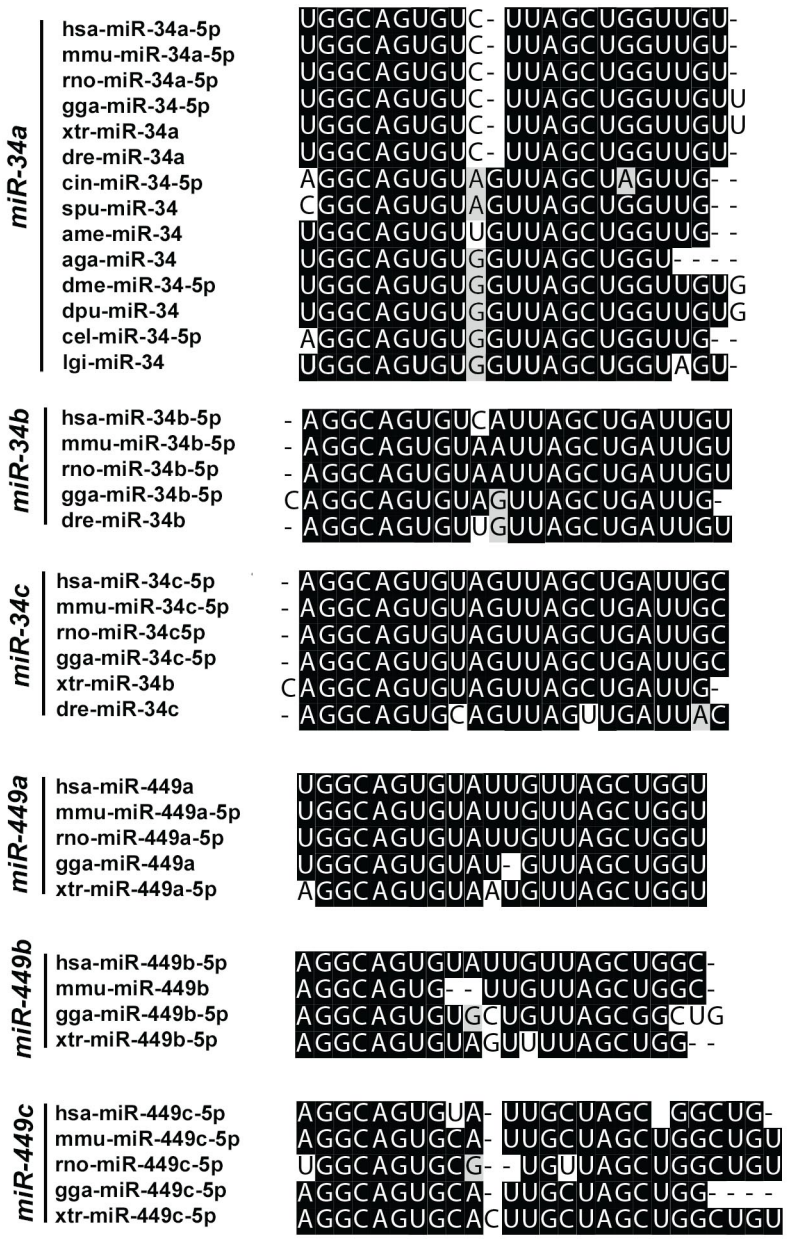

Supplemental Figure 6.
The *mir-34* and *mir-449* miRNAs are highly conserved across vertebrates.

Conclusions

In the Chapters above, I presented our discoveries that *mir-19* is a key oncogenic component of the polycistronic miRNA cluster, *mir-17-92,* and accelerates B-lymphoma by promoting cell survival through its downregulation of Pten (Chapter 1). Following, I presented our finding that *mir-92* provides an internal tumor suppressive function within *mir-17-92* in the *Eμ-myc* B-lymphoma mouse model. We found that *mir-92* targets the ubiquitin ligase Fbw7, responsible for inducing degradation of Myc. Thereby, overexpression of *mir-92* increases Myc protein levels and Myc-induced apoptosis, antagonizing *mir-19's* cell survival signals (Chapter 2). We saw that as tumors develop there is an increase in the ratio of *miR-19:miR-92*, indicating that cells with increased *mir-19* are selected for during tumor development. For this selection, these tumor cells either acquire the ability to increase the stability of *miR-19* or to process *miR-19* more efficiently; such mechanisms remain to be determined. While we have a better understanding of the functions *mir-17-92,* we do not know whether different miRNAs in the *mir-17-92* cluster exhibit similar antagonistic relationships across different cell types and in response to other oncogenic signals. Additionally, we have yet to determine whether other polycistronic miRNA clusters have similar internally built-in mechanisms to regulate their cellular effects.

In the final chapter, I presented our discovery of the *mir-34*/*mir-449* family's tumor suppressive functions. Deletion of each of these three miRNA loci accelerates *Eμ-myc* lymphomagenesis, while the complete deletion of *mir-34a* and *mir-34b/mir-34c* loci abolishes the acceleration. The acceleration is likely lost in the complete *mir-34* knockout mice because E2f1 is upregulated, which drives a compensatory upregulation of *mir-449.* Our discoveries of the fine-tuned regulation of the *mir-34* and *mir-449* miRNAs illuminate their importance in further linking the E2f1 and p53 pathways. Other work from our lab has shown that the *mir-34* and *mir-449* in fact share redundant functions as complete loss of this miRNA family impairs development of multiciliated cells and consequently the ability of these mice to thrive. However, the effects of complete loss of the *mir-34/mir-449* miRNAs in other cell types, including B-lymphoma, remains unclear. While we have some data suggesting that complete loss of *mir-34/mir-449* may protect normal B-cells from apoptosis, a different phenotype may be exhibited under the constitutive expression of the c-Myc oncogene. All in all, our discoveries suggest that miRNAs may have evolved and maintained such polycistronic structures, and seemingly redundant family members copies in order to cross-activate regulatory pathways for maintenance of normal cell growth.

References

1. Abubaker, J. *et al*. PIK3CA mutations are mutually exclusive with PTEN loss in diffuse large B-cell lymphoma. *Leukemia* **21,** 2368–70 (2007).

2. Adams, J. M. *et al*. The c-myc oncogene driven by immunoglobulin enhancers induces lymphoid malignancy in transgenic mice. *Nature* **318,** 533–538 (1985).

3. Ambros, V. The functions of animal microRNAs. *Nature* **431,** 350–5 (2004).

4. Ameres, S. L. & Zamore, P. D. Diversifying microRNA sequence and function. *Nat. Rev. Mol. Cell Biol.* **14,** 475–88 (2013).

5. Amir, S. *et al*. Oncomir miR-125b suppresses p14(ARF) to modulate p53-dependent and p53-independent apoptosis in prostate cancer. *PLoS One* **8,** e61064 (2013).

6. Arrate, M. P. *et al*. MicroRNA Biogenesis Is Required for Myc-Induced B-Cell Lymphoma Development and Survival. *Cancer Res.* **70,** 6083–6092 (2010).

7. Asangani, I. A. *et al*. MicroRNA-21 (miR-21) post-transcriptionally downregulates tumor suppressor Pdcd4 and stimulates invasion, intravasation and metastasis in colorectal cancer. *Oncogene* **27,** 2128–36 (2008).

8. Audrito, V. *et al*. Nicotinamide blocks proliferation and induces apoptosis of chronic lymphocytic leukemia cells through activation of the p53/miR-34a/SIRT1 tumor suppressor network. *Cancer Res.* **71,** 4473–83 (2011).

9. Ayala de la Peña, F. *et al*. Loss of p53 and acquisition of angiogenic microRNA profile are insufficient to facilitate progression of bladder urothelial carcinoma in situ to invasive carcinoma. *J. Biol. Chem.* **286,** 20778–87 (2011).

10. Baek, D. *et al*. The impact of microRNAs on protein output. *Nature* **455,** 64–71 (2008).

11. Bao, J. *et al*. MicroRNA-449 and microRNA-34b/c function redundantly in murine testes by targeting E2F transcription factor-retinoblastoma protein (E2F-pRb) pathway. *J. Biol. Chem.* **287,** 21686–98 (2012).

12. Bartel, D. P. MicroRNAs: target recognition and regulatory functions. *Cell* **136,** 215–33 (2009).

13. Böhlig, L., Friedrich, M. & Engeland, K. p53 activates the PANK1/miRNA-107 gene leading to downregulation of CDK6 and p130 cell cycle proteins. *Nucleic Acids Res.* **39,** 440–53 (2011).

14. Boldin, M. P. *et al*. miR-146a is a significant brake on autoimmunity, myeloproliferation, and cancer in mice. *J. Exp. Med.* **208,** 1189–201 (2011).

15. Bonci, D. *et al*. The miR-15a-miR-16-1 cluster controls prostate cancer by targeting multiple oncogenic activities. *Nat. Med.* **14,** 1271–7 (2008).

16. Boon, R. A. *et al*. MicroRNA-34a regulates cardiac ageing and function. *Nature* **495,** 107–10 (2013).

17. Borchert, G. M., Lanier, W. & Davidson, B. L. RNA polymerase III transcribes human microRNAs. *Nat. Struct. Mol. Biol.* **13,** 1097–101 (2006).

18. Bottoni, A. *et al.* miR-15a and miR-16-1 down-regulation in pituitary adenomas. *J. Cell. Physiol.* **204,** 280–5 (2005).

19. Bouchard, C. *et al.* FoxO transcription factors suppress Myc-driven lymphomagenesis via direct activation of Arf. *Genes Dev.* **21,** 2775–2787 (2007).

20. Bousquet, M., Harris, M. H., Zhou, B. & Lodish, H. F. MicroRNA miR-125b causes leukemia. *Proc. Natl. Acad. Sci. U. S. A.* **107,** 21558–63 (2010).

21. Bracken, C. P. *et al.* A double-negative feedback loop between ZEB1-SIP1 and the microRNA-200 family regulates epithelial-mesenchymal transition. *Cancer Res.* **68,** 7846–54 (2008).

22. Braun, C. J. *et al.* p53-Responsive micrornas 192 and 215 are capable of inducing cell cycle arrest. *Cancer Res.* **68,** 10094–104 (2008).

23. Brennecke, J., Hipfner, D. R., Stark, A., Russell, R. B. & Cohen, S. M. bantam encodes a developmentally regulated microRNA that controls cell proliferation and regulates the proapoptotic gene hid in Drosophila. *Cell* **113,** 25–36 (2003).

24. Brenner, J. L., Jasiewicz, K. L., Fahley, A. F., Kemp, B. J. & Abbott, A. L. Loss of individual microRNAs causes mutant phenotypes in sensitized genetic backgrounds in C. elegans. *Curr. Biol.* **20,** 1321–5 (2010).

25. Bu, P. *et al.* A microRNA miR-34a-regulated bimodal switch targets Notch in colon cancer stem cells. *Cell Stem Cell* **12,** 602–15 (2013).

26. Burger, M. L., Xue, L., Sun, Y., Kang, C. & Winoto, A. Premalignant PTEN-deficient thymocytes activate microRNAs miR-146a and miR-146b as a cellular defense against malignant transformation. *Blood* (2014). doi:10.1182/blood-2013-11-539411

27. Burns, D. M., D'Ambrogio, A., Nottrott, S. & Richter, J. D. CPEB and two poly(A) polymerases control miR-122 stability and p53 mRNA translation. *Nature* **473,** 105–8 (2011).

28. Butler, M. P., Wang, S. I., Chaganti, R. S., Parsons, R. & Dalla-Favera, R. Analysis of PTEN mutations and deletions in B-cell non-Hodgkin's lymphomas. *Genes. Chromosomes Cancer* **24,** 322–7 (1999).

29. Calin, G. A. *et al.* Frequent deletions and down-regulation of micro- RNA genes miR15 and miR16 at 13q14 in chronic lymphocytic leukemia. *Proc. Natl. Acad. Sci. U. S. A.* **99,** 15524–9 (2002).

30. Calin, G. A. *et al.* Human microRNA genes are frequently located at fragile sites and genomic regions involved in cancers. *Proc. Natl. Acad. Sci. U. S. A.* **101,** 2999–3004 (2004).

31. Campaner, S. & Amati, B. Two sides of the Myc-induced DNA damage response: from tumor suppression to tumor maintenance. *Cell Div.* **7,** 6 (2012).

32. Cao, X., Bennett, R. L. & May, W. S. c-Myc and caspase-2 are involved in activating Bax during cytotoxic drug-induced apoptosis. *J. Biol. Chem.* **283,** 14490–6 (2008).

33. Carraro, G. *et al*. miR-17 family of microRNAs controls FGF10-mediated embryonic lung epithelial branching morphogenesis through MAPK14 and STAT3 regulation of E-Cadherin distribution. *Dev. Biol*. **333,** 238–50 (2009).

34. Chakraborty, S., Mehtab, S., Patwardhan, A. & Krishnan, Y. Pri-miR-17-92a transcript folds into a tertiary structure and autoregulates its processing. *RNA* **18,** 1014–28 (2012).

35. Chan, J. A., Krichevsky, A. M. & Kosik, K. S. MicroRNA-21 is an antiapoptotic factor in human glioblastoma cells. *Cancer Res*. **65,** 6029–33 (2005).

36. Chang, C.-J. *et al*. p53 regulates epithelial-mesenchymal transition and stem cell properties through modulating miRNAs. *Nat. Cell Biol*. **13,** 317–23 (2011).

37. Chang, T.-C. *et al*. Transactivation of miR-34a by p53 broadly influences gene expression and promotes apoptosis. *Mol. Cell* **26,** 745–52 (2007).

38. Chang, T.-C. *et al*. Widespread microRNA repression by Myc contributes to tumorigenesis. *Nat. Genet*. **40,** 43–50 (2008).

39. Chaudhuri, A. A. *et al*. Oncomir miR-125b regulates hematopoiesis by targeting the gene Lin28A. *Proc. Natl. Acad. Sci. U. S. A*. **109,** 4233–8 (2012).

40. Chaulk, S. G. *et al*. Role of pri-miRNA tertiary structure in miR-17~92 miRNA biogenesis. *RNA Biol*. **8,** 1105–14

41. Chen, L. *et al*. P53-induced microRNA-107 inhibits proliferation of glioma cells and down-regulates the expression of CDK6 and Notch-2. *Neurosci. Lett*. **534,** 327–32 (2013).

42. Chen, X., Ko, L. J., Jayaraman, L. & Prives, C. p53 levels, functional domains, and DNA damage determine the extent of the apoptotic response of tumor cells. *Genes Dev*. **10,** 2438–2451 (1996).

43. Cheng, C.-Y. *et al*. miR-34 Cooperates with p53 in Suppression of Prostate Cancer by Joint Regulation of Stem Cell Compartment. *Cell Rep*. **6,** 1000–7 (2014).

44. Chi, S. W., Zang, J. B., Mele, A. & Darnell, R. B. Argonaute HITS-CLIP decodes microRNA-mRNA interaction maps. *Nature* **460,** 479–86 (2009).

45. Chou, J. *et al*. GATA3 suppresses metastasis and modulates the tumour microenvironment by regulating microRNA-29b expression. *Nat. Cell Biol*. **15,** 201–13 (2013).

46. Christoffersen, N. R. *et al*. p53-independent upregulation of miR-34a during oncogene-induced senescence represses MYC. *Cell Death Differ*. **17,** 236–45 (2010).

47. Cimmino, A. *et al*. miR-15 and miR-16 induce apoptosis by targeting BCL2. *Proc. Natl. Acad. Sci. U. S. A*. **102,** 13944–9 (2005).

48. Comer, F. I. & Parent, C. A. PI 3-Kinases and PTEN. *Cell* **109,** 541–544 (2002).

49. Concepcion, C. P. *et al*. Intact p53-dependent responses in miR-34-deficient mice. *PLoS Genet*. **8,** e1002797 (2012).

50. Conkrite, K. *et al*. miR-17~92 cooperates with RB pathway mutations to promote retinoblastoma. *Genes Dev*. **25,** 1734–45 (2011).

51. Costinean, S. *et al*. Pre-B cell proliferation and lymphoblastic leukemia/high-grade lymphoma in E(mu)-miR155 transgenic mice. *Proc. Natl. Acad. Sci. U. S. A.* **103,** 7024–9 (2006).

52. Craig, V. J. *et al*. Myc-mediated repression of microRNA-34a promotes high-grade transformation of B-cell lymphoma by dysregulation of FoxP1. *Blood* **117,** 6227–36 (2011).

53. Crusio, K. M., King, B., Reavie, L. B. & Aifantis, I. The ubiquitous nature of cancer: the role of the SCF(Fbw7) complex in development and transformation. *Oncogene* **29,** 4865–73 (2010).

54. Cui, J.-W. *et al*. Retroviral insertional activation of the Fli-3 locus in erythroleukemias encoding a cluster of microRNAs that convert Epo-induced differentiation to proliferation. *Blood* **110,** 2631–40 (2007).

55. Cummins, J. M. *et al*. The colorectal microRNAome. *Proc. Natl. Acad. Sci. U. S. A.* **103,** 3687–92 (2006).

56. Czyzyk-Krzeska, M. F. & Zhang, X. MiR-155 at the heart of oncogenic pathways. *Oncogene* **33,** 677–8 (2014).

57. Dar, A. A. *et al*. The role of miR-18b in MDM2-p53 pathway signaling and melanoma progression. *J. Natl. Cancer Inst*. **105,** 433–42 (2013).

58. Davis, B. N., Hilyard, A. C., Lagna, G. & Hata, A. SMAD proteins control DROSHA-mediated microRNA maturation. *Nature* **454,** 56–61 (2008).

59. Denli, A. M., Tops, B. B. J., Plasterk, R. H. A., Ketting, R. F. & Hannon, G. J. Processing of primary microRNAs by the Microprocessor complex. *Nature* **432,** 231–5 (2004).

60. Dennis, G. *et al*. DAVID: Database for Annotation, Visualization, and Integrated Discovery. *Genome Biol*. **4,** P3 (2003).

61. Dews, M. *et al*. Augmentation of tumor angiogenesis by a Myc-activated microRNA cluster. *Nat. Genet*. **38,** 1060–5 (2006).

62. Di Cristofano, A., Pesce, B., Cordon-Cardo, C. & Pandolfi, P. P. Pten is essential for embryonic development and tumour suppression. *Nat. Genet*. **19,** 348–55 (1998).

63. Di Cristofano, A. & Pandolfi, P. P. The Multiple Roles of PTEN in Tumor Suppression. *Cell* **100,** 387–390 (2000).

64. Dimri, G. P., Itahana, K., Acosta, M. & Campisi, J. Regulation of a Senescence Checkpoint Response by the E2F1 Transcription Factor and p14ARF Tumor Suppressor. *Mol. Cell. Biol*. **20,** 273–285 (2000).

65. Dudda, J. C. *et al*. MicroRNA-155 is required for effector CD8+ T cell responses to virus infection and cancer. *Immunity* **38,** 742–53 (2013).

66. Egle, A., Harris, A. W., Bouillet, P. & Cory, S. Bim is a suppressor of Myc-induced mouse B cell leukemia. *Proc. Natl. Acad. Sci. U. S. A.* **101,** 6164–9 (2004).

67. Eischen, C. M., Roussel, M. F., Korsmeyer, S. J. & Cleveland, J. L. Bax loss impairs Myc-induced apoptosis and circumvents the selection of p53 mutations during Myc-mediated lymphomagenesis. *Mol. Cell. Biol.* **21,** 7653–62 (2001).

68. Eischen, C. M., Woo, D., Roussel, M. F. & Cleveland, J. L. Apoptosis triggered by Myc-induced suppression of Bcl-X(L) or Bcl-2 is bypassed during lymphomagenesis. *Mol. Cell. Biol.* **21,** 5063–70 (2001).

69. Eischen, C. M., Weber, J. D., Roussel, M. F., Sherr, C. J. & Cleveland, J. L. Disruption of the ARF-Mdm2-p53 tumor suppressor pathway in Myc-induced lymphomagenesis. *Genes Dev.* **13,** 2658–2669 (1999).

70. Eulalio, A., Huntzinger, E. & Izaurralde, E. GW182 interaction with Argonaute is essential for miRNA-mediated translational repression and mRNA decay. *Nat. Struct. Mol. Biol.* **15,** 346–53 (2008).

71. Evan, G. I. & Vousden, K. H. Proliferation, cell cycle and apoptosis in cancer. *Nature* **411,** 342–8 (2001).

72. Fabbri, M. *et al.* Association of a microRNA/TP53 feedback circuitry with pathogenesis and outcome of B-cell chronic lymphocytic leukemia. *JAMA* **305,** 59–67 (2011).

73. Fabbri, M. *et al.* MicroRNA-29 family reverts aberrant methylation in lung cancer by targeting DNA methyltransferases 3A and 3B. *Proc. Natl. Acad. Sci. U. S. A.* **104,** 15805–10 (2007).

74. Farh, K. K.-H. *et al.* The widespread impact of mammalian MicroRNAs on mRNA repression and evolution. *Science* **310,** 1817–21 (2005).

75. Feldser, D. M. & Greider, C. W. Short telomeres limit tumor progression in vivo by inducing senescence. *Cancer Cell* **11,** 461–9 (2007).

76. Filipowicz, W., Bhattacharyya, S. N. & Sonenberg, N. Mechanisms of post-transcriptional regulation by microRNAs: are the answers in sight? *Nat. Rev. Genet.* **9,** 102–14 (2008).

77. Fornari, F. *et al.* MiR-122/cyclin G1 interaction modulates p53 activity and affects doxorubicin sensitivity of human hepatocarcinoma cells. *Cancer Res.* **69,** 5761–7 (2009).

78. Fujita, Y. *et al.* Effects of miR-34a on cell growth and chemoresistance in prostate cancer PC3 cells. *Biochem. Biophys. Res. Commun.* **377,** 114–9 (2008).

79. Fukuda, T. *et al.* DEAD-box RNA helicase subunits of the Drosha complex are required for processing of rRNA and a subset of microRNAs. *Nat. Cell Biol.* **9,** 604–11 (2007).

80. Garrison, S. P. *et al.* Selection against PUMA gene expression in Myc-driven B-cell lymphomagenesis. *Mol. Cell. Biol.* **28,** 5391–402 (2008).

81. Gefen, N. *et al.* Hsa-mir-125b-2 is highly expressed in childhood ETV6/RUNX1 (TEL/AML1) leukemias and confers survival advantage to growth inhibitory signals independent of p53. *Leukemia* **24,** 89–96 (2010).

82. Geng, L. *et al.* MicroRNA-192 suppresses liver metastasis of colon cancer. *Oncogene* (2013). doi:10.1038/onc.2013.478

83. Georges, S. A. *et al*. Coordinated regulation of cell cycle transcripts by p53-Inducible microRNAs, miR-192 and miR-215. *Cancer Res*. **68,** 10105–12 (2008).

84. Gibbons, D. L. *et al*. Contextual extracellular cues promote tumor cell EMT and metastasis by regulating miR-200 family expression. *Genes Dev*. **23,** 2140–51 (2009).

85. Giraldez, A. J. *et al*. Zebrafish MiR-430 promotes deadenylation and clearance of maternal mRNAs. *Science* **312,** 75–9 (2006).

86. Gottlieb, T. M., Leal, J. F. M., Seger, R., Taya, Y. & Oren, M. Cross-talk between Akt, p53 and Mdm2: possible implications for the regulation of apoptosis. *Oncogene* **21,** 1299–303 (2002).

87. Gregory, P. A. *et al*. The miR-200 family and miR-205 regulate epithelial to mesenchymal transition by targeting ZEB1 and SIP1. *Nat. Cell Biol*. **10,** 593–601 (2008).

88. Griffiths-Jones, S. miRBase: the microRNA sequence database. *Methods Mol. Biol*. **342,** 129–38 (2006).

89. Grim, J. E. *et al*. Isoform- and cell cycle-dependent substrate degradation by the Fbw7 ubiquitin ligase. *J. Cell Biol*. **181,** 913–20 (2008).

90. Grim, J. E. *et al*. Fbw7 and p53 cooperatively suppress advanced and chromosomally unstable intestinal cancer. *Mol. Cell. Biol*. **32,** 2160–7 (2012).

91. Grimson, A. *et al*. MicroRNA targeting specificity in mammals: determinants beyond seed pairing. *Mol. Cell* **27,** 91–105 (2007).

92. Grishok, A. *et al*. Genes and mechanisms related to RNA interference regulate expression of the small temporal RNAs that control C. elegans developmental timing. *Cell* **106,** 23–34 (2001).

93. Gu, S., Jin, L., Zhang, F., Sarnow, P. & Kay, M. a. Biological basis for restriction of microRNA targets to the 3' untranslated region in mammalian mRNAs. *Nat. Struct. Mol. Biol*. **16,** 144–50 (2009).

94. Guil, S. & Cáceres, J. F. The multifunctional RNA-binding protein hnRNP A1 is required for processing of miR-18a. *Nat. Struct. Mol. Biol*. **14,** 591–6 (2007).

95. Ha, T.-Y. The role of regulatory T cells in cancer. *Immune Netw*. **9,** 209–35 (2009).

96. Hagan, J. P., Piskounova, E. & Gregory, R. I. Lin28 recruits the TUTase Zcchc11 to inhibit let-7 maturation in mouse embryonic stem cells. *Nat. Struct. Mol. Biol*. **16,** 1021–5 (2009).

97. Han, J. *et al*. The Drosha-DGCR8 complex in primary microRNA processing. *Genes Dev*. **18,** 3016–27 (2004).

98. Han, Y.-C. *et al*. microRNA-29a induces aberrant self-renewal capacity in hematopoietic progenitors, biased myeloid development, and acute myeloid leukemia. *J. Exp. Med*. **207,** 475–89 (2010).

99. Hanahan, D., Wagner, E. F. & Palmiter, R. D. The origins of oncomice: a history of the first transgenic mice genetically engineered to develop cancer. *Genes Dev*. **21,** 2258–70 (2007).

100. Harris, A. W. *et al*. The E mu-myc transgenic mouse. A model for high-incidence spontaneous lymphoma and leukemia of early B cells. *J. Exp. Med.* **167,** 353–71 (1988).

101. Harvey, K. F., Zhang, X. & Thomas, D. M. The Hippo pathway and human cancer. *Nat. Rev. Cancer* **13,** 246–57 (2013).

102. Hatley, M. E. *et al*. Modulation of K-Ras-dependent lung tumorigenesis by MicroRNA-21. *Cancer Cell* **18,** 282–93 (2010).

103. Hayashita, Y. *et al*. A polycistronic microRNA cluster, miR-17-92, is overexpressed in human lung cancers and enhances cell proliferation. *Cancer Res.* **65,** 9628–32 (2005).

104. He, L. *et al*. A microRNA component of the p53 tumour suppressor network. *Nature* **447,** 1130–1134 (2007).

105. He, L. & Hannon, G. J. MicroRNAs: small RNAs with a big role in gene regulation. *Nat. Rev. Genet.* **5,** 522–31 (2004).

106. He, L., He, X., Lowe, S. W. & Hannon, G. J. microRNAs join the p53 network--another piece in the tumour-suppression puzzle. *Nat. Rev. Cancer* **7,** 819–22 (2007).

107. He, L. *et al*. A microRNA polycistron as a potential human oncogene. *Nature* **435,** 828–33 (2005).

108. Hemann, M. T. *et al*. Evasion of the p53 tumour surveillance network by tumour-derived MYC mutants. *Nature* **436,** 807–11 (2005).

109. Hemann, M. T. *et al*. An epi-allelic series of p53 hypomorphs created by stable RNAi produces distinct tumor phenotypes in vivo. *Nat. Genet.* **33,** 396–400 (2003).

110. Hemann, M. T. *et al*. Suppression of tumorigenesis by the p53 target PUMA. *Proc. Natl. Acad. Sci. U. S. A.* **101,** 9333–8 (2004).

111. Heo, I. *et al*. Mono-uridylation of pre-microRNA as a key step in the biogenesis of group II let-7 microRNAs. *Cell* **151,** 521–32 (2012).

112. Heo, I. *et al*. Lin28 mediates the terminal uridylation of let-7 precursor MicroRNA. *Mol. Cell* **32,** 276–84 (2008).

113. Hermeking, H. The miR-34 family in cancer and apoptosis. *Cell Death Differ.* **17,** 193–9 (2010).

114. Hermeking, H. MicroRNAs in the p53 network: micromanagement of tumour suppression. *Nat. Rev. Cancer* **12,** 613–26 (2012).

115. Hershko, T., Chaussepied, M., Oren, M. & Ginsberg, D. Novel link between E2F and p53: proapoptotic cofactors of p53 are transcriptionally upregulated by E2F. *Cell Death Differ.* **12,** 377–83 (2005).

116. Hill, D. A. *et al*. DICER1 mutations in familial pleuropulmonary blastoma. *Science* **325,** 965 (2009).

117. Hong, L. *et al*. The miR-17-92 cluster of microRNAs confers tumorigenicity by inhibiting oncogene-induced senescence. *Cancer Res.* **70,** 8547–57 (2010).

118. Hossain, A., Kuo, M. T. & Saunders, G. F. Mir-17-5p regulates breast cancer cell proliferation by inhibiting translation of AIB1 mRNA. *Mol. Cell. Biol.* **26,** 8191–201 (2006).

119. Hu, W. *et al.* MiR-29a Maintains Hematopoietic Stem Cell Self-Renewal and Is Required For Myeloid Leukemogenesis. *Blood* **122,** 1190– (2013).

120. Hu, W. *et al.* Negative regulation of tumor suppressor p53 by microRNA miR-504. *Mol. Cell* **38,** 689–99 (2010).

121. Huang, Q. *et al.* The microRNAs miR-373 and miR-520c promote tumour invasion and metastasis. *Nat. Cell Biol.* **10,** 202–10 (2008).

122. Huse, J. T. *et al.* The PTEN-regulating microRNA miR-26a is amplified in high-grade glioma and facilitates gliomagenesis in vivo. *Genes Dev.* **23,** 1327–37 (2009).

123. Hutvágner, G. *et al.* A cellular function for the RNA-interference enzyme Dicer in the maturation of the let-7 small temporal RNA. *Science* **293,** 834–8 (2001).

124. Hwang, H.-W., Wentzel, E. A. & Mendell, J. T. Cell-cell contact globally activates microRNA biogenesis. *Proc. Natl. Acad. Sci. U. S. A.* **106,** 7016–21 (2009).

125. Iannello, A., Thompson, T. W., Ardolino, M., Lowe, S. W. & Raulet, D. H. p53-dependent chemokine production by senescent tumor cells supports NKG2D-dependent tumor elimination by natural killer cells. *J. Exp. Med.* **210,** 2057–69 (2013).

126. Incoronato, M. *et al.* miR-212 increases tumor necrosis factor-related apoptosis-inducing ligand sensitivity in non-small cell lung cancer by targeting the antiapoptotic protein PED. *Cancer Res.* **70,** 3638–46 (2010).

127. Inomata, M. *et al.* MicroRNA-17-92 down-regulates expression of distinct targets in different B-cell lymphoma subtypes. *Blood* **113,** 396–402 (2009).

128. Jacobs, J. J. L. *et al.* Bmi-1 collaborates with c-Myc in tumorigenesis by inhibiting c-Myc-induced apoptosis via INK4a/ARF. *Genes Dev.* **13,** 2678–2690 (1999).

129. Jazdzewski, K. *et al.* Common SNP in pre-miR-146a decreases mature miR expression and predisposes to papillary thyroid carcinoma. *Proc. Natl. Acad. Sci. U. S. A.* **105,** 7269–74 (2008).

130. Ji, Q. *et al.* Restoration of tumor suppressor miR-34 inhibits human p53-mutant gastric cancer tumorspheres. *BMC Cancer* **8,** 266 (2008).

131. Jiang, S. *et al.* A novel miR-155/miR-143 cascade controls glycolysis by regulating hexokinase 2 in breast cancer cells. *EMBO J.* **31,** 1985–98 (2012).

132. Johnson, S. M. *et al.* RAS is regulated by the let-7 microRNA family. *Cell* **120,** 635–47 (2005).

133. Kato, M. *et al.* The mir-34 microRNA is required for the DNA damage response in vivo in C. elegans and in vitro in human breast cancer cells. *Oncogene* **28,** 2419–24 (2009).

134. Kawai, S. & Amano, A. BRCA1 regulates microRNA biogenesis via the DROSHA microprocessor complex. *J. Cell Biol.* **197,** 201–8 (2012).

135. Keklikoglou, I. *et al*. MicroRNA-520/373 family functions as a tumor suppressor in estrogen receptor negative breast cancer by targeting NF-κB and TGF-β signaling pathways. *Oncogene* **31,** 4150–63 (2012).

136. Kent, O. A. *et al*. Repression of the miR-143/145 cluster by oncogenic Ras initiates a tumor-promoting feed-forward pathway. *Genes Dev*. **24,** 2754–9 (2010).

137. Khvorova, A., Reynolds, A. & Jayasena, S. D. Functional siRNAs and miRNAs exhibit strand bias. *Cell* **115,** 209–16 (2003).

138. Kim, H.-R., Roe, J.-S., Lee, J.-E., Cho, E.-J. & Youn, H.-D. p53 regulates glucose metabolism by miR-34a. *Biochem. Biophys. Res. Commun*. **437,** 225–31 (2013).

139. Kim, N. H. *et al*. p53 and microRNA-34 are suppressors of canonical Wnt signaling. *Sci. Signal*. **4,** ra71 (2011).

140. Kim, S.-W. *et al*. MicroRNAs miR-125a and miR-125b constitutively activate the NF-κB pathway by targeting the tumor necrosis factor alpha-induced protein 3 (TNFAIP3, A20). *Proc. Natl. Acad. Sci. U. S. A*. **109,** 7865–70 (2012).

141. Kim, T. *et al*. p53 regulates epithelial-mesenchymal transition through microRNAs targeting ZEB1 and ZEB2. *J. Exp. Med*. **208,** 875–83 (2011).

142. Kim, V. N., Han, J. & Siomi, M. C. Biogenesis of small RNAs in animals. *Nat. Rev. Mol. Cell Biol*. **10,** 126–39 (2009).

143. Kim, Y.-K. & Kim, V. N. Processing of intronic microRNAs. *EMBO J*. **26,** 775–83 (2007).

144. Kiriakidou, M. *et al*. An mRNA m7G cap binding-like motif within human Ago2 represses translation. *Cell* **129,** 1141–51 (2007).

145. Kistner, A. *et al*. Doxycycline-mediated quantitative and tissue-specific control of gene expression in transgenic mice. *Proc. Natl. Acad. Sci*. **93,** 10933–10938 (1996).

146. Klein, U. *et al*. The DLEU2/miR-15a/16-1 cluster controls B cell proliferation and its deletion leads to chronic lymphocytic leukemia. *Cancer Cell* **17,** 28–40 (2010).

147. Klusmann, J.-H. *et al*. miR-125b-2 is a potential oncomiR on human chromosome 21 in megakaryoblastic leukemia. *Genes Dev*. **24,** 478–90 (2010).

148. Knobbe, C. B., Lapin, V., Suzuki, A. & Mak, T. W. The roles of PTEN in development, physiology and tumorigenesis in mouse models: a tissue-by-tissue survey. *Oncogene* **27,** 5398–415 (2008).

149. Kong, W. *et al*. MicroRNA-155 is regulated by the transforming growth factor beta/Smad pathway and contributes to epithelial cell plasticity by targeting RhoA. *Mol. Cell. Biol*. **28,** 6773–84 (2008).

150. Kota, J. *et al*. Therapeutic microRNA delivery suppresses tumorigenesis in a murine liver cancer model. *Cell* **137,** 1005–17 (2009).

151. Kozomara, A. & Griffiths-Jones, S. miRBase: annotating high confidence microRNAs using deep sequencing data. *Nucleic Acids Res*. **42,** D68–73 (2014).

152. Kress, T. R. *et al*. The MK5/PRAK kinase and Myc form a negative feedback loop that is disrupted during colorectal tumorigenesis. *Mol. Cell* **41,** 445–57 (2011).

153. Kumar, M. *et al*. Negative regulation of the tumor suppressor p53 gene by microRNAs. *Oncogene* **30,** 843–53 (2011).

154. Kumar, M. S. *et al*. HMGA2 functions as a competing endogenous RNA to promote lung cancer progression. *Nature* **505,** 212–7 (2014).

155. Kumar, M. S. *et al*. Suppression of non-small cell lung tumor development by the let-7 microRNA family. *Proc. Natl. Acad. Sci. U. S. A.* **105,** 3903–8 (2008).

156. Kumar, M. S., Lu, J., Mercer, K. L., Golub, T. R. & Jacks, T. Impaired microRNA processing enhances cellular transformation and tumorigenesis. *Nat. Genet.* **39,** 673–7 (2007).

157. Kumar, M. S. *et al*. Dicer1 functions as a haploinsufficient tumor suppressor. *Genes Dev.* **23,** 2700–4 (2009).

158. Lal, A. *et al*. Capture of microRNA-bound mRNAs identifies the tumor suppressor miR-34a as a regulator of growth factor signaling. *PLoS Genet.* **7,** e1002363 (2011).

159. Landais, S., Landry, S., Legault, P. & Rassart, E. Oncogenic potential of the miR-106-363 cluster and its implication in human T-cell leukemia. *Cancer Res.* **67,** 5699–707 (2007).

160. Lander, E. S. *et al*. Initial sequencing and analysis of the human genome. *Nature* **409,** 860–921 (2001).

161. Langdon, W. Y., Harris, A. W., Cory, S. & Adams, J. M. The c-myc oncogene perturbs B lymphocyte development in Eμ-myc transgenic mice. *Cell* **47,** 11–18 (1986).

162. Le, M. T. N. *et al*. MicroRNA-125b is a novel negative regulator of p53. *Genes Dev.* **23,** 862–76 (2009).

163. Lee, E. J. *et al*. Systematic evaluation of microRNA processing patterns in tissues, cell lines, and tumors. *RNA* **14,** 35–42 (2008).

164. Lee, R. C., Feinbaum, R. L. & Ambros, V. The C. elegans heterochronic gene lin-4 encodes small RNAs with antisense complementarity to lin-14. *Cell* **75,** 843–854 (1993).

165. Lee, Y. S. & Dutta, A. The tumor suppressor microRNA let-7 represses the HMGA2 oncogene. *Genes Dev.* **21,** 1025–30 (2007).

166. Lee, Y. *et al*. The nuclear RNase III Drosha initiates microRNA processing. *Nature* **425,** 415–9 (2003).

167. Lee, Y. *et al*. MicroRNA genes are transcribed by RNA polymerase II. *EMBO J.* **23,** 4051–60 (2004).

168. Lenz, G. *et al*. Molecular subtypes of diffuse large B-cell lymphoma arise by distinct genetic pathways. *Proc. Natl. Acad. Sci. U. S. A.* **105,** 13520–5 (2008).

169. Levine, A. J. & Oren, M. The first 30 years of p53: growing ever more complex. *Nat. Rev. Cancer* **9,** 749–58 (2009).

170. Lewis, B. P., Burge, C. B. & Bartel, D. P. Conserved seed pairing, often flanked by adenosines, indicates that thousands of human genes are microRNA targets. *Cell* **120,** 15–20 (2005).

171. Lewis, B. P., Shih, I., Jones-Rhoades, M. W., Bartel, D. P. & Burge, C. B. Prediction of Mammalian MicroRNA Targets. *Cell* **115,** 787–798 (2003).

172. Li, J. *et al*. Correction: miR-30 Regulates Mitochondrial Fission through Targeting p53 and the Dynamin-Related Protein-1 Pathway. *PLoS Genet*. **6,** (2010).

173. Li, N., Muthusamy, S., Liang, R., Sarojini, H. & Wang, E. Increased expression of miR-34a and miR-93 in rat liver during aging, and their impact on the expression of Mgst1 and Sirt1. *Mech. Ageing Dev*. **132,** 75–85 (2011).

174. Lim, L. P. *et al*. Microarray analysis shows that some microRNAs downregulate large numbers of target mRNAs. *Nature* **433,** 769–73 (2005).

175. Liu, C. *et al*. The microRNA miR-34a inhibits prostate cancer stem cells and metastasis by directly repressing CD44. *Nat. Med*. **17,** 211–5 (2011).

176. Liu, G., Min, H., Yue, S. & Chen, C.-Z. Pre-miRNA loop nucleotides control the distinct activities of mir-181a-1 and mir-181c in early T cell development. *PLoS One* **3,** e3592 (2008).

177. Liu, J. *et al*. Argonaute2 is the catalytic engine of mammalian RNAi. *Science* **305,** 1437–41 (2004).

178. Liu, J. *et al*. A role for the P-body component GW182 in microRNA function. *Nat. Cell Biol*. **7,** 1261–6 (2005).

179. Liu, N. *et al*. The microRNA miR-34 modulates ageing and neurodegeneration in Drosophila. *Nature* **482,** 519–23 (2012).

180. Liu, N. *et al*. microRNA-133a regulates cardiomyocyte proliferation and suppresses smooth muscle gene expression in the heart. *Genes Dev*. **22,** 3242–54 (2008).

181. Lodygin, D. *et al*. Inactivation of miR-34a by aberrant CpG methylation in multiple types of cancer. *Cell Cycle* **7,** 2591–600 (2008).

182. Lowe, S. W., Cepero, E. & Evan, G. Intrinsic tumour suppression. *Nature* **432,** 307–15 (2004).

183. Lu, J. *et al*. MicroRNA expression profiles classify human cancers. *Nature* **435,** 834–8 (2005).

184. Lu, Y., Thomson, J. M., Wong, H. Y. F., Hammond, S. M. & Hogan, B. L. M. Transgenic over-expression of the microRNA miR-17-92 cluster promotes proliferation and inhibits differentiation of lung epithelial progenitor cells. *Dev. Biol*. **310,** 442–53 (2007).

185. Lujambio, A. *et al*. Non-cell-autonomous tumor suppression by p53. *Cell* **153,** 449–60 (2013).

186. Lujambio, A. *et al*. A microRNA DNA methylation signature for human cancer metastasis. *Proc. Natl. Acad. Sci. U. S. A.* **105,** 13556–61 (2008).

187. Lund, E., Güttinger, S., Calado, A., Dahlberg, J. E. & Kutay, U. Nuclear export of microRNA precursors. *Science* **303,** 95–8 (2004).

188. Lund, E., Sheets, M. D., Imboden, S. B. & Dahlberg, J. E. Limiting Ago protein restricts RNAi and microRNA biogenesis during early development in Xenopus laevis. *Genes Dev*. **25,** 1121–31 (2011).

189. Lytle, J. R., Yario, T. A. & Steitz, J. A. Target mRNAs are repressed as efficiently by microRNA-binding sites in the 5' UTR as in the 3' UTR. *Proc. Natl. Acad. Sci. U. S. A.* **104,** 9667–72 (2007).

190. Ma, L., Teruya-Feldstein, J. & Weinberg, R. A. Tumour invasion and metastasis initiated by microRNA-10b in breast cancer. *Nature* **449,** 682–8 (2007).

191. Ma, X. *et al*. Loss of the miR-21 allele elevates the expression of its target genes and reduces tumorigenesis. *Proc. Natl. Acad. Sci. U. S. A.* **108,** 10144–9 (2011).

192. Ma, Y. *et al*. Elevated oncofoetal miR-17-5p expression regulates colorectal cancer progression by repressing its target gene P130. *Nat. Commun.* **3,** 1291 (2012).

193. Mandke, P. *et al*. MicroRNA-34a modulates MDM4 expression via a target site in the open reading frame. *PLoS One* **7,** e42034 (2012).

194. Manfè, V. *et al*. miR-122 regulates p53/Akt signalling and the chemotherapy-induced apoptosis in cutaneous T-cell lymphoma. *PLoS One* **7,** e29541 (2012).

195. Manni, I. *et al*. The microRNA miR-92 increases proliferation of myeloid cells and by targeting p63 modulates the abundance of its isoforms. *FASEB J.* **23,** 3957–66 (2009).

196. Marcet, B. *et al*. Control of vertebrate multiciliogenesis by miR-449 through direct repression of the Delta/Notch pathway. *Nat. Cell Biol.* **13,** 693–9 (2011).

197. Maroney, P. A., Yu, Y., Fisher, J. & Nilsen, T. W. Evidence that microRNAs are associated with translating messenger RNAs in human cells. *Nat. Struct. Mol. Biol.* **13,** 1102–7 (2006).

198. Martinez, I., Cazalla, D., Almstead, L. L., Steitz, J. A. & DiMaio, D. miR-29 and miR-30 regulate B-Myb expression during cellular senescence. *Proc. Natl. Acad. Sci. U. S. A.* **108,** 522–7 (2011).

199. Martinez, J., Patkaniowska, A., Urlaub, H., Lührmann, R. & Tuschl, T. Single-stranded antisense siRNAs guide target RNA cleavage in RNAi. *Cell* **110,** 563–74 (2002).

200. Matsuoka, S. *et al*. Fbxw7 acts as a critical fail-safe against premature loss of hematopoietic stem cells and development of T-ALL. *Genes Dev*. **22,** 986–91 (2008).

201. Mavrakis, K. J. *et al*. A cooperative microRNA-tumor suppressor gene network in acute T-cell lymphoblastic leukemia (T-ALL). *Nat. Genet.* **43,** 673–8 (2011).

202. Mavrakis, K. J. *et al*. Genome-wide RNA-mediated interference screen identifies miR-19 targets in Notch-induced T-cell acute lymphoblastic leukaemia. *Nat. Cell Biol.* **12,** 372–9 (2010).

203. Medina, P. P., Nolde, M. & Slack, F. J. OncomiR addiction in an in vivo model of microRNA-21-induced pre-B-cell lymphoma. *Nature* **467,** 86–90 (2010).

204. Megraw, M., Sethupathy, P., Corda, B. & Hatzigeorgiou, A. G. miRGen: a database for the study of animal microRNA genomic organization and function. *Nucleic Acids Res*. **35,** D149–55 (2007).

205. Melo, S. A. *et al*. A genetic defect in exportin-5 traps precursor microRNAs in the nucleus of cancer cells. *Cancer Cell* **18,** 303–15 (2010).

206. Melo, S. A. *et al*. A TARBP2 mutation in human cancer impairs microRNA processing and DICER1 function. *Nat. Genet*. **41,** 365–70 (2009).

207. Mendell, J. T. miRiad roles for the miR-17-92 cluster in development and disease. *Cell* **133,** 217–22 (2008).

208. Mendell, J. T. & Olson, E. N. MicroRNAs in stress signaling and human disease. *Cell* **148,** 1172–87 (2012).

209. Meng, F. *et al*. MicroRNA-21 regulates expression of the PTEN tumor suppressor gene in human hepatocellular cancer. *Gastroenterology* **133,** 647–58 (2007).

210. Meyer, N. & Penn, L. Z. Reflecting on 25 years with MYC. *Nat. Rev. Cancer* **8,** 976–90 (2008).

211. Michalak, E. M. *et al*. Puma and to a lesser extent Noxa are suppressors of Myc-induced lymphomagenesis. *Cell Death Differ*. **16,** 684–96 (2009).

212. Minella, A. C., Grim, J. E., Welcker, M. & Clurman, B. E. p53 and SCFFbw7 cooperatively restrain cyclin E-associated genome instability. *Oncogene* **26,** 6948–53 (2007).

213. Minella, A. C. *et al*. Cyclin E phosphorylation regulates cell proliferation in hematopoietic and epithelial lineages in vivo. *Genes Dev*. **22,** 1677–89 (2008).

214. Miranda, K. C. *et al*. A pattern-based method for the identification of MicroRNA binding sites and their corresponding heteroduplexes. *Cell* **126,** 1203–17 (2006).

215. Mitchell, K. O. *et al*. Bax is a transcriptional target and mediator of c-myc-induced apoptosis. *Cancer Res*. **60,** 6318–25 (2000).

216. Mori, M. *et al*. Hippo signaling regulates microprocessor and links cell-density-dependent miRNA biogenesis to cancer. *Cell* **156,** 893–906 (2014).

217. Morlando, M. *et al*. FUS stimulates microRNA biogenesis by facilitating co-transcriptional Drosha recruitment. *EMBO J*. **31,** 4502–10 (2012).

218. Moser, R. *et al*. MYC-driven tumorigenesis is inhibited by WRN syndrome gene deficiency. *Mol. Cancer Res*. **10,** 535–45 (2012).

219. Mott, J. L., Kobayashi, S., Bronk, S. F. & Gores, G. J. mir-29 regulates Mcl-1 protein expression and apoptosis. *Oncogene* **26,** 6133–40 (2007).

220. Mu, P. *et al*. Genetic dissection of the miR-17~92 cluster of microRNAs in Myc-induced B-cell lymphomas. *Genes Dev*. **23,** 2806–11 (2009).

221. Mudduluru, G. *et al*. Regulation of Axl receptor tyrosine kinase expression by miR-34a and miR-199a/b in solid cancer. *Oncogene* **30,** 2888–99 (2011).

222. Mudhasani, R. *et al*. Loss of miRNA biogenesis induces p19Arf-p53 signaling and senescence in primary cells. *J. Cell Biol*. **181,** 1055–63 (2008).

223. Murakami, Y. *et al*. Comprehensive analysis of microRNA expression patterns in hepatocellular carcinoma and non-tumorous tissues. *Oncogene* **25,** 2537–45 (2006).

224. Murphy, D. J. *et al*. Distinct thresholds govern Myc's biological output in vivo. *Cancer Cell* **14,** 447–57 (2008).

225. Nalls, D., Tang, S.-N., Rodova, M., Srivastava, R. K. & Shankar, S. Targeting epigenetic regulation of miR-34a for treatment of pancreatic cancer by inhibition of pancreatic cancer stem cells. *PLoS One* **6,** e24099 (2011).

226. Navarro, A. *et al*. MicroRNA expression, chromosomal alterations, and immunoglobulin variable heavy chain hypermutations in Mantle cell lymphomas. *Cancer Res*. **69,** 7071–8 (2009).

227. Nittner, D. *et al*. Synthetic lethality between Rb, p53 and Dicer or miR-17-92 in retinal progenitors suppresses retinoblastoma formation. *Nat. Cell Biol*. **14,** 958–65 (2012).

228. Noonan, E. J. *et al*. miR-449a targets HDAC-1 and induces growth arrest in prostate cancer. *Oncogene* **28,** 1714–24 (2009).

229. O'Connell, R. M., Chaudhuri, A. A., Rao, D. S. & Baltimore, D. Inositol phosphatase SHIP1 is a primary target of miR-155. *Proc. Natl. Acad. Sci. U. S. A*. **106,** 7113–8 (2009).

230. O'Connell, R. M. *et al*. Sustained expression of microRNA-155 in hematopoietic stem cells causes a myeloproliferative disorder. *J. Exp. Med*. **205,** 585–94 (2008).

231. O'Donnell, K. A., Wentzel, E. A., Zeller, K. I., Dang, C. V & Mendell, J. T. c-Myc-regulated microRNAs modulate E2F1 expression. *Nature* **435,** 839–43 (2005).

232. Ogawara, Y. *et al*. Akt enhances Mdm2-mediated ubiquitination and degradation of p53. *J. Biol. Chem*. **277,** 21843–50 (2002).

233. Okada, N. *et al*. A positive feedback between p53 and miR-34 miRNAs mediates tumor suppression. *Genes Dev*. **28,** 438–450 (2014).

234. Olive, V. *et al*. miR-19 is a key oncogenic component of mir-17-92. *Genes Dev*. **23,** 2839–49 (2009).

235. Onoyama, I. *et al*. Conditional inactivation of Fbxw7 impairs cell-cycle exit during T cell differentiation and results in lymphomatogenesis. *J. Exp. Med*. **204,** 2875–88 (2007).

236. Ota, A. Identification and Characterization of a Novel Gene, C13orf25, as a Target for 13q31-q32 Amplification in Malignant Lymphoma. *Cancer Res*. **64,** 3087–3095 (2004).

237. Paik, J. H. *et al*. MicroRNA-146a downregulates NFκB activity via targeting TRAF6 and functions as a tumor suppressor having strong prognostic implications in NK/T cell lymphoma. *Clin. Cancer Res*. **17,** 4761–71 (2011).

238. Pallasch, C. P. *et al*. miRNA deregulation by epigenetic silencing disrupts suppression of the oncogene PLAG1 in chronic lymphocytic leukemia. *Blood* **114,** 3255–64 (2009).

239. Pandey, D. P. & Picard, D. miR-22 inhibits estrogen signaling by directly targeting the estrogen receptor alpha mRNA. *Mol. Cell. Biol.* **29,** 3783–90 (2009).

240. Park, S.-Y., Lee, J. H., Ha, M., Nam, J.-W. & Kim, V. N. miR-29 miRNAs activate p53 by targeting p85 alpha and CDC42. *Nat. Struct. Mol. Biol.* **16,** 23–9 (2009).

241. Paroo, Z., Ye, X., Chen, S. & Liu, Q. Phosphorylation of the human microRNA-generating complex mediates MAPK/Erk signaling. *Cell* **139,** 112–22 (2009).

242. Pasquinelli, A. E. *et al*. Conservation of the sequence and temporal expression of let-7 heterochronic regulatory RNA. *Nature* **408,** 86–9 (2000).

243. Pekarsky, Y. *et al*. Tcl1 expression in chronic lymphocytic leukemia is regulated by miR-29 and miR-181. *Cancer Res.* **66,** 11590–3 (2006).

244. Petersen, C. P., Bordeleau, M.-E., Pelletier, J. & Sharp, P. A. Short RNAs repress translation after initiation in mammalian cells. *Mol. Cell* **21,** 533–42 (2006).

245. Petrocca, F. *et al*. E2F1-regulated microRNAs impair TGFbeta-dependent cell-cycle arrest and apoptosis in gastric cancer. *Cancer Cell* **13,** 272–86 (2008).

246. Pichiorri, F. *et al*. Downregulation of p53-inducible microRNAs 192, 194, and 215 impairs the p53/MDM2 autoregulatory loop in multiple myeloma development. *Cancer Cell* **18,** 367–81 (2010).

247. Pillai, R. S. *et al*. Inhibition of translational initiation by Let-7 MicroRNA in human cells. *Science* **309,** 1573–6 (2005).

248. Post, S. *et al*. p53-dependent senescence delays Eμ-myc-induced B-cell lymphomagenesis. *Oncogene* 1–10 (2009).

249. Radhakrishnan, S. K. *et al*. Constitutive expression of E2F-1 leads to p21-dependent cell cycle arrest in S phase of the cell cycle. *Oncogene* **23,** 4173–6 (2004).

250. Rao, D. S. *et al*. MicroRNA-34a perturbs B lymphocyte development by repressing the forkhead box transcription factor Foxp1. *Immunity* **33,** 48–59 (2010).

251. Raver-Shapira, N. *et al*. Transcriptional activation of miR-34a contributes to p53-mediated apoptosis. *Mol. Cell* **26,** 731–43 (2007).

252. Reimann, M. *et al*. Tumor Stroma-Derived TGF-β Limits Myc-Driven Lymphomagenesis via Suv39h1-Dependent Senescence. *Cancer Cell* **17,** 262–272 (2010).

253. Reinhart, B. J. *et al*. The 21-nucleotide let-7 RNA regulates developmental timing in Caenorhabditis elegans. *Nature* **403,** 901–6 (2000).

254. Robledo, C. *et al*. Array comparative genomic hybridization identifies genetic regions associated with outcome in aggressive diffuse large B-cell lymphomas. *Cancer* **115,** 3728–37 (2009).

255. Rossi, D. J. & Weissman, I. L. Pten, tumorigenesis, and stem cell self-renewal. *Cell* **125,** 229–31 (2006).

256. Roybal, J. D. *et al*. miR-200 Inhibits lung adenocarcinoma cell invasion and metastasis by targeting Flt1/VEGFR1. *Mol. Cancer Res.* **9,** 25–35 (2011).

257. Ruby, J. G., Jan, C. H. & Bartel, D. P. Intronic microRNA precursors that bypass Drosha processing. *Nature* **448,** 83–6 (2007).

258. Sachdeva, M. *et al*. p53 represses c-Myc through induction of the tumor suppressor miR-145. *Proc. Natl. Acad. Sci. U. S. A.* **106,** 3207–12 (2009).

259. Sandhu, S. K. *et al*. miR-155 targets histone deacetylase 4 (HDAC4) and impairs transcriptional activity of B-cell lymphoma 6 (BCL6) in the Eμ-miR-155 transgenic mouse model. *Proc. Natl. Acad. Sci. U. S. A.* **109,** 20047–52 (2012).

260. Schmitt, C. A., McCurrach, M. E., de Stanchina, E., Wallace-Brodeur, R. R. & Lowe, S. W. INK4a/ARF mutations accelerate lymphomagenesis and promote chemoresistance by disabling p53. *Genes Dev.* **13,** 2670–2677 (1999).

261. Schmitt, C. A., Wallace-Brodeur, R. R., Rosenthal, C. T., Mccurrach, M. E. & Lowe, S. W. DNA Damage Responses and Chemosensitivity in the E -myc Mouse Lymphoma Model. *Cold Spring Harb. Symp. Quant. Biol.* **65,** 499–510 (2000).

262. Schmitt, C. A. *et al*. Dissecting p53 tumor suppressor functions in vivo. *Cancer Cell* **1,** 289–298 (2002).

263. Schratt, G. M. *et al*. A brain-specific microRNA regulates dendritic spine development. *Nature* **439,** 283–9 (2006).

264. Schulte, J. H. *et al*. MYCN regulates oncogenic MicroRNAs in neuroblastoma. *Int. J. Cancer* **122,** 699–704 (2008).

265. Seitz, H., Ghildiyal, M. & Zamore, P. D. Argonaute loading improves the 5' precision of both MicroRNAs and their miRNA* strands in flies. *Curr. Biol.* **18,** 147–51 (2008).

266. Selbach, M. *et al*. Widespread changes in protein synthesis induced by microRNAs. *Nature* **455,** 58–63 (2008).

267. Seoane, J., Le, H.-V. & Massagué, J. Myc suppression of the p21(Cip1) Cdk inhibitor influences the outcome of the p53 response to DNA damage. *Nature* **419,** 729–34 (2002).

268. Shachaf, C. M. *et al*. MYC inactivation uncovers pluripotent differentiation and tumour dormancy in hepatocellular cancer. *Nature* **431,** 1112–7 (2004).

269. Shan, S. W. *et al*. MicroRNA MiR-17 retards tissue growth and represses fibronectin expression. *Nat. Cell Biol.* **11,** 1031–8 (2009).

270. Shen, J. *et al*. EGFR modulates microRNA maturation in response to hypoxia through phosphorylation of AGO2. *Nature* **497,** 383–7 (2013).

271. Shen, J. *et al*. A functional polymorphism in the miR-146a gene and age of familial breast/ovarian cancer diagnosis. *Carcinogenesis* **29,** 1963–6 (2008).

272. Shi, L. *et al*. p53-induced miR-15a/16-1 and AP4 form a double-negative feedback loop to regulate epithelial-mesenchymal transition and metastasis in colorectal cancer. *Cancer Res*. **74,** 532–42 (2014).

273. Shi, X.-B. *et al*. miR-125b promotes growth of prostate cancer xenograft tumor through targeting pro-apoptotic genes. *Prostate* **71,** 538–49 (2011).

274. Shimono, Y. *et al*. Downregulation of miRNA-200c links breast cancer stem cells with normal stem cells. *Cell* **138,** 592–603 (2009).

275. Shin, C. *et al*. Expanding the microRNA targeting code: functional sites with centered pairing. *Mol*. *Cell* **38,** 789–802 (2010).

276. Siemens, H. *et al*. miR-34 and SNAIL form a double-negative feedback loop to regulate epithelial-mesenchymal transitions. *Cell Cycle* **10,** 4256–71 (2011).

277. Siemens, H., Jackstadt, R., Kaller, M. & Hermeking, H. Repression of c-Kit by p53 is mediated by miR-34 and is associated with reduced chemoresistance, migration and stemness. *Oncotarget* **4,** 1399–415 (2013).

278. Slack, F. J. *et al*. The lin-41 RBCC gene acts in the C. elegans heterochronic pathway between the let-7 regulatory RNA and the LIN-29 transcription factor. *Mol*. *Cell* **5,** 659–69 (2000).

279. Smith, K. M. *et al*. miR-29ab1 deficiency identifies a negative feedback loop controlling Th1 bias that is dysregulated in multiple sclerosis. *J*. *Immunol*. **189,** 1567–76 (2012).

280. So, A. Y.-L., Zhao, J. L. & Baltimore, D. The Yin and Yang of microRNAs: leukemia and immunity. *Immunol*. *Rev*. **253,** 129–45 (2013).

281. Song, S. J. *et al*. MicroRNA-antagonism regulates breast cancer stemness and metastasis via TET-family-dependent chromatin remodeling. *Cell* **154,** 311–24 (2013).

282. Song*, R. *et al*. miR-34/449 miRNAs are required for motile ciliogenesis by repressing cp110. *Nature* **In Press,** (2014).

283. Sonoki, T., Iwanaga, E., Mitsuya, H. & Asou, N. Insertion of microRNA-125b-1, a human homologue of lin-4, into a rearranged immunoglobulin heavy chain gene locus in a patient with precursor B-cell acute lymphoblastic leukemia. *Leukemia* **19,** 2009–10 (2005).

284. Starczynowski, D. T. *et al*. Identification of miR-145 and miR-146a as mediators of the 5q-syndrome phenotype. *Nat*. *Med*. **16,** 49–58 (2010).

285. Strasser, A., Harris, A. W., Bath, M. L. & Cory, S. Novel primitive lymphoid tumours induced in transgenic mice by cooperation between myc and bcl-2. *Nature* **348,** 331–3 (1990).

286. Suzuki, H. I. *et al*. Modulation of microRNA processing by p53. *Nature* **460,** 529–33 (2009).

287. Swarbrick, A. *et al*. miR-380-5p represses p53 to control cellular survival and is associated with poor outcome in MYCN-amplified neuroblastoma. *Nat*. *Med*. **16,** 1134–40 (2010).

288. Sylvestre, Y. *et al*. An E2F/miR-20a autoregulatory feedback loop. *J*. *Biol*. *Chem*. **282,** 2135–43 (2007).

289. Taganov, K. D., Boldin, M. P., Chang, K.-J. & Baltimore, D. NF-kappaB-dependent induction of microRNA miR-146, an inhibitor targeted to signaling proteins of innate immune responses. *Proc. Natl. Acad. Sci. U. S. A.* **103,** 12481–6 (2006).

290. Tagawa, H. & Seto, M. A microRNA cluster as a target of genomic amplification in malignant lymphoma. *Leukemia* **19,** 2013–6 (2005).

291. Tagawa, H., Karube, K., Tsuzuki, S., Ohshima, K. & Seto, M. Synergistic action of the microRNA-17 polycistron and Myc in aggressive cancer development. *Cancer Sci.* **98,** 1482–90 (2007).

292. Takakura, S. *et al*. Oncogenic role of miR-17-92 cluster in anaplastic thyroid cancer cells. *Cancer Sci.* **99,** 1147–54 (2008).

293. Takamizawa, J. *et al*. Reduced expression of the let-7 microRNAs in human lung cancers in association with shortened postoperative survival. *Cancer Res.* **64,** 3753–6 (2004).

294. Tam, W., Ben-Yehuda, D. & Hayward, W. S. bic, a novel gene activated by proviral insertions in avian leukosis virus-induced lymphomas, is likely to function through its noncoding RNA. *Mol. Cell. Biol.* **17,** 1490–502 (1997).

295. Tanzer, A. & Stadler, P. F. Molecular evolution of a microRNA cluster. *J. Mol. Biol.* **339,** 327–35 (2004).

296. Tarasov, V. *et al*. Differential regulation of microRNAs by p53 revealed by massively parallel sequencing: miR-34a is a p53 target that induces apoptosis and G1-arrest. *Cell Cycle* **6,** 1586–93 (2007).

297. Tay, Y., Zhang, J., Thomson, A. M., Lim, B. & Rigoutsos, I. MicroRNAs to Nanog, Oct4 and Sox2 coding regions modulate embryonic stem cell differentiation. *Nature* **455,** 1124–8 (2008).

298. Thomson, J. M. *et al*. Extensive post-transcriptional regulation of microRNAs and its implications for cancer. *Genes Dev.* **20,** 2202–7 (2006).

299. Tian, S. *et al*. MicroRNA-1285 inhibits the expression of p53 by directly targeting its 3' untranslated region. *Biochem. Biophys. Res. Commun.* **396,** 435–9 (2010).

300. Tie, J. *et al*. MiR-218 inhibits invasion and metastasis of gastric cancer by targeting the Robo1 receptor. *PLoS Genet.* **6,** e1000879 (2010).

301. Trabucchi, M. *et al*. The RNA-binding protein KSRP promotes the biogenesis of a subset of microRNAs. *Nature* **459,** 1010–4 (2009).

302. Trotman, L. C. *et al*. Pten dose dictates cancer progression in the prostate. *PLoS Biol.* **1,** E59 (2003).

303. Tsuchida, A. *et al*. miR-92 is a key oncogenic component of the miR-17-92 cluster in colon cancer. *Cancer Sci.* **102,** 2264–71 (2011).

304. Tsuruta, T. *et al*. miR-152 is a tumor suppressor microRNA that is silenced by DNA hypermethylation in endometrial cancer. *Cancer Res.* **71,** 6450–62 (2011).

305. Tu, Y. *et al*. MicroRNA-218 inhibits glioma invasion, migration, proliferation, and cancer stem-like cell self-renewal by targeting the polycomb group gene Bmi1. *Cancer Res*. **73,** 6046–55 (2013).

306. Tusher, V. G., Tibshirani, R. & Chu, G. Significance analysis of microarrays applied to the ionizing radiation response. *Proc. Natl. Acad. Sci. U. S. A.* **98,** 5116–21 (2001).

307. Ugalde, A. P. *et al*. Aging and chronic DNA damage response activate a regulatory pathway involving miR-29 and p53. *EMBO J*. **30,** 2219–32 (2011).

308. Uziel, T. *et al*. The miR-17~92 cluster collaborates with the Sonic Hedgehog pathway in medulloblastoma. *Proc. Natl. Acad. Sci. U. S. A.* **106,** 2812–7 (2009).

309. van Rooij, E. *et al*. A family of microRNAs encoded by myosin genes governs myosin expression and muscle performance. *Dev. Cell* **17,** 662–73 (2009).

310. van Rooij, E. *et al*. Control of stress-dependent cardiac growth and gene expression by a microRNA. *Science* **316,** 575–9 (2007).

311. Venkataraman, S. *et al*. MicroRNA 218 acts as a tumor suppressor by targeting multiple cancer phenotype-associated genes in medulloblastoma. *J. Biol. Chem*. **288,** 1918–28 (2013).

312. Ventura, A. *et al*. Targeted deletion reveals essential and overlapping functions of the miR-17 through 92 family of miRNA clusters. *Cell* **132,** 875–86 (2008).

313. Vogt, M. *et al*. Frequent concomitant inactivation of miR-34a and miR-34b/c by CpG methylation in colorectal, pancreatic, mammary, ovarian, urothelial, and renal cell carcinomas and soft tissue sarcomas. *Virchows Arch*. **458,** 313–22 (2011).

314. Volinia, S. *et al*. A microRNA expression signature of human solid tumors defines cancer gene targets. *Proc. Natl. Acad. Sci. U. S. A.* **103,** 2257–61 (2006).

315. Vousden, K. H. & Lu, X. Live or let die: the cell's response to p53. *Nat. Rev. Cancer* **2,** 594–604 (2002).

316. Walker, J. C. & Harland, R. M. microRNA-24a is required to repress apoptosis in the developing neural retina. *Genes Dev*. **23,** 1046–51 (2009).

317. Wang, C. *et al*. Interactions between E2F1 and SirT1 regulate apoptotic response to DNA damage. *Nat. Cell Biol*. **8,** 1025–31 (2006).

318. Wang, C. L. *et al*. Activation of an oncogenic microRNA cistron by provirus integration. *Proc. Natl. Acad. Sci. U. S. A.* **103,** 18680–4 (2006).

319. Wang, G. *et al*. Critical regulation of miR-200/ZEB2 pathway in Oct4/Sox2-induced mesenchymal-to-epithelial transition and induced pluripotent stem cell generation. *Proc. Natl. Acad. Sci. U. S. A.* **110,** 2858–63 (2013).

320. Wang, P. *et al*. Elevated Mdm2 expression induces chromosomal instability and confers a survival and growth advantage to B cells. *Oncogene* **27,** 1590–8 (2008).

321. Wang, P. *et al*. Inducible microRNA-155 feedback promotes type I IFN signaling in antiviral innate immunity by targeting suppressor of cytokine signaling 1. *J. Immunol*. **185,** 6226–33 (2010).

322. Wang, X.-S. *et al*. MicroRNA-29a and microRNA-142-3p are regulators of myeloid differentiation and acute myeloid leukemia. *Blood* **119,** 4992–5004 (2012).

323. Wang, Z. *et al*. Tumor suppressor functions of FBW7 in cancer development and progression. *FEBS Lett*. **586,** 1409–18 (2012).

324. Watanabe, G. *et al*. Inhibition of Cyclin D1 Kinase Activity Is Associated with E2F-Mediated Inhibition of Cyclin D1 Promoter Activity through E2F and Sp1. *Mol. Cell. Biol*. **18,** 3212–3222 (1998).

325. Weber, J. D. & Zambetti, G. P. Renewing the debate over the p53 apoptotic response. *Cell Death Differ*. **10,** 409–12 (2003).

326. Wei, J. S. *et al*. The MYCN oncogene is a direct target of miR-34a. *Oncogene* **27,** 5204–13 (2008).

327. Wei, J. *et al*. miR-34s inhibit osteoblast proliferation and differentiation in the mouse by targeting SATB2. *J. Cell Biol*. **197,** 509–21 (2012).

328. Welch, C., Chen, Y. & Stallings, R. L. MicroRNA-34a functions as a potential tumor suppressor by inducing apoptosis in neuroblastoma cells. *Oncogene* **26,** 5017–22 (2007).

329. Welcker, M. & Clurman, B. E. FBW7 ubiquitin ligase: a tumour suppressor at the crossroads of cell division, growth and differentiation. *Nat. Rev. Cancer* **8,** 83–93 (2008).

330. Wendel, H.-G. *et al*. Determinants of sensitivity and resistance to rapamycin-chemotherapy drug combinations in vivo. *Cancer Res*. **66,** 7639–46 (2006).

331. Wiggins, J. F. *et al*. Development of a lung cancer therapeutic based on the tumor suppressor microRNA-34. *Cancer Res*. **70,** 5923–30 (2010).

332. Wightman, B., Ha, I. & Ruvkun, G. Posttranscriptional regulation of the heterochronic gene lin-14 by lin-4 mediates temporal pattern formation in C. elegans. *Cell* **75,** 855–862 (1993).

333. Wolyniec, K. *et al*. E6AP ubiquitin ligase regulates PML-induced senescence in Myc-driven lymphomagenesis. *Blood* **120,** 822–32 (2012).

334. Woods, K., Thomson, J. M. & Hammond, S. M. Direct regulation of an oncogenic micro-RNA cluster by E2F transcription factors. *J. Biol. Chem*. **282,** 2130–4 (2007).

335. Wortham, N. C. *et al*. The DEAD-box protein p72 regulates ERalpha-/oestrogen-dependent transcription and cell growth, and is associated with improved survival in ERalpha-positive breast cancer. *Oncogene* **28,** 4053–64 (2009).

336. Wu, L., Fan, J. & Belasco, J. G. MicroRNAs direct rapid deadenylation of mRNA. *Proc. Natl. Acad. Sci. U. S. A*. **103,** 4034–9 (2006).

337. Wu, Z., Huang, X., Huang, X., Zou, Q. & Guo, Y. The inhibitory role of Mir-29 in growth of breast cancer cells. *J. Exp. Clin. Cancer Res*. **32,** 98 (2013).

338. Wu, Z., Irizarry, R., Gentleman, R., Murillo, F. M. & Spencer, F. *A Model Based Background Adjustment for Oligonucleotide Expression Arrays*. *Johns Hopkins Univ. Dept. Biostat. Work. Pap.* (2004). at <http://biostats.bepress.com/jhubiostat/paper1>

339. Xiao, C. *et al*. Lymphoproliferative disease and autoimmunity in mice with increased miR-17-92 expression in lymphocytes. *Nat. Immunol.* **9,** 405–14 (2008).

340. Xiao, J., Lin, H., Luo, X., Luo, X. & Wang, Z. miR-605 joins p53 network to form a p53:miR-605:Mdm2 positive feedback loop in response to stress. *EMBO J.* **30,** 524–32 (2011).

341. Xu, D. *et al*. miR-22 represses cancer progression by inducing cellular senescence. *J. Cell Biol.* **193,** 409–24 (2011).

342. Xu, P., Vernooy, S. Y., Guo, M. & Hay, B. A. The Drosophila microRNA Mir-14 suppresses cell death and is required for normal fat metabolism. *Curr. Biol.* **13,** 790–5 (2003).

343. Xu, Q. *et al*. A regulatory circuit of miR-148a/152 and DNMT1 in modulating cell transformation and tumor angiogenesis through IGF-IR and IRS1. *J. Mol. Cell Biol.* **5,** 3–13 (2013).

344. Xu, Y., Sengupta, T., Kukreja, L. & Minella, A. C. MicroRNA-223 regulates cyclin E activity by modulating expression of F-box and WD-40 domain protein 7. *J. Biol. Chem.* **285,** 34439–46 (2010).

345. Xue, W. *et al*. Senescence and tumour clearance is triggered by p53 restoration in murine liver carcinomas. *Nature* **445,** 656–60 (2007).

346. Yamakuchi, M., Ferlito, M. & Lowenstein, C. J. miR-34a repression of SIRT1 regulates apoptosis. *Proc. Natl. Acad. Sci. U. S. A.* **105,** 13421–6 (2008).

347. Yamakuchi, M. *et al*. P53-induced microRNA-107 inhibits HIF-1 and tumor angiogenesis. *Proc. Natl. Acad. Sci. U. S. A.* **107,** 6334–9 (2010).

348. Yang, M.-H. *et al*. Connective tissue growth factor modulates oral squamous cell carcinoma invasion by activating a miR-504/FOXP1 signalling. *Oncogene* **31,** 2401–11 (2012).

349. Yang, X. *et al*. Both mature miR-17-5p and passenger strand miR-17-3p target TIMP3 and induce prostate tumor growth and invasion. *Nucleic Acids Res.* **41,** 9688–704 (2013).

350. Yang, X. *et al*. miR-449a and miR-449b are direct transcriptional targets of E2F1 and negatively regulate pRb-E2F1 activity through a feedback loop by targeting CDK6 and CDC25A. *Genes Dev.* **23,** 2388–93 (2009).

351. Yang, Z.-Z., Novak, A. J., Ziesmer, S. C., Witzig, T. E. & Ansell, S. M. Attenuation of CD8(+) T-cell function by CD4(+)CD25(+) regulatory T cells in B-cell non-Hodgkin's lymphoma. *Cancer Res.* **66,** 10145–52 (2006).

352. Yi, R., Qin, Y., Macara, I. G. & Cullen, B. R. Exportin-5 mediates the nuclear export of pre-microRNAs and short hairpin RNAs. *Genes Dev.* **17,** 3011–6 (2003).

353. Yu, F. *et al*. let-7 regulates self renewal and tumorigenicity of breast cancer cells. *Cell* **131,** 1109–23 (2007).

354. Zaidi, M. R., Okada, Y. & Chada, K. K. Misexpression of full-length HMGA2 induces benign mesenchymal tumors in mice. *Cancer Res*. **66,** 7453–9 (2006).

355. Zamore, P. D. & Haley, B. Ribo-gnome: the big world of small RNAs. *Science* **309,** 1519–24 (2005).

356. Zauli, G. *et al*. miR-34a induces the downregulation of both E2F1 and B-Myb oncogenes in leukemic cells. *Clin*. *Cancer Res*. **17,** 2712–24 (2011).

357. Zhang, J. *et al*. Loss of microRNA-143/145 disturbs cellular growth and apoptosis of human epithelial cancers by impairing the MDM2-p53 feedback loop. *Oncogene* **32,** 61–9 (2013).

358. Zhang, Y. *et al*. A novel epigenetic CREB-miR-373 axis mediates ZIP4-induced pancreatic cancer growth. *EMBO Mol*. *Med*. **5,** 1322–34 (2013).

359. Zhao, J., Lammers, P., Torrance, C. J. & Bader, A. G. TP53-independent function of miR-34a via HDAC1 and p21(CIP1/WAF1.). *Mol*. *Ther*. **21,** 1678–86 (2013).

360. Zhao, J.-J. *et al*. microRNA expression profile and identification of miR-29 as a prognostic marker and pathogenetic factor by targeting CDK6 in mantle cell lymphoma. *Blood* **115,** 2630–9 (2010).

361. Zhu, S., Si, M.-L., Wu, H. & Mo, Y.-Y. MicroRNA-21 targets the tumor suppressor gene tropomyosin 1 (TPM1). *J*. *Biol*. *Chem*. **282,** 14328–36 (2007).

362. Zindy, F. *et al*. Myc signaling via the ARF tumor suppressor regulates p53-dependent apoptosis and immortalization. *Genes Dev*. **12,** 2424–2433 (1998).

Appendix A:

Eμ-myc^{+}*;p53+/-* tumors have increased numbers of T regulatory cells

Introductory Summary:
T regulatory cells (Tregs) are known to protect the host from autoimmune disorders by repressing, and even killing self-reactive cells. Consequently, Treg cells have the capability to protect cancer cells from immune attack. There are increasing examples illustrating the correlation between increased numbers of Treg cells at the tumor site, and poor survival of the patients (Ha, 2009). Loss of p53 enhances the malignancy of tumors through numerous mechanisms by inhibiting apoptosis and senescence, and increasing proliferation and metastatic capabilities. More recently, studies have linked loss of p53 to a repression of the immune system in responses to cancer. One example, is that deletion of p53 dampens the recruitment of NK cells to the tumor site (Ianello et al., 2013). In this appendix, I show that deletion of p53 in the *Eμ-myc* mouse model increases the number intratumoral Tregs. The mechanism and functional significance of this phenomenon has yet to be determined.

Results:
Eμ-myc^{+}*;p53+/-* tumors exhibit an increase in the number of Treg cells in their tumor mass when compared to *Eμ-myc* only cells (Fig 1A). Similar results were observed for *Eμ-myc*$^{+}$*;p53ER/-* tumor cells kindly provided by Daniel Garcia from the Evans lab.

To test whether the increased number of Tregs in the *Eμ-myc*$^{+}$*;p53+/-* tumors might be having an effect on anti-tumor immune surveillance mechanisms we analyzed the number of CD8+ effector cells, and compared them to the total number of CD4+ cells and the total number of Tregs within the tumor samples. In the *Eμ-myc*$^{+}$*;p53+/-* samples, there was a decrease in the ratio of the percentage CD8+ T cells compared total CD4+ cells (Fig. 1B), and total Tregs (Fig. 1C) in comparison to *Eμ-myc* tumors. Yang *et al* has previously shown in humans that the number of CD8 T cells are inversely correlated with number of intratumoral CD4+CD25+ T cells in B-lymphoma samples (Yang et al., 2006). Yang *et al* also show that the patient matched Tregs can inhibit proliferation of the patient's CD8 T cells.

Discussion
While the modest increase of Treg cells in the *Eμ-myc*$^{+}$*;p53+/-* tumors may assist in the rapid tumor development that occurs in the *Eμ-myc*$^{+}$*;p53+/-* mice, many more experiments are required to understand the mechanism of Treg increase to the *Eμ-myc*$^{+}$*;p53+/-* tumors. One question is whether loss of p53 increases the number of Treg cells present in the animal or whether loss of p53 alters signaling pathways that allow for a greater recruitment of cells to the site. It has been shown that B-lymphoma cells can secrete the chemokine CCL22 to induce chemotaxis of Treg cells (Yang et al., 2006). It is possible that *Eμ-myc*$^{+}$*;p53+/-* B-lymphoma cells secrete more CCL22 or a different chemokine to attract an increased number of Tregs to the tumor site.

Before proceeding, we need to investigate whether increased numbers of Treg cells can accelerate the development of *Eμ-myc* B-lymphoma. There are tools for blocking Treg immunosuppressive function, and for depleting Tregs *in vivo* that would

allow us to inhibit the Treg population in the *Eμ-myc*$^{+}$*;p53*+/- mice, and observe the effects on the rate of tumorigenesis. The data presented here provides a platform from which we can begin to further investigate the controversial role of Tregs in promoting B-lymphoma, and the effects of the loss of p53 on Treg survival and activity, and recruitment to lymphoma sites.

Materials and Methods:

$4x10^6$ cells of lymphoma samples were resuspended in 1ul/1ml Fixable Viability Dye eFluor 660 **(**65-0864-14, eBioscience) in PBS for 20min on ice. Cells were washed with PBS, and stained in 100ul of 3% FBS/PBS containing PerCPBy5.5 anti-CD4 1:80 (clone RM4-5) and PE-Cy7 anti-CD25 1:100 (Clone PC61.5) for 20min on ice. Cells were incubated in 1ml Fix/Perm buffer **(**00-5523-00, eBioscience**)** for 30min on ice, and washed 2x with 1ml Perm Buffer. Cells were blocked for 15min at 4C in 100ul of 24G2 supernatant diluted in Perm buffer. 1ul of PE-Foxp3 or PE-RatIgG2a K Isotype (12-5773-82 or 12-4321-80, eBioscience) control was added, and cells were stained for 30min on ice, washed 2x and resuspended in 400ul of 3% FBS/PBS before analysis with BD's LSR II, and FlowJo (TreeStar). Additional staining was performed on the same samples using the same protocol and staining with PacBlue-CD8a (Clone 53-6.7) 1:600 and PerCPBy5.5 anti-CD4 1:80 (clone RM4-5).

Appendix A: Figure 1

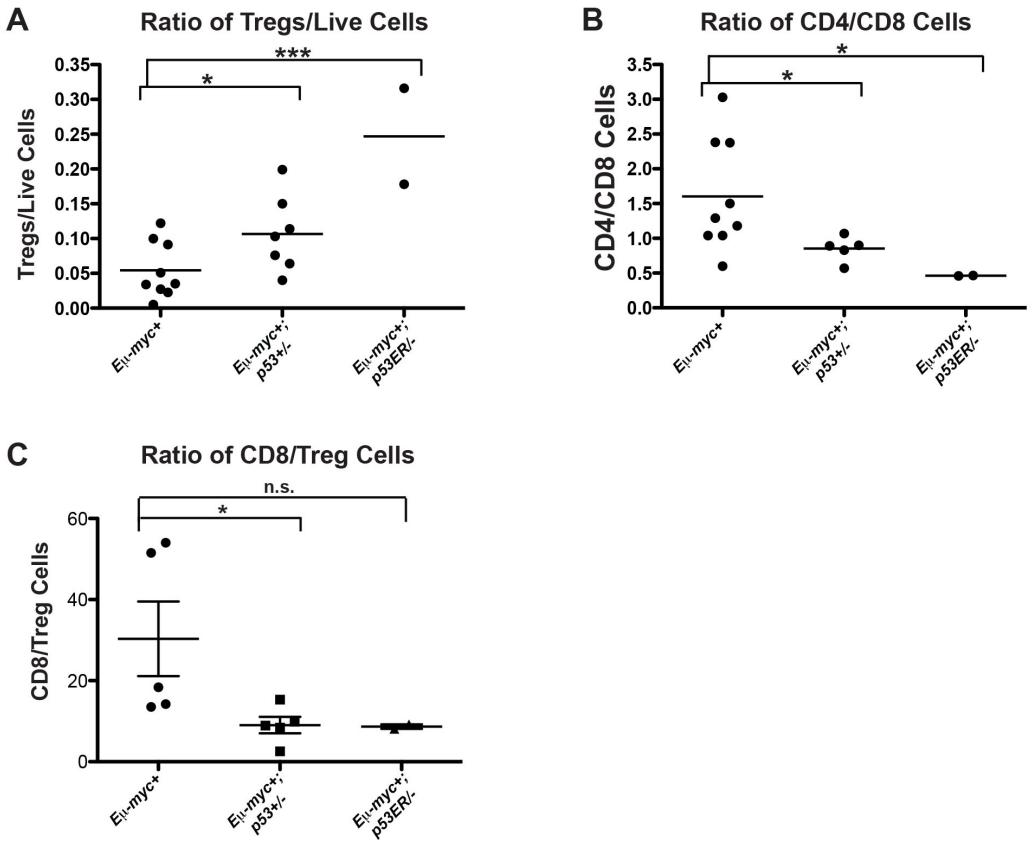

Figure 1. *Eμ-myc*$^{+}$*;p53+/-* tumors have increased numbers of T regulatory cells
A. . *Eμ-myc*$^{+}$*;p53+/-* tumors have increased numbers of Treg cells ($p<0.0219$), and two *Eμ-myc*$^{+}$*;p53ER/-* tumors show an even greater increase ($p<0.0004$). **B.** *Eμ-myc*$^{+}$*;p53+/-* tumors exhibit a decrease in the ratio of CD8cells:CD4 cells ($p<0.0316$) and so do the *Eμ-myc*$^{+}$*;p53ER/-* tumors ($p<0.429$). **C.** The ratio of CD8cells:Tregs is decreased in *Eμ-myc*$^{+}$*;p53+/-* tumors ($p<0.0269$), and the same trend is observed in *Eμ-myc*$^{+}$*;p53ER/-* tumors but more animals are needed to determine the significance.

Appendix B:

Eμ-myc^{+}*;mir-34b/c+/-* mice exhibit increased lymphoma dissemination to the meningeal space

Bennett, MJ., Chen, Y., Zhong, Y., and He, L. Unpublished data 2014

Introductory Summary:
As previously discussed in the above thesis, p53 suppresses tumor development through many mechanisms including inducing apoptosis and senescence, and inhibiting proliferation and metastasis. In the *Eμ-myc* mouse model, mice deleted for p53 develop tumors at an accelerated rate (Eischen et al, 1999; Schmitt et al). This accelerated rate of lymphoma is mostly attributed to the reduced apoptosis of *Eμ-myc*$^{+}$*;p53+/-* B-cells, as well as increased proliferation and dissemination throughout the animals organs (Schmitt et al, 2001). In our comparison of *Eμ-myc*$^{+}$*;p53+/-* and *Eμ-myc*$^{+}$ *mir-34* knockout animals, we observed a significant increase in dissemination to the meningeal space between the brain and the skull of *Eμ-myc*$^{+}$*;p53+/-* mice that has gone previously undescribed. In comparing the *mir-34* knockout mice to deletion of p53 in the *Eμ-myc*$^{+}$ mouse model, we observed a similar increase in dissemination to the brain in the *Eμ-myc*$^{+}$*;mir-34b/c+/-* mice.

Results:
The *Eμ-myc*$^{+}$*;p53+/-* succumb to lymphoma at a faster rate (average time of 7 weeks) than *Eμ-myc* only animals **(**average time of 19 weeks) (Eischen et al, 1999**)**. The *Eμ-myc*$^{+}$*;mir-34b/c+/-* mice exhibit a similar increased acceleration of lymphomagenesis (average time of 13 weeks - Chapter 3, Sup.Fig. 2A), though to a lesser degree than the *Eμ-myc*$^{+}$*;p53+/-* animals.

Many aspects of tumorigenesis contribute to the *Eμ-myc*$^{+}$*;p53+/-* succumbing more quickly to tumorigenesis. One contributing factor of accelerated lymphomagenesis is that the *Eμ-myc*$^{+}$*;p53+/-* mice exhibit an increase in dissemination (Schmitt et al, 2001). We specifically observed an increase of dissemination to the meningeal space between the brain and the skull of these *Eμ-myc*$^{+}$*;p53+/-* mice (Fig. 1B). This phenotype is currently being further characterized by students in the lab since our initial discovery.

In an effort to characterize the *mir-34* knockout mice in the *Eμ-myc* mouse model, we analyzed whether the deletion of either *mir-34a, mir-34b/c,* or the combined deletion of *mir-34a* and *mir-34b/c* mimicked the dissemination phenotype seen in the *Eμ-myc*$^{+}$*;p53+/-* mice. Fascinatingly, we observed a similar phenotype in the *Eμ-myc*$^{+}$*;mir-34b/c+/-* mice (Fig. 2), but not in the *Eμ-myc*$^{+}$*;mir-34b/c-/-* or any of the *mir-34* knockout mice (data not shown). We show here by immunohistochemical staining for the B-cell marker, B220, that the increased cell mass in the meningeal space is in fact B-cell lymphoma (Fig. 2A). We further illustrate that the increased dissemination seen in *Eμ-myc*$^{+}$*;mir-34b/c+/-* mice is significant, by analyzing the area of the infiltrating tumor normalized to the size of the skull (Fig. 2B).

Discussion:

While it is clear that both *Eμ-myc*$^{+}$*;p53*+/- and *Eμ-myc*$^{+}$;*mir-34b/c*+/- mice exhibit an increase in meningeal dissemination, the mechanisms driving this phenotype remain unknown. It seems logical that the meningeal dissemination contributes to the acceleration of lymphomagenesis of these mice, however, the *Eμ-myc*$^{+}$;*mir-34b/c-/-* mice succumb to death at the same rate as the *Eμ-myc*$^{+}$;*mir-34b/c*+/- mice but the *Eμ-myc*$^{+}$;*mir-34b/c-/-*do not exhibit this meningeal dissemination. Therefore, it is likely that this phenotype is not the major driver for mice and even perhaps humans to succumb to lymphomagenesis, but instead impacts quality of life.

A confusing puzzle is what is driving the *Eμ-myc*$^{+}$;*mir-34b/c*+/- animals to acquire these disseminated tumors, while their *Eμ-myc*$^{+}$;*mir-34b/c-/-* littermates do not. The difference between the phenotypes of these mice suggest that the mechanism is likely very refined to be altered under such a small change in dosage of the miRNAs. Further characterization of the *Eμ-myc*$^{+}$*;p53*+/- meningeal dissemination phenotype and discovery of the mechanisms behind this phenotype will hopefully shed light on why *Eμ-myc*$^{+}$;*mir-34b/c*+/- exhibit dissemination and *Eμ-myc*$^{+}$;*mir-34b/c-/-* do not.

Materials and Methods:

Skulls were fixed for 5-7 days in formalin (SF100-4; Fisher), at room temperature and then washed for 1-3 hours with 3 changes of PBS. Skulls were decalcified in Saturated EDTA (100g of EDTA (disodium salt dihydrate) / Liter of H2O2 – stir until dissolved) for 4 days at room temperature, and washed 3 times with PBS with the 3rd time overnight at room temperature. The samples were then stored in 70% EtOH at 4C until embedding in paraffin (AC41677-0020; Fisher). Before embedding, the skulls were sagittally cut in half.

Embedding was performed starting with two 30min washes of each 80% and 90% EtOH. Following skulls were washed for 30min in 95% EtOH, and then incubated overnight in 95% EtOH at 4C. Then skulls were washed twice in 100% EtOH for 30min, and then 30min each of 50%EtOH/50%Histoclear (HS-200, National Diagnostics) then 100% Histoclear, 50%Histoclear/50% Paraffin wax, and then three 1 hour washes of 100% Paraffin (keep at 65C), with a final step of embedded and cooling overnight.

Skulls were than sectioned in 5-6uM sections, and subjected to Histoclear and graded alcohols before staining with hematoxylin and eosin (7211 & 7111, Fisher) or antigen retrieval with 10mM sodium citrate buffer with 10min in a pressure cooking and overnight incubation with anti-B220 (14-0452-85, 1:100; eBioscience). Detection of antibody staining was carried out following standard procedures from the avidin-biotin immunoperoxidase methods. Diaminobenzidine (002014, Invitrogen) was used as the chromogen and hematoxylin as the nuclear counter stain.

Appendix B: Figure 1

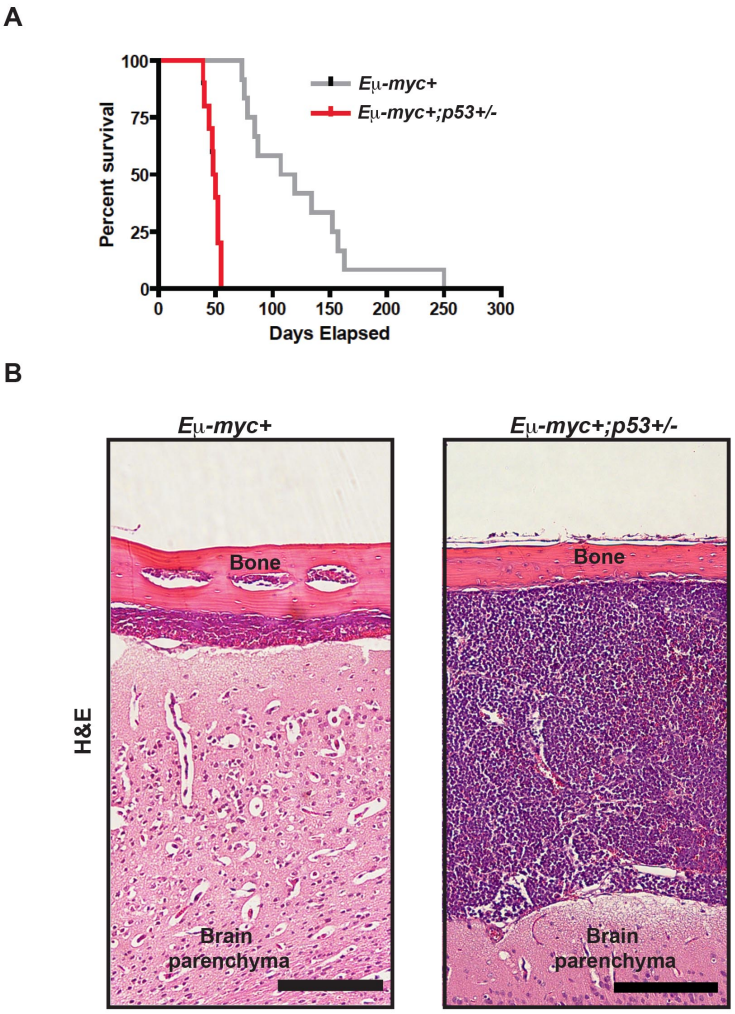

Figure 1: *Eμ-myc*$^{+}$*;p53+/-* mice exhibit increased lymphoma dissemination to the meningeal space.

A. Kaplan-Meier curve showing that *Eμ-myc*$^{+}$*;p53+/-* succumb to lymphoma at a faster rate than *Eμ-myc*$^{+}$ mice. Represented in this graph are mice analyzed for brain dissemination. **B.** H&E staining of a representative example of lymphoma disseminated into the meningeal space of an *Eμ-myc*$^{+}$*;p53+/-* mouse but not in the *Eμ-myc*$^{+}$ mouse.

Figure 2

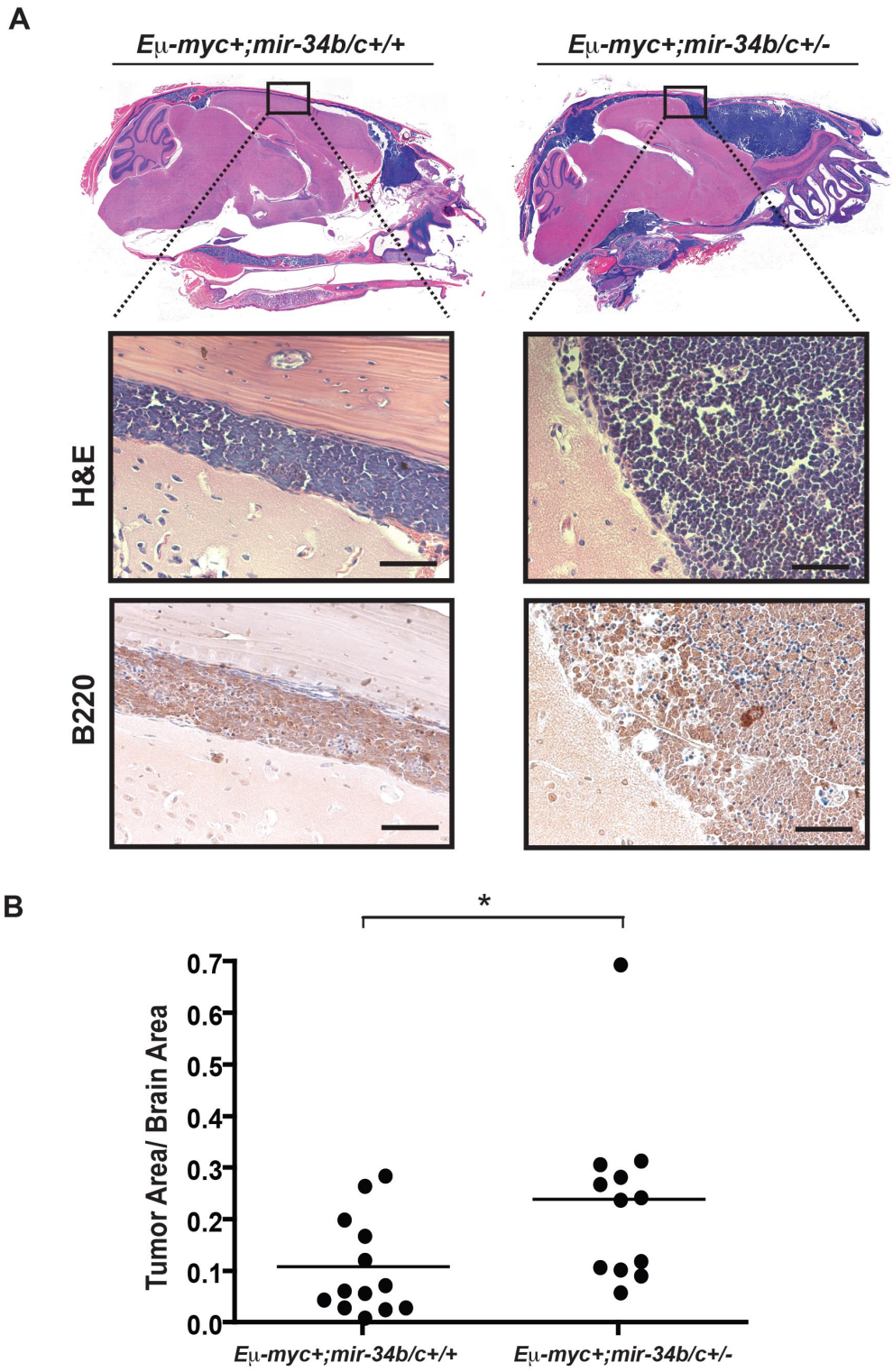
A
Eμ-myc+;mir-34b/c+/+
Eμ-myc+;mir-34b/c+/-
H&E
B220
B
*
Tumor Area/ Brain Area
0.7
0.6
0.5
0.4
0.3
0.2
0.1
0.0
Eμ-myc+;mir-34b/c+/+
Eμ-myc+;mir-34b/c+/-

Figure 2: *Eμ-myc*$^{+}$*;mir-34b/c+/-* mice exhibit increased lymphoma dissemination to the meninges.

A. H&E staining and immunohistochemical B220 staining of representative *Eμ-myc*$^{+}$ and *Eμ-myc*$^{+}$*;mir-34b/c+/-* skulls illustrating the increased lymphoma dissemination to the meninges in the *Eμ-myc*$^{+}$*;mir-34b/c+/-* mice. Represented in this graph are mice analyzed for brain dissemination. **B.** H&E staining of a representative example of lymphoma disseminated into the meningeal space of an *Eμ-myc*$^{+}$*;p53+/-* mouse but not in the *Eμ-myc*$^{+}$ mouse.